

A microscopic image of nasal epithelial cells, showing various cell shapes and structures, including nuclei and cytoplasm, stained in shades of orange and red against a dark background.

Nasal epithelial cells as model for cystic fibrosis

Lisa W. Rodenburg

Nasal epithelial cells as model for cystic fibrosis

Neus epitheelcellen als model voor taaislijmziekte

(met een samenvatting in het Nederlands)

Lisa Willemijn Rodenburg

Nasal epithelial cells as model for cystic fibrosis
Neus epitheelcellen als model voor taaislijmziekte

(met een samenvatting in het Nederlands)

Lisa Willemijn Rodenburg

ISBN: 978-94-6483-633-2

DOI: 10.33540/2079

Provided by thesis specialist Ridderprint, ridderprint.nl

Printing: Ridderprint

Layout and cover design: Harma Makken, persoonlijkproefschrift.nl

Copyright 2023 © Lisa Willemijn Rodenburg

The Netherlands. All rights reserved. No parts of this thesis may be reproduced, stored in a retrieval system or transmitted in any form or by any means without permission of the author.

Nasal epithelial cells as model for cystic fibrosis

Neus epitheelcellen als model voor taaislijmziekte
(met een samenvatting in het Nederlands)

Proefschrift

ter verkrijging van de graad van doctor aan de
Universiteit Utrecht
op gezag van de
rector magnificus, prof. dr. H.R.B.M. Kummeling,
ingevolge het besluit van het college voor promoties
in het openbaar te verdedigen op

donderdag 8 februari 2024 des middags te 2.15 uur

door

Lisa Willemijn Rodenburg

geboren op 7 april 1994
te Amersfoort

Promotoren:

Prof. dr. J.M. Beekman

Prof. dr. C.K. van der Ent

Copromotor:

Dr. G.D. Amatngalim

Beoordelingscommissie:

Prof. dr. L.J. Bont

Dr. M. Carlon

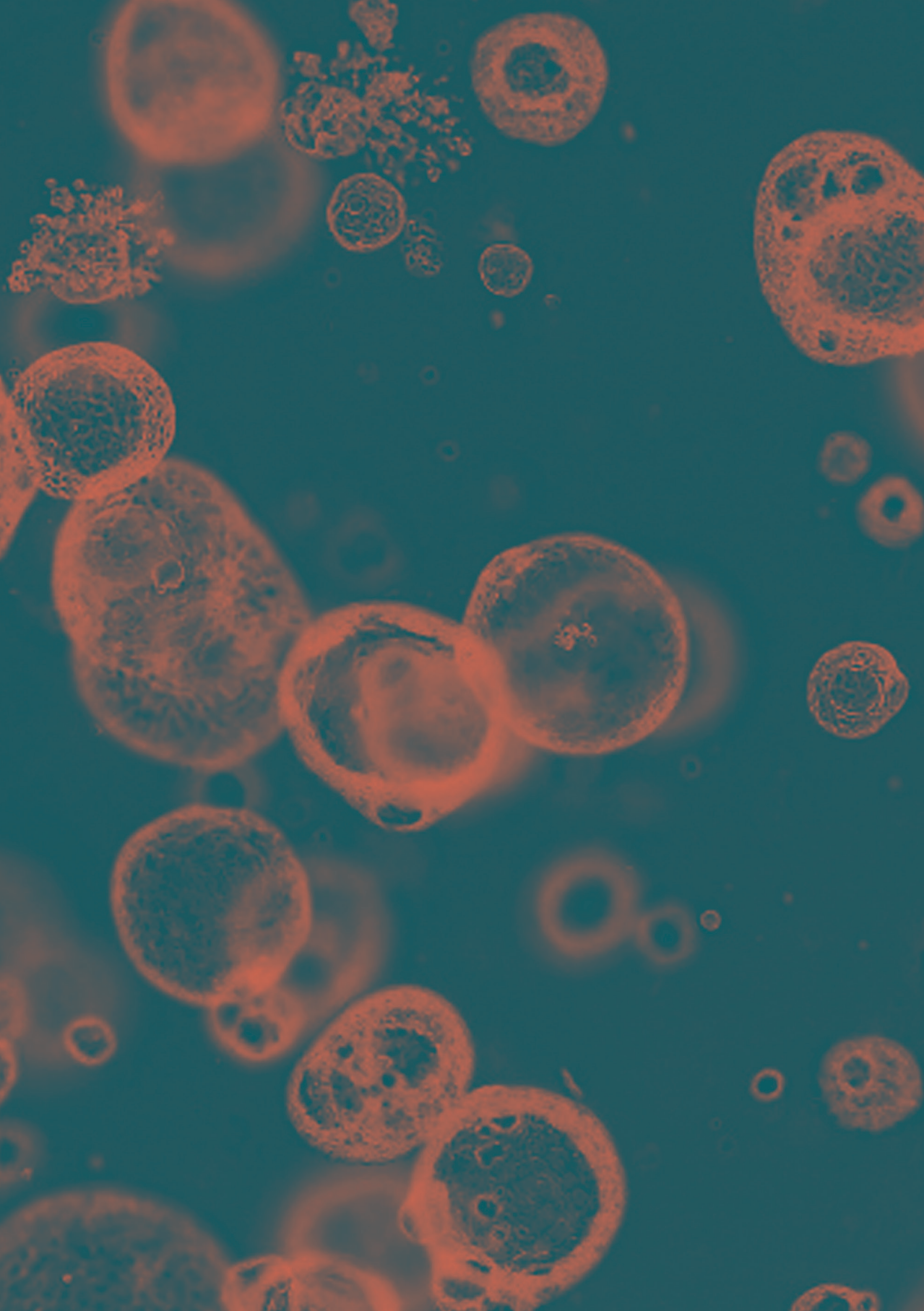
Prof. dr. H.G.M. Heijerman (voorzitter)

Prof. dr. H.I. Heijink

Prof. dr. P.S. Hiemstra

CONTENT

General introduction	6
Chapter 1 Protocol for generating airway organoids from 2D air-liquid interface-differentiated nasal epithelia for use in a functional CFTR assay	24
Chapter 2 Measuring cystic fibrosis drug responses in organoids derived from 2D differentiated nasal epithelia	66
Chapter 3 Drug repurposing for cystic fibrosis: identification of drugs that induce CFTR-independent fluid secretion in nasal organoids	98
Chapter 4 Examining CRISPR knockouts of non-CFTR ion channels or transporters in cystic fibrosis nasal organoid fluid secretion	138
Chapter 5 Exploring intrinsic variability between cultured nasal and bronchial epithelia in cystic fibrosis	158
General discussion	188
Nederlandse samenvatting	204
Acknowledgements – Dankwoord	214
List of publications	222
About the author	226



General introduction

CYSTIC FIBROSIS AND CFTR MODULATOR THERAPIES

Cystic fibrosis (CF) is one of the most common autosomal recessive inherited diseases, caused by mutations in the *cystic fibrosis transmembrane conductance regulator (CFTR)* gene. The *CFTR* gene encodes an anion channel that is mainly expressed in the apical membrane of epithelial tissues, such as the airway epithelium. It is a cAMP-activated channel secreting chloride and bicarbonate, accompanied by passive water transport due to osmosis. CFTR thus facilitates mucus hydration by modulation of ion and water transport, and it regulates pH of the airway surface liquid^{1,2}. A dysfunctional CFTR protein leads to impaired salt and water transport, causing mucus dehydration in multiple organs such as the lungs. The accumulation of thick dehydrated mucus in the lungs increases the risk for infections with opportunistic respiratory pathogens, such as *Pseudomonas aeruginosa*³. This may lead to hospitalizations and early death due to respiratory failure. Furthermore, people with CF may develop, among other things, pancreatic insufficiency, CF-related diabetes, CF liver disease, intestinal disease or infertility¹.

The incidence of CF is 1:4.500 in Western Europe^{1,2}. People with CF are diagnosed early in life during the newborn screening, based on elevated pancreatic protein concentrations and DNA analysis for common *CFTR* mutations¹. The diagnosis is further confirmed by a sweat chloride test, as a dysfunctional CFTR leads to reduced chloride reabsorption in the sweat ducts and high sweat chloride concentrations⁴. Over 2.000 different mutations in the *CFTR* gene have been discovered so far⁵. These mutations can be classified in seven classes according to mechanistic principles and their functional effects⁶. The most common mutation is the F508del mutation, carried by around 73% of people with CF⁵. This is a class II mutation, typified by impaired protein folding. Other mutation classes range from gating defects (class III) to no mRNA or protein production at all (class I and VII respectively)⁶.

The life expectancy for people with CF has dramatically increased the past years. The median survival age for Americans born with CF between 2017-2021 is predicted to be around 53 years old, which was around 43 years of age for people with CF born 4 years earlier, between 2012-2016^{2,7}. The main reason for this increase in survival age is the development of novel CFTR-modulating therapies. Before the era of these therapies, people with CF only received symptomatic therapy, including mucolytics to facilitate airway clearance, antibiotic treatment to treat pulmonary exacerbations and pancreatic enzymes to improve nutrition⁸.

CFTR modulators caused a paradigm shift from symptomatic treatment towards disease-modifying treatment that could potentially fully arrest or even reverse CF

disease progression. The first CFTR modulator (ivacaftor, VX-770) was introduced in 2012. This small molecule therapy directly targets the dysfunctional CFTR protein and acts as a CFTR potentiator by prolongation of channel opening. Clinical trials demonstrated a 10.6% increase in FEV1 in people with CF carrying a gating mutation⁹. However, despite this impressive increase in lung function, only ~6% of people with CF are eligible for ivacaftor treatment due to the low prevalence of responsive mutations⁸. In 2015 and 2018, the CFTR correctors lumacaftor (VX-809) and tezacaftor (VX-661) were developed respectively, both improving CFTR folding and trafficking. Combination treatment of these correctors with the potentiator ivacaftor (orkambi and symkevi) facilitated treatment for people with CF carrying folding mutations, including the most common F508del mutation⁸. Despite a step forward in CF treatment, lung function improvements were small with a 2.6% and 4.0% improvement in FEV1 for orkambi and symkevi respectively, and only observed in people carrying two copies of the *F508del* gene mutation^{10,11}. The most recent breakthrough was the launch of triple therapy, consisting of two CFTR correctors (tezacaftor, VX-661 and elexacaftor, VX-445) combined with the CFTR potentiator ivacaftor⁸. Multiple clinical trials demonstrated its high efficacy with an increase in FEV1 ranging from 10.0 - 14.3%^{12,13}. As all people with CF carrying at least one F508del CFTR allele are eligible, ~80% of all people with CF might benefit from this therapy¹⁴. It is therefore expected that the survival of people with CF will increase even more the coming years.

THE CURRENT UNMET NEED FOR PEOPLE WITH CF

Despite the increased life expectancy for the majority of people with CF, there still exists an unmet need for people with CF not having access to CFTR modulator therapy. It is estimated that only 12% of people with CF receive triple combination therapy¹⁵, while ~80% are eligible¹⁴, showing that access to care is limited. This is mainly caused by high costs that hinder reimbursement in many countries. Besides the issue of access, another group of people with CF does not receive treatment because they are not eligible for CFTR modulator treatment based on their mutation type. This number ranges from 7.6 – 30% of the CF population, dependent on race and ethnicity¹⁶. These include individuals with rare or with non-responding *CFTR* mutations. For the rare mutations, it is unknown how they will respond to CFTR-modulating therapies. Health insurances will not reimburse the high costs for CFTR modulator therapy with the uncertainty of therapy effectiveness. The people with non-responding mutations, which are class I and VII mutations, will not benefit from therapy as they do not have any *CFTR* mRNA or protein. New therapeutic approaches are needed for this group, such as read-through agents, mRNA therapy or gene editing to stimulate the production of

functional CFTR¹⁷. Despite huge progress in this field of research, efficient delivery and safety remain challenging issues¹⁷. Another therapeutic approach for the people with CF with an unmet need could be the stimulation of alternative chloride channels to restore epithelial fluid secretion in a CFTR-independent manner¹⁸ (Figure 1).

The concept to stimulate alternative chloride channels was introduced in 1991, by the discovery of CFTR-independent chloride transport in CF airway epithelia after stimulation with ATP or UTP¹⁹. These nucleotides enhance intracellular calcium via stimulation of purinergic receptors, thus suggesting the presence of a calcium-dependent chloride channel. In 2008, TMEM16A, also known as anoctamin-1 (ANO1), was identified as the responsible chloride channel by three different research groups²⁰⁻²². However, TMEM16A is also associated with mucus secretion and airway smooth muscle contraction^{23,24}. Controversy therefore exists whether the channel should be activated to increase chloride transport or inhibited to reduce mucus secretion and airway smooth muscle contraction²⁵. Despite this controversy, the TMEM16A potentiator ETD002 showed promising results in preclinical studies by stimulating chloride secretion without increased mucus production or bronchoconstriction^{26,27}. It is now being investigated in a clinical trial²⁸.

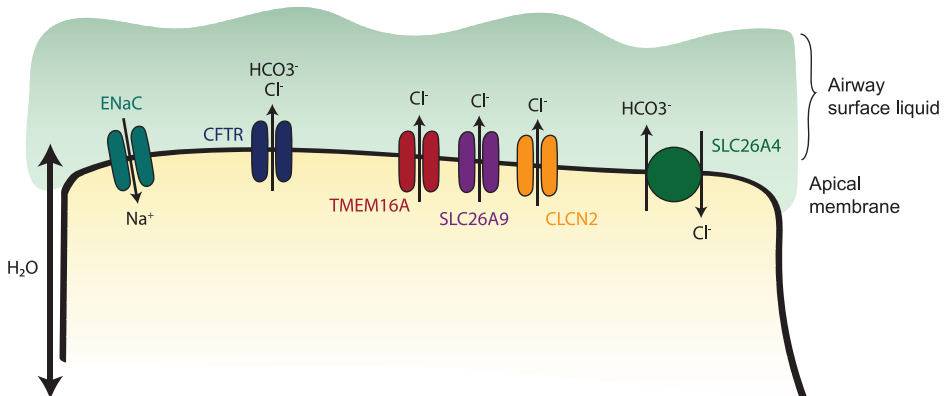


Figure 1. Schematic drawing of ion channels and transporters at the apical airway epithelium, involved in chloride transport. Only ion channels and transporters discussed in this thesis are depicted.

TMEM16A is the most studied non-CFTR chloride channel in the airway epithelium, but more channels or transporters might act as therapeutic target as they are directly or indirectly involved with chloride secretion^{4,29}. For example, the airway epithelium contains more chloride channels (e.g. SLC26A9) or transporters (e.g. SLC26A4) at the apical and basolateral membrane. Furthermore, ion transport is a complex process

with many interacting channels and transporters. Targeting sodium or potassium transporters might therefore indirectly influence chloride transport. One example is the sodium transporter ENaC which is hyperactivated in CF airway epithelia, thereby causing sodium hyperabsorption³⁰.

PERSONALIZED *IN VITRO* MODEL SYSTEMS FOR CYSTIC FIBROSIS

In vitro model systems can be employed to determine the efficacy of CFTR modulator therapies, for patient stratification or to find new therapeutic strategies for people with CF with an unmet need. Traditionally, many research has been performed with cell lines expressing CFTR or other ion channels or transporters. Cell lines are easy to culture, have unlimited growth and provide a standardized cellular source for preclinical studies. For example, Fischer rat thyroid (FRT) cells expressing mutant CFTR were used for high-throughput screenings to find new CFTR-activating compounds³¹, the identity of TMEM16A as a calcium-activated chloride channel was discovered by use of TMEM16A-expressing FRT cells²¹ and FRT cells were used to study the role of the chloride channel SLC26A9 in epithelial fluid transport³². However, cell lines usually have undergone substantial genetic changes, hardly recapitulate their parental line, rely on supra-physiological readouts (e.g. fluorescent reporters) and are often not derived from affected epithelial tissues³³. Patient-derived primary cells are therefore considered as a better resource to model human tissues³⁴. Moreover, they can be used as personalized disease model as they maintain the genetic, epigenetic and cellular features from individual donors.

As example of a personalized disease model in CF, 3D cultured intestinal organoids are currently being used to predict CFTR function and modulator responses with the forskolin-induced swelling (FIS) assay³⁵. Intestinal organoids are derived from painless rectal biopsies. Stem-cell rich intestinal crypts are isolated from these biopsies and self-organize into 3D structures when surrounded by an extracellular matrix-like environment³⁶. Intestinal organoids can be expanded over a long period of time and cryostored for later use while keeping phenotypic and genetic stability. Due to abundant expression of CFTR in the distal colon, stimulation with the cAMP agonist forskolin induces chloride secretion into the organoid lumen, which is passively followed by sodium and water transport. This causes CFTR-dependent swelling of the organoids. Quantification of organoid swelling can be used as measure for CFTR function and the potential rescue by CFTR modulator drugs. *In vitro* drug responses were shown to correlate with *in vivo* improvements in lung function and sweat chloride upon CFTR modulator treatment³⁷.

Furthermore, the FIS assay in intestinal organoids already facilitated access to treatment for CF subjects whose intestinal organoids showed a good response to CFTR modulator therapy³⁸. However, as people with CF mainly suffer from respiratory symptoms, it is argued that an airway epithelial model system would be more suited to predict CFTR modulator therapy efficacy and to develop new therapeutic strategies that reduce respiratory symptoms. Furthermore, intestinal organoids are not suitable to study CFTR-bypassing therapies by activation of alternative chloride channels or transporters as they do not show substantial CFTR-independent fluid secretion^{39,40}.

THE AIRWAY EPITHELIUM

The airway epithelium is a continuous cellular layer lining the respiratory tract. It consists of a diversity of cells which collaboratively maintain homeostasis in the airways (Figure 2). It functions as a protective barrier against environmental stimuli from the air we breathe, such as pathogens and pollutants. This physical barrier is maintained by tight junctions and adhesion proteins between the epithelial cells. Other functions of the airway epithelium include host defence, immunomodulation, mucociliary clearance and maintenance of the lung fluid balance⁴¹.

Healthy airways possess a pseudostratified epithelial layer. The principal cells are **basal cells**, connected to the basement membrane. They contribute to one third of the airway epithelial cells and are identifiable by the expression of cytokeratin 5 (KRT5) and the tumour protein 63 (p63)⁴⁴. Basal cells are multipotent stem cells, with the ability to self-renew and differentiate towards luminal cell types, including goblet cells, club cells, ciliated cells and ionocytes⁴⁵. They have this ability during steady state, but also when epithelial repair is needed in response to injury⁴⁶. **Ciliated cells** are present throughout the respiratory tract and their beating cilia contribute to mucociliary clearance. Mucociliary clearance is the process in which microorganisms and debris are captured in gel forming mucins and cleared from the airways by rhythmic ciliary beating movements. Ciliated cells are characterized by the expression of the transcription factor forkhead box protein J1 (FOXP1), which is necessary for cilia formation⁴⁷. The other cell types contributing to mucociliary clearance are secretory epithelial cells, which produce gel-forming mucins, i.e. MUC5AC and MUC5B. In the upper airways, **goblet cells** represent the main secretory cell type of the surface airway epithelium and mainly produce MUC5AC. Furthermore, goblet cells are characterized by the transcription factor SPDEF, which mediates goblet cell differentiation⁴⁸. Although a subpopulation of goblet cells also display expression of MUC5B, submucosal glands are mainly responsible for producing this gel-forming mucin in the upper airways

⁴⁹. The main secretory cells residing in the lower airways are **club cells**, formerly known as Clara cells. They have an immunomodulatory function by the production of anti-microbial and anti-inflammatory peptides, such as SCGB1A1 (also known as CC10 or CC16). Furthermore, club cells mediate the production of MUC5B, whereas MUC5AC production in the lower airways is normally lacking ^{49,50}.

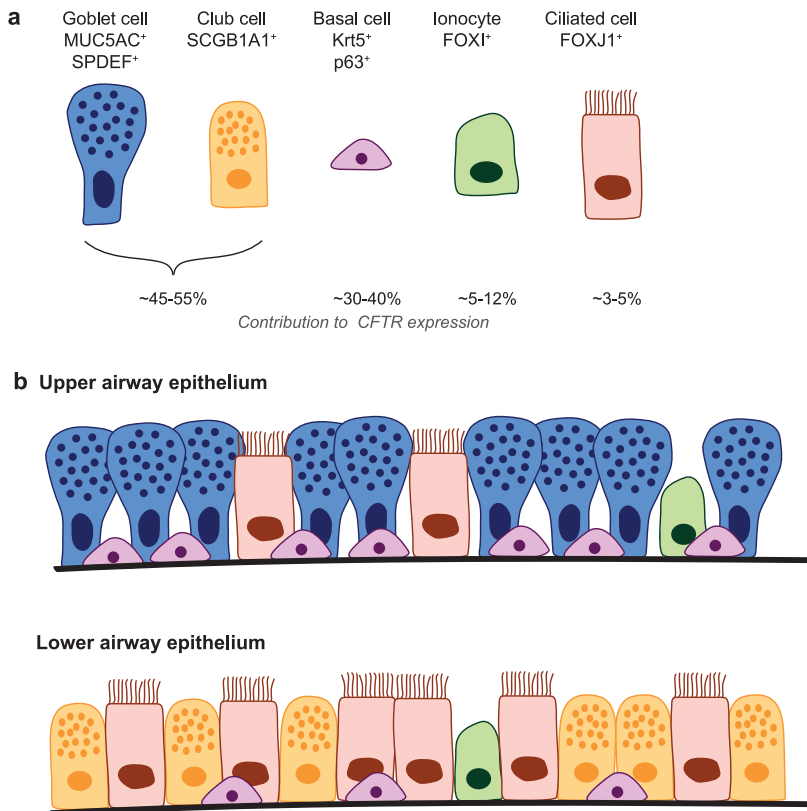


Figure 2. Composition of the airway epithelium

(A) Schematic drawing of the most common cell types, and ionocytes, in the airway epithelium and an estimation of their contribution to CFTR expression, based on earlier studies ^{42,43}. (B) Schematic drawing of the cellular composition of the upper and lower airway epithelium.

Besides basal, ciliated and secretory cells, some rare cell types exist in the airway epithelium including tuft cells, neuroendocrine cells and ionocytes. Pulmonary **ionocytes**, identifiable by the expression of FOXI1, have been identified in 2018 and are mainly interesting because of their abundant expression of CFTR ^{51,52}. However, the role of ionocytes in CFTR function is debatable because of their low prevalence, namely 1-2% of all human airway epithelial cells. Other reports argued that secretory

cells might be more important for CFTR function in the airway epithelium because of their higher prevalence^{42,43}. Besides CFTR, the alternative chloride channel TMEM16A is predominantly being expressed in mucus-producing goblet cells²³.

The cellular composition of the airway epithelium changes along the proximal-to-distal axis, corresponding to a change in function. The upper respiratory tract, consisting of the nasal cavity, pharynx and larynx functions, mainly functions as a protective barrier against pathogens. The lower respiratory tract consists of the trachea, bronchi and bronchioles and is specialized in air conduction towards the distal small airways, consisting of the respiratory bronchioles and alveoli⁵³. Along the proximal-to-distal axis, the prevalence of basal progenitor cells decreases from 31% in the large airways to 6% in the small airways⁵⁴. In contrast, the number of ciliated cells increases along this axis^{44,55}. Regarding secretory cells, mucus-producing goblet cells are dominant in the upper airways and substituted by secretory club cells in the smaller airways⁵⁶. The knowledge about the composition of the airway epithelium along the respiratory tract has been expanded the last years due to advances in single-cell RNA-sequencing (scRNA-seq) techniques. This led to the discovery of new cellular subtypes, such as the previously mentioned ionocytes⁵³. For basal, secretory and ciliated cells, differences in gene expression profiles were found at different anatomical locations along the respiratory tract⁴⁴. For example, secretory cells in the nasal epithelium have higher expression of genes related to cell motility and differentiation compared to secretory cells in the tracheobronchial epithelium, which have higher expression of genes related to innate immunity and wound healing responses^{44,53}. Moreover, intermediate cell types have been discovered. Examples are the deuterosomal cells, precursors of multiciliated cells^{44,57}, and mucus ciliated cells (MUC5AC⁺FOXJ1⁺), suggesting that goblet cells can transdifferentiate towards ciliated cells^{44,57,58}.

PRIMARY AIRWAY EPITHELIAL CELLS AS MODEL FOR CYSTIC FIBROSIS

To model the airway epithelium of individuals with CF in cell culture models, cells can be derived from brushings, biopsies or bronchoalveolar lavage during a bronchoscopy³³. From these samples, human bronchial epithelial cells (HBEC) are isolated and expanded using irradiated feeder cells, which improve the proliferative lifespan⁵⁹. Feeder-free culture conditions have recently been established, depending on small molecules which inhibit signaling transduction pathways, such as TGF- β /BMP signaling⁶⁰. Expanded HBEC display an undifferentiated basal cell phenotype, which lack ciliated and in particular CFTR-expressing secretory cells. To recapitulate the differentiated airway

epithelium, cells are further differentiated on porous membrane filters (Transwell inserts) at air-liquid interface (ALI) conditions³⁴. This triggers differentiation towards a pseudostratified airway epithelium containing luminal cells and an epithelial barrier with tight junctions and adherent proteins.

CFTR activity can be measured in these epithelial cell cultures by transepithelial short circuit current (Isc) measurements with the Ussing chamber (Figure 3, number 1)⁶¹. This is a physiological system which measures ion transport across an epithelial layer, such as ALI-differentiated cells. To specifically measure CFTR-dependent transepithelial electric currents, sodium transport is first inhibited with the ENaC blocker amiloride. CFTR is then activated with the cAMP agonists forskolin and IBMX. CFTR inhibitors can be added to evaluate CFTR specificity. The potential efficacy of CFTR modulator therapy is assessed by addition of these drugs before CFTR activation. Besides CFTR function measurements, the Ussing Chamber can also be used to measure chloride transport by non-CFTR channels or transporters. Currents induced by the calcium agonists A3 and UTP rely on calcium-activated chloride channels, including TMEM16A⁶². The activity of the sodium channel ENaC can be quantified by the decrease in current after addition of the ENaC inhibitor amiloride⁶². As specific activators or inhibitors of other chloride channels (e.g. SLC26A9) are lacking, these channels are mainly studied with overexpressing or knockdown experiments in cell lines^{32,63}.

Ussing chamber measurements are widely used and assumed as the golden standard for CFTR function measurements *in vitro*. Their importance is shown with their major role in the preclinical phase of the development of the current CFTR modulators⁶⁴. However, limitations of this technique are the low-throughput setting and invasive procedures to obtain HBEC, which makes it unsuitable for personalized diseased modeling.

To facilitate scalability, primary airway epithelial cells can be cultured as 3D organoids (Figure 3, number 2). In 2019, a protocol was published for the long-term expansion of airway organoids, derived from resected lung tissue or bronchoalveolar lavage⁴⁰. Airway organoids were used to measure CFTR-dependent organoid swelling and the effect of CFTR modulator therapy in the FIS assay. Improvements still have to be made to decrease the heterogeneity in organoid morphology and swelling responses. Interestingly, observations of not completely blocked FIS by CFTR inhibitors, and organoid swelling induced by the calcium agonist E_{act} , suggest the presence of alternative chloride channels in airway organoids. This in contrast to the intestinal organoids where FIS is completely CFTR-dependent, and no calcium-dependent swelling exists. This study therefore shows that airway organoids provide an *in vitro* model system to study alternative ion channels or transporters, next to their potential for scalability. However, invasive procedures are still needed to obtain primary airway cells.

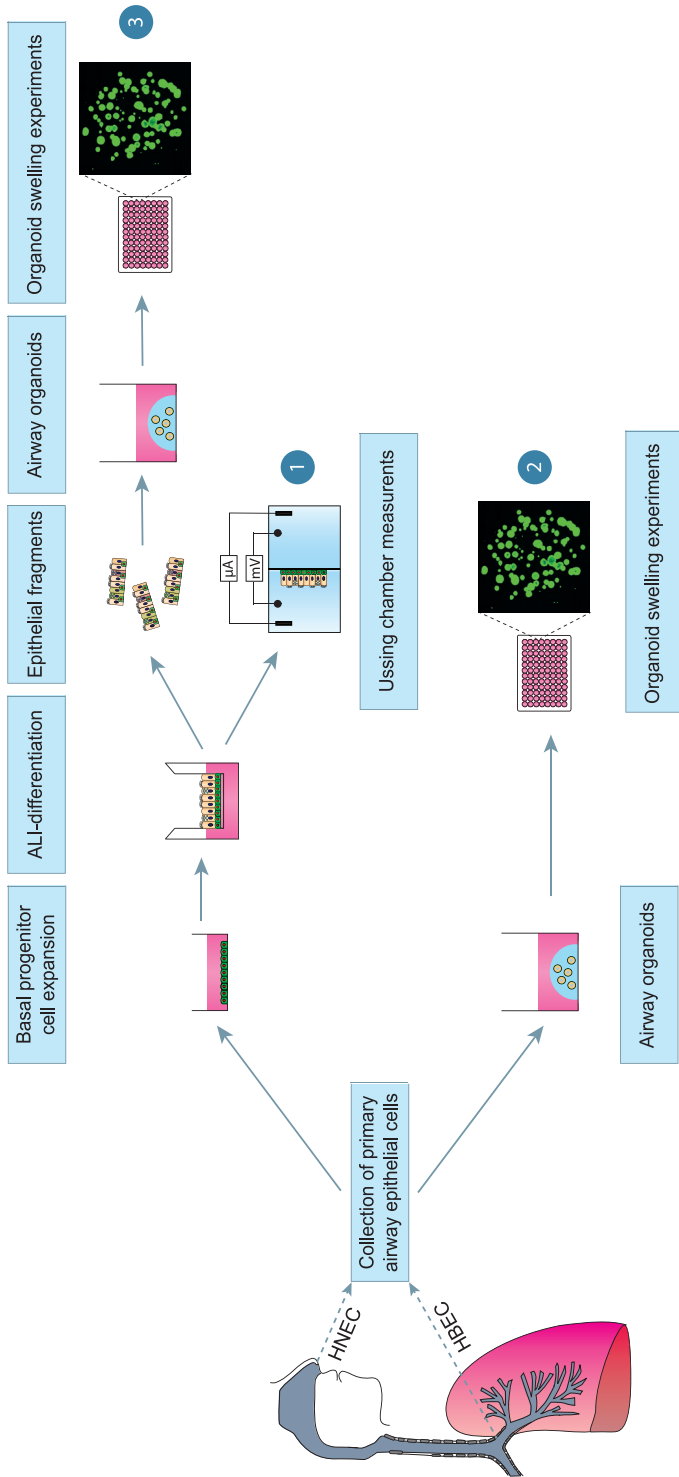


Figure 3. Primary epithelial cells can be collected via nasal (HNEC) or bronchial brushing (HBEC).

Basal progenitor cells can be expanded and ALI-differentiated to be used for electrophysiological measurements in the Ussing chamber (indicated by number 1). This method is traditionally seen as the golden standard. Alternatively, epithelial cells can be expanded as airway organoids and used in organoid swelling experiments as measure for fluid secretion (indicated by number 2). In this thesis, we propose an alternative method to generate airway organoids from ALI-differentiated nasal epithelia to decrease heterogeneity in individual organoid morphology and swelling responses (indicated by number 3).

NASAL EPITHELIAL CELLS AS MODEL FOR CYSTIC FIBROSIS

Because of the invasive procedures needed to obtain HBEC, it is proposed that human nasal epithelial cells (HNEC) might be applied as proxy model for the lower airways. HNEC can be obtained by non-invasive nasal brushings, which enables their use for personalized disease modeling. As the genetic CFTR mutation is present in both the upper and airway epithelium, it is expected that HNEC are usable for CFTR function measurements. Moreover, the involvement of the upper airways in CF is demonstrated by a high prevalence of sinonasal problems⁶⁵ and the use of nasal potential difference (NPD) measurements as diagnostic tool^{66,67}. However, nasal cells originate from a different germ layer and show a somewhat different cellular composition. The role for nasal cells in disease modeling should therefore be investigated by comparison studies between nasal and bronchial epithelial cells. These types of studies already showed that both HBEC and HNEC can be expanded as basal progenitor cells and ALI-differentiated towards a pseudostratified mucociliary epithelium with the presence of adherent proteins⁶⁸⁻⁷⁰.

Several groups already investigated the use of nasal epithelial cells as model for CF and correlated the efficacy of CFTR modulators in Ussing Chamber measurements with clinical drug responses⁷¹⁻⁷³. For example, one group showed that *in vitro* responses to VX770/VX809 correlated with the ppFEV1 increase after 6 months of therapy in 16 patients with a F508del/F508del mutation⁷². Another study focused on 12 patients with a G551D/R117H mutation and showed a correlation between *in vitro* VX770 response with the *in vivo* drug responses on sweat chloride and lung function⁷³. CFTR function measurements were not only performed in 2D ALI-cultured nasal epithelial cells, but also in fluid secretion assays with 3D cultured nasal organoids. For example, nasospheroids with the apical side faced outwards were used for CFTR-dependent shrinking assays⁷⁴ and nasospheroids with the apical side facing inwards for CFTR-dependent swelling assays^{75,76}. CFTR modulator responses in the latter were shown to correlate with CFTR modulator-induced chloride currents in Ussing chamber measurements and with *in vivo* lung function^{75,76}. Altogether, all these studies already show the potential of nasal epithelial cells as model for CF. However, as far as we know, all studies used low passage nasal epithelial cells which could not be cryopreserved and are thus for single use. This hampers their use for biobanking and their use in multiple and future experiments.

THESIS OUTLINE

This thesis investigates the use of nasal brushing-derived airway epithelial cells in 3D organoid cultures as personalized disease model of CF (Figure 3, number 3). Nasal organoids are used to find therapeutic strategies for the people with CF with an existing unmet need by restoring epithelial fluid transport by activation of CFTR or alternative ion channels or transporters (Figure 4).

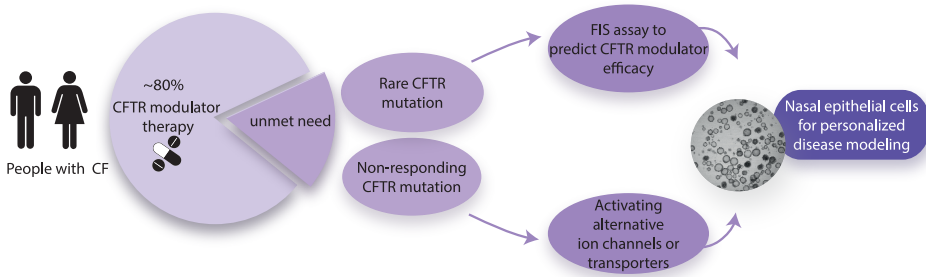


Figure 4. The use of nasal organoids for personalized disease modeling in CF to find therapeutic strategies for the people with CF with an unmet need.

On the one hand, they can be applied to predict CFTR modulator efficacy with FIS assays in cell cultures from people with CF with rare CFTR mutations. On the other hand, they can be applied to find drugs activating alternative ion channels or transporters in cell cultures from people with CF without any functional CFTR protein.

Chapter 1 describes the procedures to generate nasal organoids. These include the sampling of nasal brushings and the isolation, expansion and cryostorage of airway basal progenitor cells. Furthermore, it explains how basal progenitor cells are differentiated in ALI-cultures, and how to convert ALI-differentiated cells into airway organoids for the application in the CFTR-dependent FIS-assay.

Chapter 2 describes the optimization of culturing conditions to employ the FIS assay in nasal organoids. It investigates the feasibility to predict efficacy of CFTR modulators on individual basis for people with CF.

Chapter 3 describes the application of nasal organoids to find drugs which restore epithelial fluid transport by activation of alternative ion channels or transporters, thus bypassing the dysfunctional CFTR protein. A screening assay was performed to find FDA-approved drugs inducing CFTR-independent epithelial fluid secretion.

Chapter 4 describes a further investigation in the mechanism behind CFTR-independent fluid secretion. Knockout studies were performed to investigate which ion channel or transporter is involved in the CFTR-independent nasal organoid swelling.

Chapter 5 focuses on the comparison between nasal and bronchial epithelial cell cultures to investigate how nasal epithelial cells represent the lower airway epithelium. Donor-matched nasal and bronchial epithelial cells and organoids were analyzed on phenotypic and transcriptomic characteristics. It was further investigated how the differences affect epithelial fluid secretion in nasal and bronchial organoids.

Finally, in the general discussion I will provide a summary of the results and discuss the strengths and limitations of the use of nasal epithelial cells as *in vitro* model for cystic fibrosis. Furthermore, I will discuss the potential of HNEC in personalized disease modeling.

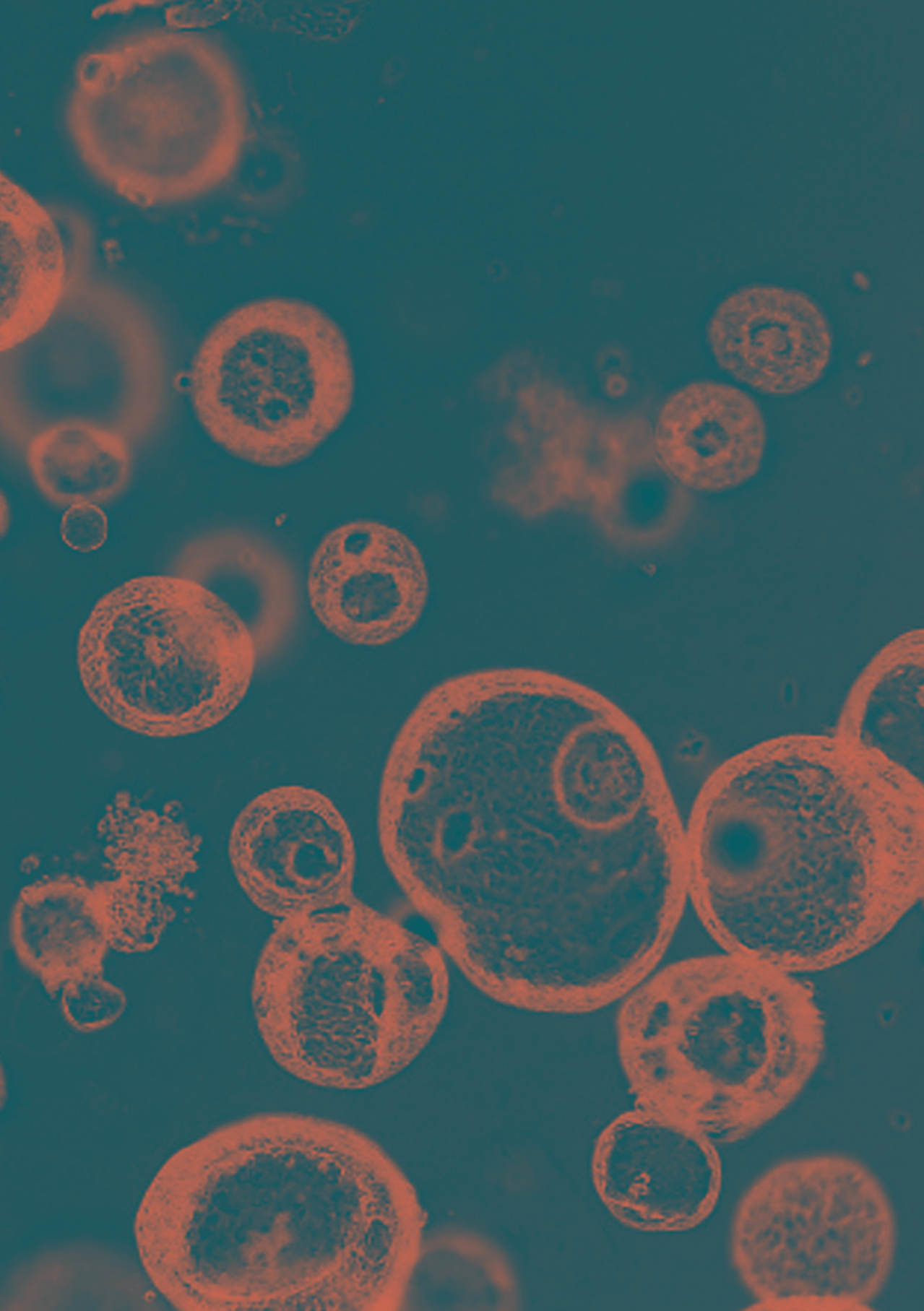
REFERENCES

1. Shteinberg, M., Haq, I. J., Polineni, D. & Davies, J. C. Cystic fibrosis. *Lancet* 397, 2195–2211 (2021).
2. Scotet, V., L'hostis, C. & Férec, C. The Changing Epidemiology of Cystic Fibrosis: Incidence, Survival and Impact of the CFTR Gene Discovery. *Genes (Basel)* 11, 589 (2020).
3. Chmiel, J. F. *et al.* Antibiotic management of lung infections in cystic fibrosis: II. Nontuberculous mycobacteria, anaerobic bacteria, and fungi. *Ann Am Thorac Soc* 11, 1298–1306 (2014).
4. Saint-Criq, V. & Gray, M. A. Role of CFTR in epithelial physiology. *Cellular and Molecular Life Sciences* 74, 93–115 (2017).
5. US CF Foundation, Johns Hopkins University & The Hospital for Sick Children. The Clinical and Functional Translation of CFTR (CFTR2); available at <http://cftr2.org>. <https://cftr2.org/> (2011).
6. de Boeck, K. & Amaral, M. D. Progress in therapies for cystic fibrosis. *Lancet Respir Med* 4, 662–674 (2016).
7. US Cystic Fibrosis Registry (Cystic Fibrosis Foundation). Patient registry annual data report 2021. (2021).
8. McBennett, K. A., Davis, P. B. & Konstan, M. W. Increasing life expectancy in cystic fibrosis: Advances and challenges. *Pediatr Pulmonol* 57 Suppl 1, S5–S12 (2022).
9. Ramsey, B. W. *et al.* A CFTR potentiator in patients with cystic fibrosis and the G551D mutation. *N Engl J Med* 365, 1663–1672 (2011).
10. Taylor-Cousar, J. L. *et al.* Tezacaftor–Ivacaftor in Patients with Cystic Fibrosis Homozygous for Phe508del. *New England Journal of Medicine* 377, 2013–2023 (2017).
11. Wainwright, C. E. *et al.* Lumacaftor–Ivacaftor in Patients with Cystic Fibrosis Homozygous for Phe508del CFTR. *New England Journal of Medicine* 373, 220–231 (2015).
12. Middleton, P. G. *et al.* Elexacaftor–Tezacaftor–Ivacaftor for Cystic Fibrosis with a Single Phe508del Allele. *N Engl J Med* 381, 1809–1819 (2019).
13. Heijerman, H. G. M. *et al.* Efficacy and safety of the elexacaftor plus tezacaftor plus ivacaftor combination regimen in people with cystic fibrosis homozygous for the F508del mutation: a double-blind, randomised, phase 3 trial. *Lancet* 394, 1940–1948 (2019).
14. Fajac, I. & Sermet, I. Therapeutic Approaches for Patients with Cystic Fibrosis Not Eligible for Current CFTR Modulators. *Cells* 10, 2793 (2021).
15. Guo, J., Garratt, A. & Hill, A. Worldwide rates of diagnosis and effective treatment for cystic fibrosis. *Journal of Cystic Fibrosis* 21, 456–462 (2022).
16. McGarry, M. E. & McColley, S. A. Cystic Fibrosis Patients of Minority Race and Ethnicity Less Likely Eligible for CFTR Modulators Based on CFTR Genotype. *Pediatr Pulmonol* 56, 1496 (2021).
17. Allan, K. M., Farrow, N., Donnelley, M., Jaffe, A. & Waters, S. A. Treatment of Cystic Fibrosis: From Gene- to Cell-Based Therapies. *Front Pharmacol* 12, 241 (2021).
18. Mall, M. A. & Galiotta, L. J. V. Targeting ion channels in cystic fibrosis. *Journal of Cystic Fibrosis* 14, 561–570 (2015).
19. Knowles, M. R., Clarke, L. L. & Boucher, R. C. Activation by extracellular nucleotides of chloride secretion in the airway epithelia of patients with cystic fibrosis. *N Engl J Med* 325, 533–538 (1991).
20. Schroeder, B. C., Cheng, T., Jan, Y. N. & Jan, L. Y. Expression cloning of TMEM16A as a calcium-activated chloride channel subunit. *Cell* 134, 1019–1029 (2008).
21. Caputo, A. *et al.* TMEM16A, a membrane protein associated with calcium-dependent chloride channel activity. *Science* 322, 590–594 (2008).
22. Yang, Y. D. *et al.* TMEM16A confers receptor-activated calcium-dependent chloride conductance. *Nature* 455, 1210–1215 (2008).
23. Scudieri, P. *et al.* Association of TMEM16A chloride channel overexpression with airway goblet cell metaplasia. *J Physiol* 590, 6141–6155 (2012).

24. Huang, F. *et al.* Calcium-activated chloride channel TMEM16A modulates mucin secretion and airway smooth muscle contraction. *Proc Natl Acad Sci U S A* 109, 16354–16359 (2012).
25. Kunzelmann, K. *et al.* TMEM16A in Cystic Fibrosis: Activating or Inhibiting? *Front Pharmacol* 10, 1–18 (2019).
26. Danahay, H. L. *et al.* TMEM16A Potentiation: A Novel Therapeutic Approach for the Treatment of Cystic Fibrosis. *Am J Respir Crit Care Med* 201, 946–954 (2020).
27. Danahay, H. *et al.* Potentiating TMEM16A does not stimulate airway mucus secretion or bronchial and pulmonary arterial smooth muscle contraction. *FASEB Bioadv* 2, 464 (2020).
28. A First in Human Study to Evaluate the Safety, Tolerability and Pharmacokinetics of Single and Multiple Ascending Doses of Inhaled ETD002 in Healthy Subjects - Full Text View - ClinicalTrials.gov. <https://clinicaltrials.gov/ct2/show/NCT04488705?term=etd002&draw=2&rank=1>.
29. Hollenhorst, M. I., Richter, K. & Fronius, M. Ion Transport by Pulmonary Epithelia. *J Biomed Biotechnol* 2011, 174306 (2011).
30. Mall, M., Bleich, M., Greger, R., Schreiber, R. & Kunzelmann, K. The amiloride-inhibitable Na⁺ conductance is reduced by the cystic fibrosis transmembrane conductance regulator in normal but not in cystic fibrosis airways. *J Clin Invest* 102, 15–21 (1998).
31. Galletta, L. J. V. *et al.* Novel CFTR Chloride Channel Activators Identified by Screening of Combinatorial Libraries Based on Flavone and Benzoquinolinizinium Lead Compounds. *Journal of Biological Chemistry* 276, 19723–19728 (2001).
32. Salomon, J. J. *et al.* Ion Channels and Transporters in Lung Function and Disease: Generation and functional characterization of epithelial cells with stable expression of SLC26A9 Cl⁻ channels. *Am J Physiol Lung Cell Mol Physiol* 310, L593 (2016).
33. Awatade, N. T. *et al.* Human Primary Epithelial Cell Models: Promising Tools in the Era of Cystic Fibrosis Personalized Medicine. *Front Pharmacol* 9, 1429 (2018).
34. Pezzulo, A. A. *et al.* The air-liquid interface and use of primary cell cultures are important to recapitulate the transcriptional profile of in vivo airway epithelia. *Am J Physiol Lung Cell Mol Physiol* 300, L25–31 (2011).
35. Dekkers, J. F. *et al.* A functional CFTR assay using primary cystic fibrosis intestinal organoids. *Nat Med* 19, 939–945 (2013).
36. Sachs, N. *et al.* Long-term expanding human airway organoids for disease modeling. *EMBO J* 38, (2019).
37. Berkers, G. *et al.* Rectal Organoids Enable Personalized Treatment of Cystic Fibrosis. *Cell Rep* 26, 1701–1708.e3 (2019).
38. Ramalho, A. S. *et al.* Correction of CFTR function in intestinal organoids to guide treatment of cystic fibrosis. *European Respiratory Journal* 57, 1902426 (2021).
39. Zomer-van Ommen, D. D. *et al.* Comparison of ex vivo and in vitro intestinal cystic fibrosis models to measure CFTR-dependent ion channel activity. *J Cyst Fibros* 17, 316–324 (2018).
40. Sachs, N. *et al.* Long-term expanding human airway organoids for disease modeling. *EMBO J* 38, e100300 (2019).
41. Knight, D. A. & Holgate, S. T. The airway epithelium: structural and functional properties in health and disease. *Respirology* 8, 432–446 (2003).
42. Okuda, K. *et al.* Secretory Cells Dominate Airway CFTR Expression and Function in Human Airway Superficial Epithelia. *Am J Respir Crit Care Med* 203, 1275–1289 (2021).
43. Carraro, G. *et al.* Transcriptional analysis of cystic fibrosis airways at single-cell resolution reveals altered epithelial cell states and composition. *Nat Med* 27, 806–814 (2021).
44. Deprez, M. *et al.* A Single-Cell Atlas of the Human Healthy Airways. *Am J Respir Crit Care Med* 202, 1636–1645 (2020).
45. Davis, J. D. & Wypych, T. P. Cellular and functional heterogeneity of the airway epithelium. *Mucosal Immunol* 14, 978–990 (2021).
46. Rock, J. R. *et al.* Basal cells as stem cells of the mouse trachea and human airway epithelium. *Proc Natl Acad Sci U S A* 106, 12771–5 (2009).

47. You, Y. *et al.* Role of f-box factor foxj1 in differentiation of ciliated airway epithelial cells. *Am J Physiol Lung Cell Mol Physiol* 286, L650-7 (2004).
48. Chen, G. *et al.* SPDEF is required for mouse pulmonary goblet cell differentiation and regulates a network of genes associated with mucus production. *J Clin Invest* 119, 2914 (2009).
49. Okuda, K. *et al.* Localization of Secretory Mucins MUC5AC and MUC5B in Normal/Healthy Human Airways. *Am J Respir Crit Care Med* 199, 715–727 (2019).
50. Zuo, W. L. *et al.* Ontogeny and Biology of Human Small Airway Epithelial Club Cells. *Am J Respir Crit Care Med* 198, 1375–1388 (2018).
51. Plasschaert, L. W. *et al.* A single-cell atlas of the airway epithelium reveals the CFTR-rich pulmonary ionocyte. *Nature* 560, 377–381 (2018).
52. Montoro, D. T. *et al.* A revised airway epithelial hierarchy includes CFTR-expressing ionocytes. *Nature* 560, 319–324 (2018).
53. Hewitt, R. J. & Lloyd, C. M. Regulation of immune responses by the airway epithelial cell landscape. *Nature Reviews Immunology* 2021 21:6 21, 347–362 (2021).
54. Boers, J. E., Ambergen, A. W. & Thunnissen, F. B. Number and proliferation of basal and parabasal cells in normal human airway epithelium. *Am J Respir Crit Care Med* 157, 2000–2006 (1998).
55. Hogan, B. L. M. *et al.* Repair and regeneration of the respiratory system: complexity, plasticity, and mechanisms of lung stem cell function. *Cell Stem Cell* 15, 123–138 (2014).
56. Boers, J. E., Ambergen, A. W. & Thunnissen, F. B. J. M. Number and Proliferation of Clara Cells in Normal Human Airway Epithelium. *Am J Respir Crit Care Med* 159, 1585–91 (1999).
57. Garcíá, S. R. *et al.* Novel dynamics of human mucociliary differentiation revealed by single-cell RNA sequencing of nasal epithelial cultures. *Development* 146, dev177428 (2019).
58. Vieira Braga, F. A. *et al.* A cellular census of human lungs identifies novel cell states in health and in asthma. *Nat Med* 25, 1153–1163 (2019).
59. Liu, X. *et al.* ROCK inhibitor and feeder cells induce the conditional reprogramming of epithelial cells. *American Journal of Pathology* 180, 599–607 (2012).
60. Mou, H. *et al.* Dual SMAD Signaling Inhibition Enables Long-Term Expansion of Diverse Epithelial Basal Cells. *Cell Stem Cell* 19, 217–231 (2016).
61. Ramalho, A. S. *et al.* Assays of CFTR Function In Vitro, Ex Vivo and In Vivo. *Int J Mol Sci* 23, (2022).
62. Gianotti, A., Delpiano, L. & Caci, E. In vitro Methods for the Development and Analysis of Human Primary Airway Epithelia. *Front Pharmacol* 9, 1176 (2018).
63. Pinto, M. C. *et al.* Synergy in cystic fibrosis therapies: Targeting SLC26A9. *Int J Mol Sci* 22, 13064 (2021).
64. Van Goor, F. *et al.* Correction of the F508del-CFTR protein processing defect in vitro by the investigational drug VX-809. *Proc Natl Acad Sci U S A* 108, 18843–18848 (2011).
65. Oomen, K. P. Q. & April, M. M. Sinonasal Manifestations in Cystic Fibrosis. *Int J Otolaryngol* 2012, 1–7 (2012).
66. Rowe, S. M., Clancy, J. P. & Wilschanski, M. Nasal potential difference measurements to assess CFTR ion channel activity. *Methods Mol Biol* 741, 69–86 (2011).
67. Knowles, M., Gatzky, J. & Boucher, R. Increased bioelectric potential difference across respiratory epithelia in cystic fibrosis. *N Engl J Med* 305, 1489–1495 (1981).
68. Lopez-Souza, N., Avila, P. C. & Widdicombe, J. H. Polarized cultures of human airway epithelium from nasal scrapings and bronchial brushings. *In Vitro Cell Dev Biol Anim* 39, 266–269 (2003).
69. Pranke, I. M. *et al.* Correction of CFTR function in nasal epithelial cells from cystic fibrosis patients predicts improvement of respiratory function by CFTR modulators. *Scientific Reports* 2017 7:1 7, 1–11 (2017).
70. Brewington, J. J. *et al.* Brushed nasal epithelial cells are a surrogate for bronchial epithelial CFTR studies. *JCI Insight* 3, e99385 (2018).

71. de Courcey, F. *et al.* Development of primary human nasal epithelial cell cultures for the study of cystic fibrosis pathophysiology. *Am J Physiol Cell Physiol* 303, C1173-9 (2012).
72. Pranke, I. *et al.* Might Brushed Nasal Cells Be a Surrogate for CFTR Modulator Clinical Response? *Am J Respir Crit Care Med* 199, 123–126 (2019).
73. Debley, J. S. *et al.* Correlation between ivacaftor-induced CFTR activation in airway epithelial cells and improved lung function: A proof-of-concept study. *Ann Am Thorac Soc* 17, 1024–1027 (2020).
74. Guimbellot, J. S. *et al.* Nasospheroids permit measurements of CFTR-dependent fluid transport. *JCI Insight* 2, e95734 (2017).
75. Anderson, J. D., Liu, Z., Odom, L. V., Kersh, L. & Guimbellot, J. S. CFTR function and clinical response to modulators parallel nasal epithelial organoid swelling. *Am J Physiol Lung Cell Mol Physiol* 321, L119–L129 (2021).
76. Brewington, J. J. *et al.* Detection of CFTR function and modulation in primary human nasal cell spheroids. *J Cyst Fibros* 17, 26–33 (2018).



Chapter 1

Protocol for generating airway organoids from 2D air-liquid interface-differentiated nasal epithelia for use in a functional CFTR assay

Lisa W. Rodenburg, Isabelle S. van der Windt, Henriette H.M. Dreyer, Shannon M.A. Smits, Loes A. den Hertog - Oosterhoff, Ellen M. Aarts, Jeffrey M. Beekman and Gimano D. Amatngalim

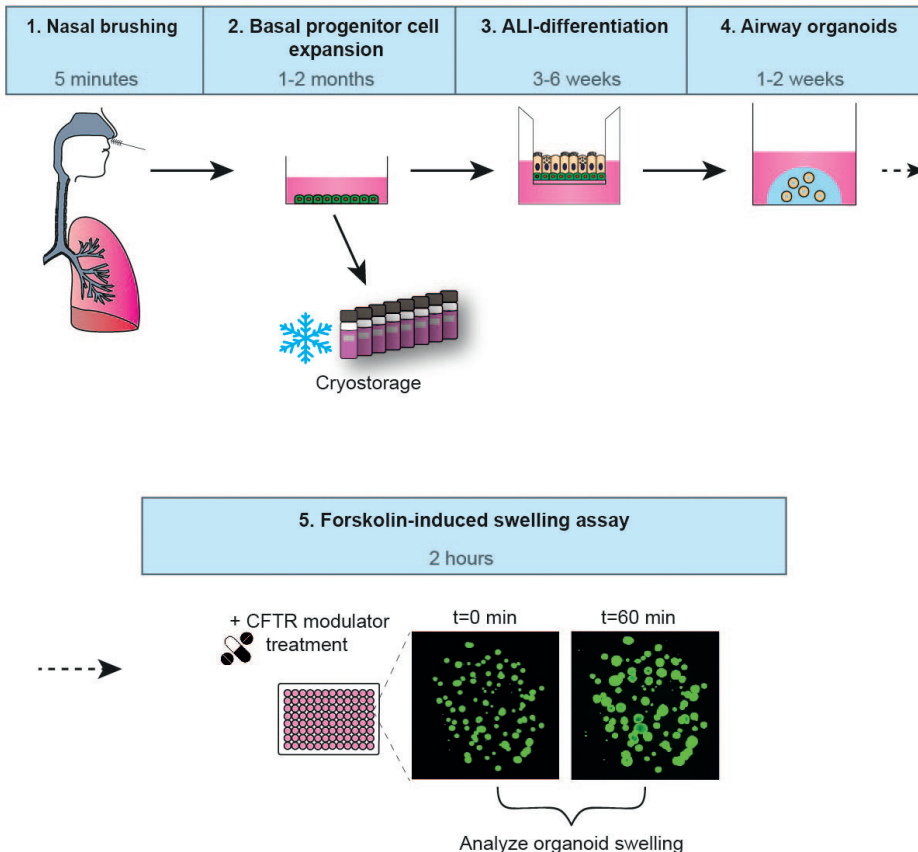
STAR protocols 2023, 4 (3); 102337

SUMMARY

We present a protocol to generate organoids from air-liquid interface (ALI)-differentiated nasal epithelia. We detail their application as cystic fibrosis (CF) disease model in the cystic fibrosis transmembrane conductance regulator (CFTR)-dependent forskolin-induced swelling (FIS) assay. We describe steps for isolation, expansion and cryostorage of nasal brushing-derived basal progenitor cells, and their differentiation in ALI-cultures. Furthermore, we detail the conversion of differentiated epithelial fragments into organoids of healthy controls and CF subjects for validating CFTR function and modulator responses.

For complete details on the use and execution of this protocol, please refer to Amatngalim et al.¹

GRAPHICAL ABSTRACT



BEFORE YOU BEGIN

Institutional permissions

All human samples used for this study were acquired with informed consent of the subjects and approval of a specific ethical board for the use of biobanked materials TcBIO (Toetsingscommissie Biobanks), an institutional Medical Research Ethics Committee of the University Medical Center Utrecht (protocol ID: 16/586).

CRITICAL: This protocol describes the use of primary human nasal epithelial cells. It is important that permission has been received from relevant institutions and it should meet regulatory standards, including informed consent from all subjects.

Preparation: precoating of well plates for basal progenitor cell expansion

Timing: 1.5 - 24 hours

1. Coat wells in a 12- or 6-well plate with collagen IV (50 µg/mL in PBS0) and incubate at 37 °C and 5% CO₂ for 1 – 24 hours.
 - a. For one well in a 12-well plate: add 500 µL collagen IV solution.
 - b. For one well in a 6-well plate: add 1000 µL collagen IV solution.

Note: After 24 hours of incubation with the coating, precoated wells can be stored in the fridge for a maximum of 14 days. For storage, replace the collagen coating solution with 1 mL (12-well plate) or 2 mL (6-well plate) PBS0, wrap the plate in foil and store at 4 °C.

Preparation: precoating of Transwell inserts for ALI-differentiation

Timing: 1.5 - 24 hours

2. Coat Transwell inserts at the apical side with PureCol (30 µg/mL in PBS0) and incubate at 37 °C and 5% CO₂ for 1 – 24 hours.
 - a. For one 6.5 mm insert (24-well plate): add 200 µL PureCol solution.
 - b. For one 12 mm insert (12-well plate): add 400 µL PureCol solution.

Note: After 24 hours of incubation with the coating, precoated wells can be stored in the fridge for a maximum of 14 days. For storage, replace the PureCol coating solution with 300 µL (6.5 mm insert) or 600 µL (12 mm insert) PBS0, fill the basolateral compartment with PBS0, wrap the plate in foil and store at 4 °C.

KEY RESOURCES TABLE

REAGENT or RESOURCE	SOURCE	IDENTIFIER
Antibodies		
N/A		
Bacterial and virus strains		
N/A		
Biological samples		
Human nasal airway epithelial cells (HNEC) from nasal brushing	UMC Utrecht	Protocol ID: 16/586, NL54885.041.16
Chemicals, peptides, and recombinant proteins		
Phosphate Buffered Saline 0, without Ca and Mg (PBS0)	Sigma-Aldrich/ Thermo Fisher Scientific/sterile homemade	Cat#D5652; Cat#14190250
Acetic acid	Sigma-Aldrich	Cat#A6283-1L
Collagen IV	Sigma-Aldrich	Cat#C7521
PureCol Type I Collagen Solution	Advanced BioMatrix	Cat#5005
TrypLE express enzyme	Thermo Fisher Scientific	Cat#12605010
Sputolysin	Calbiochem	Cat#560000-10
CryoStor CS10	STEMCELL Technologies	Cat#07930
Advanced DMEM/F-12 (Ad-DF)	Thermo Fisher Scientific	Cat#12634-028
Bronchial epithelial cell medium-basal (BEpiCM-b)	ScienCell	Cat#3211
B-27 Supplement, serum free	Thermo Fisher Scientific	Cat#17504001
GlutaMAX Supplement	Thermo Fisher Scientific	Cat#35050-061
HEPES	Thermo Fisher Scientific	Cat#15630080
3,3',5-Triiodo-L-thyronine sodium salt	Sigma-Aldrich	Cat#T6397
(±)-Epinephrine hydrochloride	Sigma-Aldrich	Cat#E4642
Hydrocortisone	Sigma-Aldrich	Cat#H0888
N-Acetyl-L-cysteine	Sigma-Aldrich	Cat#A9165
Nicotinamide	Sigma-Aldrich	Cat#N0636
A83-01 (TGF-βi)	Tocris	Cat#2939/10
DAPT (NOTCHi)	Thermo Fisher Scientific	Cat#15467109
DMH-1 (BMPi)	Selleck Chemicals	Cat#S7146
SB 202190 (p38i)	Sigma-Aldrich	Cat#S7067
TTNPB (Retinoic acid agonist)	Cayman	Cat#16144-1
Y-27632 (ROCKi)	Selleck Chemicals	Cat#S1049
Recombinant human Fibroblast growth factor 7 (FGF-7)	PeptoTech	Cat#100-19
Recombinant human Fibroblast growth factor 10 (FGF-10)	PeptoTech	Cat#100-26
Recombinant human Pro-epidermal growth factor (EGF)	PeptoTech	Cat#AF-100-15
Recombinant human Hepatocyte growth factor (HGF)	PeptoTech	Cat#100-39H
Recombinant Neuregulin-1β	PeptoTech	Cat#100-03

Key resources table (continued)

REAGENT or RESOURCE	SOURCE	IDENTIFIER
Recombinant Interleukin-1 β	PeproTech	Cat#200-01B
RSPO3-Fc Fusion Protein conditioned medium (R-spondin 3)	U-Protein Express	Cat#R001 - 100 ml
Amphotericin B	Thermo Fisher Scientific	Cat#15290018
Gentamicin	Sigma-Aldrich	Cat#G1397
Penicillin–Streptomycin	Thermo Fisher Scientific	Cat#15070-063
Primocin	InvivoGen	Cat#ant-pm-2
Vancomycin	Sigma-Aldrich	Cat#SBR00001
Collagenase type II	Thermo Fisher Scientific	Cat#17101-015
Cultrex Basement Membrane Extract, Type 2, Pathclear (BME)	Trevigen	Cat#3532-010-02
Matrigel® Growth Factor Reduced (GFR) Basement Membrane Matrix, LDEV-free	Corning	Cat#354230
Cell recovery solution	Corning	Cat#354253
VX-445	MedChemExpress	Cat#HY-111772
VX-661	Selleck Chemicals	Cat#S7059
VX-809	Selleck Chemicals	Cat#S1565
VX-770	Selleck Chemicals	Cat#S1144
Forskolin	Sigma-Aldrich	Cat#F3917-10mg
Calcein green acetoxymethyl (AM)	Invitrogen	Cat#C34852
Critical commercial assays		
N/A		
Deposited data		
N/A		
Experimental models: Cell lines		
N/A		
Experimental models: Organisms/strains		
N/A		
Oligonucleotides		
N/A		
Recombinant DNA		
N/A		
Software and algorithms		
Zen Blue Software	Zeiss	https://www.zeiss.com/microscopy/int/products/microscope-software/zen.html

Key resources table (continued)

REAGENT or RESOURCE	SOURCE	IDENTIFIER
Prism 8	GraphPad Software Inc.	https://www.graphpad.com/scientific-software/prism/
Microsoft Excel	Microsoft Corporation	https://office.microsoft.com/excel
R (version 4.2.2)	R Core Team (2022)	https://www.R-project.org/
RStudio (version 2022.7.2.576)	RStudio Team (2022)	http://www.rstudio.com/
ImageJ/FIJI	Wayne Rasband, NIH, USA	https://imagej.net/Fiji/Downloads
Other		
Cytological brush	CooperSurgical	Cat#C0004
Interdental brush 3-5 mm	E.g. Lactona	N/A
pluriStrainer® 30 µm	ITK Diagnostics	Cat#43-50030
pluriStrainer® 100 µm	ITK Diagnostics	Cat#43-57100-51
MACS SmartStrainers (100 µm)	Miltenyi Biotec bv	Cat#130-098-463
12-mm Transwell with 0.4-µm Pore Polyester Membrane Insert	Corning	Cat#3460
6.5-mm Transwell with 0.4-µm Pore Polyester Membrane Insert	Corning	Cat#3470
CELLSTAR® 6-well plate, TC	Greiner Bio-One	Cat#657160
CELLSTAR® 12-well plate, TC	Greiner Bio-One	Cat#655180
CELLSTAR® 24-well plate, suspension	Greiner Bio-One	Cat#662102
CELLSTAR® 96-well plate, F-bottom, µClear®, black, TC	Greiner Bio-One	Cat#655090
CELLSTAR® 96-well plate, U-bottom, TC	Greiner Bio-One	Cat#650180
CoolCell™ LX Cell Freezing Container	Corning	Cat#CLS432001-1EA
Zeiss LSM800 confocal microscope	Zeiss	N/A
Liquid nitrogen tank	N/A	N/A

MATERIALS AND EQUIPMENT

Stock preparation of medium compounds

Timing: 16 - 20 hours

Compound	Stock preparation	Stock concentration	Storage
Advanced DMEM/F-12 (Ad-DF)	Ready to use	-	4 °C for 1 year
Bronchial epithelial cell medium-basal (BEpiCM-b)	Ready to use	-	4 °C for 1 year
B-27 Supplement, serum free	Ready to use	-	-20 °C for 1 year
GlutaMAX Supplement	Ready to use	-	4 °C for 2 years
HEPES	Ready to use	1 M	4 °C for 2 years
3,3',5-Triiodo-L-thyronine sodium salt	Dissolve 100 mg in 100 mL NaOH (0.2 M) and filter sterilize (0.22 µm)	1 mg/mL	-80 °C for 1 year
(±)-Epinephrine hydrochloride	Dissolve 25 mg in 5 mL PBS0 and filter sterilize (0.22 µm)	5 mg/mL	-20 °C for 1 year
Hydrocortisone	Dissolve 5 mg in 1 mL Ethanol 100% and subsequently in 49 mL Ad-DF. Filter sterilize (0.22 µm)	100 µg/mL	-80 °C for 1 year
N-Acetyl-L-cysteine	Dissolve 3.26 g in 40 mL PBS0 MQ and filter sterilize (0.22 µm)	500 mM	-20 °C for 3 months
Nicotinamide	Dissolve 5 g in 41 mL PBS0 MQ and filter sterilize (0.22 µm)	1 M	-20 °C for 3 months
A83-01 (TGF-βi)	Dissolve 10 mg in 4.74 mL DMSO	5 mM	-80 °C or -20 °C for 3 months
DAPT (NOTCHi)	Dissolve 10 mg in 1.16 mL DMSO	20 mM	-20 °C for 1 year
DMH-1 (BMPi)	Dissolve 10 mg in 5.2571 mL DMSO	5 mM	-20 °C for 2 years
SB 202190 (p38i)	Dissolve 5 mg in 500 µL DMSO	30 mM	-20 °C for 2 years
TTNPB (Retinoic acid agonist)	Dissolve 1 mg in 2.9 mL DMSO	1 mM	-20 °C for 1 year
Y-27632 (ROCKi)	Dissolve 50 mg in 1.56 mL DMSO	100 mM	-20 °C for 2 years
Recombinant human Pro-epidermal growth factor (EGF)	Dissolve 100 µg in 2 mL PBS0-BSA 0.1%	50 µg/mL	-20 °C for 1 year
Recombinant human Fibroblast growth factor 10 (FGF-10)	Dissolve 1 mg in 1 mL PBS0-BSA 0.1%	1 mg/mL	-20 °C for 1 year
Recombinant human Fibroblast growth factor 7 (FGF-7)	Dissolve 100 µg in 1 mL PBS0-BSA 0.1%	100 µg/mL	-20 °C for 1 year
Recombinant human Hepatocyte growth factor (HGF)	Dissolve 100 µg in 0.4 mL PBS0-BSA 0.1%	250 µg/mL	-20 °C for 1 year
Recombinant Neuregulin-1β	Dissolve 100 µg in 1333 µL PBS-BSA 0.1 %	10 µM	-20 °C for 1 year
Recombinant Interleukin-1β	Dissolve 10 µg in 1000 µL PBS-BSA 0.1 %	10 µg/mL	20 °C for 1 year
RSPO3-Fc Fusion Protein conditioned medium (R-spondin 3)	Ready to use	-	-80 °C or -20 °C for 3 months

Compound	Stock preparation	Stock concentration	Storage
Collagen IV	Dissolve 10 mg in filter sterilized (0.22 µm filter) 10 mL acetic acid (0.5 M)	20x	-20 °C for 1 year
Collagenase type II	Dissolve 1 g in 50 mL PBS0 MQ	20 mg/mL	-20 °C for 1 year
PureCol Type I Collagen Solution	Ready to use	3 mg/mL	4 °C for 6 months
Amphotericin B	Ready to use	250 mg/mL	-20 °C for 1 year
Gentamicin	Ready to use	50 mg/mL	4 °C for 2 years
Penicillin-Streptomycin	Ready to use	-	-20 °C for 1 year
Primocin	Ready to use	50 mg/mL	-20 °C for 1 year
Vancomycin	Ready to use	100 mg/mL	-20 °C for 2 years

Overview of media

Overview of all different media used in the protocol

Name	Abbreviation	Preparation	Application
Collection medium	N/A	Section "Preparation of collection medium"	Collection and storage of nasal brushings
Basic basal cell medium	BC medium	Section "Basic BC medium"	Basic medium which is used to prepare BC isolation or BC expansion medium
Basal cell isolation medium	BC isolation medium	Section "BC isolation medium"	Basic BC medium with supplements to culture basal progenitor cells the first week after isolation
Basal cell expansion medium	BC expansion medium	Section "BC expansion medium"	Basic BC medium with supplements to expand basal progenitor cells
Freezing medium	Freezing medium	Add 5 µL Y-27632 (stock 100 mM) to 100 mL CryoStor CS10	Medium to freeze basal progenitor cells
Basic ALI-differentiation medium	ALI-diff medium	Section "ALI-diff medium"	Basic medium for ALI-differentiation of basal progenitor cells on Transwell inserts
ALI-differentiation medium + A83-01	ALI-diff phase 1 medium	Section "ALI-diff phase 1 medium"	Medium used for the submerged culturing phase on Transwell inserts
ALI-differentiation medium + A83-01 + neuregulin-1β	ALI-diff phase 2 medium	Section "ALI-diff phase 2 medium"	Medium used the first days after air-exposure on Transwell inserts
ALI-differentiation medium + neuregulin-1β	ALI-diff phase 3 medium	Section "ALI-diff phase 3 medium"	Medium used for the rest of differentiation on Transwell inserts
Airway organoid medium	AO medium	Section "AO medium"	Basic medium for airway organoids

Overview of all different media used in the protocol (continued)

Name	Abbreviation	Preparation	Application
Airway organoid culture medium	AO culture medium	Section "AO culture medium"	Medium for organoid formation and maintenance
Airway organoid FIS assay medium	AO FIS assay medium	Section "AO FIS assay medium"	Medium used to enhance CFTR expression in organoids used in the FIS assay

Preparation of collection medium

Collection medium is used for the collection and preservation of nasal brushings. It can be stored at 4 °C for a maximum of one year.

Collection medium

Reagent	Final concentration	Amount
Advanced DMEM/F-12 (Ad-DF)	97.8% (v/v)	489 mL
GlutaMAX Supplement (100x)	1% (v/v)	5 mL
Penicillin-Streptomycin (100x)	1% (v/v)	5 mL
Primocin (50 mg/mL)	100 µg/mL	1 mL
Total	n/a	500 mL

Preparation of basic BC medium, BC isolation and BC expansion medium

Basic basal cell (BC) medium is first prepared and can be used to make BC isolation medium or BC expansion medium by addition of fresh supplements. Basic BC medium can be stored at -20 °C for a maximum of 6 months, if desirable as 10 mL or 40 mL aliquots. BC isolation and expansion medium can be stored at 4 °C for 2 weeks. BC isolation medium is used for the culturing of basal progenitor cells the first 7 days after isolation. BC expansion medium is used for further expansion of basal progenitor cells.

Basic BC medium

Reagent	Final concentration	Amount
Advanced DMEM/F-12 (Ad-DF)	44% (v/v)	220 mL
Bronchial epithelial cell medium-basal (BEpiCM-b) (100%)	49.6% (v/v)	248 mL
B-27 Supplement, serum free (100%)	2% (v/v)	10 mL
GlutaMAX Supplement (100x)	1% (v/v)	5 mL
HEPES (1 M)	10 mM	5 mL
3,3',5-Triiodo-L-thyronine sodium salt (1 mg/mL)	100 nM	34 µL
(±)-Epinephrine hydrochloride (5 mg/mL)	0.5 µg/mL	50 µL
Hydrocortisone (100 µg/mL)	0.5 µg/mL	2.5 mL
N-Acetyl-L-cysteine (500 mM)	1.25 mM	1.25 mL

Basic BC medium (*continued*)

Reagent	Final concentration	Amount
Nicotinamide (1M)	5 mM	2.5 mL
A83-01 (TGF- β i) (5 mM)	1 μ M	100 μ L
DMH-1 (BMPi) (5 mM)	1 μ M	100 μ L
SB 202190 (p38i) (30 mM)	500 mM	8 μ L
Y-27632 (ROCKi) (100 mM)	5 μ M	25 μ L
Penicillin-Streptomycin (100x)	1% (v/v)	5 mL
Primocin (50 mg/mL)	100 μ g/mL	1 mL
Total	n/a	500 mL

BC isolation medium

Reagent	Final concentration	Amount
Basic BC medium (100%)	100% (v/v)	10 mL
Recombinant human Pro-epidermal growth factor (EGF) (50 μ g/mL)	5 ng/mL	1 μ L
Recombinant human Fibroblast growth factor 7 (FGF-7) (100 μ g/mL)	25 ng/mL	2.5 μ L
Recombinant human Fibroblast growth factor 10 (FGF-10) (1 mg/mL)	100 ng/mL	1 μ L
Recombinant human Hepatocyte growth factor (HGF) (250 μ g/mL)	25 ng/mL	1 μ L
RSPO3-Fc Fusion Protein conditioned medium (100%)	2% (v/v)	200 μ L
Amphotericin B (250 mg/mL)	250 μ g/mL	10 μ L
Gentamicin (50 mg/mL)	50 μ g/mL	10 μ L
Vancomycin (100 mg/mL)	50 μ g/mL	5 μ L
Total	n/a	10 mL

BC expansion medium

Reagent	Final concentration	Amount
Basic BC medium (100%)	98% (v/v)	490 mL
DAPT (NOTChi) (20 mM)	5 μ g/mL	125 μ L
Recombinant human Pro-epidermal growth factor (EGF) (50 μ g/mL)	5 ng/mL	50 μ L
Recombinant human Fibroblast growth factor 7 (FGF-7) (100 μ g/mL)	25 ng/mL	125 μ L
Recombinant human Fibroblast growth factor 10 (FGF-10) (1 mg/mL)	100 ng/mL	50 μ L
Recombinant human Hepatocyte growth factor (HGF) (250 μ g/mL)	25 ng/mL	50 μ L
RSPO3-Fc Fusion Protein conditioned medium (100%)	2% (v/v)	10 mL
Total	n/a	500 mL

Preparation of ALI-differentiation medium

ALI differentiation (ALI-diff) medium is used for the differentiation of basal progenitor cells and can be stored at 4 °C for 2 weeks.

ALI-diff medium

Reagent	Final concentration	Amount
Advanced DMEM/F-12 (Ad-DF)	98.4% (v/v)	492 mL
3,3',5-Triiodo-L-thyronine sodium salt (1.5 mM)	100 nM	34 μ L
Hydrocortisone (100 μ g/mL)	0.5 μ g/mL	2.5 mL
(\pm)-Epinephrine hydrochloride (5 mg/mL)	0.5 μ g/mL	50 μ L
A83-01 (TGF- β i) (5 mM)	50 nM	5 μ L
TTNPB (Retinoic acid agonist) (1 mM)	100 nM	50 μ L
Recombinant human EGF (50 μ g/mL)	0.5 ng/mL	5 μ L
Penicillin-Streptomycin (100x)	1% (v/v)	5 mL
Total	n/a	500 mL

The following variations of ALI-diff medium are used for different stages of differentiation:

ALI-diff phase 1 medium:

- Add 4 μ L A83-01 (final concentration 500 nM) to 40 mL basic ALI-diff medium.

ALI-diff phase 2 medium:

- Add 4 μ L A83-01 (final concentration 500 nM) and 2 μ L Neuregulin-1 β (final concentration 0.5 nM) to 40 mL basic ALI-diff medium.

ALI-diff phase 3 medium:

- Add 2 μ L Neuregulin-1 β (final concentration 0.5 nM) to 40 mL basic ALI-diff medium.

Preparation of airway organoid medium

Airway organoid (AO) medium is the basic medium for airway organoids. It can be stored at -20 °C for 6 months or at 4 °C for 2 weeks.

AO medium

Reagent	Final concentration	Amount
Advanced DMEM/F-12 (Ad-DF)	94.8% (v/v)	474 mL
B-27 Supplement, serum free (100%)	2% (v/v)	10 mL
GlutaMAX Supplement (100x)	1% (v/v)	5 mL
HEPES (1 M)	10 mM	5 mL
N-Acetyl-L-cysteine (500 mM)	1.25 mM	1.25 mL
Nicotinamide (1 M)	5 mM	2.5 mL
A83-01 (TGF- β i) (5 mM)	500 nM	50 μ L
Penicillin-Streptomycin (100x)	0.5% (v/v)	2.5 mL
Total	n/a	500 mL

The following variations of AO medium are used:

AO culture medium:

- Add 10 μL DAPT (final concentration 5 μM), 2 μL FGF-7 (final concentration 5 ng/mL) and 0.4 μL FGF-10 (final concentration 10 ng/mL) to 40 mL AO medium.

AO FIS assay medium:

- Add 2 μL Neuregulin-1 β (final concentration 0.5 nM) and 40 μL Interleukin-1 β (stock 10 ng/mL) to 40 mL AO medium.

STEP-BY-STEP METHOD DETAILS

Workflow to culture nasal brushing-derived basal progenitor cells

Timing: 1 - 2 months

This part describes the workflow to culture nasal epithelial basal progenitor cells and includes the isolation, expansion and cryostorage of nasal brushing-derived basal progenitor cells (Figure 1).

1. Obtain nasal cells by nasal brushing, according to the section “Obtaining nasal cells by nasal brushing”.
2. Expand human nasal epithelial cells (HNEC) passage 0 (p0) in one well of a 12-well plate until a 90% confluent cell layer exists.
3. Passage HNEC p0 cells to 2 wells of a 6-well plate according to the section “Passaging and expansion of nasal epithelial basal progenitor cells” for further expansion as HNEC p1 cells.
4. When confluent, freeze HNEC p1 cells as a master cell bank (MCB) according to the section “Freezing nasal epithelial basal progenitor cells”.

Note: All cells can be frozen as a MCB, or 0.5×10^6 cells can be passaged to another collagen-coated well on a 6-well plate for further expansion.

5. Expand HNEC p2 cells.

Note: Use cells from the previous step or thaw a MCB vial according to the section “Thawing and further expansion of cryostored nasal epithelial basal progenitor cells”.

6. Once confluent, freeze as a p2 working cell bank (WCB).

Note: All cells can be frozen as a WCB, or 0.5×10^6 cells can be passaged to another collagen-coated well on a 6-well plate for further expansion.

7. Expand HNEC p3 cells.

Note: Use cells from the previous step or thaw a WCB vial according to the section “Thawing and further expansion of cryostored nasal epithelial basal progenitor cells”.

8. Once confluent, these cells are ready for differentiation as ALI-cultures.

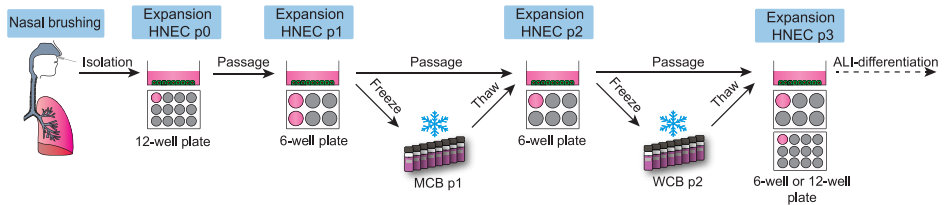


Figure 1: Workflow to culture nasal brushing-derived basal progenitor cells.

Obtaining nasal cells by nasal brushing

Timing: 15 minutes

This section describes the collection of nasal cells through brushing of the inferior nasal turbinates.

Preparations

9. Prepare a 15 mL tube with 7 mL collection medium.
10. Prepare a 15 mL tube with 5 mL PBS0.

Note: Smaller nasal brushes may be needed for younger children. These can be created by connecting a p200 non-filter tip to an interdental brush with parafilm (Figure 2).

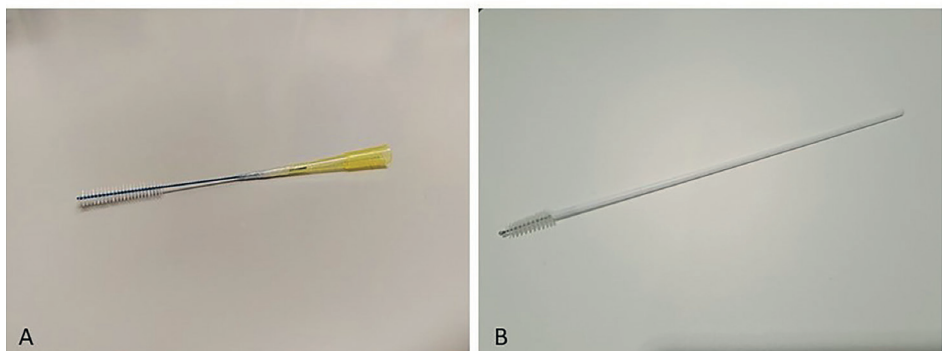


Figure 2: Nasal brushes.

- (A) Nasal brush for younger children, created from an interdental brush connected to a p200 non-filter tip.
- (B) Cytological brush used for adults.

Nasal brushing

11. Inform the nasal cell donor about the procedure and intended use of the cells. Explain that the lacrimal gland will be stimulated by the brushing procedure, which might cause tearing eyes. Infrequently, it causes a nosebleed.
12. Make sure informed consent is documented through signing of appropriate informed consent forms.
13. Ask the donor to blow their nose.
14. Ask the donor to sit straight and sideways to the person taking the brush.
15. Wet the nasal brush in the tube with PBS0.
16. Hold one hand at the back of the head to prevent head movements during the procedure.
17. Insert the brush horizontally into the nostril and the inferior turbinate until mild resistance. Turn the brush twice and remove the brush from the nose.
18. Place the brush in the 15 mL tube with collection medium, properly labelled, and keep on ice.
19. Repeat the procedure for the other nostril with a new brush and place in the same 15 mL tube with collection medium.
20. Cut the top of the brushes and close the 15 mL tube.
21. Maintain the collection tube with brushes on ice or in a refrigerator at 4 °C until further processing, which should be performed within 6 hours.

Isolation of nasal epithelial basal progenitor cells from nasal brushes

Timing: 45 - 60 minutes

This part describes the isolation of nasal epithelial basal progenitor cells from nasal brushes. Half of the cells will be plated for expansion and the other half will be cryopreserved.

CRITICAL: All laboratory procedures with nasal cells should be performed in a laminar flow and sterile compounds should be used to prevent contamination.

Preparations

22. Coat a well in 12-well plate according to the section “Preparation: precoating of well plates for basal progenitor cell expansion”.
23. Prepare and pre-warm BC isolation medium in a water bath at 37 °C.
24. Prepare freezing medium, according to the section “Overview of media”.

Isolation of epithelial cells from nasal brushes

25. Cut the tip (approximately 0.5 cm) of a non-filter p1000 pipette tip with scissors to allow the nasal brush to fit through the opening of the tip (Figure 3).

Note: This procedure can be performed in a sterile environment with ethanol-cleaned scissors. Another option is to autoclave tips after cutting.

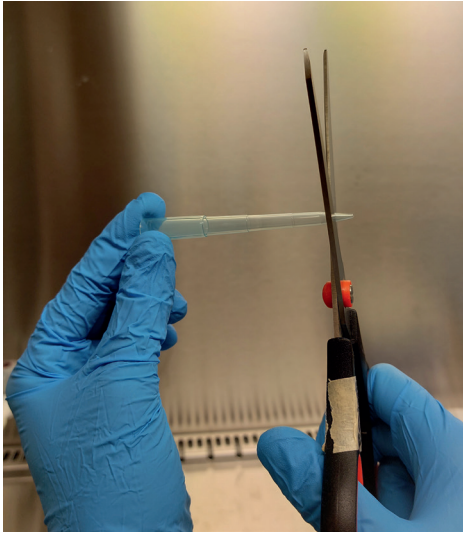


Figure 3: The tip of a non-filter p1000 pipette tip is cut off to make the opening large enough for passing of a nasal brush.

26. Place one of the brushes temporarily in an empty 15 mL tube to provide space for scraping cells from the brush.
27. Dissociate nasal cells in the tube with collection medium by scraping the brush through the opening of the p1000 pipette tip. Move the brush approximately ten times up and down through the p1000 pipette tip (Figure 4). Discard the brush afterwards.
28. Repeat the previous step for the second brush. The cut tip used for the first brush can be re-used.
29. Centrifuge the 15 mL tube with nasal cells at 400 g for 5 min at 4 °C.
30. Aspirate the supernatant and resuspend the pellet in 4 mL TrypLE express enzyme + 20 μ L Sputolysin (0.5% (v/v)).

CRITICAL: Be careful with aspiration when a lot of mucus is present in the pellet to prevent unintended loss of cells.

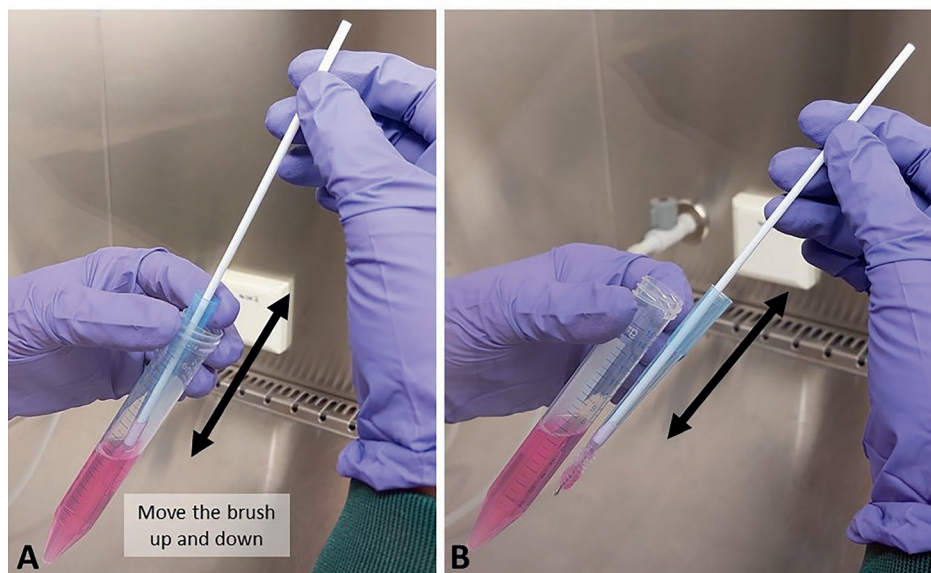


Figure 4: Scraping cells off the brush.

(A) The brush is moved up and down through the pipette tip to scrape cells from the brush and collect them in the tube with collection medium. (B) A close-up of how to move the brush up and down through the pipette tip. The procedure must be carried out in the collection medium inside the 15 mL tube.

31. Incubate the cell suspension for 5 minutes at 37 °C (water bath or incubator).
32. Resuspend the cells by pipetting up and down approximately 5 times with a p1000 pipette to dissolve mucus.
33. Incubate the suspension for an additional 5 minutes at 37 °C (water bath or incubator).
34. Add 8 mL of Ad-DF to inactivate the TrypLE express enzyme by dilution.
35. Strain the cell suspension through a 100 µm cell strainer.
36. Wash the strainer with 2 mL Ad-DF.
37. Transfer half of the cell suspension to a new 15 mL tube.
38. Centrifuge both 15 mL tubes at 400 g for 5 min at 4 °C.
39. Use one 15 mL tube with cells for freezing:
 - b. Aspirate the supernatant and resuspend the cell pellet in 500 µL CryoStor CS10 freezing medium (supplemented with 5 µM Y-27632).
 - c. Transfer the cell suspension to a sterile cryovial, labelled with donor number.
 - d. Gradually freeze the cells by placing the cryovials in a cell freezing container at -80 °C.
 - e. Transfer the vials to a liquid nitrogen freezer after 24 hours.

CRITICAL: Cells are first placed in a -80°C freezer for gradual cooling. For optimal cell viability after thawing, cells should be transferred to the liquid nitrogen freezer as soon as possible after reaching a temperature of -80°C .

40. Use the other 15 mL tube with cells for the expansion of nasal epithelial basal progenitor cells:
 - a. Aspirate the supernatant and resuspend the cell pellet in 1 mL BC isolation medium.
 - b. Remove the collagen coating solution or PBS0 from the precoated well in a 12-well plate.
 - c. Transfer the cell suspension to the precoated well.
 - d. Label the plate, indicating passage number (p0) and donor number.
 - e. Refresh the medium three times a week, with a maximum of 2 consecutive non-refreshing days, with 1 mL BC isolation medium.
 - f. After 7 days, change BC isolation medium for BC expansion medium.
 - g. Culture the cells until ~90% confluence (Figure 5). This will usually take 7 - 14 days.

CRITICAL: It is recommended to culture only one donor per plate because of the risk for infections in HNEC p0 cells.

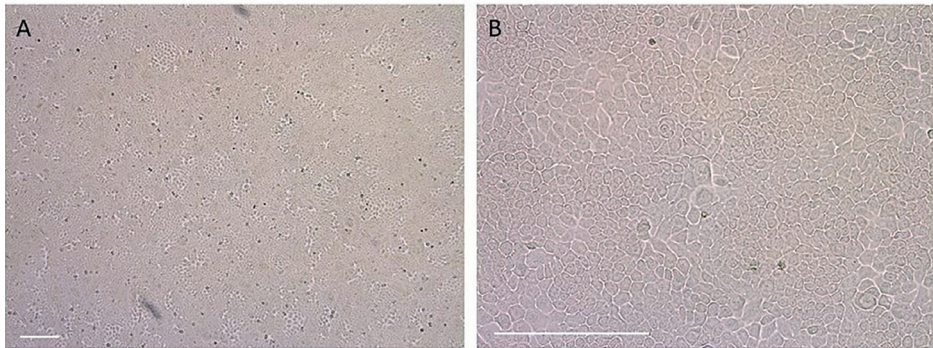


Figure 5: 90% confluent nasal epithelial basal progenitor cell culture, ready for passaging. The cell layer is shown in a low (A) and high (B) magnification. Scale bar equals 200 μm .

Passaging and expansion of nasal epithelial basal progenitor cells

Timing: 45 - 60 minutes

This part describes the procedure of passaging and further expansion of basal progenitor cells in 12- or 6-well plates. This step is applied as indicated in the section “Workflow to culture nasal brushing-derived basal progenitor cells”.

Preparations

41. Coat wells in 12- or 6-well plates according to the section “Preparation: precoating of well plates for basal progenitor cell expansion”.
42. Prepare and pre-warm BC expansion medium in a water bath at 37 °C.

Passaging procedure

43. Proceed with passaging when the cell culture is approximately 90% confluent (Figure 5).
44. Remove medium and wash the cells with PBS0.
 - a. For one well in a 12-well plate: add 500 μ L PBS0.
 - b. For one well in a 6-well plate: add 1000 μ L PBS0.
45. After removal of PBS0, add TrypLE express enzyme to the cells.
 - a. For one well in a 12-well plate: add 500 μ L TrypLE express enzyme.
 - b. For one well in a 6-well plate: add 1000 μ L TrypLE express enzyme.
46. Incubate the cells with TrypLE at 37 °C until the cells detach. This takes approximately 10-15 minutes. Check the detachment of the cells under a light microscope (Figure 6). If not detached, incubate for an additional 5 minutes.



Figure 6: Detached cells after incubation with TrypLE express enzyme. Scale bar equals 200 μ m.

47. Pipette the TrypLE a few times up and down to detach all cells from the well and transfer the cell suspension to a 15 mL tube.

48. Wash the well with Ad-DF to remove all remaining cells and transfer to the 15 mL tube to inactivate the TrypLE.
 - a. For one well in a 12-well plate: 1000 μ L Ad-DF.
 - b. For one well in a 6-well plate: 2000 μ L Ad-DF.
49. Determine cell numbers with a cell counter (e.g. with a BioRad Automated Cell Counter).

Note: The average yield for a confluent well is $1\text{-}3 \times 10^6$ cells in a 12-well plate and $4\text{-}7 \times 10^6$ cells in a 6-well plate.

50. Centrifuge the cell suspension at 400 g for 5 min at 4 °C.
51. Remove the collagen solution or PBS0 from the precoated wells and transfer the cells dissolved in BC expansion medium to these wells:
 - a. For one well in a 12-well plate: add 0.2×10^6 cells to 1 mL BC expansion medium.
 - b. For one well in a 6-well plate: add 0.5×10^6 cells to 2 mL BC expansion medium.
52. Refresh the medium three times a week with BC expansion medium, until approximately 90% confluence (Figure 5).
 - a. For one well in a 12-well plate: refresh with 1 mL BC expansion medium
 - b. For one well in a 6-well plate: refresh with 2 mL BC expansion medium

Freezing nasal epithelial basal progenitor cells

Timing: 45 - 60 minutes

This part describes the general procedure of freezing nasal brushing-derived basal progenitor cells after expansion.

Preparations

53. Prepare freezing medium, according to the section “Overview of media”.

Freezing procedure

54. After expansion, detach basal progenitor cells from the well plate according to step 41-46 from the section “Passaging and expansion of nasal epithelial basal progenitor cells”.
55. Determine cell concentration with a cell counter (e.g. BioRad Automated Cell Counter).
56. Centrifugate the cell suspension at 400 g for 5 min at 4 °C.
57. After centrifugation, aspirate the supernatant and resuspend the cells in CryoStor CS10 freezing medium (containing Y-27632) to obtain a cell suspension with a final concentration of $1\text{-}2 \times 10^6$ cells per mL.

58. Divide 0.5 mL of the cell suspension over sterile cryovials. Depending on the dilution at step 55, each cryovial should contain $0.5 \cdot 10^6$ cells. Label the cryovials, indicating passage number and donor number.
59. Gradually freeze the cells by placing the cryovials in a cell freezing container at -80°C and subsequently transfer them to a liquid nitrogen freezer.

CRITICAL: Cells are first placed in a -80°C freezer for gradual cooling. For optimal cell viability after thawing, cells should be transferred to the liquid nitrogen freezer as soon as possible after reaching a temperature of -80°C .

Thawing and further expansion of cryostored nasal epithelial basal progenitor cells

Timing: 15 - 30 minutes

This part describes the general procedure of thawing and further expansion of cryostored nasal brushing-derived basal progenitor cells.

Preparation

60. Coat wells in 12- or 6-well plates according to the section “Preparation: precoating of well plates for basal progenitor cell expansion”.
61. Prepare and pre-warm BC expansion medium.
62. Prepare a 15 mL tube containing 5 mL Ad-DF.

Thawing procedure

63. Take a cryovial with cells from the liquid nitrogen freezer and store on dry ice. If not processed immediately, store in the -80°C freezer for a maximum of 14 days.
64. Place the cryovial with cells in a 37°C water bath until the cell suspension is almost thawed and rapidly transfer the cell suspension to the 15 mL tube.
65. Wash the cryovial with 1 mL of Ad-DF and add to the 15 mL tube.
66. Centrifuge at 400 g for 5 min at 4°C .
67. Remove the collagen solution or PBS0 from the precoated wells and transfer the cells dissolved in BC expansion medium to these wells:
 - a. For one well in a 12-well plate: add 1 mL BC expansion medium.
 - b. For one well in a 6-well plate: add 2 mL BC expansion medium.
68. Refresh cell cultures three times a week with BC expansion medium.
 - a. For one well in a 12-well plate: refresh with 1 mL BC expansion medium.
 - b. For one well in a 6-well plate: refresh with 2 mL BC expansion medium.

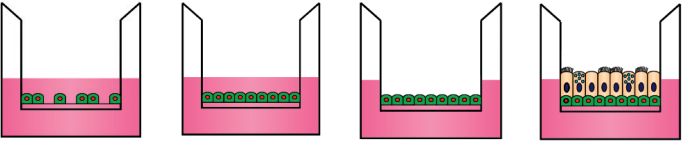
2D ALI differentiation of nasal epithelial cells

Timing: 3 – 6 weeks

This section describes the 2D ALI differentiation of HNEC. Basal progenitor cells are transferred to Transwell inserts and cultured in submerged conditions with BC expansion medium to obtain a confluent cell layer. Medium is then changed to ALI-diff medium supplemented with the TGF- β inhibitor A83-01 for habituation to a new medium but without directly starting differentiation. In the next step, the apical medium is removed to culture the cells air-exposed to stimulate differentiation towards a pseudostratified airway epithelium, including secretory and ciliated cells. The day of air-exposure is called $t=0$. Neuregulin-1 β is added to the medium to boost CFTR expression (Table 1).

Table 1. Different stages of ALI differentiation.

Step	1	2	3	4
Number of days	\pm 4-7 days	\pm 4-10 days	3-5 days	13-15 days
Goal	Confluent cell layer	Adaptation to differentiation medium	Start differentiation at air-exposed conditions	Mucociliary differentiation
Medium	BC expansion	ALI-diff phase 1	ALI-diff phase 2	ALI-diff phase 3



	Apical compartment		Air-exposed		Air-exposed	
6.5 mm 24-well insert	200 μ L	200 μ L	0 μ L	0 μ L	0 μ L	0 μ L
12 mm 12-well insert	200 μ L	200 μ L	0 μ L	0 μ L	0 μ L	0 μ L
Basal compartment						
6.5 mm 24-well insert	800 μ L	800 μ L	600 μ L	600 μ L	600 μ L	600 μ L
12 mm 12-well insert	1000 μ L	1000 μ L	1000 μ L	1000 μ L	1000 μ L	1000 μ L

ALI = air-liquid interface, A = A83-01, NR = Neuregulin-1 β .

Preparations

69. Coat Transwell inserts according to the section “Preparation: precoating of Transwell inserts for ALI-differentiation”.
70. Prepare and pre-warm ALI-diff medium.

Transfer basal progenitor cells to Transwell inserts

71. Dissociate basal progenitor cells from a well plate according to step 41-46 from “Passaging and expansion of nasal epithelial basal progenitor cells”.
72. Centrifuge the cell suspension at 400 g for 5 min at 4 °C.
73. Remove the coating solution from the Transwell inserts.
74. Seed basal progenitor cells on the apical side of the Transwell inserts:
 - a. For 6.5 mm inserts (24-well plate): 0.2×10^6 cells in 200 μ L BC expansion medium.
 - b. For 12 mm inserts (12-well plate): 0.5×10^6 cells in 200 μ L BC expansion medium.
75. Add BC expansion medium to the basolateral side:
 - a. For 6.5 mm inserts (24-well plate): 800 μ L BC expansion medium.
 - b. For 12 mm inserts (12-well plate): 1 mL BC expansion medium.
76. Refresh the medium three times a week and culture the cells under submerged conditions until full confluence is reached. This takes approximately 4-7 days.
77. When confluent, change apical and basolateral medium for ALI-diff phase 1 medium (ALI-diff medium supplemented with A83-01 (500 nM)).
78. Refresh the medium three times a week until a homogeneous monolayer exists with all cells having a similar size and morphology (Figure 7). This takes approximately 4-10 days.

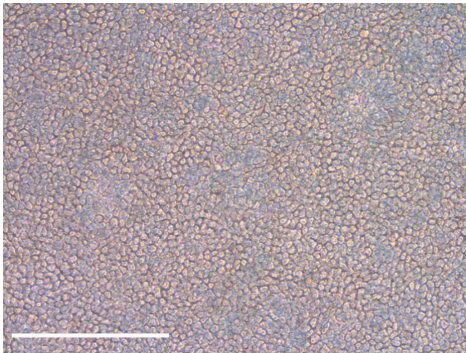


Figure 7: Transwell insert with a 100% confluent cell layer with homogeneous morphology, ready for the switch to air-exposed conditions. Scale bar equals 200 μ m.

79. Remove medium from the apical side and culture the cells under air-exposed conditions. Change medium at the basolateral side for ALI-diff phase 2 medium (ALI-diff medium supplemented with A83-01 (500 nM) and neuregulin-1 β (0.5 nM)).
 - a. For 6.5 mm inserts (24-well plate): add 600 μ L ALI-diff phase 2 medium.
 - b. For 12 mm inserts (12-well plate): add 1 mL ALI-diff phase 2 medium.

Note: The moment of air-exposure is called t=0 of differentiation.

80. After 3-5 days, replace ALI-diff phase 2 medium for ALI-diff phase 3 medium (ALI-diff medium supplemented with neuregulin-1 β (0.5 nM)). Refresh the basolateral medium twice a week.
81. Wash the cells once a week at the apical surface, by incubation with PBS0 in a tissue incubator at 37 °C for 5-10 minutes.
 - a. For 6.5 mm inserts (24-well plate): wash with 125 μ L PBS0.
 - b. For 12 mm inserts (12-well plate): wash with 200 μ L PBS0.
82. Differentiation starts from the moment of air-exposure (t=0) and can be observed by the observation of beating cilia under a light microscope. Cells are ready for the next step when beating cilia are observed, or after 18 days of differentiation.

Note: A high abundance of ciliated cells might cause the unwanted formation of inside-out oriented organoids during the conversion of ALI-differentiated nasal epithelial cells into airway organoids. It is therefore recommended to proceed to the next step as soon as beating cilia are visible and not wait too long before proceeding.

Conversion of ALI-differentiated nasal epithelial cells into airway organoids

Timing: 2 - 3 hours

This section describes the conversion of ALI-differentiated nasal epithelial cells into airway organoids. The ALI-differentiated epithelial cell layer is detached from the Transwell insert with collagenase. Epithelial sheets are then manually disrupted and strained to generate 30-100 μ m fragments to be plated in Matrigel droplets. The complete workflow from ALI-differentiated cell cultures towards airway organoids is shown in figure 8.

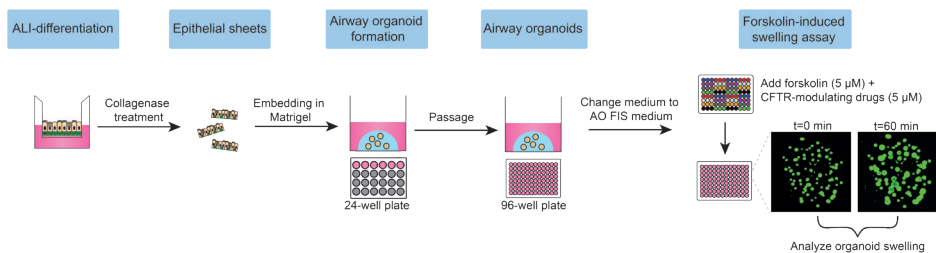


Figure 8: Workflow from ALI-differentiated cells towards airway organoids.

Preparations

83. Pre-warm 24-well suspension plates in a tissue incubator for at least 24 hours.
84. Thaw Matrigel on ice or at 4 °C.
85. Prepare and pre-warm AO culture medium.

Alternative: BME (100%) can be used as an alternative to Matrigel (100%).

Conversion of ALI-differentiated nasal epithelial cells into airway organoids

86. Wash the differentiated ALI-cultures at the apical surface with PBS0. Incubate for 5 minutes in a tissue incubator.
 - a. For 6.5 mm inserts (24-well plate): 125 μ L PBS0.
 - b. For 12 mm inserts (12-well plate): 200 μ L PBS0.
87. Remove the PBS0 or medium at the apical and basolateral side of the ALI-culture. Add collagenase type II solution (1 mg/mL in Ad-DF) to the basolateral side.
 - a. For 6.5 mm inserts (24-well plate): 600 μ L collagenase solution.
 - b. For 12 mm inserts (12-well plate): 1000 μ L collagenase solution.
88. Incubate for 45 - 60 minutes in a tissue incubator.

Note: The epithelial layer will dissociate from the insert during this procedure.

89. Add Ad-DF to the apical surface of the Transwell insert and transfer the dissociated epithelial layer to a 15 mL tube.
 - a. For 6.5 mm inserts (24-well plate): add 100 μ L Ad-DF per Transwell insert.
 - b. For 12 mm inserts (12-well plate): add 200 μ L Ad-DF per Transwell insert.
90. Wash the apical side of the Transwell insert with Ad-DF and transfer remaining epithelial fragments to the 15 mL tube containing the epithelial layer.
 - a. For 6.5 mm inserts (24-well plate): 100 μ L Ad-DF per Transwell insert.
 - b. For 12 mm inserts (12-well plate): 200 μ L Ad-DF per Transwell insert.

Note: Epithelial fragments might stick to the edge of the Transwell membrane, which can be checked with a light microscope. In this case, a P200 pipet can be used to scrape the epithelial layer off the membrane.

91. Disrupt the epithelial layer into smaller fragments with a P1000 pipet tip. Evaluate the size of the fragments by eye or a light microscope. The majority of the epithelial fragments should have a diameter of approximately 30-100 μ m (Figure 9).

Optional: When having difficulties to obtain small fragments, an additional P200 non-filter tip can be placed on top of the P1000 pipet tip.

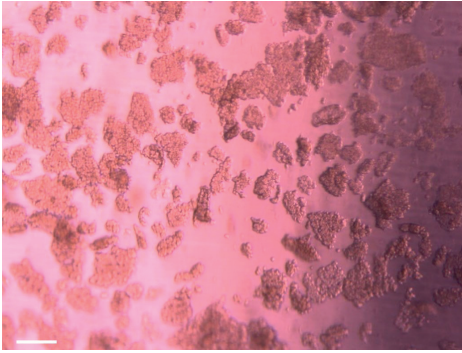


Figure 9: Correct size of epithelial fragments in a 15 mL tube after disruption. Scale bare equals 200 μm .

92. Strain the epithelial fragments with a combination of a 100 μm pluriStrainer[®] placed on top of a 30 μm pluriStrainer[®].
 - a. Add an additional 4 mL Ad-DF to the 15 mL tube with epithelial fragments, and transfer the fragments through the strainers (Figure 10A).
 - b. Discard the 100 μm strainer (Figure 10B).
 - c. Flip the 30 μm strainer upside down on top of a new 50 mL tube (Figure 10C-D).
 - d. Add 5 mL Ad-DF to the reversed 30 μm pluriStrainer[®] to collect the epithelial fragments (size between 30-100 μm) in the 50 mL tube (Figure 10E).

Note: Wash both sides of the 100 μm and 30 μm pluriStrainers[®] before use with 1 mL Ad-DF to enable efficient flow-through.

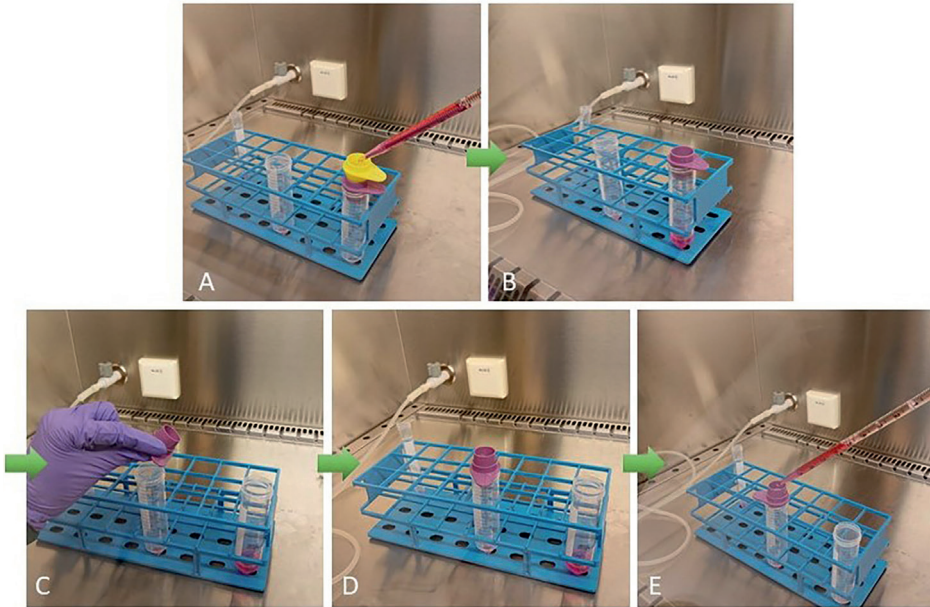


Figure 10: The steps (A-E) of the straining procedure to obtain epithelial fragments with a size between 30-100 µm.

A 100 µm (yellow) and 30 µm pluriStrainer® (purple) are used.

93. Transfer the epithelial fragments to a 15 mL tube and centrifuge at 400 g at 4°C for 5 min.
94. Remove the supernatant and add 100% Matrigel to the pellet and mix well.
 - a. For epithelial fragments from a 6.5 mm 24-well insert: add 60 µL Matrigel, to plate 2 x 30 µL droplets.
 - b. For epithelial fragments from a 12 mm 12-well insert: add 180 µL Matrigel, to plate 6 x 30 µL droplets.

CRITICAL: This step should be performed on ice to prevent solidification of Matrigel.

CRITICAL: Avoid formation of bubbles during resuspension of the epithelial fragments in Matrigel.

95. Place a pre-warmed 24-well suspension plate on top of a T175 flask filled with hand warm tap water (Figure 11). Apply 30 µL droplets per well. After 2 minutes, flip the plate upside down and solidify the droplets in a tissue incubator for 15-30 minutes.

Note: The plate is flipped upside down to distribute the epithelial fragments equally through the Matrigel, enabling equal access to nutrients.

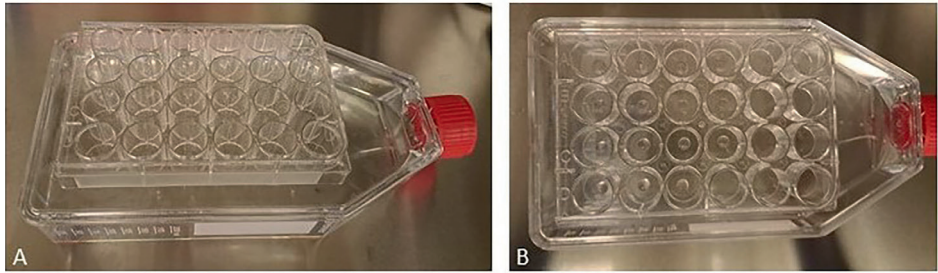


Figure 11: Epithelial fragments embedded in Matrigel are plated in a 24-well plate placed on top of a T175 flask filled with warm water.

(A) Side view. (B) Top view.

96. Add 500 μ L pre-warmed AO culture medium to the epithelial fragments embedded in Matrigel (Figure 12A).

97. Refresh the medium twice a week.

Note: Gently add the medium to avoid disruption of the Matrigel droplets.

Epithelial fragments self-organize into organoids and develop lumen in 3-5 days (Figure 12B). Organoids can be passaged to a 96-well plate after lumen formation.

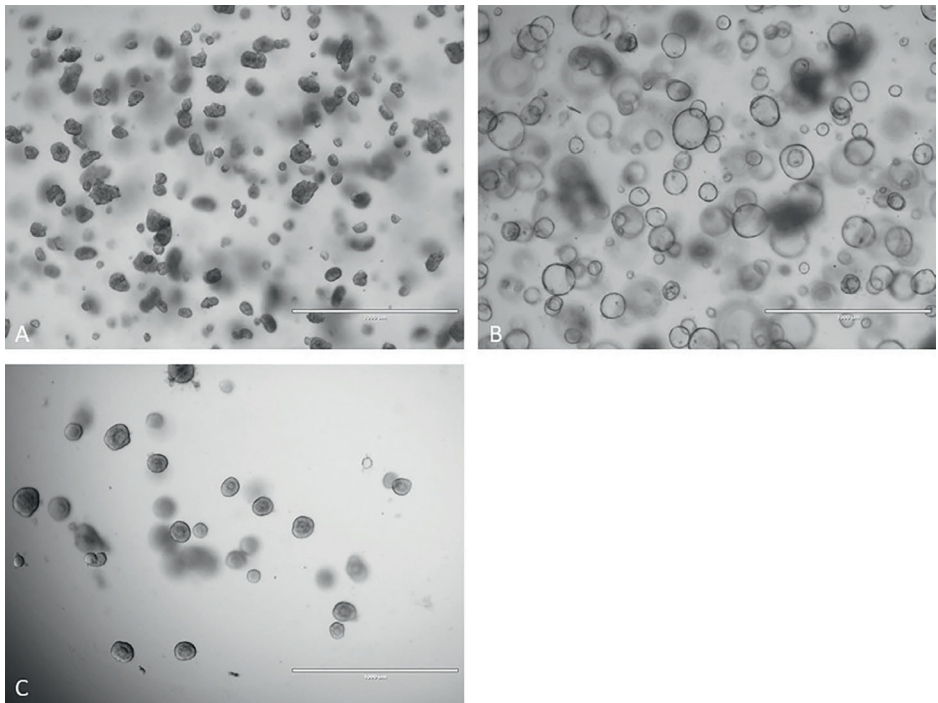


Figure 12: Formation of airway organoids.

Figure 12: *(continued)*

(A) Epithelial fragments embedded in Matrigel, 30 minutes after plating and solidification of the Matrigel in the 24-well plate. (B) Airway organoids acquired intrinsic lumen, 3 days after plating. (C) Airway organoids lose their intrinsic lumen by changing medium to AO FIS medium, 5 days after medium change and after passaging to a 96-well plate. Scalebar equals 1000 μm .

Passaging of nasal organoids to a 96-well plate

Timing: 1 - 2 hours

This section describes the passaging of nasal organoids to 96-well plates, which can be used for FIS assays.

Preparations

99. Pre-warm black flat-bottom tissue culture-treated 96-well plates in a tissue incubator for at least 24 hours.
100. Thaw Matrigel on ice or at 4 °C.
101. Prepare and pre-warm AO culture medium.

Passaging of nasal organoids to 96-well plates

102. Remove culture medium and add 400 μL cell recovery solution per well.
103. Resuspend the Matrigel droplet once in cell recovery solution.
104. Incubate the well plate at 4 °C in the fridge for 5-10 min until the Matrigel is dissolved.

Alternative: Cell recovery solution is recommended to dissolve the Matrigel efficiently. As an alternative, ice cold Ad-DF can be used, in which case the 4 °C incubation step can be skipped.

105. Transfer the organoids to a 15 mL tube with 7 mL ice cold Ad-DF to inactivate the cell recovery solution. Keep the tube on ice.
106. Centrifuge the organoids at 400 g and 4 °C for 5 min.
107. Remove supernatant and resuspend the organoid pellet in 100% Matrigel. Keep the tube on ice. The plating volume is $4 \mu\text{L} \times \text{number of wells in 96-well plate} + 10\%$ extra medium.
 - a. With good quality organoid cultures, one 30 μL Matrigel droplet from a 24-well plate can be seeded into 16 wells of a 96-well plate.
 - b. To avoid too sparsely seeded wells, it is recommended to first resuspend the organoids in a Matrigel volume sufficient to seed half of the wells. Plate a 4 μL test droplet and check density under a light microscope. In case the organoid density is too high, organoids can be diluted by adding more Matrigel (Figure 13).

Note: The Matrigel-embedded organoids can be transferred to an Eppendorf tube for easier handling.

108. Take a pre-warmed 96-well plate and add 4 μL Matrigel droplets with organoids in each well.

CRITICAL: Regularly resuspend the organoids in the Eppendorf tube to keep a homogeneous suspension.

CRITICAL: Tap the 96-well plate regularly on a flat surface during plating (\pm after every 16-24 wells) to distribute the organoids in the same plane.

109. Solidify the Matrigel droplets by placing the plate in a tissue incubator for 15-25 minutes.

110. Add 100 μL AO culture medium to each well and place the plate in a tissue incubator at 37 $^{\circ}\text{C}$ and 5% CO_2 .

111. Refresh the medium twice a week.

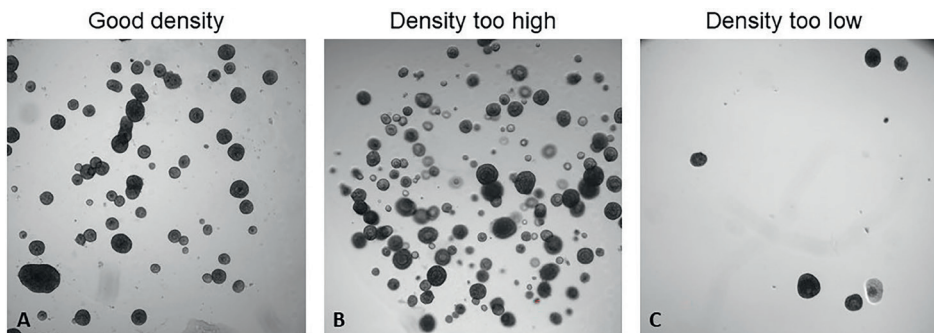


Figure 13: Organoids plated in different densities.

(A) Well containing an appropriate number of organoids. (B) Well with too many organoids and in different Z planes. (C) Well with too few organoids.

FIS assay for nasal organoids

Timing: 2 - 2.5 hours

This section describes the FIS assay which can be used to visualize and quantify the functional rescue of CFTR protein function by CFTR modulator treatment in nasal organoid swelling experiments.

Preparations: 5-10 days prior to the FIS assay

112. Replace organoid medium with 100 μL pre-warmed AO FIS assay medium, 5-10 days prior to the FIS assay.

Note: Organoids display complete loss of lumen formation 2-5 days after the media change to AO FIS assay medium (Figure 12C).

Preparations: 48 hours prior to the FIS assay

113. Refresh the organoid medium with 100 μL AO FIS assay medium supplemented with CFTR correctors (i.e. VX-809, VX-445, VX-661; 5 μM) or vehicle control, 48 hours prior to the FIS assay.

Preparations: similar day as the FIS assay

114. Turn on the environmental control of the confocal microscope at least 1 hour before start of the experiment at 37 $^{\circ}\text{C}$ and 5% CO_2 .

115. Dissolve calcein green (50 μg) in 6 μL DMSO and prepare calcein green solution (1:750 v/v) in Ad-DF (10 $\mu\text{L}/\text{well}$).

116. Prepare 2x concentrated dilutions of compounds to be added acute: i.e. forskolin (10 μM), CFTR potentiators (VX-770; 10 μM) or vehicle in Ad-DF. Dispense 125 μL of the compound solutions per well in a new U-bottom 96-well suspension plate.

Note: The stimuli will be further diluted 1:1 when added to the well plate with organoids, already containing 100 μL medium. So final concentrations of both forskolin and CFTR potentiators are 5 μM .

FIS assay

117. Dispense 10 μL calcein green solution to each well of the 96-well plate with organoids. Mix the calcein green solution through gentle resuspension (2-3 times pipetting) with a multichannel.

Alternative: Instead of adding the calcein green solution with a multichannel, an automatic repetitive pipet (such as the Eppendorf Multipette E3) with a high dispensing speed could be used.

118. Incubate the plate in a tissue incubator for 30 minutes.

119. Position the 96-well plate with organoids in the place holder of a confocal microscope and ensure the plate is fixed in position.

120. Set the live cell imaging settings:

- a. Use the 2.5x objective.
- b. Calcein green staining can be visualized with an emission at 488 nm and excitation at 515 nm.
- c. Set the laser intensity, ensuring that the calcein green signal in the organoid structures is slightly oversaturated.
- d. Set the right position (X, Y) and focus (Z) for each well to obtain a good view of the organoids, or use autofocus when possible.
- e. Set a time lapse for 1 hour measurement:
 - a. Interval = 10 minutes
 - b. Cycles = 7 (cycle 1 is $t = 0$)

Optional: If possible, include brightfield/DIC imaging to obtain a better view of organoid morphology.

121. Add 100 μ L from the 96-well plate with acute stimuli to the well plate with organoids, using a multichannel. Immediately start imaging after addition of the acute stimuli.

CRITICAL: It is important to start imaging quickly after addition of the acute stimuli, as organoids might directly start swelling.

EXPECTED OUTCOMES

The FIS assay with intestinal organoids is already an established and widely used assay to predict CFTR modulator efficacy on individual basis.^{2,3} However, it is proposed that an airway model might be more convenient as people with CF are mostly suffering from respiratory symptoms. Furthermore, a nasal brushing is less invasive compared to an intestinal biopsy. Here we describe a protocol to perform the FIS assay in nasal brushing-derived airway organoids, of which we recently showed their ability to predict CFTR modulator responses.¹ To guarantee evenly differentiated organoids, we differentiated basal progenitor cells as ALI-cultures before their transformation into organoids.¹ This will diminish the variation in organoid morphology and in FIS between individual organoids in a single well.

By use of this protocol, investigators should be able to isolate, expand and differentiate basal progenitor cells from nasal brushes, to generate nasal airway organoids and to conduct the FIS assay to determine CFTR function and CFTR modulator response efficacy.

From nasal brushings of one donor, approximately 5×10^6 cells can be isolated and cryostored as a MCB p1 (10 vials containing 5×10^5 cells). Each MCB vial can be further expanded in the next passage (p2) to a yield of approximately 5×10^6 cells, indicating that in total approximately 5×10^7 basal progenitor cells (p2) can be generated from the MCB and 5×10^8 cells at a higher passage (p3). These basal progenitor cells (p3) are transferred to Transwell filters for ALI-differentiation. 5×10^5 basal progenitor cells are seeded on a 12 mm 12-well insert, which yields approximately 48-96 wells with organoids in a 96-well plate. When smaller Transwell inserts are used, 2×10^5 basal progenitor cells are seeded on a 6.5 mm 24-well insert, which yields approximately 16-32 wells with organoids in a 96-well plate.

Figures 14 and 15 illustrate example results of a FIS assay experiment. In non-CF nasal organoids, forskolin stimulation induces organoid swelling (Figure 14). CF nasal organoids lack swelling in response to forskolin, but the swelling response is restored upon treatment with CFTR modulators (Figure 15).

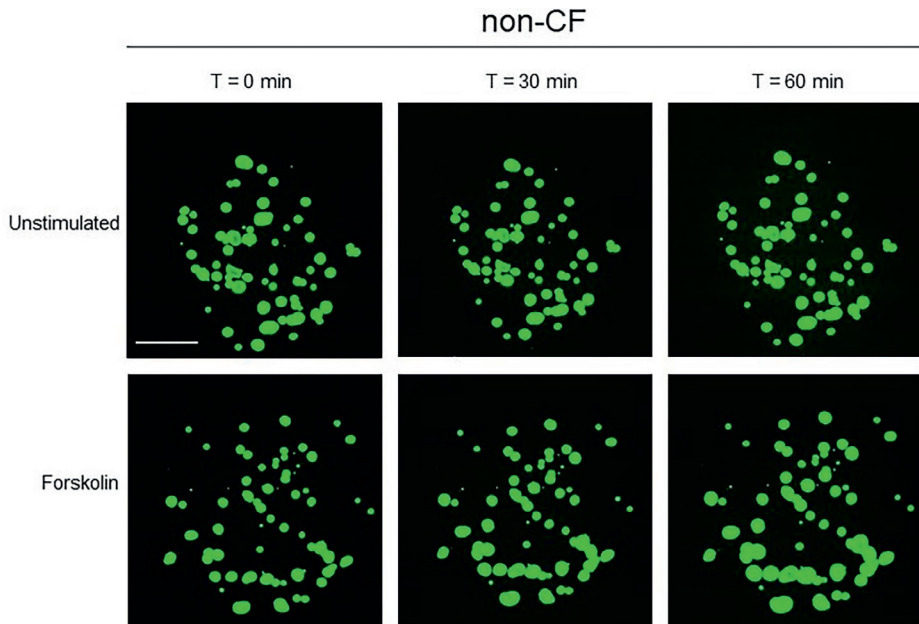


Figure 14: Confocal images of calcein green stained organoids from a non-CF donor, unstimulated or stimulated with forskolin. Scale bar equals 500 μm .

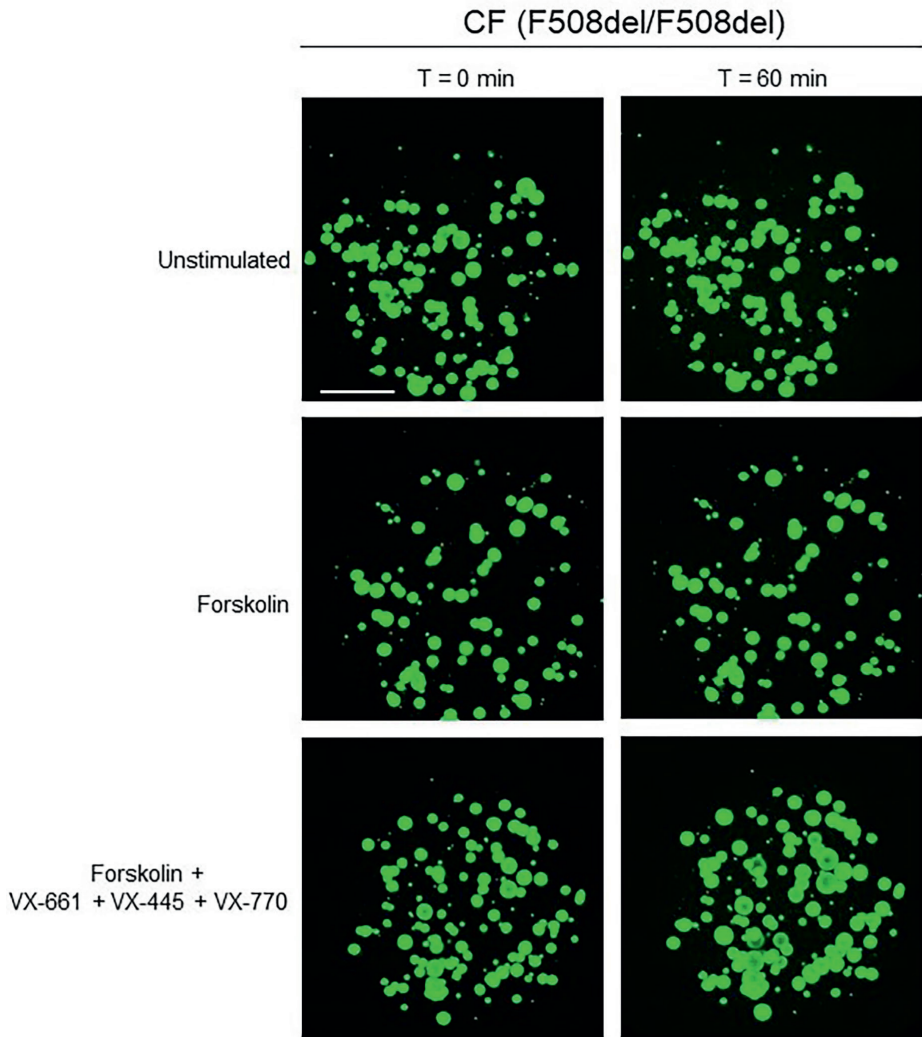


Figure 15: Confocal images of calcein green stained organoids from a CF donor (F508del/F508del) unstimulated or stimulated with either forskolin alone or with forskolin + CFTR modulator treatment (48h pre-incubation with VX-661 and VX-445 and acute stimulation with VX-770). Scale bar equals 500 μ m.

QUANTIFICATION AND STATISTICAL ANALYSIS

The output of the FIS assay is a time series of confocal images containing calcein green stained organoids. For quantification and interpretation of the results, organoid swelling is calculated as the relative increase of total organoid area over time, according to the following steps:

1. Determination of total organoid area in each image (Table 2):
 - a. Total organoid area is determined in each individual image using image analysis software, such as Zen blue (Zeiss), or open-source software, such as ImageJ or CellProfiler.⁴ Further processing can be performed with Excel, GraphPad or R.
 - b. Particles with a size smaller than $6.000 \mu\text{m}^2$ are excluded from analysis.
2. Normalization of total organoid area to baseline (Table 3):
 - a. Organoid swelling is usually expressed as relative increase to baseline ($t=0$), which is set at 100%. The formula to calculate normalized organoid area for individual wells at a specific timepoint x is:

$$\text{Normalized organoid area at } t = x = \frac{\text{Total organoid surface area at } t = x}{\text{Total organoid surface area at } t = 0} \times 100\%$$

- b. The average normalized organoid area (%) of technical replicates within a plate can be plotted against time (minutes) to visualize the kinetics of organoid swelling (Figure 16A).

Note: Individual wells can be excluded from analysis when less than 10 organoids are present in a well, or when out of focus organoids are not recognized in all timepoints of the experiment.

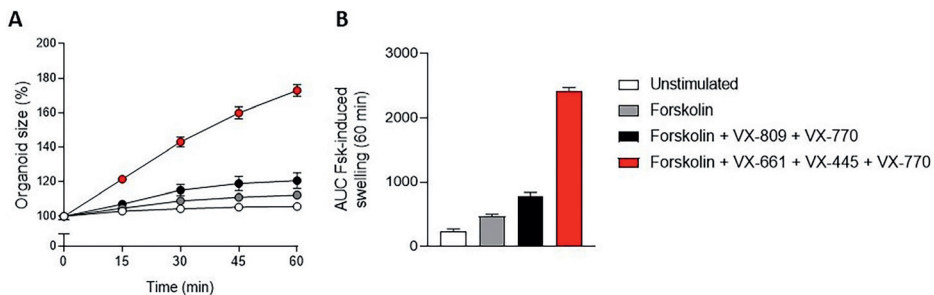


Figure 16: Quantification of a FIS assay with the experimental data from table 2 and table 3.

Panel (A) shows normalized organoid area (%) over time and panel (B) shows the corresponding AUC values. Data is shown as mean \pm SD from 4 technical replicates per condition. Fsk = forskolin.

3. Calculation of area under the curve (AUC) values as a measure for organoid swelling:
 - a. AUC values are calculated as a measure for organoid swelling. This creates a single data point per well which can be used to compare organoid swelling in response to different stimuli.
 - b. Mean AUC values of technical replicates within a plate can be visualized with bar graphs (Figure 16B).
4. Statistical analysis:
 - a. Statistical analysis can be performed to compare different groups with a student t-test or ANOVA, dependent on the number of groups.

Table 2. Example dataset showing total organoid area (mm²) per well and per timepoint for a FIS experiment. Quadruplicates are used as technical replicates within an experimental plate.

Time (min)	Well number + condition															
	1	2	3	4	5	6	7	8	9	10	11	12	13	14	15	16
	Unstimulated				Forskolin				Forskolin + Vx-809 + Vx-770				Forskolin + Vx-661 + Vx-445 + Vx-770			
0	1.63	1.98	1.70	1.86	1.97	2.01	1.95	1.74	2.26	1.91	1.96	1.58	1.81	2.07	1.80	2.11
15	1.69	2.01	1.78	1.91	2.09	2.09	2.04	1.80	2.38	2.04	2.09	1.73	2.22	2.49	2.15	2.61
30	1.71	2.02	1.81	1.94	2.19	2.17	2.13	1.86	2.52	2.18	2.26	1.89	2.64	2.93	2.52	3.06
45	1.73	2.04	1.83	1.95	2.23	2.23	2.17	1.89	2.58	2.25	2.34	1.97	2.96	3.27	2.81	3.42
60	1.74	2.04	1.83	1.97	2.26	2.26	2.19	1.90	2.60	2.28	2.37	2.00	3.19	3.54	3.05	3.69

Table 3. Normalized organoid area (%) of the experimental dataset from table 2. Total organoid area is normalized to baseline (t=0, 100%).

Time (min)	Well number + condition															
	1	2	3	4	5	6	7	8	9	10	11	12	13	14	15	16
	Unstimulated				Forskolin				Forskolin + Vx-809 + Vx-770				Forskolin + Vx-661 + Vx-445 + Vx-770			
0	100	100	100	100	100	100	100	100	100	100	100	100	100	100	100	100
15	103.6	101.4	104.5	102.4	106.1	104.0	105.1	103.6	105.3	107.0	106.9	109.4	123.0	120.4	119.2	123.2
30	105.0	102.3	106.4	104.0	111.4	108.2	109.6	106.8	111.5	114.2	115.7	119.3	146.1	141.6	139.9	144.6
45	106.2	102.9	107.5	104.6	113.5	110.9	111.4	108.4	114.1	118.0	119.5	124.3	163.7	158.0	156.1	161.8
60	106.6	103.2	107.7	105.4	114.9	112.6	112.6	109.3	115.1	119.7	121.3	126.3	176.7	171.3	169.0	174.5

LIMITATIONS

This protocol describes the use of primary nasal cell cultures. It is important to realize that working with primary cell cultures is different compared to cell lines. Primary cell cultures have an increased risk of microbial outgrowth during the first day of cell isolation, especially in cell cultures derived from individuals with CF. Furthermore, donor to donor variation exists, such as differences in the expansion rate of basal progenitor cells, in differentiation time of ALI-cultures and in the organoid yield. This variation might be related to donor characteristics, to the yield of cells from the nasal brushing, to environmental conditions or to the freeze/thawing procedure. It is recommended to prevent changes in medium batches and guarantee correct freeze/thawing procedures. Be aware that changing manufacturer of medium compounds or using alternative culture ware may affect the quality of the cell and organoid cultures.

TROUBLESHOOTING

Problem 1:

Fungal infection of basal cell cultures, related to the section “Isolation of nasal epithelial basal progenitor cells from nasal brushes”.

Potential solution:

Add the antifungal reagent Fungin (50 µg/mL) to the cell culture medium, wrap the plate in foil, keep the cell culture isolated from other cell cultures and check if the infection disappears in the coming 3 days. If not, the cell culture should be thrown away to prevent contamination of other cell cultures.

Problem 2:

Squamous cell differentiation in basal cell cultures or ALI-cultures related to the section “Passaging and expansion of nasal epithelial basal progenitor cells” or “2D ALI differentiation of nasal epithelial cells” (Figure 17).

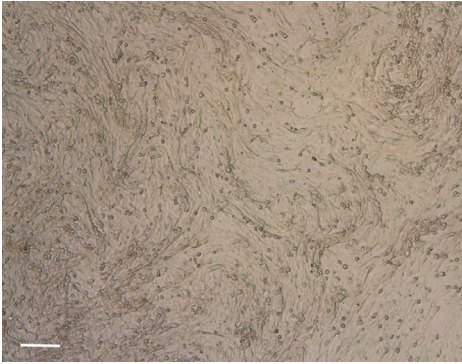


Figure 17: Squamous cell differentiation of basal progenitor cells. Scale bar equals 200 μm .

Potential solution:

In general, basal progenitor cells displaying squamous cell differentiation cannot be used for ALI-differentiation or organoid formation.

When squamous cell differentiation occurs in multiple donors cultured in parallel, it might be caused by incorrect preparation of the culture medium, e.g. the use of compounds past their expiring date, or incorrect storage or preparation of stock compounds or media batches. Renew compounds or medium when needed.

The occurrence of squamous cell differentiation might also relate to a specific donor. Thaw and expand cells of other vials from this donor and determine whether squamous cell differentiation occurs. If this is the case, the cells of this donor cannot be further used. Consider to repeat the isolation of nasal cells from the frozen back up vial or to collect new nasal brushes.

Problem 3:

Cells have difficulty starting up after thawing, related to the section “Thawing and further expansion of cryostored nasal epithelial basal progenitor cells”.

Potential solution:

Thaw cells in a smaller well, or thaw cells from a lower passage number to create a new working cell bank.

Problem 4:

Inside out-oriented organoids, related to the section “Conversion of ALI-differentiated nasal epithelial cells into airway organoids”.

Potential solution:

When differentiated ALI cultures display high numbers of ciliated cells, this may impede formation of organoids with the lumen facing inward. Cilia beating in highly ciliated epithelial fragments prevents solidification of the Matrigel, leading to formation of inside out-oriented organoids. Therefore, cells should not be differentiated too long at the ALI and should be converted into organoids as soon as cilia appear during differentiation.

Problem 5:

Nonoptimal organoid density in 96-well plates for a FIS assay experiment, related to the section “Passaging of nasal organoids to a 96-well plate”.

Potential solution:

For optimal performance of the FIS assay, it is important to seed organoids in the right density in 96-well plates (Figure 13). A high seeding density might cause problems for organoid recognition during image analysis, especially when organoids are in different planes. A low seeding density will provide unreliable results.

Problem 6:

Organoids swell during the experiment without any stimulation, related to the section “FIS assay for nasal organoids”.

Potential solution:

Check temperature and CO₂ settings of the microscope incubator as organoid swelling might be pH dependent.

RESOURCE AVAILABILITY

Lead contact

Further information and requests for resources and reagents should be directed to and will be fulfilled by the lead contact, Jeffrey Beekman, j.beekman@umcutrecht.nl

Materials availability

This study did not generate new unique reagents.

Data and code availability

This study did not generate datasets or code.

ACKNOWLEDGMENTS

This work was supported by grants of the Dutch Cystic Fibrosis Foundation (NCFS, HIT-CF grant), SRC 013 from CF Trust-UK and Health Holland.

AUTHOR CONTRIBUTIONS

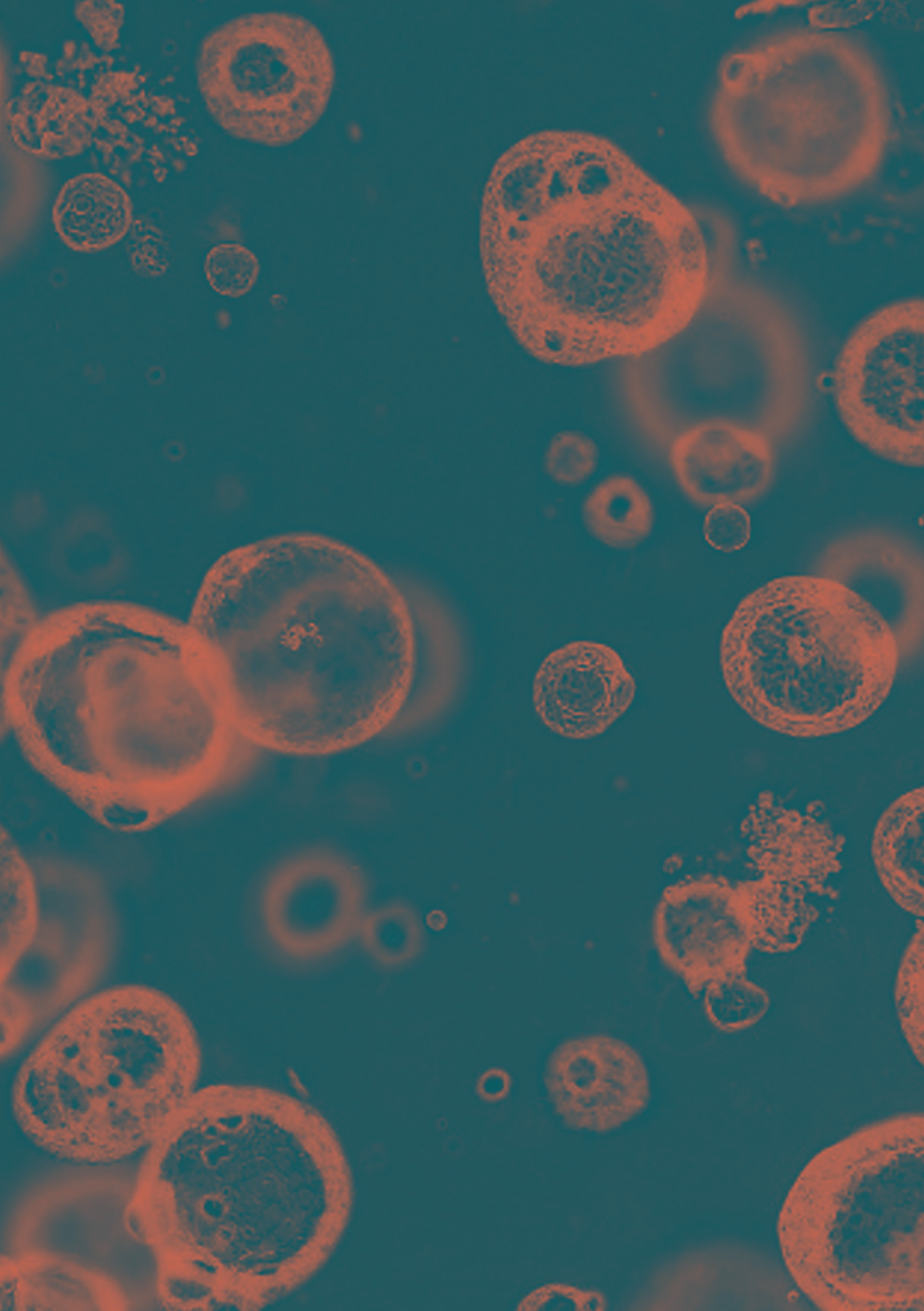
Conceptualization, J.M.B. and G.D.A.; Methodology, G.D.A.; Validation, Formal Analysis, Investigation and Data Curation, L.W.R., I.S.W., H.H.M.D., S.M.A.S., L.A.H.O., E.M.A. and G.D.A.; Resources, J.M.B.; Writing – Original Draft, L.W.R. and I.S.W.; Writing – Review & Editing, H.H.M.D., S.M.A.S., L.A.H.O., E.M.A., J.M.B. and G.D.A.; Visualization, L.W.R. and I.S.W.; Supervision, J.M.B. and G.D.A.; Funding Acquisition, J.M.B. and G.D.A..

DECLARATION OF INTERESTS

J.M.B. has a patent granted (10006904) related to CFTR function measurements in intestinal organoids and received personal fees from HUB/Royal Dutch academy of sciences, during the conduct of the study. He received nonfinancial support from Vertex Pharmaceuticals and personal fees and nonfinancial support from Proteostasis Therapeutics, outside the submitted work.

REFERENCES

1. Amatngalim, G. D. *et al.* Measuring cystic fibrosis drug responses in organoids derived from 2D differentiated nasal epithelia. *Life Sci Alliance* 5, e202101320 (2022).
2. Vonk, A. M. *et al.* Protocol for Application , Standardization and Validation of the Forskolin-Induced Swelling Assay in Cystic Fibrosis Human Colon Organoids Protocol for Application , Standardization and Validation of the Forskolin-Induced Swelling Assay in Cystic Fibrosis. *STAR Protoc* 1, 100019 (2020).
3. Dekkers, J. F. *et al.* Characterizing responses to CFTR-modulating drugs using rectal organoids derived from subjects with cystic fibrosis. *Sci Transl Med* 8, 344ra84 (2016).
4. Hagemeyer, M. C. *et al.* An open-source high-content analysis workflow for CFTR function measurements using the forskolin-induced swelling assay. *Bioinformatics* 36, 5686–5694 (2020).



Chapter 2

Measuring cystic fibrosis drug responses in organoids derived from 2D differentiated nasal epithelia

Gimano D. Amatngalim, Lisa W. Rodenburg, Bente L. Aalbers, Henriette H. M. Raeven, Ellen M. Aarts, Dounia Sarhane, Sacha Spelier, Juliet W. Lefferts, Iris A.L. Silva, Wilco Nijenhuis, Sacha Vrendenburg, Evelien Kruisselbrink, Jesse E. Brunsveld, Cornelis M. van Drunen, Sabine Michel, Karin M. de Winter-de Groot, Harry G. Heijerman, Lukas C. Kapitein, Margarida D. Amaral, Cornelis K. van der Ent and Jeffrey M. Beekman

Life Science Alliance 2022, 5 (12); e202101320

ABSTRACT

Cystic Fibrosis (CF) is caused by genetic defects that impair the cystic fibrosis transmembrane conductance regulator (CFTR) channel in airway epithelial cells. These defects may be overcome by specific CFTR modulating drugs, for which the efficacy can be predicted in a personalized manner using 3D nasal-brushing-derived airway organoids in a forskolin-induced swelling assay. Despite of this, previously described CFTR function assays in 3D airway organoids were not fully optimal, due to inefficient organoid differentiation and limited scalability. In this report we therefore describe an alternative method of culturing nasal brushing-derived airway organoids, which are created from an equally differentiated airway epithelial monolayer of a 2D air-liquid interface culture. In addition, we have defined organoid culture conditions, with the growth factor/cytokine combination neuregulin-1 β and interleukine-1 β , which enabled consistent detection of CFTR modulator responses in nasal airway organoids cultures from subjects with CF.

INTRODUCTION

Cystic fibrosis (CF) is a monogenic epithelial disease caused by mutations in the *cystic fibrosis conductance transmembrane regulator* (*CFTR*) gene¹. This defect impairs CFTR-dependent anion conductance in airway epithelia², which leads to a severe respiratory disease³. CFTR modulators are target-specific drugs that may restore CFTR function in individuals with CF⁴. However, the efficiency of modulators largely depends on the *CFTR* genotype of an individual with CF. More than 2,000 distinct *CFTR* mutations have been reported (<http://www.genet.sickkids.on.ca/>) with variable effects on CFTR expression or function. In addition to common mutations, such as the F508del allele, approximately 1,000 rare mutations have been identified that each affect less than 5 individuals worldwide. This low prevalence makes it unfeasible to determine CFTR modulator drug efficacy in large cohort clinical studies.

As an alternative of determining drug efficacy directly in individuals with CF, the effects of CFTR modulators can be predicted using patient-derived epithelial cultures in functional CFTR assays⁵. This is traditionally done with 2D air-liquid interface (ALI)-differentiated airway epithelia by assessment of CFTR-dependent chloride (Cl) conductance via electrophysiology⁶⁻⁸. However, a major disadvantage of the ALI-culture model system is the limited scalability. In contrast, CFTR-expressing epithelial organoids from various tissues, i.e. airway, intestine, kidney, are emerging as a novel model system in which drug efficacy can be tested more efficiently in a mid-to high-throughput fashion⁹⁻¹¹. Previously, we and others have shown that intestinal organoids from subjects with CF can be used to predict drug responses in a forskolin-induced swelling (FIS) assay, reflecting CFTR-dependent fluid secretion¹²⁻¹⁵. Nevertheless, based on the origin of CF respiratory disease, it remains postulated that airway epithelial models are more predictive for determining CFTR modulator responses.

Indeed, we previously reported CFTR modulator response measurements in long-term expanded distal airway organoids using FIS¹¹. However, we observed large variations in FIS measurements, as swelling was limited to well-differentiated spherical structures. Others have successfully used 3D nasal airway organoids (NAOs) derived from minimal-invasive nasal brushings in functional CFTR assays¹⁶⁻¹⁸, which are a more suitable option for personalized drug testing compared to cultures derived from invasive (tracheo)bronchial and intestinal tissues. However, previously described functional CFTR assays using NAOs were low-in throughput¹⁶⁻¹⁹. Therefore, there is a remaining need for a further optimized and scalable FIS assay using airway organoids, especially derived from nasal brushings, which enables CFTR modulator response measurements in subjects with CF. In this report, we describe an alternative organoid culture method,

in which NAOs are derived from 2D differentiated human nasal epithelial cell (HNEC) monolayers. We furthermore describe optimized airway organoid culture condition to improve CFTR modulator response measurements, by including the growth factor/cytokine combination neuregulin-1 β and IL-1 β . Validation studies using this culture condition showed consistent detection of genotype-specific responses to CFTR modulators in FIS assays, including repairing effects of the FDA-approved CFTR triple modulator therapy VX-661/VX-445/VX-770²⁰.

RESULTS AND DISCUSSION

We previously reported CFTR function measurements in distal airway organoids in FIS assays¹¹. Upon passaging of mechanically disrupted organoids, we observed however large variation in organoid morphology, corresponding with differences in differentiation of individual organoid structures within the same culture (Fig S1A and B). CFTR function is mediated by differentiated cells. Therefore, this unsynchronized organoid differentiation reduces the accuracy of quantifying FIS, which is based on measuring the total surface area increase of all organoids within a single culture well (Fig S1C and Video 1). To generate evenly differentiated airway organoids that display FIS (Fig S1D and Video 2), we set up a method in which organoids are established from a 2D differentiated human nasal epithelial cells (HNEC) monolayer (Fig 1A). In the culture procedure, HNEC derived from nasal brushings were first isolated and expanded in regular 2D cell cultures (Fig 1B). HNEC stained positive for p63 and cytokeratin 5 (KRT5), confirming a basal stem cell phenotype (Fig 1C). After expansion, HNEC were cryo-preserved as a master (passage 2) and working (passage 3) cell bank to enable repeated usage of donor materials (detailed description in the methods section). HNEC expanded from a working cell bank were subsequently differentiated in conventional 2D air-liquid interface (ALI) Transwell-cultures, to recapitulate the mucociliary airway epithelium. Similar to the native nasal epithelial tissue (Fig 1D), ALI-HNEC cultures displayed a pseudostratified morphology and consisted of all major airway epithelial subsets, i.e. MUC5AC/CC10⁺ secretory cell, β -tubulin IV⁺ ciliated cells, and p63/KRT5⁺ basal cells (Fig 1D and Fig S2A). Further studies are required to determine the presence of rare cell types, such as ionocytes^{21,22}. CFTR function and effects of modulators were confirmed in ALI-HNEC from a healthy control (HC) and individual with CF and a F508del/F508del genotype (Fig S2B and C). During isolation of airway organoids from resected airway tissues, based on the method described by Sachs et al.¹¹, we observed that large epithelial fragments, obtained after collagenase treatment, self-organized into differentiated organoids within a few days after gel embedding. Based on this observation we proposed that epithelial fragments from 2D- differentiated ALI cultures

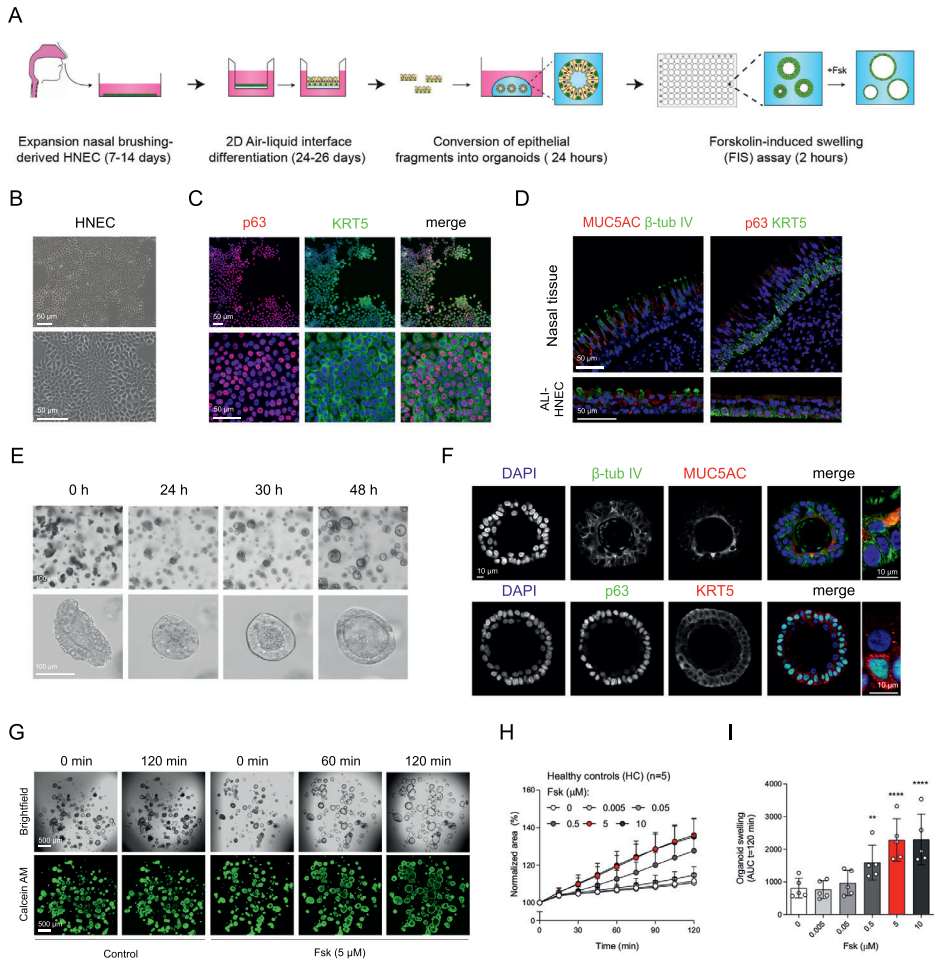


Figure 1: Conversion of differentiated ALI-HNEC cultures into nasal airway organoids and use in FIS assays.

(A) Graphic illustration showing workflow of culturing nasal airway organoids (NAOs) from 2D differentiated human nasal epithelial cells (HNEC) and use in FIS assays. (B) Brightfield images of HNEC. (C) IF staining of HNEC with basal cell markers p63 (red) and cytokeratin 5 (KRT5, green). (D) Sections of nasal tissue (top) and 18 days differentiated air-liquid interface (ALI-) cultured HNEC (bottom), demonstrating IF staining of MUC5AC (goblet cells, red), β -tubulin IV (ciliated cells, green), p63 and KRT5 (basal cell markers, green and red respectively). (E) Time course showing self-organization of differentiated ALI-HNEC-derived epithelial fragments into organoids. (F) Confocal images showing in the top panels staining with DAPI (blue), β -tubulin IV (green), and MUC5AC (red). The bottom panels show staining with DAPI (blue), p63 (green), and KRT5 (red). (G) Representative brightfield images (top) and images of calcein green AM esters-stained (bottom) organoids from a HC subject, which were unstimulated (Control) or treated with forskolin (Fsk, 5 μ M). Images were taken at t=0, 60, and 120 min after stimulation. (H and I) NAOs from HC subjects (n=5 independent donors) were stimulated with different concentrations of Fsk (0-10 μ M), followed by quantification of FIS. Data information: DAPI (blue) was used as nuclear staining (C, D, F). Quantification of FIS is depicted as the percentage change in surface area relative to t=0 (normalized area) measured at 15-minute time intervals for 2 h (means \pm SD) (H), and area under the curve (AUC) plots (t=120 min, means \pm SD, datapoints represent individual donors) (I). Analysis of differences was determined with a one-way ANOVA and Bonferroni *post-hoc* test (I). ** $p < 0.01$, **** $p < 0.0001$.

could be converted into 3D organoids as well. Indeed, embedding of differentiated ALI-derived epithelial fragments in a 3D extracellular matrix led to formation of organoids within 24 h, with visible lumens formation within 48 h (Fig 1E). From a single 12 mm Transwell insert we can generate a yield of organoids that is sufficient for 48 independent wells (approx. 25-50 organoids/well) of a 96 well plate. In terms of scalability and cost-efficiency, this demonstrates a major advantage compared to the conventional use of 2D ALI-cultures. ALI-culture-derived NAOs directly displayed a differentiated phenotype. This was confirmed by visual observation of beating cilia and accumulation of mucus (Video 3), as well as by immunofluorescence imaging, demonstrating β -tubulin IV⁺ cilia and MUC5AC⁺ secretory cells inside of the organoids, and p63⁺/KRT5⁺ basal cells at the basal side (Fig 1F, and Fig S2D).

Next, we determined whether ALI-derived NAOs could be used to measure CFTR function in FIS assays in a 96 well plate format. Forskolin (Fsk) stimulation of organoids from HC subjects increased swelling in time, which was dose-dependent and reached a plateau at a concentration of 5 μ M (Fig 1G-I). Organoid swelling was partly attenuated with the Na(+)-K(+)-Cl(-) co-transporter (NKCC1) inhibitor bumetanide, demonstrating chloride-dependence of forskolin-induced organoid fluid secretion (Fig S2E and F). Lack of complete inhibition may be explained by reabsorption and recycling of luminal secreted chloride, or an ion channel-independent mechanism underlying fluid secretion caused by mechanical forces^{23,24}. Moreover, chemical CFTR inhibitors significantly reduced FIS in HC NAOs (Fig S2G and H), indicating CFTR dependence. Upon comparison of cultures from HC subjects and subject with CF, we observed that both HC and CF NAOs displayed cystic lumens, which were not significant different in size (Fig 2A and B). This corresponded with observations made in distal airway organoids¹¹, and suggests intrinsic CFTR-independent fluid secretion mediated by alternative chloride channels. In line with this observation, stimulation with the Ca²⁺-activated Cl⁻ channel (CaCC) activator E_{act}^{Cl} induced organoid swelling in CF NAOs, which was significant higher compared to HC cultures (Fig S2I and J). This further suggests dominant CFTR-independent fluid secretion in CF NAOs, also observed by others in Ussing chamber measurements in ALI-cultures²⁵.

FIS measurements in NAOs from HC subjects was significantly higher compared to subjects with CF (Fig 2C and D). Although CF and HC NAOs could be distinguished phenotypically based on FIS, we were unable to observe repairing effects of the CFTR corrector and potentiator combination VX-809/VX-770 in CF F508del/F508del NAOs (Fig 2E-G), likely due to dominant CFTR-independent fluid secretion and low CFTR expression. Therefore, we aimed to optimize CFTR modulator response measurements by modifying organoid culture conditions. Recent studies suggested that secretory cells

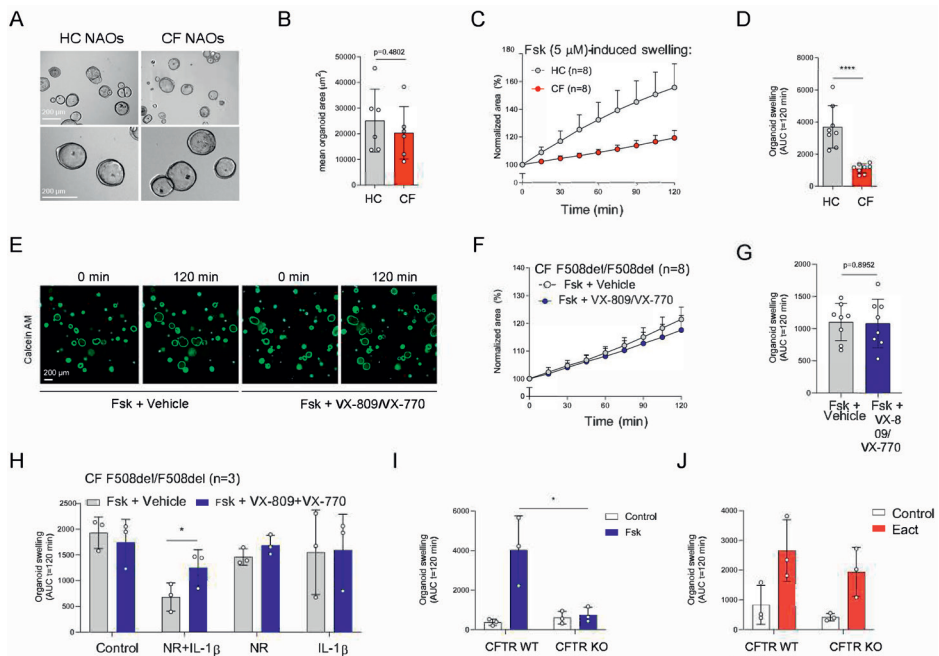


Figure 2: Comparison between HC and CF NAOs and validation of NR/IL-1 β organoid culture conditions.

(A) Representative brightfield images of HC and CF NAOs. (B) Quantification of the mean organoid area (μm^2 , means \pm SD) of HC and CF NAOs (both $n=6$ independent donors). (C and D) Comparison of FIS between HC and CF NAOs (both $n=8$ independent donors) after forskolin (Fsk, $5 \mu\text{M}$) stimulation. (E) Representative images of calcein green AM esters-stained organoids from a CF F508del/F508del subject, treated with vehicle or VX-809/VX-770. Images were taken at $t=0$ and 120 min after stimulation with Fsk. (F and G) CF F508del/F508del NAOs ($n=8$ independent donors) were pre-treated with VX-809 or vehicle control for 48 h. Subsequently, FIS was determined after acute stimulation with Fsk, together with VX-770 or vehicle control. (H) CF F508del/F508del NAOs ($n=3$ independent donors) were cultured at control conditions, or with NR, IL-1 β , or combination (NR+IL-1 β). Afterwards, FIS was determined in response to VX-809/VX-770. (I) FIS and (J) E_{act} -induced swelling measured in CFTR WT or KO NAOs ($n=3$ independent donors). Data information: Results of organoid swelling are depicted as the percentage change in surface area relative to $t=0$ (normalized area) measured at 15-minute time intervals for 2 h (means \pm SD) (C, F), and area under the curve (AUC) plots ($t=120$ min, means \pm SD, datapoints represent individual donors) (D, G-J). Analysis of differences was determined with an unpaired t-test (B, D, G, I), and one-way ANOVA and Bonferroni *post-hoc* test (H). * $p < 0.05$, **** $p < 0.0001$.

are the primary airway epithelial cell type mediating CFTR function^{26,27}. Therefore, we examined a panel of growth factors and cytokines that could modulate secretory cell functions, added after plating of the epithelial fragments and during organoid culturing (Fig S3A). The examined factors included, neuregulin-1 β (NR), which has been reported to enhance epithelial polarization and differentiation of secretory cells in ALI-cultures^{28,29}. Moreover, the effect of the pro-inflammatory cytokine IL-1 β was examined, which has been shown to enhance goblet cell differentiation, CFTR mRNA expression, chloride conductance, and CFTR modulator responses in ALI-cultures³⁰⁻³⁴. In contrast to independent factors, a combination of NR/IL-1 β enabled detection

of VX-809/VX-770 modulator responses in CF F508del/F508del NAOs (Fig 2H and Fig S3B). The combined effect is likely required, because of the activation of distinct signaling transduction pathways, i.e. mitogen-activated protein kinases and NF- κ B respectively, based on studies in ALI-cultures^{28,34}. In contrast to CF NAOs, NR/IL-1 β did not reduce FIS measured in HC NAOs (Fig S3C and D). Corresponding with reduced CFTR-independent fluid secretion, NR/IL-1 β attenuated lumen formation in CF NAOs (Fig S4A and B). Moreover, in line with enhanced specificity of CFTR function, NR/IL-1 β increased and reducing the expression of CFTR and the CaCC ANO1 respectively (Fig S4C). The Cl⁻ channel SLC26A9 was also increased upon stimulation with NR/IL-1 β , which may support CFTR protein stability or function, as proposed by others³⁵. NR/IL-1 β did not affect the expression of ciliated and goblet cells markers (Fig S4D and E), suggesting that increased CFTR and SLC26A9 expression is not caused by alterations in mucociliary differentiation. To further demonstrate CFTR-dependence of FIS in the NR/IL-1 β culture condition, and to exclude potential inadequate inhibition of CFTR with chemical inhibitors earlier used, we generated CFTR gene KO HNEC using CRISPR gene editing (Fig S5A). WT and CFTR KO cells were differentiated in ALI-cultures, converted into NAOs, and cultured with NR/IL-1 β , which attenuated lumen formation (Fig S5B). CFTR KO NAOs displayed attenuated FIS compared to WT controls (Fig 2I and Fig S5C). In contrast, comparable swelling was observed in response to E_{act} (Fig 2J and Fig S5D). This corresponded with persistent E_{act} -induced swelling in CF NAOs cultured with NR/IL-1 β (Fig S5E and F). Altogether, studies in CFTR KO NAOs further confirmed CFTR-dependence of FIS in the NR/IL-1 β culture condition.

Next, we further validated CFTR function and modulator responses in the NR/IL-1 β organoid culture condition. Similar to cultures without NR/IL-1 β (Fig 2C and D), HC NAOs displayed a significant higher swelling response when compared to cultures from CF F508del/F508del subjects (Fig 3A-C, and Fig S6A). Moreover, the CFTR modulator combination VX-809/VX-770 consistently enhanced FIS measured in CF F508del/F508del NAOs from 7 independent subjects (Fig 3B, C, and Fig S6B). In addition, consistent responses to VX-809/VX-770 were observed in CF F508del/F508del NAOs derived from the same donor, differentiated in ALI-cultures at passage 4-6, and derived from two separate cryopreserved vials from the same work cell bank (Fig S6C). In addition to VX-809, FIS in CF F508del/F508del NAOs were selectively modulated upon treatment with other CFTR correctors (Fig S6D). Moreover, genotype-specific VX-770 potentiator responses were observed in NAOs from subjects with CF and a S1251N gating mutation (Fig 3D and F, and Fig S7A). The CFTR triple modulator therapy VX-445/VX-661/VX-770²⁰, induced a high increase in FIS in CF F508del/F508del NAOs cultured with NR/IL-1 β (Fig 3F, G, and Fig S7B). VX-445 by itself did not increase FIS in CF F508del/F508del NAO, whereas chemical CFTR inhibition completely diminished increases in swelling

by VX-445/VX-661/VX-770 (Fig S7C and D). VX-445/VX-661/VX-770 did not improve FIS in NAOs from an individual with CF and a severe R553X/R553X genotype (Fig S7E and F). Altogether, these findings demonstrate robust increases in FIS by VX-445/VX-661/VX-770 in a CFTR specificity specific manner.

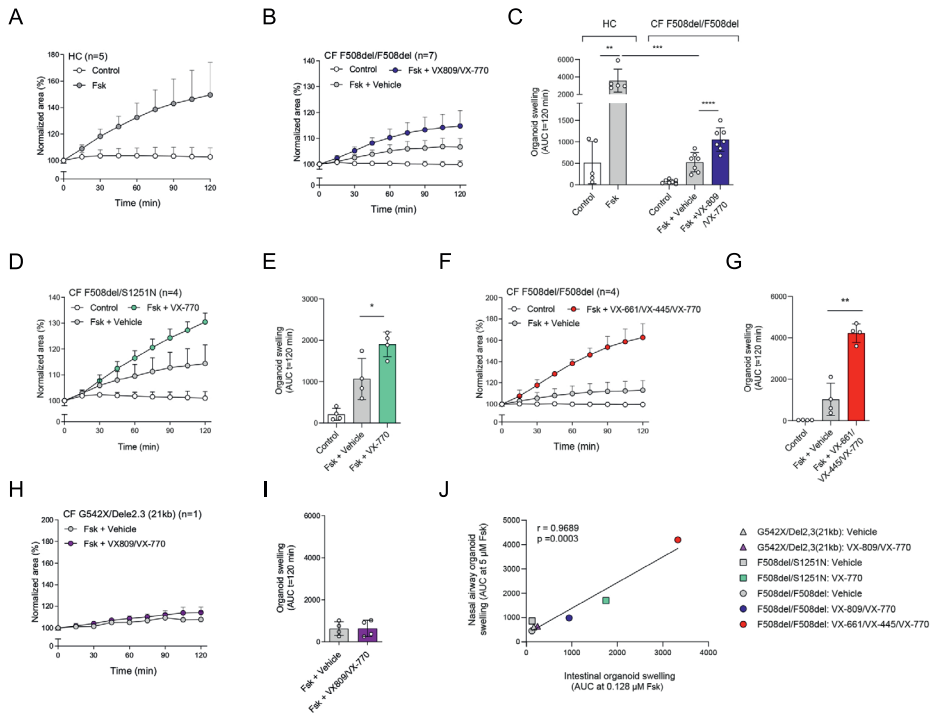


Figure 3: Validation of CFTR modulator responses in NR/IL-1 β -cultured NAOs.

(A) FIS measured in HC NAOs (n=5 independent donors) and (B) CF F508del/F508del NAOs (n=7 independent donors) cultured with NR/IL-1 β . FIS responses in CF NAOs were determined in response to VX-809/VX-770. (C) Comparison of FIS measured in HC and CF F508del/F508del NAOs. (D and E) FIS in NR/IL-1 β cultured NAOs of CF F508del/S1251N subjects (n=4 independent subjects), stimulated with Fsk and VX-770 or vehicle. (F and G) CF F508del homozygous NAOs cultured with NR/IL-1 β (n=4 independent donors) were pre-treated with vehicle or VX-661/VX-445. Swelling was determined afterwards following acute stimulation with Fsk together with VX-770 or vehicle. (H and I) FIS in NR/IL-1 β cultured NAOs of an individual with CF and a severe R553X/R553X genotype. Organoids were pre-treated with VX-809 or vehicle. Swelling was determined afterwards following acute stimulation with Fsk with or without VX-770. (J) Pearson correlation between FIS measured in NAOs and CFTR genotype matched intestinal organoids. Data information: Swelling results *** p<0.001 are depicted as (A, B, D, F, H) the percentage change in surface area relative to t=0 (normalized area) measured at 15-minute time intervals for 2 h (means \pm SD), and (C, E, G, I, J) area under the curve (AUC) plots (t=120 min, means \pm SD), datapoints represent individual donors (C, E, and G) or technical replicates (I). Correlation between nasal and intestinal organoid FIS was examined with AUC values at 5 and 0.128 μ M Fsk respectively. Analysis of differences was determined with a paired t-test (C; within groups, E, G, and I), unpaired t-test (C; HC compared to CF), and Pearson correlation (J). * p<0.05, ** p<0.01, *** p<0.001, **** p<0.0001.

As a final validation study, we determined the correlation between FIS in NAOs from individuals with CF and FIS in CFTR genotype-matched intestinal organoids (Fig S7G). We compared the effect of VX-770 in F508del/S1251N organoids (Fig 3E), VX-809/VX-770 (Fig 3C) and VX-445/VX-661/VX-770 (Fig 3G) in F508del/F508del organoids, and the effect of VX-809/VX-770 in organoids of individuals with a severe G542X/Dele2,3(21kb) genotype (Fig 3H and I). We observed a strong correlation ($r=0.9689$, $p=0003$) between FIS in CF NAOs and intestinal organoids (Fig 3J). This suggests that CFTR function and modulator responses in NAOs are comparable to the CFTR-dependent intestinal organoid model.

In summary, we described a new method of culturing nasal brushing-derived airway organoids, which can be used to determine CFTR modulator responses in individuals with CF. Starting with a nasal brush till assessment of CFTR modulator response in NAOs with FIS (Fig S8), the procedure takes approx. 57-66 days, varying between donors. However, for personalized medicine purposes, the procedure can be reduced to 36-45 days, by excluding de generation of cryopreserved cell banks, and instead using freshly isolated cells. Previously we have shown that long-term expanded airway organoids can be cultured as 2D differentiated ALI-cultures¹¹. In this report, we demonstrate further flexibility between 2D and 3D airway culture models, by showing the possibility to convert 2D differentiated ALI-cultures into 3D organoids. We furthermore described airway organoid culture conditions that improved quantification of CFTR modulator responses in FIS assays. The NR/IL-1 β culture condition may reflect the chronically inflamed airway epithelium of individuals with CF, and therefore may act as physiological condition for testing CFTR modulator responses in NAOs. Further research is required to determine whether NR/IL-1 β also improve CFTR modulator responses in other airway model systems, such as distal airway organoids, or other CFTR-expressing epithelial cells.

Limitation of our model is that we cannot discriminate HC from CF NAOs based on steady-state lumen size, due to CFTR-independent fluid secretion, which is in contrast to the CFTR-dependent intestinal organoid model^{9,13}. Furthermore, we are unable to use CFTR modulator response measurements in NAOs to estimate the level of CFTR repair that is achieved as compared to HC activity, as exemplified by comparable FIS in HC NAOs and F508del/F508del CF NAOs treated with VX-445/VX-661/VX-770 (Fig 3C and G). Furthermore, comparison studies remain required to determine whether CFTR modulator responses based on short-circuit current measurements conducted in ALI-cultures, correlate with organoid swelling, as recently shown by others^{19,36}.

Indeed, we observed a correlation between CFTR modulator responses in nasal- and intestinal organoids. FIS in intestinal organoids is fully CFTR dependent, and previously it has been shown that CFTR modulator responses in intestinal organoids correlate with drug efficacy in individuals with CF^{12,15,37}. Therefore, a correlation between nasal and intestinal organoids provides early evidence that FIS in NAOs can also be used to predict CFTR modulator efficacy in a genotype dependent manner. However, the potential clinical impact of our method requires follow up studies, such as further exploration whether CFTR modulator responses in ALI-derived NAOs correlate with clinical outcome in a large cohort of individuals with CF, and how this relates to other *in vitro* measurements, i.e. patient-matched intestinal organoids and 2D ALI- airway cultures. CFTR function measurements in ALI-culture derived NAOs may also be used to examine novel target-specific therapies for subjects with CF with unmet, such as assessment of CRISPR-gene editing, read-through agents, or compounds targeting nonsense mediated decay. Moreover, complementary to the widely used 2D ALI-cultures, airway organoids derived from this model may be further used to study other respiratory tract disorders.

MATERIALS AND METHODS

Reagents and Tools Table

Reagent or Resource	Source	Identifier
Antibodies		
Mouse IgG1 anti- β -tubulin IV	Emergo Biogenex	#MU178-UC
Rabbit anti- β -tubulin IV	Abcam	#ab179509
Rabbit anti-MUC5AC	Abcam	#ab198294
Rabbit anti-P63	Abcam	#ab124762
Mouse IgG1 anti cytokeratin 5	Abcam	#ab17130
Mouse IgG1 anti-CC10	Acris, Origene	#AM26360PU-N
Goat anti-Mouse IgG1, Alexa Fluor 488	Invitrogen	#A-21121
Goat anti-Mouse IgG1, Alexa Fluor 647	Invitrogen	#A-21240
Goat anti-Rabbit IgG, Alexa Fluor 488	Invitrogen	#A-11034
Goat anti-Rabbit IgG, Alexa Fluor 546	Invitrogen	#A-11035
Biological Samples		
Nasal brushings	UMC Utrecht	Protocol ID: 16/586, NL54885.041.16
Nasal turbinate tissue	Academic Medical Center Amsterdam	N/A
Intestinal organoids	HUB	https://huborganoids.nl/
Chemicals, Peptides, and Recombinant Proteins		
TrypLE express enzyme	Fisher scientific	# 12605010

Reagents and Tools Table (continued)

Reagent or Resource	Source	Identifier
Sputolysin	Calbiochem	#560000-10
Collagen IV	Sigma-Aldrich	#C7521
CryoStor® CS10	StemCell Technologies	#07930
PureCol	Advanced BioMatrix	#5005
Bronchial epithelial cell medium-basal (BEpiCM-b)	Sciencell	#3211
Advanced DMEM F12	Thermo Fisher	#12634-028
B-27 Supplement, serum free	Thermo Fisher	#12587010
GlutaMAX Supplement	Thermo Fisher	#35050-061
HEPES	Thermo Fisher	#15630080
(±)-Epinephrine hydrochloride	Sigma-Aldrich	#E4642
Hydrocortisone	Sigma-Aldrich	#H0888
3,3',5-Triiodo-L-thyronine sodium salt	Sigma-Aldrich	#T6397
N-Acetyl-L-cysteine	Sigma-Aldrich	#A9165
Nicotinamide	Sigma-Aldrich	#N0636
SB02190	Sigma-Aldrich	#S7067
DMH-1	Selleck Chemicals	#S7146
A83-01	Tocris	#2939/10
Y-27632	Selleck Chemicals	#S1049
DAPT	Fisher Scientific	#15467109
TTNPB	Cayman	#16144-1
Recombinant human FGF-7	Peprtech	#100-19
Recombinant human FGF-10	Peprtech	#100-26
Recombinant human EGF	Peprtech	#AF-100-15
Recombinant human HGF	Peprtech	#100-39H
Recombinant Neuregulin-1 β	Peprtech	#100-03
Recombinant Interleukin 1 β	Peprtech	#200-01B
Penicillin-Streptomycin	Thermo Fisher	#15070-063
Primocin	Invivogen	#ant-pm-2
Amphotericin B	Thermo Fisher	#15290018
Gentamicin	Sigma-Aldrich	#G1397
Vancomycin	Sigma-Aldrich	#SBR00001
Collagenase type II	Thermo Fisher	#17101-015
CFTR multi-guide sgRNA	Synthego	
2NLS-Cas9 nuclease	Synthego	
OptiMEM	Thermo Fisher	#31985062
CFTRinh-172	Sigma-Aldrich	#C2992

Reagents and Tools Table (continued)

Reagent or Resource	Source	Identifier
GlyH101	Sigma-Aldrich	#219671
VX-809	Selleck Chemicals	# S1565
VX-661	Selleck Chemicals	#S7059
VX-770	Selleck Chemicals	#S1144
Correctors C1-18	Cystic Fibrosis Foundation Therapeutics	https://www.cff.org/Research/Researcher-Resources/Tools-and-Resources/CFTR-Chemical-Compound-Program/
Forskolin	Sigma-Aldrich	#F3917
3-Isobutyl-1-methylxanthine	Sigma-Aldrich	# I5879
Amiloride	Sigma-Aldrich	#1019701
Calcein green acetoxymethyl (AM)	Invitrogen	#C34852
Alexa Fluor 555 Phalloidin	Invitrogen	#A34055
Phalloidin-iFluor 405	Abcam	#ab176752
Prolong Gold antifade reagent	Thermo Fischer	#P36934
Prolong Gold antifade reagent with DAPI	Thermo Fischer	#P36935
iQ SYBR Green Supermix	Bio-Rad	#1708880
Critical Commercial Assays		
RNeasy Mini Kit	Qiagen	#74104
iScript cDNA synthesis kit	Bio-Rad	#1708891
Quick-DNA Microprep Kit	Zymo research	#D3020
GoTaq G2 Flexi DNA polymerase	Promega	# M7805
Experimental Models: Cell Lines		
Human nasal airway epithelial cells (HNEC)	This paper	N/A
Hek293T - R-spondin-1 mFc cell line	Trevigen Cat# 3710-001-	N/A
Oligonucleotides		
Primers used for this manuscript		Table S5
Equipment		
Zeiss LSM800 confocal microscopy	Zeiss	N/A
Leica SP8X confocal microscope	Leica	N/A
Leica THUNDER imager	Leica	N/A
Leica TCS SP8 STED 3X microscope	Leica	N/A
NEPA21	NEPA	N/A
Ussing chamber system	Physiologic Instruments	N/A
Voltage clamp	World Precision Instruments	#DVC-1000
PowerLab	AD Instruments	#8/30
Nanodrop spectrophotometer	Thermo Fisher	N/A

Reagents and Tools Table (continued)

Reagent or Resource	Source	Identifier
CFX96 real-time detection machine	Bio-Rad	N/A
Software and Algorithms		
Zen Blue Software	Zeiss	https://www.zeiss.com/microscopy/int/products/microscope-software/zen.html
Prism 8	GraphPad Software Inc.	https://www.graphpad.com/scientific-software/prism/
Microsoft Excel	Microsoft Corporation	https://office.microsoft.com/excel
Adobe Illustrator	Adobe	https://www.adobe.com/nl/products/illustrator.html
LabChart 6	AD Instruments	https://labchart.software.informer.com/6.0/
CFX Manager 3.1	BioRad	https://www.bio-rad.com/en-us/sku/1845000-cfx-manager-software?ID=1845000
LAS X software	Leica	https://www.leica-microsystems.com/products/microscope-software/p/leica-las-x-ls/
ImageJ/FIJI		https://imagej.net/Fiji/Downloads
ICE analysis tool.	Synthego	www.ice.synthego.com
Others		
Cytological brush	CooperSurgical	#C0004
12 mm Transwell® with 0.4 µm Pore Polyester Membrane Insert	Corning	#3460
6.5 mm Transwell® with 0.4 µm Pore Polyester Membrane Insert	Corning	#3470
Matrigel	Corning	#354230
BC isolation and expansion medium		Table S2
Air-liquid interface differentiation medium		Table S3
Airway organoid culture medium		Table S4

Patient materials and sample collection

Nasal brushings were collected from healthy volunteers without respiratory tract symptoms (n=19 independent donors), and subjects with CF (n=24 independent donors) by a trained research nurse or physician, essentially as previously described³⁸. The use of donor cells in different experiments depicted in the figures has been described in Table S1. Sampling of adults was conducted using a cytological brush and without anaesthetics. Nasal brushings of infants (<6 years old) were collected with a modified interdental brush³⁹. Samples were taken from the inferior turbinates of both left and

right nostrils and stored in collection medium, consisting of advanced (ad)DMEM/F12, with GlutaMAX (1% v/v), HEPES (10 mM), Penicillin-Streptomycin (1% v/v), and Primocin (100 µg/mL). Nasal brushings were collected and stored with informed consent of all participants and was approved by a specific ethical board for the use of biobanked materials TcBIO (Toetsingscommissie Biobanks), an institutional Medical Research Ethics Committee of the University Medical Center Utrecht (protocol ID: 16/586). Nasal samples from infants with CF were collected as part of the Precision study (protocol ID: NL54885.041.16), which was approved by the Medical Research Ethics Committee of the University Medical Center Utrecht (Utrecht, The Netherlands). Intestinal organoids (n=9 independent donors) were collected, generated, and stored with informed consent of all participants and was approved by the TcBIO (UMCU; TcBio#14-008) according to the guidelines of the European Network of Research Ethics Committees (EUREC). Biobanked intestinal organoids are stored and catalogued (<https://huborganoids.nl/>) at the foundation Hubrecht Organoid Technology (<http://hub4organoids.eu>). Resected inferior nasal turbinate tissue was obtained from a subject who underwent corrective surgery for turbinate hypertrophy at the Academic Medical Center in Amsterdam, the Netherlands. The tissue was accessible for research within the framework of patient care, in accordance with the “Human Tissue and Medical Research: Code of conduct for responsible use” (2011) (www.federa.org), describing the no-objection system for coded anonymous further use of such tissue without necessary written or verbal consent.

Isolation and expansion of human nasal airway epithelial cells as 2D-cultures

Nasal cells were dissociated from the brush in the collection medium by scraping through a sterile P1000 pipette tip with the top cut off. After centrifugation (400 g for 5 min), the pellet was treated with TrypLE express enzyme, supplemented with 1x Sputolysin. The cells were incubated for 10 min at 37 °C and strained using a 100 µm strainer. After centrifugation (400 g for 5 min), the remaining pellet was used for isolation of human nasal epithelial cells (HNEC). HNEC were isolated and expanded on 6-well culture plates coated with collagen IV (50 µg/mL) and using BC isolation and expansion medium (Table S2) respectively. BC isolation medium contained additional antibiotics to suppress microbial outgrowth and was used during the first week of epithelial cell isolation, before switching to BC expansion medium. BC expansion medium included the gamma-secretase inhibitor DAPT, which reduces outgrowth of squamous cells at late passages. Growth factors (FGF7, FGF10, EGF, and HGF) were added freshly to the culture medium. Cultures were refreshed three times a week (Monday, Wednesday, Friday) and passaged after reaching 80-90% confluency, typically within 7-14 days. This varied between donors and mainly depending on the number of cells harvested during brushings. During passaging, cells were dissociated with TrypLE express enzyme. Isolated cells (passage 1) were expanded for an additional 7

days, before freezing with CryoStor® CS10, supplemented with Y-27632 (5 μ M) to create a master cell bank (passage 2). For further use, HNEC were expanded (approx. 7) days and cryo-stored as a work cell bank (passage 3).

Differentiation of 2D ALI-HNEC cultures

HNEC (passage 4-6) were cultured on Transwell inserts (0.4 μ m pore size polyester membrane), which were coated with PureCol (30 μ g/mL). Cells were seeded in a density of 0.2 or 0.5*10⁶ cells on 24 or 12 wells inserts respectively and cultured in submerged conditions in BC expansion medium until reaching confluency after 3-5 days. Afterwards, culture medium was changed with air-liquid interface (ALI)-differentiation medium (Table S3) supplemented with A83-01 (500 nM), and cells were additionally cultured in submerged condition for 1-2 days. Subsequently, culture medium at the apical side was removed and cells were further differentiated as ALI-cultures. After 3-4 days, cells were refreshed with ALI-diff medium without additional A83-01 and differentiated for at least 14 additional days at ALI-conditions. Medium was refreshed twice a week (Monday and Thursday or Tuesday and Friday), and the apical side of the cultures was washed with PBS once a week.

Conversion of 2D differentiated ALI cultures into airway organoids

Differentiated ALI-cultures were washed at the apical surface with PBS and subsequently treated at the basolateral side with collagenase type II (1 mg/mL) diluted in addMEM/F12. Cultures were incubated at 37 °C and 5% CO₂ for 45-60 min until the epithelium detaches from the Transwell insert. Next, the dissociated epithelial layer was transferred to a 15 ml tube in 1 ml addMEM/F12 + 10 % (v/v) Fetal bovine serum (FBS), mechanically disrupted into smaller fragment by pipetting, and strained with a 100 μ m filter. After centrifugation (at 400 g, 5 min), the epithelial pellet was resuspended in ice-cold 75% growth factor reduced Matrigel (v/v in airway organoid (AO) medium Table S4). Next, epithelial fragments were embedded in 30 μ l Matrigel droplets on pre-warmed 24-well suspension plates. Droplets were solidified at 37 °C and 5% CO₂ for 20-30 min, before adding 0.5 ml AO medium (Table S4). In optimized conditions for measuring CFTR modulator responses, AO culture medium was further supplemented with neuregulin-1 β (NR, 0.5 nM) and interleukin-1 β (IL-1 β ; 10 ng/ml). Besides, NR/IL-1 β we furthermore examined the effects of culturing with other interleukins i.e. IL-13, IL-4, IL-10, and the growth factors: fibroblast growth factor 2, 7, 10, hepatocyte growth factor, and insulin-like growth factor 1, which did not improve the detection of CFTR modulator responses. AO medium was refreshed twice a week (Monday and Thursday or Tuesday and Friday).

Forskolin-induced swelling (FIS) assay

ALI-derived NAOs were used in forskolin-induced swelling (FIS) assays, essentially as previously described with minor adaptation^{11,40}. In short, organoids were transferred 3-5 days after conversion in 96-well plates in 4 μ l droplets of 75% matrigel (v/v in AO medium), containing approx. 25-50 structures. After solidification of droplets, 100 μ l AO medium was added to each well. In optimized conditions for measuring CFTR modulator responses, AO culture medium was supplemented with neuregulin-1 β (0.5 nM) and interleukin-1 β (10 ng/ml). Organoid swelling was conducted with four technical replicates. In indicated experiments, organoids were pre-treated with CFTRinh-172 and GlyH101 (CFTRi, both 50 μ M) or vehicle as negative control, for 4 h. CFTR correctors: VX-809, VX-661 (both 10 μ M), VX-445 (5 μ M), C1-18 (all 10 μ M) or vehicle were pre-treated for 48 h. Before assessment of FIS, NAOs were stained with Calcein green AM (3 μ M) for 30 min. Afterwards, organoids were stimulated with forskolin with indicated concentration. In cultures from subjects with CF, the CFTR potentiator VX-770 (10 μ M) or vehicle was added together with forskolin. Swelling of NAOs was quantitated by measuring the increase of the total area of calcein green AM-stained organoids in a well during 15-min time intervals for a period of 2 h. Images were acquired with a Zeiss LSM800 confocal microscopy, using a 2.5 or 5x objective and experiments were conducted at 37°C and 95% O₂/5% CO₂ to maintain a pH of 7.4. Data was analysed using Zen Blue Software and Prism 8.

Ussing chamber experiments

For open circuit Ussing chamber measurements, Transwell inserts (\varnothing 12 mm) were mounted in the chamber device and continuously perfused at the apical and basal side with a Ringer solution of the following composition (mmol/L) 145 NaCl, 1.6 K₂HPO₄, 1 MgCl₂, 0.4 KH₂PO₄, 1.3 Ca²⁺ Gluconate and 5 Glucose, and pH adjusted to 7.4. Following a 20 min stabilization period amiloride (20 μ M) was added to the apical side to block epithelial Na⁺ channel-mediated currents, followed by forskolin/IBMX (2 μ M/100 μ M), VX-770 (3 μ M) and CFTRInh-172 (30 μ M) were added sequentially. Transepithelial Voltage (V_{te}) values were recorded at all times with Power Lab software (AD Instruments Inc.). Values for V_{te} were referred to the basal side of the epithelium and transepithelial resistance (R_{te}) was determined by applying short intermittent pulses (0.5 μ A/s), measuring pulsated deviations in V_{te} and accounting for the area of the inserts. An empty insert was previously recorded to correct the measured values. Short-circuit currents (I_{eq-sc}) were calculated according to Ohm's law from V_{te} and R_{te} ($I_{eq-sc} = V_{te} / R_{te}$).

CRISPR gene editing

CFTR gene knock-out (KO) HNEC (n=3 independent donors) were generated by electroporation of recombinant Cas9/single-guide RNA (sgRNA) ribonucleoprotein

(RNP) complexes. RNP complexes were prepared by mixing multi-guide sgRNA (30 μM , 8,3 μL), recombinant 2NLS-Cas9 nuclease (20 μM , 2,5 μL), and 14,2 μL OptiMEM supplemented with 10 μM Y-27632, followed by incubation at room temperature for 10 minutes. After expansion, HNEC (passage 3) were dissociated into single cells using TrypLE express enzyme. Next, 1×10^6 cells were diluted in 75 μL optiMEM with 10 μM Y-27632, and added to the RNP complexes. Electroporation was conducted with the NEPA21 according to previously published settings⁴¹. After electroporation, HNEC were seeded in 12 well plates in BC expansion medium. After expansion, HNEC were used for further experiments. For assessment of KO efficiency, DNA was isolated according to the manual of the Quick-DNA Microprep Kit. Regions of interest were amplified in a PCR reaction with GoTaq G2 Flexi DNA polymerase with primers, and PCR-amplified samples were run on 1,2% TBE-agarose gel for size separation. DNA fragments were excised from the gel, purified according to the Gel extraction kit, and sent for Sanger sequencing with sequencing primers. Analysis of the KO-efficiency and the specific deletions was done with the ICE analysis tool (www.ice.synthego.com). Of independent donors the calculated CFTR KO-efficiency was 69%, 76%, and 84% respectively.

RNA extraction, cDNA synthesis, and quantitative real time PCR

Total RNA was extracted from ALI-cultures using the RNeasy Mini Kit according to the manufacturer's protocol. RNA yield was determined by a Nanodrop spectrophotometer and subsequently cDNA was synthesized by use of the iScript cDNA synthesis kit according to the manufacturer's protocol. Quantitative real-time PCR (qPCR) was performed with specific primers (Table S5) using the iQ SYBR Green Supermix and a CFX96 real-time detection machine. CFX Manager 3.1 software was used to calculate relative gene expression normalized to the housekeeping genes *ATP5B* and *RPL13A*, according to the standard curve method. Housekeeping genes were selected based on stable expression in airway epithelial cells at different experimental conditions, based on the geNorm method⁴².

Immunofluorescence staining and microscopy

2D expanded HNEC and ALI-HNEC cultures were fixed in 4% paraformaldehyde for 15 min, permeabilized in 0.25% (v/v) Triton-X in PBS for 30 min and treated with blocking buffer, consisting of 1% (w/v) BSA and 0.25% (v/v) Triton-X in PBS, for 60 min. Next, primary antibodies (1:500) in blocking buffer were added at the apical side and incubated for 1-2 h or overnight. Afterwards, cells were washed three times with PBS and incubated with secondary antibodies and Phalloidin (1:500) in blocking buffer for 30 min in dark, followed by three washings in PBS. Transwell membranes were subsequently cut from the inserts and placed on slides. All samples were mounted with Prolong Gold antifade reagent with or without DAPI. Resected nasal tissue and ALI-

HNEC cultures were fixed with 4 % paraformaldehyde and embedded in paraffin after dehydration. After deparaffinization followed by antigen retrieval using citrate buffer (pH = 6) for 20 min, the 5 μ m sections were permeabilized in 0.25% (v/v) Triton-X in PBS for 15 min, then treated with blocking buffer, consisting of 5% (w/v) BSA and 0.025% (v/v) Triton-X in PBS, for 30 min. Primary antibodies in blocking buffer, were incubated for 2 h, followed by incubation of secondary antibodies for 1 h. Samples were mounted with Prolong Gold reagent with DAPI. Organoids plated in 4 μ l droplets of 75% Matrigel (v/v) in a 96 wells plate, were fixed with 4 % paraformaldehyde for 10 min, and stained as previously described^{11,43}, using indicated primary antibodies. Images were acquired with a Leica SP8X confocal microscope, Leica THUNDER imager, and Leica TCS SP8 STED 3X microscope. Images were processed using LAS X software and ImageJ/FIJI.

Intestinal organoid culturing and use in FIS assays

Intestinal organoids of individuals with CF were isolated from rectal biopsies, expanded, and used in FIS assays as previously described^{9,44}. For FIS assays, intestinal organoids were plated in 96 wells and pre-incubated with vehicle or indicated CFTR correctors, VX-809, VX-661 (both 3 μ M), and VX-445 (5 μ M) for 24 h. FIS was measured upon addition of forskolin (0.128 μ M) and the CFTR potentiator VX-770 (3 μ M) for 60 minutes. A forskolin concentration of 0.128 μ M was used, based on previous correlation studies with clinical outcome measurements¹².

Quantification and statistical analysis

Swelling assays were conducted with 4 technical replicates for each experimental condition, and results are shown as mean \pm SD of independent subjects or independent technical replicates as indicated in the figure legends. Increases in the total surface area of all organoids in a single well is calculated as normalized swelling, relative to $t=0$, which is set as baseline of 100%. For swelling assays, statistical analysis was assessed with area under the curve (AUC) values ($t=120$ min). Analysis of differences was determined with a one/two-way repeated measurements ANOVA and Bonferroni *post-hoc* test or (un)paired Student's *t*-test as indicated in the figure legends. Normal distribution was tested using the Shapiro Wilk test. Differences were considered significant at $p < 0.05$. Statistical analysis was conducted using Prism 8 (GraphPad Software Inc.).

DATA AVAILABILITY

All data is provided with the manuscript.

ACKNOWLEDGMENTS

This work was supported by grants of the Dutch Cystic Fibrosis Foundation (NCFS, HIT-CF grant); Netherlands Organization for Health Research and Development (ZonMw); Health Holland (grant no 40-41200-98-9296); SRC 013 from CF Trust-UK; UIDB/04046/2020 and UIDP/04046/2020 centre grants (to BioISI), both from FCT/MCTES Portugal; and “HIT-CF” (H2020-SC1-2017-755021) from EU. This work is supported by the European Research Council (ERC Consolidator Grant 819219 to L.C.K.).

AUTHOR CONTRIBUTION

Conception and/or design: GA, LR, CE, JMB; Acquisition, analysis, or interpretation of data: GA, LR, HR, EA, DS, SS, JL, IS, WN, SV, BA, EK, JEB, SM, KW, HH, LK, MA, CE, JMB; Drafting the work or revising it critically for important intellectual content: GA, CD, MA, CE, JMB; Final approval of the version submitted for publication; GA, LR, HR, EA, DS, SS, JL, IS, WN, SV, BA, EK, JEB, CD, SM, KW, HH, LK, MA, CE, JMB.

CONFLICT OF INTEREST

JMB has a patent granted (10006904) related to CFTR function measurements in organoids and received personal fees from HUB/ Royal Dutch academy of sciences, during the conduct of the study; non-financial support from Vertex Pharmaceuticals, and personal fees and non-financial support from Proteostasis Therapeutics, outside the submitted work. CE reports grants from GSK, Nutricia, TEVA, Gilead, Vertex, ProQR, Proteostasis, Galapagos NV, Eloxx pharmaceuticals, outside the submitted work; In addition, CE has a patent related to CFTR function measurements in organoids (10006904) with royalties paid. MA reports grants and personal fees from Vertex Pharmaceuticals, grants from Gilead Sciences, Inc., grants and personal fees from Proteostasis Therapeutics, personal fees from Translate Bio MA, Inc, during the conduct of the study.

REFERENCES

1. Riordan, J. R. *et al.* Identification of the cystic fibrosis gene: cloning and characterization of complementary DNA. *Science (New York, N.Y.)* 245, 1066–1073 (1989).
2. Knowles, M. R. *et al.* Abnormal ion permeation through cystic fibrosis respiratory epithelium. *Science (New York, N.Y.)* 221, 1067–1070 (1983).
3. Stoltz, D. A., Meyerholz, D. K. & Welsh, M. J. Origins of Cystic Fibrosis Lung Disease. *New England Journal of Medicine* 372, 351–362 (2015).
4. Boyle, M. P. & De Boeck, K. A new era in the treatment of cystic fibrosis: correction of the underlying CFTR defect. *The Lancet Respiratory Medicine* 1, 158–163 (2013).
5. Clancy, J. P. *et al.* CFTR modulator therotyping: Current status, gaps and future directions. *Journal of cystic fibrosis : official journal of the European Cystic Fibrosis Society* 18, 22–34 (2019).
6. Gentzsch, M. *et al.* Pharmacological Rescue of Conditionally Reprogrammed Cystic Fibrosis Bronchial Epithelial Cells. *American journal of respiratory cell and molecular biology* 56, 568–574 (2017).
7. Awatade, N. T. *et al.* Measurements of Functional Responses in Human Primary Lung Cells as a Basis for Personalized Therapy for Cystic Fibrosis. *EBioMedicine* 2, 147–153 (2015).
8. Pranke, I. M. *et al.* Correction of CFTR function in nasal epithelial cells from cystic fibrosis patients predicts improvement of respiratory function by CFTR modulators. *Scientific reports* 7, 7375 (2017).
9. Dekkers, J. F. *et al.* A functional CFTR assay using primary cystic fibrosis intestinal organoids. *Nature medicine* 19, 939–945 (2013).
10. Schutgens, F. *et al.* Tubuloids derived from human adult kidney and urine for personalized disease modeling. *Nature biotechnology* 37, 303–313 (2019).
11. Sachs, N. *et al.* Long-term expanding human airway organoids for disease modeling. *The EMBO journal* 38, e100300 (2019).
12. Berkers, G. *et al.* Rectal Organoids Enable Personalized Treatment of Cystic Fibrosis. *Cell reports* 26, 1701–1708.e3 (2019).
13. Dekkers, J. F. *et al.* Characterizing responses to CFTR-modulating drugs using rectal organoids derived from subjects with cystic fibrosis. *Science translational medicine* 8, 344ra84 (2016).
14. van Mourik, P., Beekman, J. M. & van der Ent, C. K. Intestinal organoids to model cystic fibrosis. *The European respiratory journal* 54, (2019).
15. Ramalho, A. S. *et al.* Correction of CFTR function in intestinal organoids to guide treatment of Cystic Fibrosis. *The European respiratory journal* (2020) doi:10.1183/13993003.02426-2019.
16. Guimbellot, J. S. *et al.* Nasospheroids permit measurements of CFTR-dependent fluid transport. *JCI insight* 2, (2017).
17. Brewington, J. J. *et al.* Detection of CFTR function and modulation in primary human nasal cell spheroids. *Journal of cystic fibrosis : official journal of the European Cystic Fibrosis Society* 17, 26–33 (2018).
18. Liu, Z. *et al.* Human Nasal Epithelial Organoids for Therapeutic Development in Cystic Fibrosis. *Genes* 11, (2020).
19. Sette, G. *et al.* Therotyping cystic fibrosis in vitro in ALI-culture and organoid models generated from patient-derived nasal epithelial Conditionally Reprogrammed Stem Cells. *The European respiratory journal* (2021) doi:10.1183/13993003.00908-2021.
20. Keating, D. *et al.* VX-445-Tezacaftor-Ivacaftor in Patients with Cystic Fibrosis and One or Two Phe508del Alleles. *The New England journal of medicine* 379, 1612–1620 (2018).
21. Plasschaert, L. W. *et al.* A single-cell atlas of the airway epithelium reveals the CFTR-rich pulmonary ionocyte. *Nature* 560, 377–381 (2018).
22. Montoro, D. T. *et al.* A revised airway epithelial hierarchy includes CFTR-expressing ionocytes. *Orit rozenblatt-rosen* 4, 19 (2018).

23. Buddington, R. K., Wong, T. & Howard, S. C. Paracellular Filtration Secretion Driven by Mechanical Force Contributes to Small Intestinal Fluid Dynamics. *Medical sciences (Basel, Switzerland)* 9, (2021).
24. Bajko, J., Duguid, M., Altmann, S., Hurlbut, G. D. & Kaczmarek, J. S. Pendrin stimulates a chloride absorption pathway to increase CFTR-mediated chloride secretion from Cystic Fibrosis airway epithelia. *FASEB bioAdvances* 2, 526–537 (2020).
25. Clarke, L. L. & Boucher, R. C. Chloride secretory response to extracellular ATP in human normal and cystic fibrosis nasal epithelia. *The American journal of physiology* 263, C348–56 (1992).
26. Okuda, K. *et al.* Secretory Cells Dominate Airway CFTR Expression and Function in Human Airway Superficial Epithelia. *American journal of respiratory and critical care medicine* 203, 1275–1289 (2021).
27. Carraro, G. *et al.* Transcriptional analysis of cystic fibrosis airways at single-cell resolution reveals altered epithelial cell states and composition. *Nature medicine* 27, 806–814 (2021).
28. Kettle, R. *et al.* Regulation of neuregulin 1beta-induced MUC5AC and MUC5B expression in human airway epithelium. *American journal of respiratory cell and molecular biology* 42, 472–481 (2010).
29. Vermeer, P. D., Panko, L., Karp, P., Lee, J. H. & Zabner, J. Differentiation of human airway epithelia is dependent on erbB2. *American journal of physiology. Lung cellular and molecular physiology* 291, L175–80 (2006).
30. Gray, T. *et al.* Regulation of MUC5AC mucin secretion and airway surface liquid metabolism by IL-1beta in human bronchial epithelia. *American journal of physiology. Lung cellular and molecular physiology* 286, L320–30 (2004).
31. Abdullah, L. H. *et al.* Mucin Production and Hydration Responses to Mucopurulent Materials in Normal versus Cystic Fibrosis Airway Epithelia. *American journal of respiratory and critical care medicine* 197, 481–491 (2018).
32. Gentzsch, M. *et al.* The cystic fibrosis airway milieu enhances rescue of F508del in a pre-clinical model. *The European respiratory journal* vol. 52 Preprint at <https://doi.org/10.1183/13993003.01133-2018> (2018).
33. Chen, G. *et al.* IL-1 β dominates the promucin secretory cytokine profile in cystic fibrosis. *The Journal of clinical investigation* 129, 4433–4450 (2019).
34. Brouillard, F. *et al.* NF-kappa B mediates up-regulation of CFTR gene expression in Calu-3 cells by interleukin-1beta. *The Journal of biological chemistry* 276, 9486–9491 (2001).
35. Balázs, A. & Mall, M. A. Role of the SLC26A9 Chloride Channel as Disease Modifier and Potential Therapeutic Target in Cystic Fibrosis. *Frontiers in pharmacology* 9, 1112 (2018).
36. Anderson, J. D., Liu, Z., Odom, L. V., Kersh, L. & Guimbellot, J. S. CFTR function and clinical response to modulators parallel nasal epithelial organoid swelling. *American journal of physiology. Lung cellular and molecular physiology* 321, L119–L129 (2021).
37. Muilwijk, D. *et al.* Forskolin-induced Organoid Swelling is Associated with Long-term CF Disease Progression. *The European respiratory journal* (2022) doi:10.1183/13993003.00508-2021.
38. Harris, C. M. *et al.* Assessment of CFTR localisation in native airway epithelial cells obtained by nasal brushing. *Journal of cystic fibrosis : official journal of the European Cystic Fibrosis Society* 3 Suppl 2, 43–48 (2004).
39. Stokes, A. B. *et al.* Comparison of three different brushing techniques to isolate and culture primary nasal epithelial cells from human subjects. *Experimental lung research* 40, 327–332 (2014).
40. Boj, S. F. *et al.* Forskolin-induced Swelling in Intestinal Organoids: An In Vitro Assay for Assessing Drug Response in Cystic Fibrosis Patients. *Journal of visualized experiments : JoVE* (2017) doi:10.3791/55159.
41. Fujii, M., Matano, M., Nanki, K. & Sato, T. Efficient genetic engineering of human intestinal organoids using electroporation. *Nature protocols* 10, 1474–1485 (2015).
42. Vandesompele, J. *et al.* Accurate normalization of real-time quantitative RT-PCR data by geometric averaging of multiple internal control genes. *Genome biology* 3, RESEARCH0034 (2002).
43. Dekkers, J. F. *et al.* High-resolution 3D imaging of fixed and cleared organoids. *Nature protocols* 14, 1756–1771 (2019).
44. Vonk, A. M. *et al.* Protocol for Application, Standardization and Validation of the Forskolin-Induced Swelling Assay in Cystic Fibrosis Human Colon Organoids. *STAR protocols* 1, 100019 (2020).

SUPPLEMENTARY FIGURES

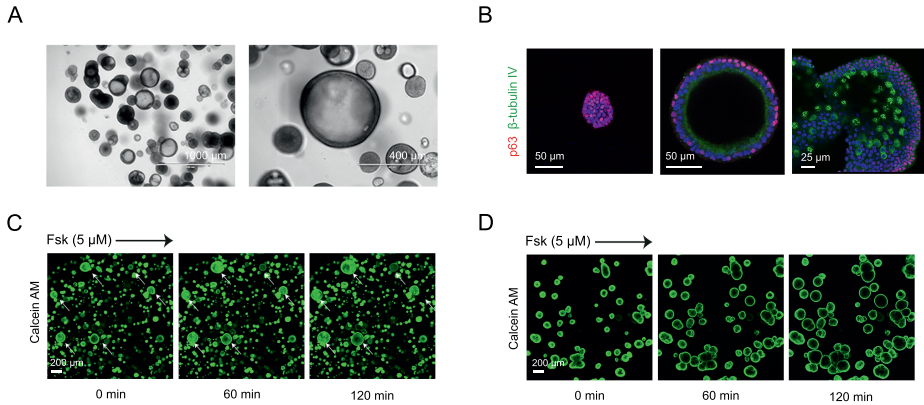


Figure S1: Heterogeneity in passaged tissue-derived airway organoid cultures.

(A) Brightfield images of airway organoids, passaged after mechanical disruption according to the method described by Sachs *et al*, 2019, showing differences in organoid morphology, i.e. structures with lumen and solid colonies. (B) Immunofluorescence confocal imaging of airway organoids from the same culture, stained for the basal cell marker p63 (red) and ciliated cell marker β -tubulin IV (green). Images show (left) a solid colony consisting solely of p63⁺ basal cells, (middle) a pseudostratified structure with lumen but without ciliated cells, and (right) a large structure displaying ciliated cells. (C) Representative images (t=0, 60 and 120 min after 5 μM forskolin stimulation) of a FIS assay using serially passaged HC airway organoids stained with calcein green-AM. Arrows indicate swelling of large-sized structures. (D) Representative images (t=0, 60 and 120 min after 5 μM forskolin stimulation) of a FIS assay using HC airway organoids derived from an ALI-culture stained with calcein green-AM.

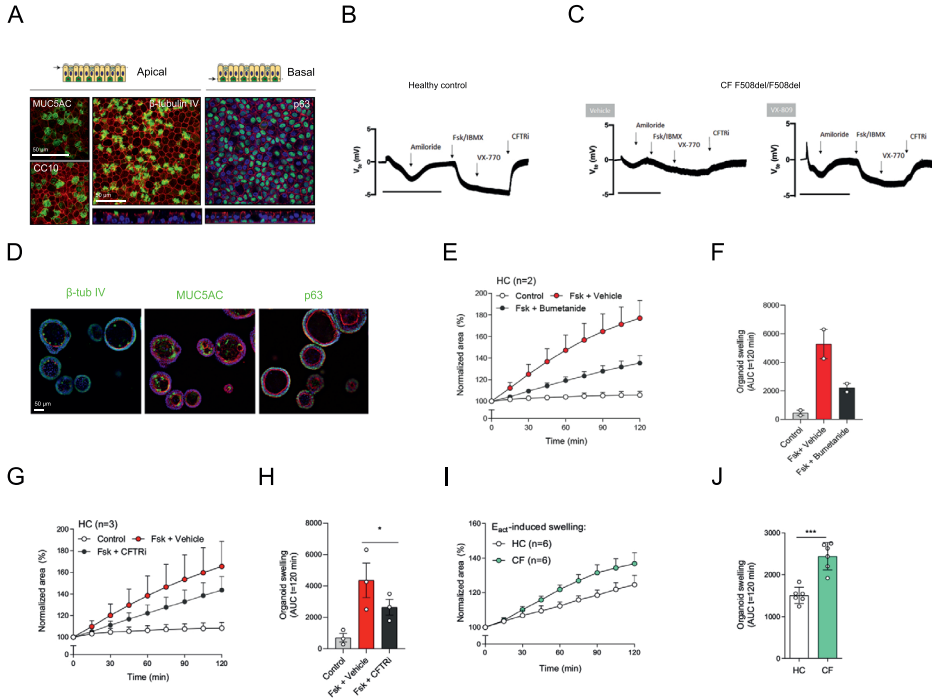
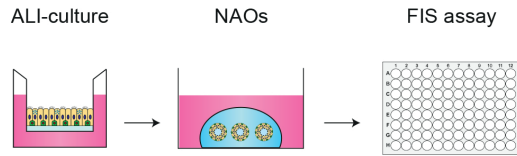


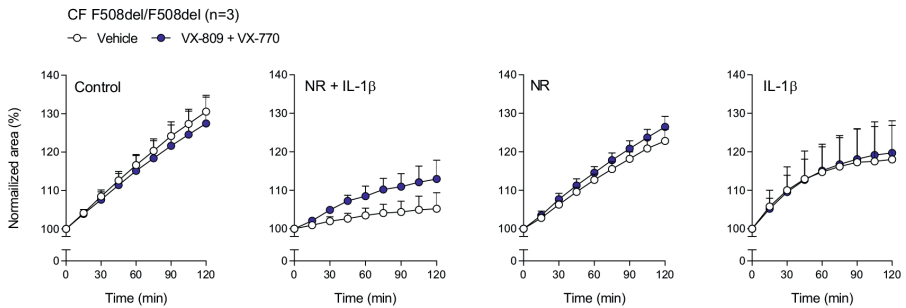
Figure S2: Characterization of ALI-HNEC and nasal airway organoid swelling assay.

(A) Whole-mount IF confocal images of ALI-HNEC, showing maximal projections of the apical side of the secretory cell markers MUC5AC and Club Cell protein 10 (CC10), and ciliated cell marker β -tubulin IV (Z-stack at the bottom). The projection of the basal side shows the basal cell marker p63 (Z-stack at the bottom). All markers are shown in green. **(B and C)** Open circuit Ussing chamber tracings showing trans-epithelial voltage measurements (V_{oc}) from Healthy control **(B)** and CF F508del/F508del **(C)** ALI-HNEC cultures. CF cultures were pre-treated with VX-809 or vehicle. During measurements, cells were treated sequentially with Amiloride, Fsk/IBMX, VX-770, and CFTRI. The bar corresponds to a 10 min frame. **(D)** IF staining of NAOs for β -tubulin IV, MUC5AC, and p63 (all in green). **(E and F)** HC nasal airway organoids (NAOs) (n=2 independent donors) were pre-treated with bumetanide or vehicle for 4 h, followed by stimulation with forskolin (Fsk) and assessment of FIS. **(G and H)** HC NAOs (n=3 independent donors) were pre-treated with CFTR inhibitors or vehicle, followed by assessment of FIS. **(I and J)** Comparison between HC and CF organoid swelling (both n=6 independent donors) after stimulation with the calcium-activated chloride channel agonist E_{act} . Data information: DAPI (blue) was used as nuclear staining, Phalloidin (red) was used as actin cytoskeleton staining (A and D). FIS assay results are depicted as the percentage change in surface area relative to $t=0$ (normalized area) measured at 15-min time intervals for 2 h (means \pm SD) **(E, G, I)** and as area under the curve (AUC) plots ($t=120$ min, means \pm SD) **(F, H, J)**. Analysis of differences was determined with a paired **(H)** or unpaired **(J)** t-test. * $p < 0.05$, *** $p < 0.001$.

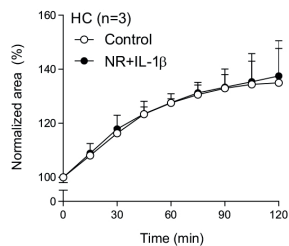
A



B



C



D

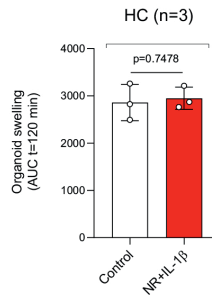


Figure S3: Optimization of CFTR modulator responses in NAOs with NR/IL-1 β .

(A) Illustration showing culturing of NAOs with neuregulin 1 β (NR) and interleukin-1 β (IL-1 β). (B) NAOs from F508del homozygous subjects with CF (n=3 independent donors) were cultured without additional stimuli (Control), with neuregulin (NR), interleukin-1 β (IL-1 β), or combination of both (NR+IL-1 β) for 5 days. At day 3, cultures were pre-treated with VX-809 or vehicle control for 48 h, and afterwards stimulated with forskolin (Fsk, 5 μ M), in combination with VX-770 or vehicle control. (C and D) Assessment of FIS in HC NAOs (n=3 independent donors) cultured under control conditions or NR+IL-1 β . FIS assay results are depicted as the percentage change in surface area relative to t=0 (normalized area) measured at 15-min time intervals for 2 h (means \pm SD) (B and C) and as area under the curve (AUC) plots (t=120 min, means \pm SD) (D). Analysis of differences was determined with a paired t-test (D).

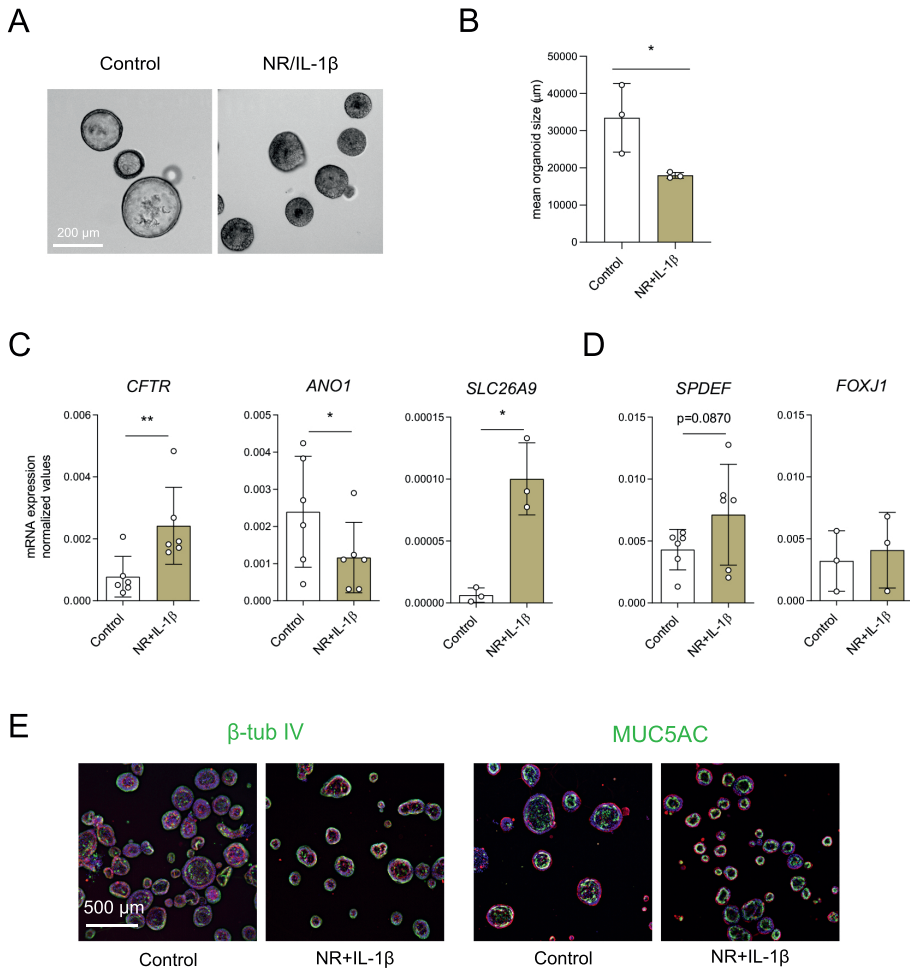


Figure S4: Characterization of NAOs cultured with NR/IL-1 β .

(A) Brightfield images of CF F508del/F508del NAOs cultured in control conditions or with NR+IL-1 β for 5 days. (B) Quantification of the mean organoid area (μ m², means \pm SD) of control and NR+IL-1 β cultured CF F508del/F508del NAOs (n=3 independent donors). (C and D) mRNA expression analysis of CF F508del/F508del NAOs (n=3-6 independent) that were left unstimulated (Control) or cultured with NR+IL-1 β for 5 days. mRNA expression was determined of (C) *CFTR*, *ANO1*, *SLC26A9*, (all chloride channels), (D) *SPDEF* (secretory cells) and *FOXJ1* (ciliated cells). Results represent target mRNA expression normalized for the geometric mean expression of the housekeeping genes *ATP5B* and *RPL13A* (means \pm SD). (E) Immunofluorescence staining of CF organoids (control and cultured with NR+IL-1 β for 5 days) was conducted of β -tubulin IV (ciliated cell) and MUC5AC (goblet cell) (green). DAPI (blue) was used for nuclear staining. Phalloidin (red) was used for actin cytoskeleton staining. Analysis of differences was determined with a paired t-test (B, C, D). * p<0.05, ** p<0.01.

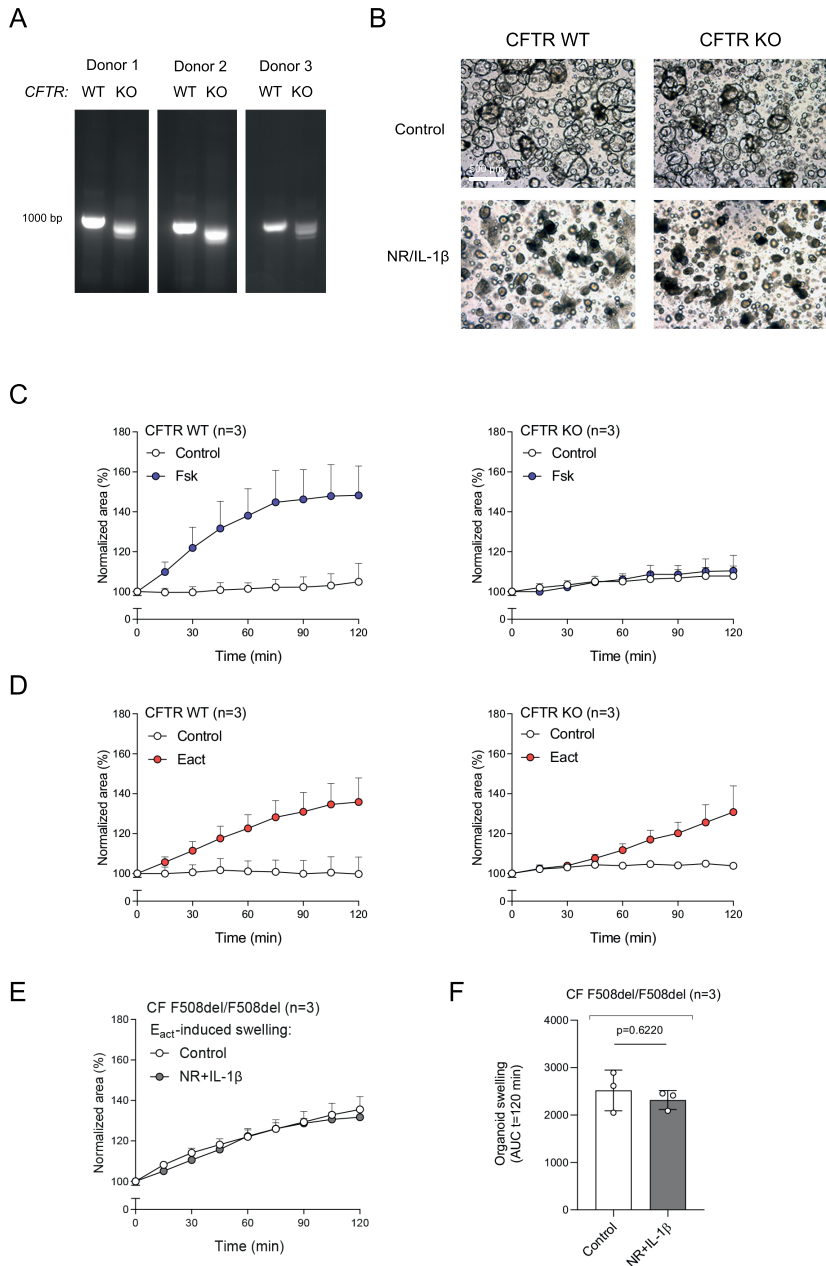


Figure S5: Validation of organoid swelling in CFTR KO cells generated with CRISPR-based gene editing.

(A) Confirmation of CFTR gene KO (n=3 independent donors) by agarose gel electrophoresis. (B) Brightfield images of CFTR WT and KO NAOs cultured in control conditions or with NR+IL-1 β for 5 days. (C) FIS and (D) E_{act} -induced swelling measured in CFTR WT or KO NAOs (n=3 independent donors). (E and F) E_{act} -induced swelling in CF F508del/F508del NAOs (n=3 independent donors). Organoid swelling results are depicted as the percentage change in surface area relative to t=0 (normalized area) measured at 15-min time intervals for 2 h (means \pm SD) (C, D, E) and as area under the curve (AUC) plots (t=120 min, means \pm SD) (F). Analysis of differences was determined with a paired t-test.

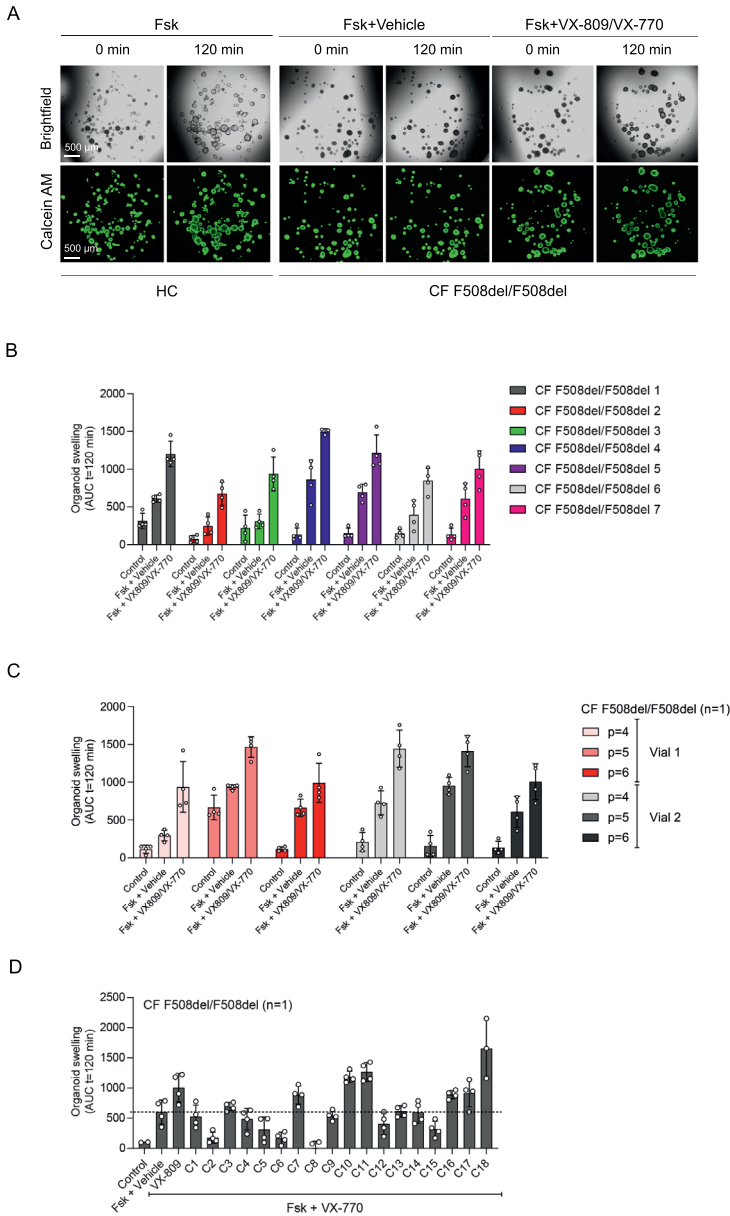


Figure S6: Comparison HC vs CF NAOs cultured with NR/IL-1 β and validation of VX-809/VX-770 responses. (A) Brightfield images (top) and images of calcein green AM-stained (bottom) NAOs cultured with NR/IL-1 β , showing FIS in HC and CF F508del/F508del cultures. FIS of CF NAOs was determined in combination with vehicle or VX809/VX-770. Images were taken at t=0, and 120 min. (B) VX-809/VX-770 modulator response measurement in NAOs of individual donor (n=7) with a CF F508del/F508del genotype. (C) Repeated measurements of VX-809/VX-770 modulator responses in CF F508del/F508del NAOs (n=1 independent donor) derived from ALI-cultures from serial passaged HNEC at p=4, p=5, and p=6, using cryopreserved cells from 2 different vials. (D) CF F508del/F508del NAOs (n=1 independent donor) were pre-treated with VX-809, or the CFTR correctors C1-18 for 48 hours. Afterwards, FIS was measured after stimulation with forskolin (Fsk) and VX-770. Vehicle was used as control. FIS assay results are depicted as area under the curve (AUC) plots (t=120 min, means \pm SD. Individual datapoints represent technical replicates.

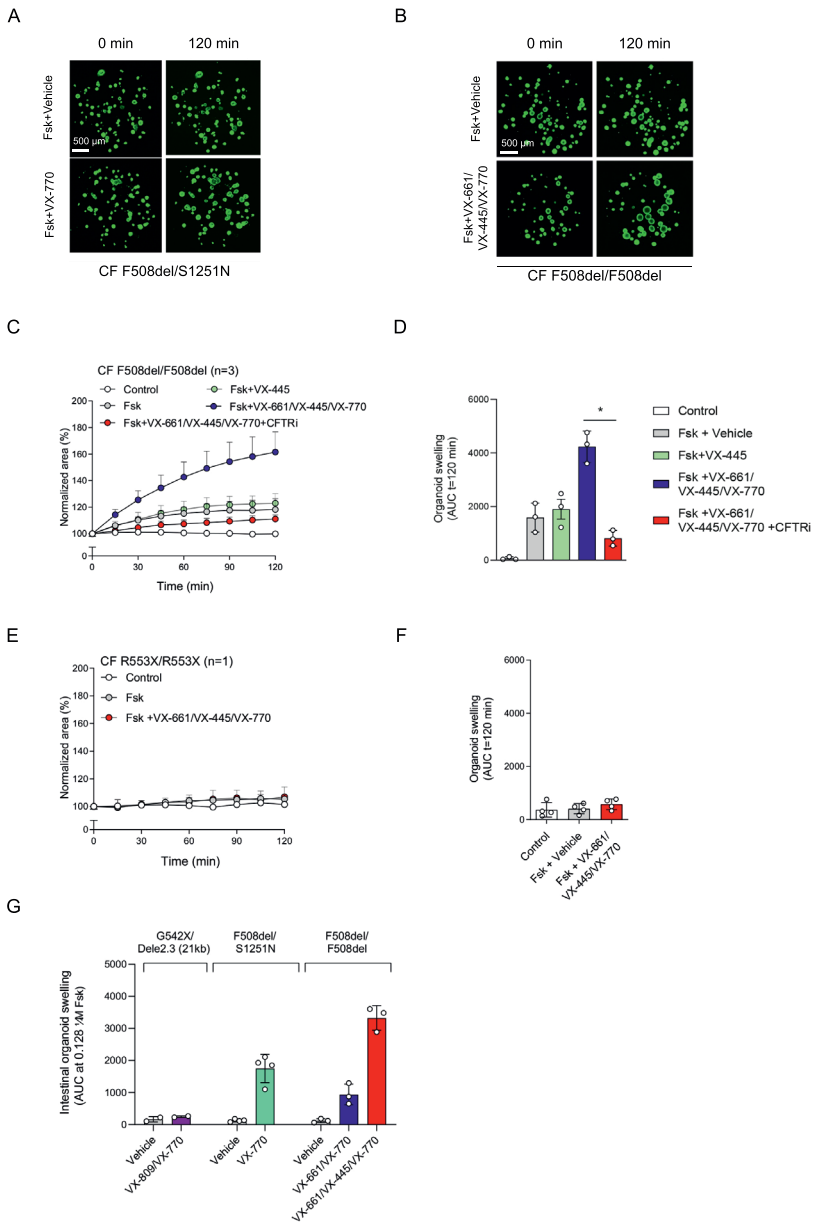


Figure S7: Validation of VX-770, VX-661/VX-445/VX-770, and FIS in intestinal organoids.

(A) Images showing FIS of NR+IL-1 β cultured NAOs from individuals with CF and F508del/S1251N genotype. NAOs were stimulated with Fsk and vehicle (top panels) or VX-770 (bottom panels). (B) Images of FIS conducted in calcein green AM-stained CF F508del/F508del NAOs cultured with NR/IL-1 β , pre-treated with vehicle (top panels) or triple CFTR modulator combination VX-661/VX-445/VX-770 (bottom panels). Images were taken at t=0, and 120 min. (C and D) CF F508del homozygous NAOs (n=3 independent donors) were pre-treated with vehicle, VX-445, or a combination of VX-661 and VX-445 for 48 h. Next, cultures were pre-treated with CFTR inhibitors CFTRinh-172 and GlyHI101 or vehicle for 4 h, followed by stimulation with Fsk together with VX-770 or vehicle as indicated. (E and F) R553X/R553X NAOs (n=1 independent donor) were pre-treated with vehicle or a combination of VX-661 and VX-445 for 48 h, followed by assessment of FIS after stimulation with Fsk together with VX-770 or vehicle as indicated. (G) FIS measured with indicated CFTR modulators in intestinal

Figure S7: (continued)

organoids from individuals with CF and G542X/Dele2,3(21kb) (n=2 independent donors), F508del/S1251N (n=4 independent donors), F508del/F508del (n=3 independent donors) genotypes, used for Pearson correlation in Figure 3J. Results are depicted as percentage increase in normalized area in time (means \pm SD) (C and E) and AUC plots (t=120 min, means \pm SD) (D, F, G). Datapoints represent individual donors (D, G) or technical replicates (F). Analysis of differences was conducted with a paired t-test (D) * $p < 0.05$.

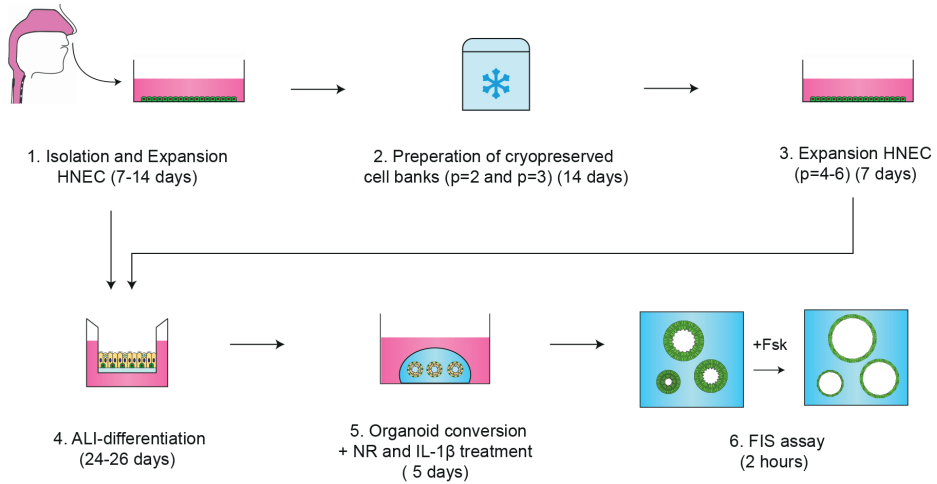


Figure S8: Graphic illustration of the whole timeline from nasal cell isolation till FIS assay in nasal airway organoids.

ONLINE SUPPLEMENTARY FILES

Supplementary information is available online at <https://doi.org/10.26508/lsa.202101320>

Video 1 - Live imaging of FIS measured in serial passaged nasal airway organoids.

Video showing FIS measured in serial passaged healthy control nasal airway organoids, showing only swelling of a few large organoids within the same culture.

Video 2 - Live imaging of FIS measured in ALI-cultured derived nasal airway organoids. Video showing FIS measured in HC nasal airway organoids, showing equal swelling of all organoids within the same culture.

Video 3 - Live imaging of an ALI-cultured derived nasal airway organoids. Video recording of a CF nasal airway organoid showing beating cilia at the luminal side of the structure and accumulated mucus.

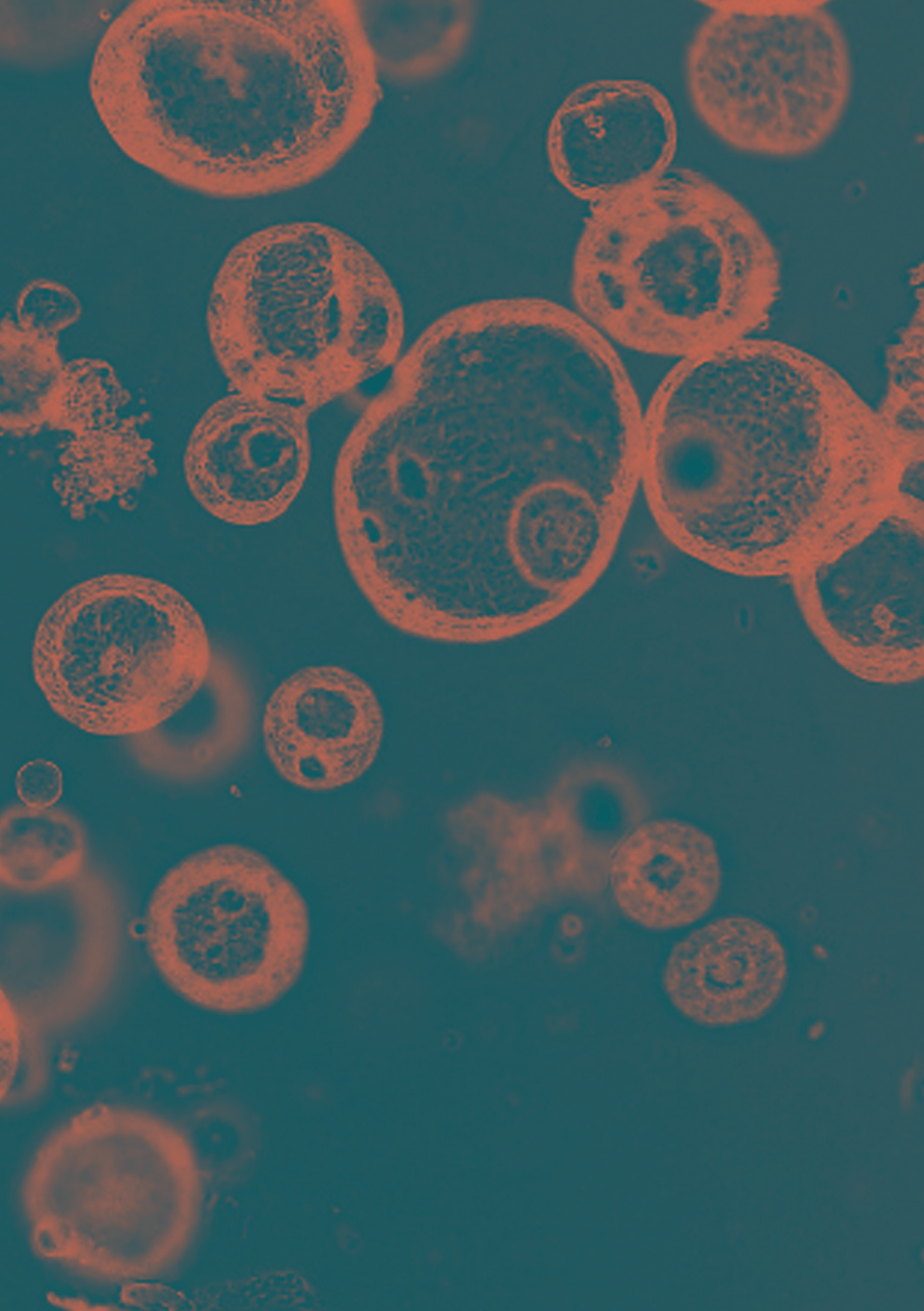
Table S1 - Use of HNEC donors in the depicted figures.

Table S2 - Composition of BC isolation and expansion medium

Table S3 - Composition of 2D air-liquid interface differentiation medium

Table S4 - Composition of airway organoid medium

Table S5 - qPCR primer sequences



Chapter 3

Drug repurposing for cystic fibrosis: identification of drugs that induce CFTR-independent fluid secretion in nasal organoids

Lisa W. Rodenburg, Livia Delpiano, Violeta Railean, Raquel Centeio, Madalena C. Pinto, Shannon M. A. Smits, Isabelle S. van der Windt, Casper F. J. van Hugten, Sam F. B. van Beuningen, Remco N. P. Rodenburg, Cornelis K. van der Ent, Margarida D. Amaral, Karl Kunzelmann, Michael A. Gray, Jeffrey M. Beekman and Gimano D. Amatngalim

International Journal of Molecular Sciences 2022, 23 (20); 12657

ABSTRACT

Individuals with cystic fibrosis (CF) suffer from severe respiratory disease due to a genetic defect in the cystic fibrosis transmembrane conductance regulator (CFTR) gene, which impairs airway epithelial ion and fluid secretion. New CFTR modulators that restore mutant CFTR function have been recently approved for a large group of people with CF (pwCF), but ~19% of pwCF cannot benefit from CFTR modulators. Restoration of epithelial fluid secretion through non-CFTR pathways might be an effective treatment for all pwCF. Here, we developed a medium-throughput 384-well screening assay using nasal CF airway epithelial organoids, with the aim to repurpose FDA-approved drugs as modulators of non-CFTR-dependent epithelial fluid secretion. From a ~1400 FDA-approved drug library, we identified and validated 12 FDA-approved drugs that induced CFTR-independent fluid secretion. Among the hits were several cAMP-mediating drugs, including β 2-adrenergic agonists. The hits displayed no effects on chloride conductance measured in the Ussing chamber, and fluid secretion was not affected by TMEM16A, as demonstrated by knockout (KO) experiments in primary nasal epithelial cells. Altogether, our results demonstrate the use of primary nasal airway cells for medium-scale drug screening, target validation with a highly efficient protocol for generating CRISPR-Cas9 KO cells and identification of compounds which induce fluid secretion in a CFTR- and TMEM16A-independent manner.

INTRODUCTION

Cystic fibrosis (CF) is a monogenic, recessive disease caused by mutations in the gene encoding for the cystic fibrosis transmembrane conductance regulator (CFTR) protein. Currently, 2110 different *CFTR* gene mutations have been described (<http://www.genet.sickkids.on.ca/>, accessed on 13 September 2022), which can be further classified based on CFTR defect, i.e., impaired CFTR mRNA/protein expression (class I/VII mutations), protein trafficking (class II) or gating (class III). Depending on the severity of the defect, CFTR dysfunction leads to impaired secretion of chloride and bicarbonate and subsequently affects fluid transport and pH regulation of secreted fluid across epithelial tissues ^{1,2}. People with CF (pwCF) may therefore experience severe dysfunction of epithelial tissues, including the respiratory tract, pancreas and liver ³.

Respiratory disease in pwCF is mainly caused by CFTR dysfunction in airway epithelial cells, which disturbs airway surface fluid secretion and causes the accumulation of thick mucus in the airways. Thick mucus leads to impaired mucociliary clearance, causing frequent and severe pulmonary infections. Restoring CFTR-dependent fluid secretion in airway epithelial cells may, therefore, reduce respiratory illness by resolving airway mucus obstruction. Recently, CFTR triple modulator therapy (elexacaftor/tezacaftor/ivacaftor), which restores CFTR-dependent anion and fluid secretion in CF airway epithelial cells, has been approved for pwCF carrying at least one copy of the most common F508del class II trafficking mutation ^{4,5}. Furthermore, CFTR potentiator therapy (ivacaftor) can improve CFTR protein function in pwCF carrying a class III gating mutation ⁶. Indeed, current therapeutic strategies to restore CFTR function highly depend on the type of CFTR defect. However, there is a remaining unmet need for ~19% of pwCF who are not eligible for CFTR modulator therapy, and only have access to symptomatic therapies ⁷. Importantly, it was reported that among pwCF who are eligible for these drugs worldwide, only 12% are actually having access to them ⁸, given their excessive cost ⁹.

Alternative therapies to restore epithelial fluid secretion in pwCF who do not respond to CFTR modulators or do not have access to them may be accomplished in a CFTR-independent manner by activating other chloride channels and transporters. As this approach bypasses CFTR, this CFTR-mutation agnostic approach may be suitable for all pwCF. A promising target for promoting CFTR-independent fluid secretion might be the calcium-activated chloride channel TMEM16A ¹⁰⁻¹². TMEM16A was chosen because it is one of the most extensively studied alternative chloride channels and the therapeutic potential is demonstrated by clinical evaluation of the compound ETD002, which enhances activity of TMEM16A in pwCF ¹³. An alternative approach to modify

airway epithelial fluid homeostasis is through modulation of the epithelial sodium channel ENaC^{14,15}. However, clinical interventions targeting ENaC have thus far not yielded clear clinical benefit^{14–16}. A large effort in the field currently aims to identify and prioritize additional therapeutic targets that modify airway epithelial ion and fluid secretion, independently of CFTR. However, the study of such pathways and targets in primary airway epithelial cells remains technically highly challenging due to lack of sufficient throughput in assays and the inability to efficiently genetically engineer primary airway cells.

In a previous study, we described a method that enables culturing of airway organoids from minimal-invasive nasal brushings¹⁷. Nasal organoids resembled a mucociliary differentiated airway epithelium. Furthermore, organoid swelling was used to measure epithelial fluid secretion induced by CFTR-modulating drugs, but we also observed CFTR-independent fluid secretion in organoids from pwCF. Based on this, we proposed that CF nasal organoids can be used as a platform to identify mechanisms of CFTR-independent fluid secretion and to identify modulators of such pathways.

Here, we miniaturized the previously described airway organoid fluid secretion assay to a 384-well plate format to facilitate primary airway epithelial fluid secretion studies at higher throughput. This assay was then used to screen ~1400 FDA-approved drugs for agonists of fluid secretion in CF primary nasal airway organoids. A brightfield image analysis platform was further developed to measure nasal organoid swelling as result of luminal organoid fluid secretion, based on a previously developed artificial intelligence-based imaging platform¹⁸. Finally, we demonstrate an efficient procedure to generate a gene knockout (KO) in primary nasal epithelium for mode-of-action studies of validated hits.

RESULTS

Nasal organoids from donors without functional CFTR display CFTR-independent fluid secretion

First, we wanted to confirm that nasal organoids can be used to measure CFTR-independent fluid secretion as suggested by previous work with F508del/F508del nasal organoids¹⁷. Cryopreserved airway basal progenitor cells were fully differentiated at an air-liquid interface (ALI), followed by formation of nasal organoids from epithelial sheets of these differentiated ALI cultures (Figure 1A). These organoids (F508del/S1251N) were well-differentiated, displaying both MUC5AC+ goblet cells and β -tubulin IV+ ciliated cells (Figure 1B). In line with earlier observations in CF nasal and bronchial organoids^{17,19}, nasal organoids from a donor without CFTR function

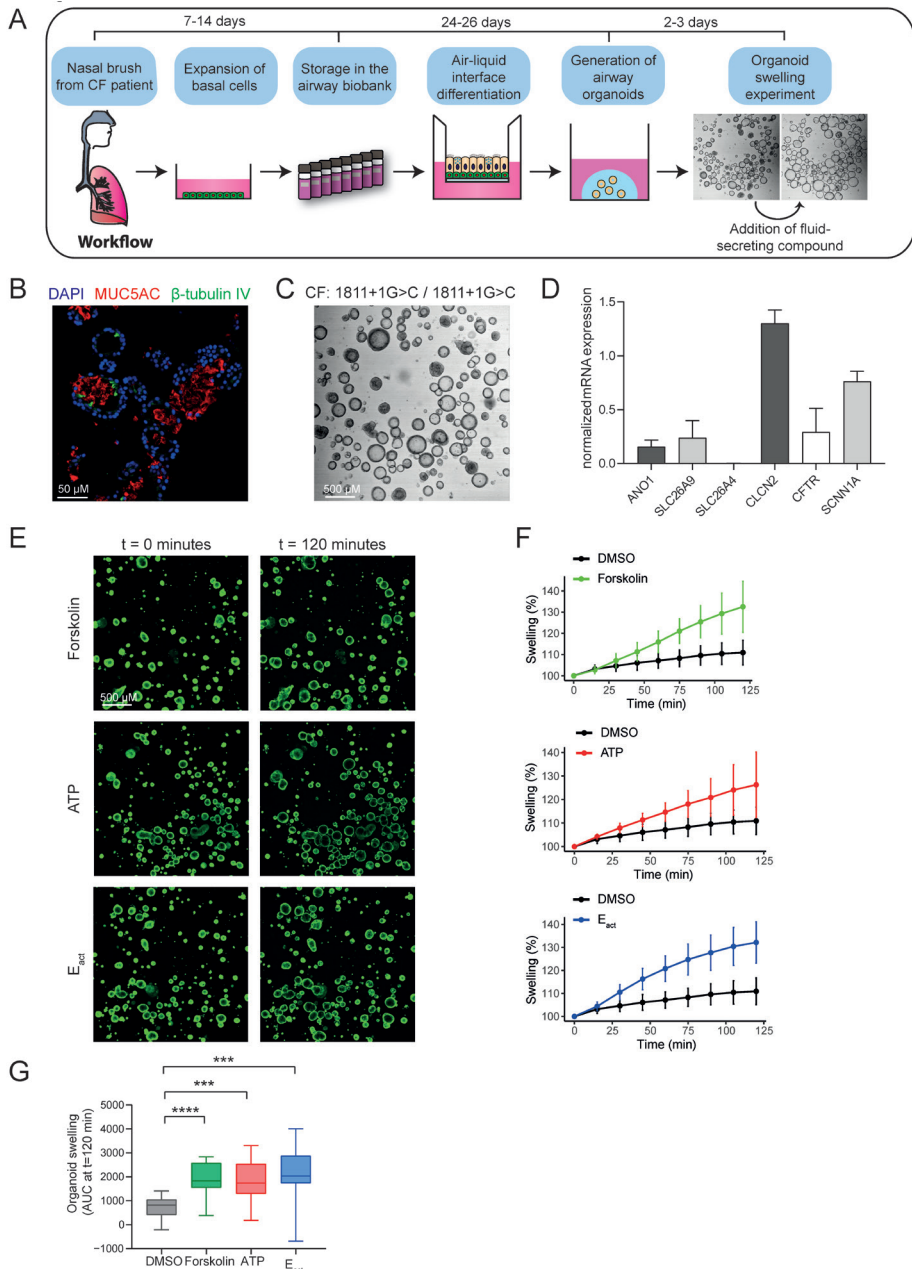


Figure 1. Characterization of CF nasal organoids and CFTR-independent organoid swelling.

(A) Schematic representation of the project workflow from nasal brush towards organoid swelling experiments; (B) immunofluorescence staining of nasal organoids with the secretory cell marker MUC5AC (red), ciliated cell marker β -tubulin IV (green) and DAPI (blue) from a CF donor (F508del/S1251N); (C) brightfield image showing intrinsic lumen formation of unstimulated nasal organoids from a CFTR-null donor (1811+1G>C/1811+1G>C);

Figure 1. (continued)

(D) mRNA expression in CFTR-null nasal organoids of the following ion channels/transporters: ANO1 (TME-M16A), SLC26A9, SLC26A4, CLCN2, SCNN1A and CFTR ($n = 3$ independent donors; W1282X/1717-1G>A, R553X/R553X, G542X/CFTRdele2.3(21 kb)); (E) confocal images of CFTR-null (G542X/CFTRdele2.3(21 kb)) nasal organoids, stimulated with forskolin (5 μ M), ATP (100 μ M) or Eact (10 μ M) at 0 and 120 min; (F) quantification of CFTR-null (G542X/CFTRdele2.3(21 kb), $n = 5$ replicates) nasal organoid swelling after stimulation with forskolin, ATP or Eact; (G) area under the curve (AUC) plots of nasal organoid swelling in three CFTR-null donors ($n = 3$ independent donors; W1282X/1717-1G>A, R553X/R553X, G542X/CFTRdele2.3(21 kb); 2–6 replicates per donor) after stimulation with forskolin, ATP or Eact. Analysis of difference with control was determined with a one-way ANOVA with Dunnett's post hoc test (G). *** $p < 0.001$, **** $p < 0.0001$.

(1811+1G>C/1811+1G>C, a severe splice mutation) showed intrinsic lumen formation without any stimulation (Figure 1C), suggesting CFTR-independent epithelial fluid transport. To demonstrate detectable expression of alternative ion channels and transporters, we conducted qPCR experiments in nasal organoids from three donors with class I/VII mutations, leading to no CFTR protein (W1282X/1717-1G>A, R553X/R553X, G542X/CFTRdele2.3(21 kb)). Here we confirmed detectable mRNA expression of ANO1/TMEM16A, SLC26A9, CLCN2 and ENaC/SCNN1A (Figure 1D). Interestingly, mRNA expression of some ion channels or transporters is higher compared to others; however, further research is needed in a larger donor cohort to demonstrate a relationship between CF disease and alternative ion channel expression. The same organoids displayed CFTR-independent forskolin-induced swelling (FIS) as quantified by 2h organoid swelling measurements (Figure 1E–G). Furthermore, organoid swelling was also observed after stimulation with ATP or Eact, potentially through modulation of calcium-dependent channels or transporters, including TMEM16A and TRPV4 (Figure 1E–G)²⁰. Altogether, these findings confirm CFTR-independent fluid secretion in CF nasal organoids.

Nasal organoid swelling in a 384-well plate format

We next set out to develop a 384-well plate fluid secretion screening assay in nasal organoids to enable analysis of ion and fluid transport studies at higher throughput. As calcein green labelling of nasal organoids was technically challenging in this plate format, we developed an alternative approach for quantifying organoid swelling based on organoid recognition with OrgaQuant¹⁸. This is an open-source deep convolutional neural network, trained to recognize cystic intestinal organoids in brightfield images. To validate organoid recognition and quantification of organoid swelling in 384-well plates using OrgaQuant, we determined the effect of the CFTR potentiators VX-770 (ivacaftor) and PTI-808 (dirocaftor), which both facilitate opening of the CFTR channel, on FIS in CF nasal organoids with a S1251N CFTR gating mutation. Assay validation was performed in this particular donor with high responses to CFTR-modulating drugs to obtain a larger range of organoid swelling measurements. The OrgaQuant model was indeed able to recognize spherical nasal organoids, and the surface area could be estimated using the OrgaQuant bounding boxes, assuming organoids

had a disk shape (Figure 2A). Moreover, based on particle tracking, we were able to follow individual organoids over time by live imaging²¹. Organoid surface areas were subsequently calculated for each time point, linear regression was performed to determine swell rates for individual organoids and the mean swell rate of all organoids within a well was calculated (Figure 2B). Based on this quantification method, we observed a significant increase in FIS of organoids stimulated with VX-770 or PTI-808 compared to vehicle control or forskolin alone (Figure 2C). Furthermore, we observed a correlation between swell rates that were measured with the OrgaQuant model and the conventional quantification method with area under the curve (AUC) values from fluorescent-labelled organoids (Figure 2D, E). In addition to CFTR modulator responses in FIS, we were able to quantify CFTR-independent Eact-induced swelling in CF nasal organoids in brightfield images using the OrgaQuant model (Figure 2F). Thus, we conclude that this newly developed method to quantify organoid swelling in brightfield images is suitable for fluid secretion assays in a 384-well plate format.

Screening of FDA-approved drugs in CF nasal organoids

Next, we aimed to identify FDA-approved drugs that could induce CFTR-independent fluid secretion in CF nasal organoids. We conducted a primary screening assay in which we examined the effect of ~1400 FDA-approved drugs on organoid swell rate over 3 h using nasal organoids from four pwCF (F508del/F508del, F508del/F508del, F508del/W846X, 1811+1G>C/1811+1G>C; Figure 3A). These donors had no functional CFTR at the plasma membrane, due to mutations leading to impaired trafficking, misfolded CFTR or no production of CFTR mRNA or protein. Two compounds were combined within a single well of a 384-well plate to reduce experimental conditions and time, and Eact, a compound known to activate calcium-dependent fluid secretion, was used as a positive control. Because of the variation in baseline swelling (without compound) among assay plates and donors (Figure S1A, B), a plate-normalization step was performed (Figure S1C). After normalization, swell rates from different replicates and donors were averaged for all compounds (Figure 3B). Wells with a plate-normalized swell rate higher than 1, corresponding to 1 interquartile range (IQR) above the median swell rate of all compounds, were defined as a hit (Figure 3B–E). This resulted in 90 compounds, divided over 45 wells, that were selected for validation in a secondary screening.

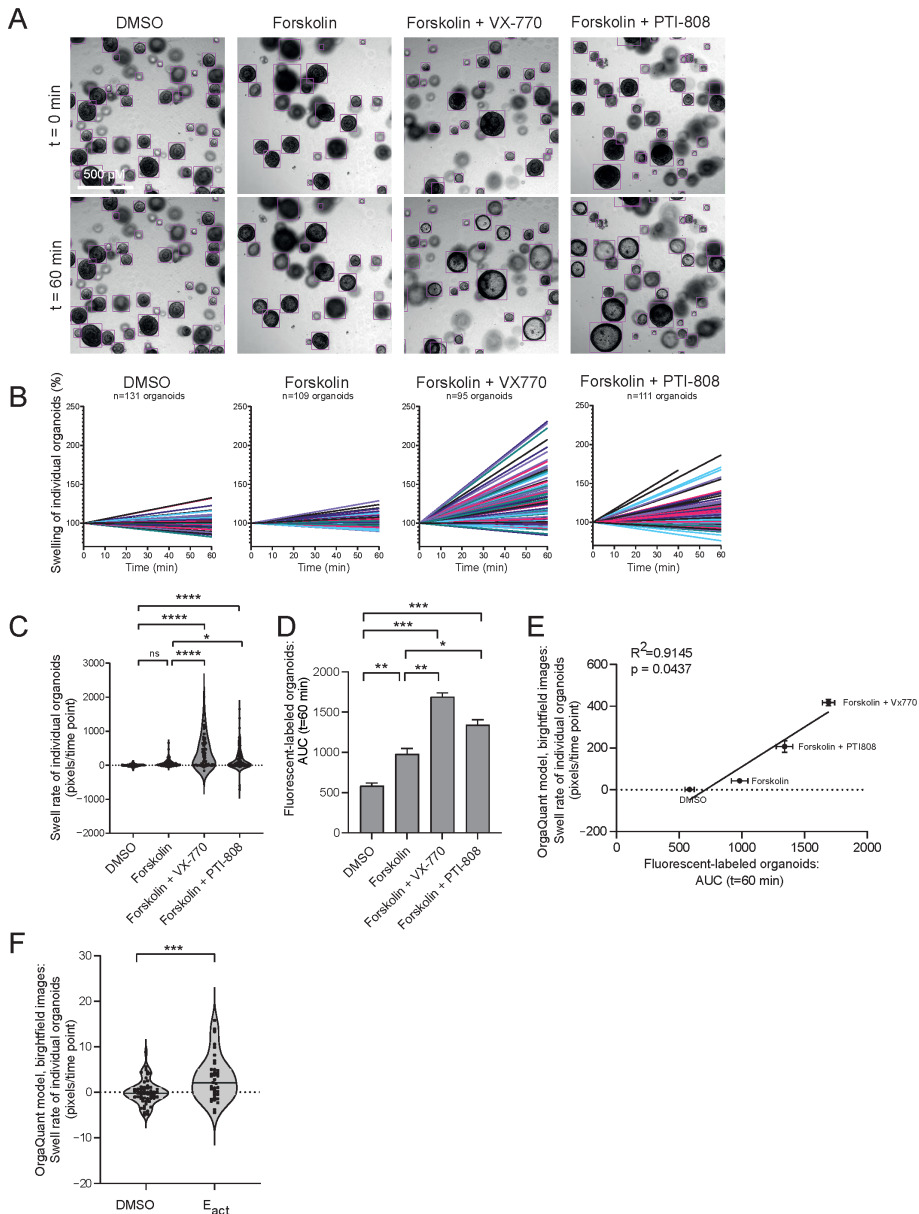


Figure 2. Quantification of nasal organoid swelling in a 384-well plate format by the OrgaQuant neural network. (A) Representative brightfield images showing automatic recognition of CF nasal organoids (F508del/S1251N) with the OrgaQuant model¹⁸. To examine swelling, organoids were treated with the vehicle DMSO, forskolin alone (5 μ M) or a combination of forskolin (5 μ M) with the CFTR potentiators VX-770 (5 μ M) or PTI-808 (1 μ M); (B) graphs show percentage change in surface area relative to t = 0 (100%) of individual organoids, treated with vehicle DMSO, forskolin, forskolin with VX-770 or forskolin with PTI-808, corresponding to the wells from (A). Each line represents an individual organoid; (C) swell rates (pixels/time point) of individual organoids from the wells shown in (A) are displayed (one representative well per condition is shown); (D) analysis of FIS using the conventional quantification method in fluorescent-labelled organoids, using the same donor as in (A–C) (n = 1 donor, F508del/S1251N, 2 biological replicates). Organoids were treated with vehicle DMSO, forskolin (5 μ M), forskolin with Vx770 (5 μ M) or forskolin with PTI-808 (1 μ M). AUC is used as outcome measurement for organoid swelling;

Figure 2. (continued)

(E) correlation between two analysis methods for FIS in a similar donor: in the new developed method, organoids in brightfield images are recognized using OrgaQuant and swell rate (pixels/time point) is used as outcome measurement for swelling. In the conventional method, fluorescent-labelled organoids are recognized with image software Zen Blue and AUC values are used as outcome measurement for swelling; (F) swell rates of individual organoids within a single well stimulated with DMSO or E_{act} (10 μ M) in a CFTR-null donor (1811+1G>C/1811+1G>C). Analysis of differences was performed using unpaired *t*-tests (F), one-way ANOVA with Tukey post hoc test (C, D) or Pearson correlation (E). ns = non-significant, * $p < 0.05$, ** $p < 0.01$, *** $p < 0.001$, **** $p < 0.0001$.

Identification of hit compounds that induce CFTR-independent organoid swelling

To further identify and validate the hit FDA-approved compounds from the primary screening assay on their potential to induce CFTR-independent fluid secretion, we conducted a secondary screening assay. This was executed using the conventional 96-well plate format. Secondary screening was conducted in the same four CF donors as the primary screening assay, which lack functional CFTR at the plasma membrane, but now testing only one compound per well (Figures 4A and S2A). Amongst the compounds that were screened in the secondary screening assay, 12 hit compounds were selected for further studies (Figure 4B, C). Selection was based on a combination of safety profile, experience with chronic use in other diseases and effectiveness in the CFTR-null donor (1811+1G>C/1811+1G>C). Additionally, a selection of compounds with a similar mode-of-action was made, as many cAMP-inducing compounds, including β 2-adrenergic agonists, were among the top compounds. Next, to exclude a potential role for residual CFTR function in mediating nasal organoid swelling by the hit compounds, we conducted a final validation study in nasal organoids from three other CFTR-null donors (W1282X/1717-1G>A, R553X/R553X, G542X/CFTRdele2.3(21 kb)). These experiments were performed with the conventional swelling assay with fluorescent-labelled organoids in 96-well plate format. All compounds, except Benidipine, significantly induced swelling of nasal organoids from CFTR-null donors (Figure 4D–F). The discrepancy in significance between compounds with a similar effect size might be due to a higher number of measurements for some compounds, resulting in higher power for statistics. Differences in the magnitude of organoid swelling and ranking of the hit compounds between the secondary screening assay (Figure 4B) and the validation in CFTR null donors (Figure 4D) might be due to the use of different donors or different compound batches (FDA drug library versus powders).

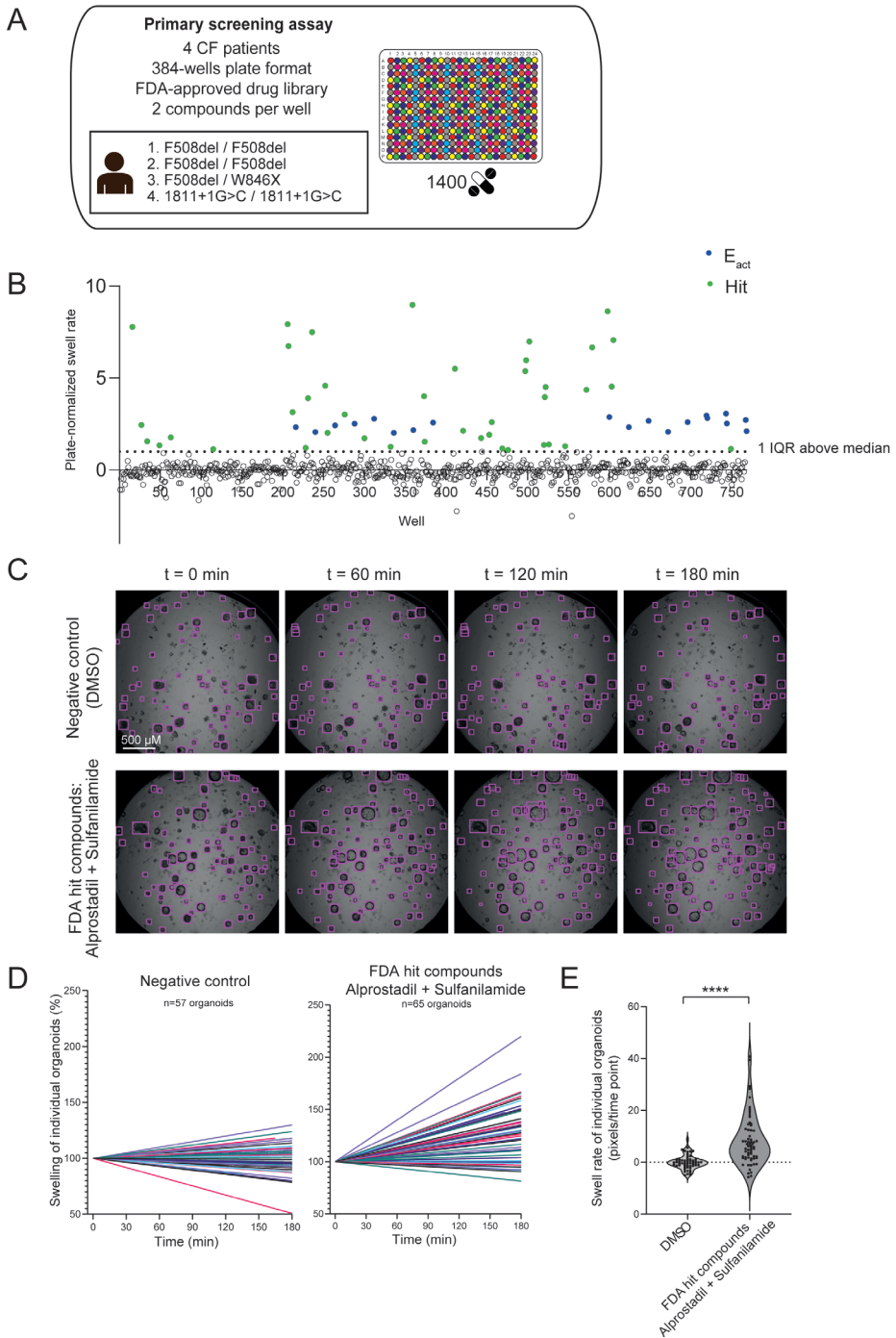


Figure 3. Primary screening assay of an FDA-approved drug library in CF nasal organoids.

(A) ~1400 FDA-approved drugs (3 μ M) were screened in a 384-well plate format in nasal organoids from 4 pwCF. Two compounds were combined in a single well; (B) the graph represents mean plate-normalized swell rates of four CF donors. A total of 90 compounds (shown in green), divided over 45 wells, with a plate-normalized swell rate above 1 IQR

Figure 3. (continued)

above the median were selected from the primary screening assay for the secondary screening assay. E_{act} (10 μ M, shown in blue) was used as positive control (n = 4 independent donors; F508del/F508del, F508del/F508del, F508del/W846X, 1811G>C/1811+1G>C, 1–3 replicates per donor); (C) representative brightfield images showing automatic recognition of nasal organoids (CF: 1811+1G>C/1811+1G>C) using the OrgaQuant model¹⁸. Examples are shown from a well containing DMSO as negative control (upper panel) and a well containing FDA hit compounds (lower panel); (D) graphs show percentage change in surface area relative to t = 0 (100%) of individual organoids, treated with vehicle DMSO (left panel) or FDA hit compounds (right panel), corresponding to the organoids shown in (C). Each line represents an individual organoid; (E) quantification of swell rates of individual organoids from the example wells shown in (C, D). Analysis of differences was performed using an unpaired *t*-test (E). *****p* < 0.0001.

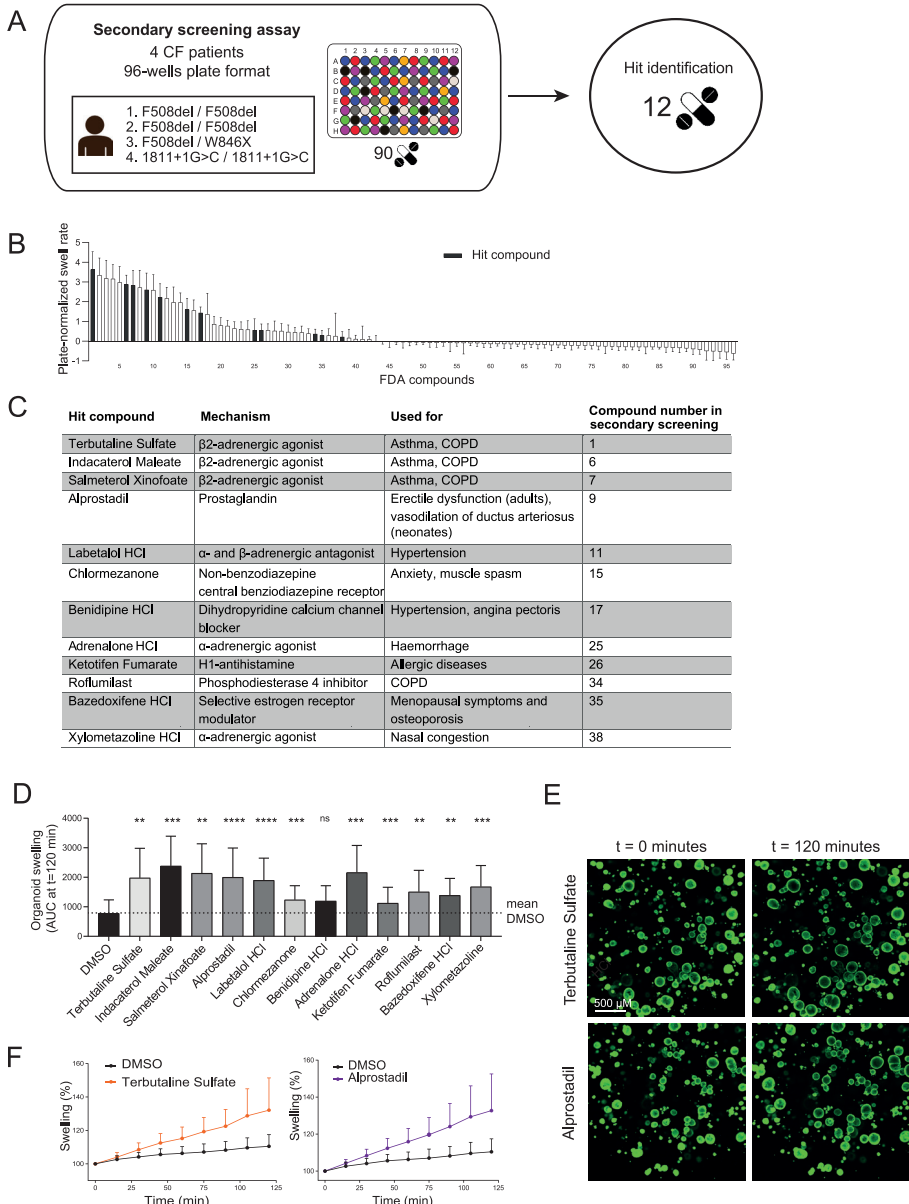
**Figure 4.** Secondary screening assay and validation of FDA hit compounds in CFTR-null donors.

Figure 4. (continued)

(A) A total of 90 hit compounds identified in the primary screening assay were further validated in the conventional 96-well plate format with one compound per well; (B) the graph represents mean plate-normalized swell rates of four donors. Hit compounds were selected based on swell rate and working mechanism ($n = 4$ independent donors; F508del/F508del, F508del/F508del, F508del/W846X, 1811G>1>C/1811>1G>C, 3 replicates per donor); (C) overview of the 12 hit compounds with their working mechanism, disease application and ranking in the secondary screening assay; (D) the 12 hit compounds were further evaluated in an organoid swelling assay with CFTR-null nasal organoids ($n = 3$ independent donors: G542X/CFTRdele2.3(21kb), W1282X/1717-1G>A, R553X/R553X, $n = 2-7$ measurements per donor). The compounds are ranked based on their effect size in the secondary screening assay, shown in (B). The conventional image analysis was applied using fluorescent-labelled organoids. Organoid swelling is shown as AUC values from measurements of 120 min; (E) representative confocal images of CFTR-null (R553X/R553X) nasal organoids, stimulated with Terbutaline Sulfate or Alprostadil (both $3 \mu\text{M}$) as example of two hit compounds at 0 and 120 min. (F) Quantification of CFTR-null (R553X/R553X) nasal organoid swelling after stimulation with Terbutaline Sulfate or Alprostadil (both $3 \mu\text{M}$). Differences with baseline are analyzed using a one-way ANOVA with Dunnett's post hoc test (D). ns = non-significant, ** $p < 0.01$, *** $p < 0.001$, **** $p < 0.0001$.

Generation and validation of TMEM16A KO nasal epithelial cells

Based on earlier results in swelling assays with the TMEM16A activator ATP (Figure 1E, F), we hypothesized that TMEM16A may contribute to CFTR-independent nasal organoid swelling. To further investigate this, we created TMEM16A gene KO nasal epithelial cells using the CRISPR-Cas9 technology. These TMEM16A KO cells were generated by use of electroporation in nasal cells from three CFTR-null donors (W1282X/1717-1G>A, R553X/R553X, G542X/CFTRdele2.3(21 kb)). To enhance efficiency, the TMEM16A locus was targeted using a mix of three different sgRNAs (Figure 5A). KO efficiency was first validated by DNA gel electrophoresis (Figure 5B) and Sanger sequencing, which revealed KO efficiencies of 95%, 87% and 88% for the three donors, respectively. Because of the high KO efficiencies, a selection step was not needed, and we therefore continued with a polyclonal cell population. For optimal validation of the TMEM16A gene KO efficiency, we also characterized cells that were stimulated with the pro-inflammatory cytokine IL-4, which is known to enhance TMEM16A expression and function^{10,22}. First, TMEM16A protein levels were assessed in ALI-differentiated KO cells using Western blot under normal and IL-4 treated conditions (for 48 h). Under both conditions, a near-complete KO phenotype was observed (Figure 5C, D). As a final functional validation, TMEM16A-dependent chloride conductance was determined in ALI-differentiated KO nasal cells in Ussing chamber experiments (Figure 5E, F). UTP-induced short-circuit currents (Isc), which were sensitive to the TMEM16A-inhibitor Ani9, were used as a measurement of TMEM16A activity²³. Quantification of the UTP-induced peak currents showed a partial Ani9-sensitivity in the control cells, suggesting TMEM16A to be responsible for more than half of the UTP-induced currents. In TMEM16A KO cells, UTP-induced currents were significantly reduced and not affected by Ani9. As expected, in IL-4-treated control cells, UTP-stimulated currents

were markedly enhanced and inhibited significantly by Ani9. In IL-4-treated KO cells, UTP-stimulated currents were small, and not affected by Ani9, similar to non-IL-4 KO cells. Altogether, these results confirm a functional TMEM16A KO in CFTR-null nasal epithelial cells, which can be further used to examine whether TMEM16A mediates nasal organoid swelling.

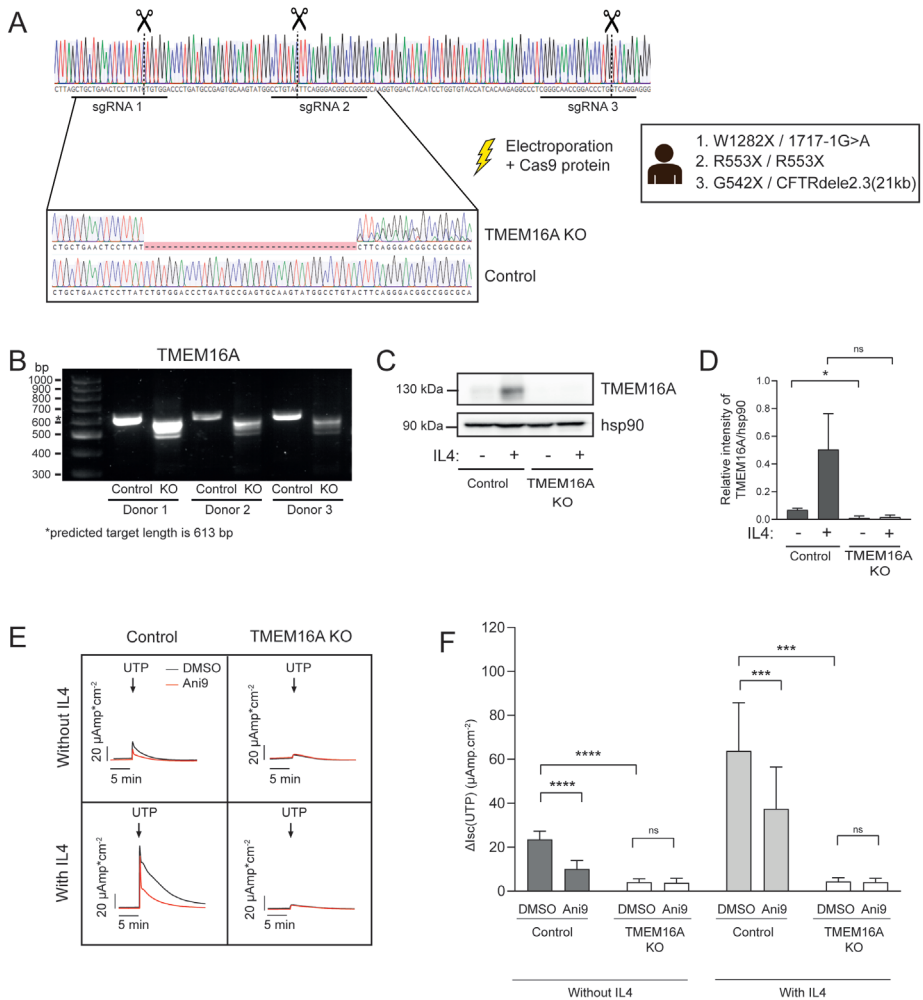


Figure 5. Generation and validation of TMEM16A KO nasal epithelial cells, generated by CRISPR-Cas9 gene editing in CFTR-null nasal cells. (A) Graphical overview showing binding sites of three sgRNA molecules and Sanger sequencing traces after electroporation; (B) DNA gel showing the PCR-amplified products of the targeted *TMEM16A* locus for KO and control samples of 3 CFTR-null donors (G542X/CFTRdele2.3(21kb), W1282X/1717-1G>A, R553X/R553X). Predicted length of the PCR product was 613 bp; (C) representative Western blot for TMEM16A protein of ALI-differentiated TMEM16A KO and control cells. To increase TMEM16A expression, some cells were treated with IL-4 for 48 h; (D) quantified band intensity of TMEM16A protein in Western blots

Figure 5. (continued)

(*n* = 3 independent donors); **(E)** functional validation of ALI-differentiated TMEM16A KO cells with Ussing chamber measurements. TMEM16A activity was determined based on Ani9-sensitive (1 μ M) UTP-induced (100 μ M) currents. Representative traces are shown of one donor and **(F)** UTP-induced currents were quantified for all donors, with and without Ani9-treatment (*n* = 3 independent donors). All cells were treated with amiloride and indicated cells were treated with IL-4 for 48 h. Analysis of differences was performed using paired *t*-tests (D) or a 2-way ANOVA with Tukey post hoc test (F). ns = non-significant, * *p* < 0.05, *** *p* < 0.001, **** *p* < 0.0001.

Hit compounds induce TMEM16A-independent fluid secretion

Next, we aimed to determine whether the 12 remaining hit compounds induced swelling of organoids, generated from ALI-differentiated TMEM16A KO nasal cells. We observed no differences in lumen formation between TMEM16A KO and control organoids without any stimulation (Figure 6A, B). This suggests no role of TMEM16A in intrinsic lumen formation of CFTR-null nasal organoids. Next, ATP-induced organoid swelling was studied, as ATP is known to activate TMEM16A. We did not observe a decline in ATP-induced swelling in TMEM16A KO organoids in regular organoid culture conditions. In contrast, ATP-induced organoid swelling was reduced in IL-4-treated TMEM16A KO organoids (Figure S3A–C). This suggests that ATP-induced swelling mediated by TMEM16A is only detected upon IL-4-stimulation. Next, we further validated the 12 FDA-approved hit compounds in TMEM16A KO nasal organoids. However, no significant differences were observed in swelling between KO and control organoids, suggesting no TMEM16A involvement in epithelial fluid secretion induced by the hit compounds (Figure 6C–E).

Effect of hit compounds on chloride conductance and TMEM16A activating effects

We further conducted mode-of-action studies with the hit compounds to determine effects on chloride conductance and TMEM16A-activating effects. First, the effect of acute addition of the hits on resting *I*_{sc} was investigated in ALI-differentiated CFTR-null nasal cells (W1282X/1717-1G>A, R553X/R553X, G542X/CFTRdele2.3(21 kb)) by Ussing chamber measurements (Figure 7A). In contrast to organoid swelling, the hit compounds did not induce any measurable change in *I*_{sc} in ALI cultures of corresponding donors (compare Figure 7A to Figure 4D). We then investigated if the hit compounds had any stimulating effect on TMEM16A-dependent chloride transport mediated by TMEM16A agonists, i.e., UTP, ATP and ionomycin. We first examined the effect of the hit compounds on the response to a range of UTP concentrations (0.1 to 100 μ M) in fully differentiated CFTR-null nasal epithelial cells with Ussing chamber measurements. However, none of the compounds enhanced these UTP-induced currents (Figures 7B and S4A). In addition to ALI-differentiated CFTR-null nasal epithelial cells, TMEM16A-dependent chloride transport was studied in YFP-quenching assays in two different cell lines. The hit compounds did not enhance Ani9-sensitive

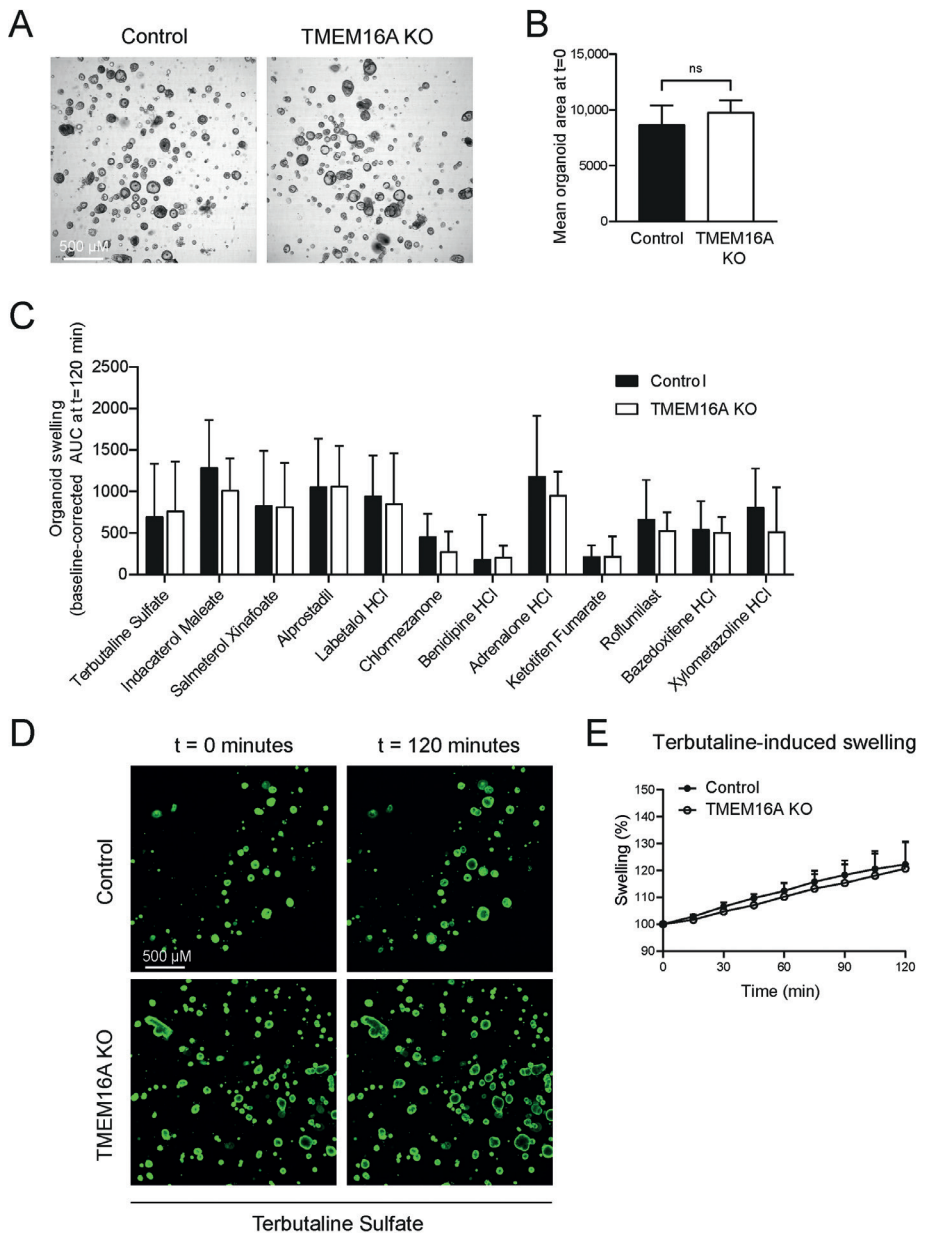


Figure 6. Hit compound validation in TMEM16A KO nasal organoids.

(A) Brightfield images showing intrinsic lumen formation, without any stimulation, in both control and TMEM16A KO nasal organoids (G542X/CFTR Δ 2.3(21kb)); (B) quantification of organoid lumen size in control and knockout organoids ($n = 3$ independent donors); (C) validation of hit compounds on nasal organoid swelling in TMEM16A KO and control organoids ($n = 3$ independent donors, 2–6 measurements per donor); (D) representative confocal images (G542X/CFTR Δ 2.3(21kb)) of TMEM16A KO and control nasal organoids, stimulated with Terbutaline Sulfate ($3 \mu\text{M}$) as example of one of the hit compounds; (E) quantification of nasal organoid swelling after stimulation with Terbutaline Sulfate ($3 \mu\text{M}$) in TMEM16A KO and control organoids ($n = 3$ independent donors). Analysis of difference was performed with a paired (B) or unpaired (C) t -test. No significant results were found. Ns = non-significant.

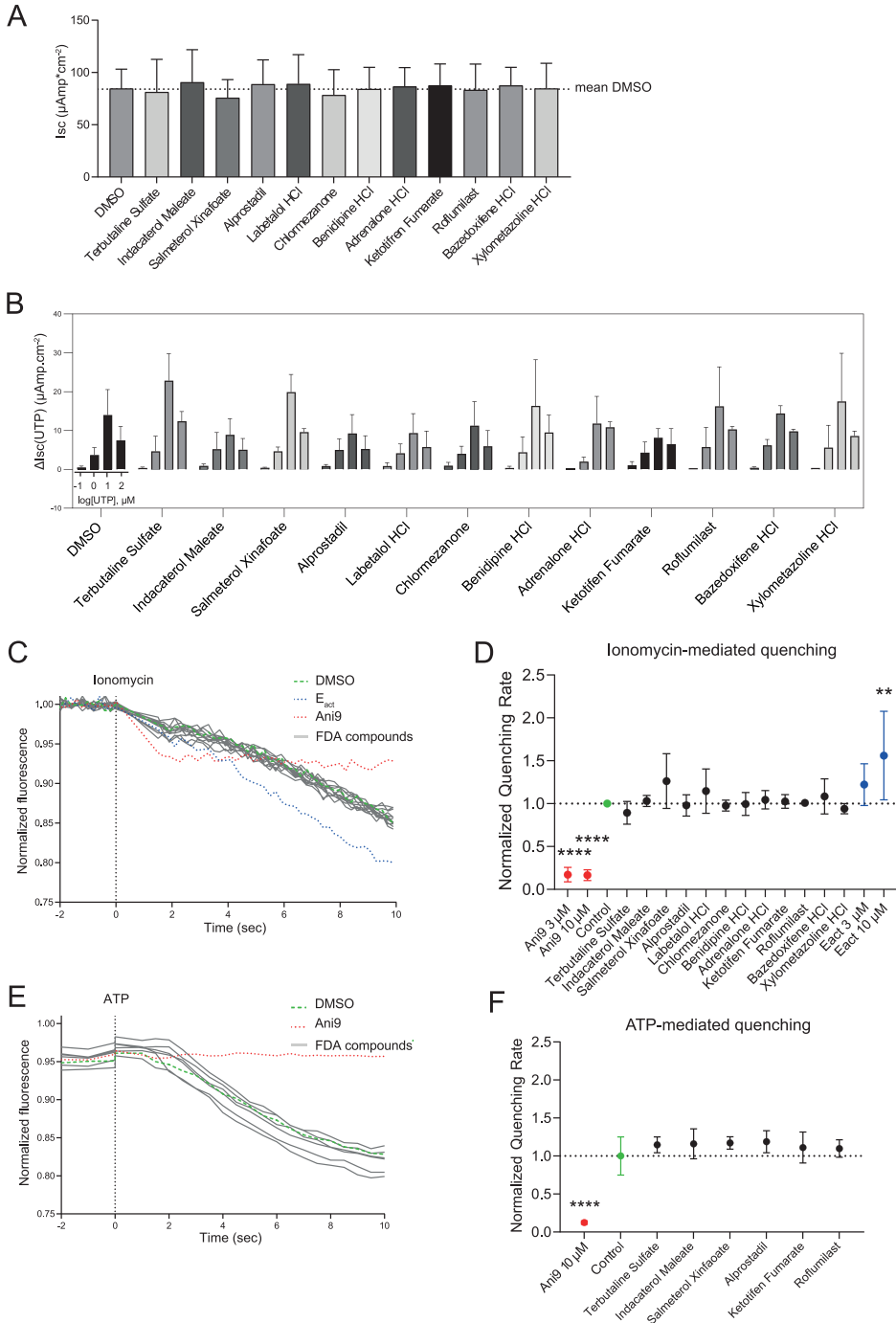


Figure 7. Effect of the hit compounds on TMEM16A in other *in vitro* model systems.

(A) The effect of the hit compounds (3 µM) on chloride conductance was determined in Ussing chamber measurements with ALI-differentiated CFTR-null nasal cells (n = 3 independent donors; each compound was measured in at least 2 different donors; n = 1–6 measurements per donor). No significant differences were found between one of the compounds and DMSO; (B) assessment whether the hit compounds (3 µM) enhance

Figure 7. (continued)

UTP-induced currents in Ussing chamber measurements. Experiments were conducted by stimulating different concentrations of UTP with hit compounds in ALI-differentiated CFTR-null nasal cells ($n = 3$ independent donors, each compound was measured in at least 2 different donors; $n = 2-3$ measurements per donor). No significant results were found between one of the compounds and DMSO, for any concentration of UTP; (C, D) effect of the 12 hit compounds ($3 \mu\text{M}$) on ionomycin-induced ($1 \mu\text{M}$) iodide influx was assessed with an YFP-quenching assay in CFBE cells. TMEM16A-dependency was demonstrated with sensitivity for Ani9 (3 and $10 \mu\text{M}$, shown in red). DMSO was used as negative control (shown in green) and E_{act} (3 and $10 \mu\text{M}$) as positive control (shown in blue). For quantification, quenching rates were normalized to the control; (E, F) effect of a selection of 6 hit compounds ($3 \mu\text{M}$) on ATP-induced ($5 \mu\text{M}$) iodide influx was analyzed in HT-29-YFP cells. TMEM16A-dependency was demonstrated with sensitivity for Ani9 ($10 \mu\text{M}$, shown in red) and DMSO was used as negative control (shown in green). For quantification, quenching rates were normalized to the control. Analysis of differences were performed with one-way ANOVA and Dunnett's post hoc test (A, D, F) or a two-way ANOVA with Dunnett's post hoc test (B). ** $p < 0.01$, **** $p < 0.0001$.

YFP-quenching upon Ionomycin stimulation of CFBE cells (Figures 7C, D and S4B), nor upon ATP stimulation in a HT-29 cell line (Figure 7E, F). Altogether, these experiments in other *in vitro* model systems indicate no effect of the hit compounds on chloride conductance measured in the Ussing chamber, and the lack of additional stimulating effect on TMEM16A-dependent chloride transport.

DISCUSSION

In this study, we performed a screening assay in CF nasal organoids, with the aim to repurpose FDA-approved drugs that stimulate CFTR-independent fluid secretion. Screening assays in 384-well plate format using airway organoids have been previously described by others²⁴⁻²⁶ and our protocol was based on a 384-well screening assay for CFTR-modulating drugs in CF intestinal organoids²⁷. However, to our knowledge, this is the first medium-throughput 384-well screening assay using nasal airway organoids that are cultured from minimal invasive nasal brushings of pwCF. In contrast to previously described assays using airway epithelial cells derived from resected tissues, the use of nasal organoids enables personalized disease modeling in airway cells of pwCF with any CFTR genotype.

Of the ~1400 FDA-approved drugs, 12 hit compounds were identified to induce fluid secretion in CFTR-null nasal organoids, based on assessment of organoid swelling. To exclude a role of CFTR in nasal organoid swelling, the hit compounds were subsequently tested in CFTR null nasal organoids. Ideally, the primary and secondary screening assays would already have been performed in these CFTR null nasal organoids, but these cells were not yet available at the beginning of the study. The screening assays were, therefore, performed on some donors with a trafficking mutation. It can be speculated that the identified compounds induce organoid swelling by restoring CFTR

function. However, we assume this is highly unlikely based on the 2 h compound incubation period, which is too short to observe CFTR functional repair caused by enhanced protein expression or trafficking.

To study the possible role of the alternative chloride channel TMEM16A in CFTR-independent nasal organoid swelling, CRISPR/Cas9 was used to create a TMEM16A KO in CFTR-null patient-derived nasal epithelial cells. We achieved high KO efficiencies (87–95%) and a selection step for clonal expansion was, therefore, not required. Despite functional validation of impaired TMEM16A function in nasal epithelial cells, nasal organoid swelling induced by the hit compounds was not reduced in TMEM16A KO cells. Further mode-of-action studies in different *in vitro* models indicated no direct effect of the hit compounds on transepithelial ion transport measured in the Ussing chamber, nor any stimulating effect on TMEM16A-dependent chloride transport, suggesting a TMEM16A-independent mode-of-action of the hit compounds. In line with previous studies^{10,22}, we observed that IL-4 could boost TMEM16A expression and TMEM16A-dependent swelling of CF nasal organoids in response to ATP. Therefore, nasal organoid culture conditions with IL-4 can potentially be used to more specifically identify TMEM16A activating compounds in future screening assays.

The discrepancy which was observed between the effects of the hit compounds on organoid swelling and Ussing chamber measurements can have multiple causes. In the Ussing chamber, changes in transepithelial ion transport are directly measured as electric currents, while organoid swelling is an indirect measurement of ion transport. Therefore, in contrast to electrical currents measured in the Ussing chamber, fluid secretion in organoids might depend on non-electrogenic transporters, e.g., by the electroneutral Cl⁻/HCO₃⁻ exchanger pendrin (SLC26A4)^{28,29}. Moreover, ALI-cultured monolayers used in the Ussing chamber might display differences in the activity of ion channels and transporters compared to organoids. For instance, the biomechanical properties of the 3D-extracellular matrix in which organoids are cultured may affect the activity of mechano-sensitive ion channels, such as TRPV4 that is activated by Eact^{20,30}. This would correspond with observations made in ALI cultures under shear stress, in which CFTR-independent chloride conductance and fluid secretion are also observed³¹. Additionally, fluid secretion experiments are cumulative assays that measure ion transport over a 2–3 h time period and might, therefore, be somewhat more sensitive to detect low signals. To further compare the differences between organoid and ALI cultures, airway surface liquid depth measurements and pH regulation studies of ALI-differentiated cells may be performed to examine fluid transport induced by the hit compounds.

The selection of hit compounds included many cAMP-inducing agents. Besides CFTR³² and also TMEM16A³³, it has been described that cAMP can modulate the activity of other ion channels and transporters. For instance, cAMP agonists activate the Cl⁻ channel CLCN2³⁴, SLC26A9³⁵, the Cl⁻/HCO₃⁻ exchanger pendrin (SLC26A4)³⁶, the Na⁺/HCO₃⁻ cotransporter NBCE1³⁷ and the H⁺/K⁺ ATPase HKA2 (ATP12A)^{29,38}. Additionally, it has been shown that cAMP modulates the expression of the Cl⁻/HCO₃⁻ exchanger type 2 (AE2 or SLC4A2) in airway epithelial cells^{29,39,40}. Furthermore, cAMP mediates K⁺ signaling, e.g., by activation of the basolateral membrane K⁺ channel KCNQ1^{39,41}, which is associated with chloride secretion⁴². Likewise, cAMP is reported to affect Ca²⁺ signaling⁴³ and, therefore, might activate a non-TMEM16A calcium-activated chloride channel⁴⁴. Lastly, cAMP is described to mediate Na⁺ transport via the epithelial sodium channel ENaC⁴⁵. Altogether, the mechanism-of-action of cAMP-enhancing drugs might depend on the interplay among different ion channels and transporters, which should be investigated in further research. Transcriptomics and proteomics can be performed to identify ion channels or transporters that are highly expressed in nasal organoids of individuals with CF. This might be followed by the creation of gene KO cells of these specific ion channels and transporters, to validate their involvement in CFTR-independent fluid secretion. In addition, studies can be conducted with chemical inhibitors to elucidate which cellular signaling transduction pathways are activated by the hit compounds.

Among the cAMP-stimulating hit compounds are multiple β 2-agonists, such as Terbutaline Sulfate, Salbutamol and Indacaterol Maleate. They seem attractive for drug repurposing as they are broadly applied as bronchodilator therapy for respiratory diseases. Indeed, a significant number of pwCF already use bronchodilator inhalation therapy to reduce respiratory symptoms of airway obstruction⁴⁶. Notably, these β 2-agonists are also described to enhance CFTR-dependent epithelial permeability in human bronchial epithelial cells⁴⁷ and to induce CFTR-dependent fluid secretion in intestinal organoids⁴⁸. As we found that they also induce non-CFTR epithelial fluid secretion, they might have a double positive effect for pwCF. Among the hit compounds, we also observed that the β 2-adrenergic antagonist Labetalol induced organoid swelling. This is potentially by acting as a partial agonist of the β -adrenoceptor, as previously shown by others⁴⁹. However, further research is needed to fully understand the working mechanism of Labetalol and other hit compounds before considering clinical use, as it is preferable to have drugs that activate specific chloride channels or transporters to prevent systemic side effects. After elucidating the working mechanisms, further studies can also be conducted to determine additive or synergistic effects of compounds with different mode of actions. To further explore the therapeutic potential, additional studies may include comparison of the effect sizes of the hit compounds with current

CFTR modulators, by determining swelling of organoids from patients that respond to CFTR modulator therapies. Moreover, the effect of the hit compounds can be determined as add-on therapy together with CFTR modulators.

In summary, we provide proof-of concept of using nasal organoids for medium-throughput screening and the ability to elucidate the mechanism-of-action of hit compounds in gene KO cells. We furthermore identified 12 FDA-approved compounds which induce CFTR- and TMEM16A-independent epithelial fluid secretion in CF nasal organoids and may potentially be used as treatment for pwCF. Moreover, our pipeline, combining screening assays in nasal organoids and validation experiments in gene KO cells can be further used for pre-clinical drug discovery. It can be used to identify novel compounds that activate alternative ion channels or transporters, which might act as treatment for pwCF who are not eligible for CFTR modulator therapy.

MATERIALS AND METHODS

Patient materials

Nasal brushings were obtained from subjects with CF. All subjects signed informed consent for use and storage of their cells, which was approved by a specific ethical board for the use of biobanked materials TcBIO (Toetsingscommissie Biobanks), an institutional Medical Research Ethics Committee of the University Medical Center Utrecht (protocol ID: 16/586). Cells were used from 9 pwCF with the following mutations: F508del/S1251N (Female (F)); F508del/S1251N (Male (M)); W1282X/1717-1G>A (F); R553X/R553X (F); G542X/Dele2.3 (21kb) (M); F508del/W846X (F); F508del/F508del (M); F508del/F508del (F); 1811+1G>C/ 1811+1G>C (F). Nasal brushings were performed by a trained nurse or physician, as described before¹⁷. Briefly, the brushings were obtained from both inferior turbinates using a cytological brush (CooperSurgical, Trumbull, CT, USA) and were collected in advanced DMEM/F12 (Gibco, Waltham, MA, USA) containing glutaMAX (1% v/v; Gibco, Waltham, MA, USA), HEPES (10 mM; Gibco, Waltham, MA, USA), penicillin-streptomycin (1% v/v; Gibco, Waltham, MA, USA) and primocin (50 mg/mL; Invivogen, San Diego, CA, USA).

Nasal epithelial cell and organoid culturing

Nasal epithelial cells were isolated and expanded as described previously¹⁷. In brief, cells were scraped off the brush and treated with TrypLE express enzyme (Fisher Scientific, Landsmeer, The Netherlands), supplemented with Sputolysin (Calbiochem, San Diego, CA, USA) for 10 min at 37 °C. Subsequently, cells were strained with a 100 µm strainer, centrifugated and plated out in a collagen IV (50 µg/mL; Sigma-Aldrich,

St. Louis, MO, USA)-precoated 6-well culturing plate with basal cell isolation medium (Table S1). Growth factors (FGF7, FGF10, EGF and HGF) were added fresh to the medium. Medium was changed three times a week. Antibiotics were withdrawn from the medium after one week of culturing and cells were further cultured with basal cell expansion medium, including the γ -secretase inhibitor DAPT (Table S1) until 80–90% confluence. Cells were then passaged using TrypLE express enzyme and further expanded until confluence. These cells were frozen as a master cell bank (passage 1) and working cell bank (passage 2) in CryoStor CS10 freezer medium (STEMCELL technologies, Vancouver, Canada), supplemented with Y-27632 (5 μ M; Selleck chemicals, Planegg, Germany). For experiments, basal cells (passage 3–5) were seeded on 12-well inserts (0.4 μ m pore size polyester membrane, 0.5 million cells per Transwell; Corning, Corning, NY, USA), precoated with PureCol (30 μ g/mL; Advanced Biomatrix, Carlsbad, CA, USA) for differentiation at air-exposed conditions. The cells were first cultured submerged with basal cell expansion medium. When reaching 100% confluence, medium was changed to ALI differentiation medium (Table S2) supplemented with A83-01 (500 nM). After 2 days, apical medium was removed to culture the cells at air-exposed conditions. After 3–4 days at air-exposed conditions, A83-01 was withdrawn from the medium. Medium was refreshed twice a week, and the apical side of the cells was washed with PBS once a week. After 14–21 days of culturing at air-exposed conditions, cells were used for further experiments. In indicated experiments, cells were treated for 48 h with IL-4 (10 ng/mL; Peprotech, Rocky Hill, NJ, USA) to increase TMEM16A expression.

To obtain nasal organoids, differentiated ALI cultures were apically washed with PBS and treated with collagenase type II (1 mg/mL; Gibco, Waltham, MA, USA), diluted in advanced DMEM/F12, at the basolateral side. The cells were incubated for 45–60 min at 37 °C until the epithelial layer detached from the Transwell. Loose epithelial sheets were collected in 1 mL advanced DMEM/F12 in a 15 mL tube. The epithelial sheets were then mechanically disrupted by pipetting and subsequently strained with a 100 μ m strainer. After centrifugation, epithelial fragments were resuspended in ice-cold 75% (*v/v*) Matrigel (diluted in airway organoid medium (Table S3); Corning, Corning, NY, USA) and kept on ice. Then, 30 μ L Matrigel droplets were plated out on a pre-warmed 24-well suspension plate. This plate was placed upside down in a tissue incubator to solidify the Matrigel droplets for 20–30 min, before adding 500 μ L airway organoid medium (supplemented with FGF7 (5 ng/mL) and FGF10 (10 ng/mL)) per well.

Organoid swelling assay

For the primary screening assay, organoids were transferred to a 384-well plate, 1–3 days after organoid formation. First, organoids were harvested by dissolving the Matrigel with Cell Recovery Solution (Corning, Corning, NY, USA) during a 10 min incubation

step at 4 °C. Afterwards, organoids were collected in a tube with ice-cold advanced DMEM/F12. After centrifugation, organoids were resuspended in 75% (*v/v*) ice-cold Matrigel (diluted in airway organoid medium) and plated out as 7 μ L-droplets in a 384-well plate. Plates were centrifuged to reach the organoids at the bottom of the wells. Matrigel droplets were solidified in a tissue incubator for 10 min and subsequently 8 μ L airway organoid medium supplemented with FGF7 (5 ng/mL) and FGF 10 (10 ng/mL) was added per well. Plates were covered with a breath sealing membrane (Sigma-Aldrich, St Louis, MO, USA) to prevent evaporation and incubated overnight at 37 °C. The next day, organoids were stimulated with compounds from an FDA-approved drug library (3 μ M; Selleckchem, Planegg, Germany; ordered in 2016), with two compounds combined in a single well, which were mixed with a plate shaker. E_{act} (10 μ M; Sigma-Aldrich, St Louis, MO, USA) was used as positive control and DMSO as negative control. Brightfield pictures were taken every 15 min for 3 h in total with a 5x objective by confocal microscopy (Zeiss LSM800) at 95% O₂/5% CO₂.

For assessment of organoid swelling in a 96-well plate format, 30 μ L Matrigel droplets were scraped from the plate and transferred to tubes with ice-cold advanced DMEM/F12 to dissolve the Matrigel, 1–3 days after organoid formation. Next, organoids were centrifuged and resuspended again in ice-cold 75% (*v/v*) Matrigel to be plated out again in 4 μ L droplets in a pre-warmed 96-well plate. The plate was placed in a tissue incubator to solidify the Matrigel droplets for 15–30 min, before adding 100 μ L culturing medium (airway organoid medium supplemented with FGF7 (5 ng/mL) and FGF10 (10 ng/mL)) per well. For specified experiments, FGF7 and FGF10 were substituted by IL-4 (10 ng/mL). A swelling assay was performed 1–2 days after plating out the organoids in a 96-well plate. Organoids were imaged with fluorescence microscopy or brightfield microscopy. For fluorescence microscopy, organoids were pre-treated with calcein green AM (3 μ M; Invitrogen, Waltham, MA, USA) for 30 min. Organoids were then stimulated with an agonist (forskolin (5 μ M; Sigma-Aldrich, St Louis, MO, USA), ATP (100 μ M; Sigma-Aldrich, St. Louis, MO, USA), E_{act} (10 μ M), FDA compound (3 μ M) or vehicle control) to analyze their effect on epithelial fluid secretion. Live imaging with confocal microscopy (Zeiss LSM800) was performed to visualize the organoids at 37 °C and 95% O₂/5% CO₂. Pictures were taken every 15 min for 2–3 h in total with a 5x objective. Organoid swelling experiments were performed in quadruplicates. FIS experiments were performed as described before ¹⁷.

Analysis of organoid swelling assays

Swelling of calcein green AM-labelled organoids was analyzed as described before ¹⁷. Total organoid area per well was determined with Zen Blue image analysis software. This was used to calculate organoid surface area over time, normalized for $t = 0$ and

with 100% as baseline. Additionally, AUC values ($t = 120$ min) were calculated. When indicated, baseline-corrected AUC values were calculated by subtraction of the AUC values from DMSO-treated wells from the same experimental plate.

For organoid swelling in experiments without fluorescent-labelled organoids, the OrgaQuant convolutional neural network was used to automatically recognize organoids in brightfield images, by use of the provided code¹⁸. Organoid surface area was estimated using OrgaQuant bounding boxes, assuming organoids had a disk shape. Particle tracking²¹ was then used to follow individual organoids over 13 time points. Next, linear regression⁵⁰ was used to determine a swell rate for individual organoids and the mean swell rate of all organoids in a single well was used for further analysis. Individual organoids were excluded from analysis (1) when not recognized in minimal 8 out of 13 time points or (2) when the standard error of swell rate was >2.5 pixels/time point. Plate-normalization was performed to compare swell rates across different plates and donors by the following formula: $(\text{swell rate}_{\text{well}} - \text{median swell rate}_{\text{plate}}) / \text{IQR swell rate}_{\text{plate}}$, where IQR is the inter quantile range.

Immunofluorescence staining and microscopy

Organoids plated in 30 μL droplets of Matrigel were used for immunofluorescence staining. Matrigel was dissolved by incubation with Cell Recovery Solution (Corning, Corning, NY, USA) for 15 min at 4 °C. Organoids were then fixed with 4% PFA (Aurion, Wageningen, Netherlands) for 15 min. Fixed organoids were stored in 70% EtOH or directly further processed. Organoids were embedded in pre-warmed HistoGel (EpreDia, Breda, The Netherlands) and dehydrated and embedded in paraffin in a Tissue Processor (Leica). Next, 3 μM -sections were deparaffinized and antigen retrieval was performed in 10 mM citrate buffer (pH = 6; Sigma-Aldrich, St Louis, MO, USA) for 10 min. The samples were then permeabilized in 0.25% (v/v) Triton-X (Sigma-Aldrich, St Louis, MO, USA) in PBS for 10 min and subsequently blocked in 5% (w/v) BSA (Sigma-Aldrich, St Louis, MO, USA) with 0.03% Triton-X in PBS for 30 min. Next, primary antibodies (Table S4) were incubated for 90 min and secondary antibodies (Table S4) together with DAPI stain (1:1.000; Sigma-Aldrich, St Louis, MO, USA) for 45 min, both diluted in blocking buffer. Last, samples were mounted in Prolong Gold reagent (Thermo Fischer Scientific, Waltham, MA, USA). Images were acquired using a Leica THUNDER imager with a 40x objective. Images were processed using Las X software and ImageJ.

RNA extraction, cDNA synthesis and quantitative real time PCR

RNA was extracted from nasal organoids with the RNeasy Mini-Kit (Qiagen, Venlo, Netherlands) according to the manufacturer's protocol together with a DNA digestion step with DNase+ (Qiagen, Venlo, Netherlands). RNA yield was measured using the

Qubit RNA BR assay kit (Thermo Fischer Scientific, Waltham, MA, USA). cDNA was produced with the iScript™ cDNA Synthesis Kit (Bio-Rad, Hercules, CA, USA) according to the manufacturer's protocol. Quantitative real-time PCR (qPCR) was performed with the iQ™ SYBR® Green Supermix (Bio-Rad, Hercules, CA, USA), specific primers listed in Table S5 and a CFX96 real-time detection machine (Bio-Rad, Hercules, CA, USA). Relative gene expression normalized to the housekeeping genes ATP5B and RPL13A was calculated using the software CFX Manager 3.1 (Bio-Rad, Hercules, CA, USA), according to the standard curve method.

Gene KO in airway epithelial basal cells using CRISPR-Cas9

TMEM16A KO nasal epithelial cells (passage 3, n = 3 independent donors) were created using CRISPR-Cas9 technology. First, ribonucleoprotein (RNP) complexes were formed by combining multi-guide sgRNA (30 μM; Synthego, Redwood City, CA, USA), recombinant 2NLS-Cas9 nuclease (20 μM, Synthego, Redwood City, CA, USA) and optiMEM (Invitrogen, Waltham, MA, USA) supplemented with Y27632 (10 μM), followed by 10 min incubation at room temperature. Next, 1 million basal epithelial cells were made single cells with TrypLE express enzyme, and after centrifugation dissolved in optiMEM, supplemented with Y27632 (10 μM). Cells were then mixed with the RNP complexes, transferred to cuvettes and electroporated in bulk using a NEPA21 electroporator (Nepa Gene, Ichikawa City, Japan), according to previously published settings⁵¹. After electroporation, the polyclonal cell suspension was resuspended in basal cell expansion medium and plated out in 12-well plates. For analysis of gene editing efficiency, DNA was isolated according to the protocol of the Quick-DNA Microprep Kit (Zymo Research, Irvine, CA, USA) and DNA concentration was measured using the Qubit ds DNA BR assay kit (Thermo Fischer Scientific, Waltham, MA, USA). Regions of interest were amplified in a PCR reaction with GoTaq G2 Flexi DNA polymerase (Promega, Madison, WI, USA), and PCR-amplified samples were run on a 1,2% TBE-agarose gel for size separation. DNA fragments were excised from the gel, purified according to the Gel Extraction Kit (Qiagen, Venlo, The Netherlands) and sent for Sanger sequencing. KO efficiency was analyzed with the ICE analysis tool (www.ice.synthego.com, accessed on 21 January 2021).

TMEM16A western blot

ALI-differentiated cells were dissociated from the Transwells with TrypLE express enzyme, washed twice with cold PBS and dissolved in Laemmli lysis buffer. Protein concentration was determined using the Pierce BCA Protein Assay Kit (Thermo Fischer Scientific, Waltham, MA, USA), according to the manufacturer's protocol. Protein extracts were separated on 8% SDS-PAGE gels and transferred to a PVDF membrane (immobilon FL; Sigma-Aldrich, St Louis, MO, USA). Membranes were blocked with 1% (for

TMEM16A protein) or 5% (for loading controls) (*w/v*) non-fat milk powder (NFM; Campina, Amersfoort, Netherlands) in Tris buffer saline with Tween-20 (Merck, Kenilworth, NJ, USA; TBS-T) for 1 h at room temperature. Primary antibodies (Table S5) were incubated overnight at 4 °C diluted in 0.5% (*w/v*) NFM/TBS-T. Hsp90 was used as loading control. Secondary antibodies were incubated for 1 h at room temperature in 0.5% (*w/v*) NFM/TBS-T. Chemiluminescent detection was performed using SuperSignal™ West Dura Extended Duration Substrate (Thermo Fischer Scientific, Waltham, MA, USA) and the Chemidoc Touch Imaging system (Bio-Rad, Hercules, CA, USA). Quantification of band intensities was performed using ImageJ and normalized to the loading control hsp90.

Ussing chamber experiments

Nasal epithelial cells differentiated at ALI conditions for 28 days were used for Ussing chamber measurements. The day before experiments, inserts were washed with sterile PBS (Thermo Fischer Scientific, Waltham, MA, USA) for 10 min at 37 °C, 5% CO₂. Epithelial cultures were mounted into the EasyMount Ussing Chamber System (Physiologic Instruments, Reno, NV, USA) and bathed in an HCO₃⁻-KRB solution, containing (in mM): 25 NaHCO₃, 115 NaCl, 5 KCl, 1 CaCl₂, 1 MgCl₂, 5 D-glucose, pH 7.4. The solution was continuously gassed with 95% O₂/5% CO₂ and maintained at 37 °C. Monolayers were voltage-clamped to 0 mV. The transepithelial short-circuit current (I_{sc}) was recorded every 10 sec using Ag-AgCl electrodes in 3M KCl agar bridges, as previously described⁵², and results were normalized to an area of 1 cm² and expressed as $\mu\text{Amp}\cdot\text{cm}^{-2}$ using the Acquire & Analyze software (Physiologic Instruments, Reno, NV, USA). Changes in short-circuit current (ΔI_{sc}) were then calculated by averaging 5 time points before and 5 points after the addition of chemicals. Chemicals were added in the following sequence: FDA compounds (3 μM , basolateral), amiloride (amil, 10 μM , apical; Sigma-Aldrich, St Louis, MO, USA), Uridine 5'-Triphosphate trisodium salt hydrate (UTP, 0.1–100 μM , apical; Sigma-Aldrich, St Louis, MO, USA).

YFP-quenching assay

For the YFP-quenching assay in CFBE cells, CFBE parental (null CFTR) cells stably expressing halide-sensitive YFP (HS-YFP) were cultured in MEM 1x (Corning, Corning, NY, USA) and 1 mg/mL of Hygromycin B (Sigma-Aldrich, St Louis, MO, USA). Cells were seeded 50,000 cells/well on clear-bottom 96-well black microplates suitable for high-content imaging (90 μL per well). Forty-eight hours after plating, cells were washed twice and incubated for 25 min at 37 °C with 65 μL of standard PBS (in mM: 137 NaCl, 2.7 KCl, 8.1 Na₂HPO₄, 1.5 KH₂PO₄, 1 CaCl₂, 0.5 MgCl₂, pH 7.4) containing vehicle alone (0.1% (*v/v*) DMSO) or with different FDA compounds (3 or 10 μM). After 25 min, the plate was transferred to a microplate reader (Tecan, Mannedorf, Switzerland). Each assay consisted of a continuous 12 s fluorescence reading—2 s before and 10 s after injection of

170 μL of iodide-rich PBS (in mM: 137 KI, 2.7 KCl, 8.1 Na_2HPO_4 , 1.5 KH_2PO_4 , 1 CaCl_2 , 0.5 MgCl_2 , pH 7.4) containing 1 μM of Ionomycin (Sigma-Aldrich, St Louis, MO, USA). Each well was normalized to their own initial fluorescence and linear fits were performed for each point. The fluorescence quenching rate (QR) represents the steepest slope within the different slopes previously calculated.

For the YFP-quenching assay in HT-29 cells, stably expressing the iodide-sensitive enhanced yellow fluorescent protein (eYFP-I152L), cells were plated in transparent 96-well plates. After 24 h of culturing to 80–90% confluence, they were incubated with or without FDA compounds (3 μM) in a gluconate-substituted Ringer solution (in mM: NaCl 100, Na-Gluconate 40, KCl 5, $\text{MgCl}_2 \cdot 6 \text{H}_2\text{O}$ 1, $\text{CaCl}_2 \cdot 2 \text{H}_2\text{O}$ 2, Glucose 10, HEPES 10). Iodide was added as a symmetrical iodide-substituted Ringer solution (in mM: NaCl 100, NaI 40, KCl 5, $\text{MgCl}_2 \cdot 6 \text{H}_2\text{O}$ 1, $\text{CaCl}_2 \cdot 2 \text{H}_2\text{O}$ 2, D-Glucose 10, HEPES 10) and 5 μM ATP was then added acutely in the final 1:1 mixed Ringer solution (NaCl 100, Na-Gluconate 20, NaI 20, KCl 5, $\text{MgCl}_2 \cdot 6 \text{H}_2\text{O}$ 1, $\text{CaCl}_2 \cdot 2 \text{H}_2\text{O}$ 2, D-Glucose 10, HEPES 10). The final iodide concentration on each well was 20 mM for every experiment. Total intracellular YFP-fluorescence intensity in each well was measured continuously with a fluorescence microplate reader (NOVOstar, BMG Labtech, Ortenberg, Germany) kept at 37 °C, using an excitation wavelength of 485 nm and emission detection at 520 nm. Background fluorescence was subtracted and data were normalized to the initial fluorescence. The initial rate of maximal fluorescence decay caused by iodide influx was then calculated as a measure of anion conductance.

Statistical analysis

For organoid swelling assays, four technical replicates were used per experimental condition. All results are shown as mean values \pm SD from biological replicates, unless indicated otherwise. For statistical analyses of differences, an (un)paired *t*-test or one/two-way ANOVA with indicated post hoc test were used, as indicated in the figure legends. *p*-values < 0.05 were considered as statistically significant. Statistical analyses were performed using Graphpad Prism 9 or R v.4.0.3.

AUTHOR CONTRIBUTIONS

Conceptualization and methodology—L.W.R., L.D., V.R., R.C., M.C.P., S.F.B.v.B., R.N.P.R., C.K.v.d.E., M.D.A., K.K., M.A.G., J.M.B. and G.D.A.; software—S.F.B.v.B. and R.N.P.R.; validation, L.W.R.; investigation, L.W.R., L.D., V.R., R.C., M.C.P., M.D.A., K.K., M.A.G., J.M.B. and G.D.A.; data curation and formal analysis, L.W.R., L.D., V.R., R.C., M.C.P., S.M.A.S., I.S.v.d.W., C.F.J.v.H. and G.D.A.; writing—original draft preparation, L.W.R., J.M.B. and G.D.A.; writing—review and editing, L.W.R., L.D., V.R., R.C., M.C.P., S.M.A.S., I.S.v.d.W., C.F.J.v.H., S.F.B.v.B., R.N.P.R., C.K.v.d.E., M.D.A., K.K., M.A.G., J.M.B. and G.D.A.; visualization, L.W.R., L.D., V.R., R.C., M.C.P. and G.D.A.; project administration, J.M.B. and G.D.A.; funding acquisition and supervision, C.K.v.d.E., M.D.A., K.K., M.A.G., J.M.B. and G.D.A.; All authors have read and agreed to the published version of the manuscript.

FUNDING

This work was funded by UK Cystic Fibrosis Trust (SRC013). Work in M.D.A. lab was also supported by UIDB/04046/2020 and UIDP/04046/2020 Centre grants (to BioISI), from FCT-Fundação para a Ciência e a Tecnologia/MCTES Portugal.

INSTITUTIONAL REVIEW BOARD STATEMENT

The study was conducted in accordance with the Declaration of Helsinki, and approved by a specific ethical board for the use of biobanked materials TcBIO (Toetsingscommissie Biobanks), an institutional Medical Research Ethics Committee of the University Medical Center Utrecht (protocol ID 16/586, approved on 25 January 2017).

INFORMED CONSENT STATEMENT

Informed consent was obtained from all subjects involved in the study.

DATA AVAILABILITY STATEMENT

All data are provided with the manuscript. Code is available at <https://github.com/UMCU-BeekmanLab/OrgaQuantBeekman>.

ACKNOWLEDGMENTS

We would like to acknowledge Valérie Daive for technical support with immunofluorescence staining.

CONFLICTS OF INTEREST

J.M.B. has a patent granted (10006904) related to CFTR function measurements in organoids and received personal fees from HUB/Royal Dutch academy of sciences, during the conduct of the study; nonfinancial support from Vertex Pharmaceuticals and personal fees and nonfinancial support from Proteostasis Therapeutics, outside the submitted work. C.K.E. reports grants from GSK, Nutricia, TEVA, Gilead, Vertex, ProQR, Proteostasis, Galapagos NV, Eloxx pharmaceuticals, outside the submitted work; In addition, C.K.E. has a patent related to CFTR function measurements in organoids (10006904) with royalties paid.

REFERENCES

1. Riordan, J. R. *et al.* Identification of the cystic fibrosis gene: cloning and characterization of complementary DNA. *Science (New York, N.Y.)* 245, 1066–1073 (1989).
2. Coakley, R. D. *et al.* Abnormal surface liquid pH regulation by cultured cystic fibrosis bronchial epithelium. *Proceedings of the National Academy of Sciences of the United States of America* 100, 16083–16088 (2003).
3. Elborn, J. S. Cystic fibrosis. *Lancet (London, England)* 388, 2519–2531 (2016).
4. Middleton, P. G. *et al.* Elexacaftor-Tezacaftor-Ivacaftor for Cystic Fibrosis with a Single Phe508del Allele. *N Engl J Med* 381, 1809–1819 (2019).
5. Heijerman, H. G. M. *et al.* Efficacy and safety of the elexacaftor plus tezacaftor plus ivacaftor combination regimen in people with cystic fibrosis homozygous for the F508del mutation: a double-blind, randomised, phase 3 trial. *Lancet (London, England)* 394, 1940–1948 (2019).
6. Ramsey, B. W. *et al.* A CFTR potentiator in patients with cystic fibrosis and the G551D mutation. *The New England journal of medicine* 365, 1663–1672 (2011).
7. Annual Reports | European Cystic Fibrosis Society (ECFS). <https://www.ecfs.eu/projects/ecfs-patient-registry/annual-reports>.
8. Guo, J., Garratt, A. & Hill, A. Worldwide rates of diagnosis and effective treatment for cystic fibrosis. *Journal of Cystic Fibrosis* 21, 456–462 (2022).
9. Guo, J., Wang, J., Zhang, J., Fortunak, J. & Hill, A. Current prices versus minimum costs of production for CFTR modulators. *Journal of Cystic Fibrosis* S1569-1993 (2022) doi:10.1016/J.JCF.2022.04.007.
10. Caputo, A. *et al.* TMEM16A, a membrane protein associated with calcium-dependent chloride channel activity. *Science* 322, 590–594 (2008).
11. Yang, Y. D. *et al.* TMEM16A confers receptor-activated calcium-dependent chloride conductance. *Nature* 455, 1210–1215 (2008).
12. Schroeder, B. C., Cheng, T., Jan, Y. N. & Jan, L. Y. Expression cloning of TMEM16A as a calcium-activated chloride channel subunit. *Cell* 134, 1019–1029 (2008).
13. A First in Human Study to Evaluate the Safety, Tolerability and Pharmacokinetics of Single and Multiple Ascending Doses of Inhaled ETD002 in Healthy Subjects - Full Text View - ClinicalTrials.gov. <https://clinicaltrials.gov/ct2/show/NCT04488705>.
14. Moore, P. J. & Tarran, R. The epithelial sodium channel (ENaC) as a therapeutic target for cystic fibrosis lung disease. *Expert Opinion on Therapeutic Targets* 22, 687–701 (2018).
15. Mall, M. A. ENaC inhibition in cystic fibrosis: potential role in the new era of CFTR modulator therapies. *European Respiratory Journal* 56, 2000946 (2020).
16. Goss, C. H. *et al.* Efficacy and safety of inhaled ENaC inhibitor BI 1265162 in patients with cystic fibrosis: BALANCE-CF 1, a randomised, phase II study. *European Respiratory Journal* 59, 2100746 (2022).
17. Amatngalim, G. D. *et al.* Measuring cystic fibrosis drug responses in organoids derived from 2D differentiated nasal epithelia. *Life science alliance* 5, e202101320 (2022).
18. Kassis, T., Hernandez-Gordillo, V., Langer, R. & Griffith, L. G. OrgaQuant: Human Intestinal Organoid Localization and Quantification Using Deep Convolutional Neural Networks. *Scientific Reports* 9, 12479 (2019).
19. Sachs, N. *et al.* Long-term expanding human airway organoids for disease modeling. *The EMBO Journal* 38, e100300 (2019).
20. Genovese, M. *et al.* TRPV4 and purinergic receptor signalling pathways are separately linked in airway epithelia to CFTR and TMEM16A chloride channels. *J Physiol* 597, 5859–5878 (2019).
21. Allan, D. B., Caswell, T., Keim, N. C., van der Wel, C. M. & Verweij, R. W. soft-matter/trackpy: Trackpy v0.5.0. (2021) doi:10.5281/ZENODO.4682814.

22. Scudieri, P. *et al.* Association of TMEM16A chloride channel overexpression with airway goblet cell metaplasia. *Journal of Physiology* 590, 6141–6155 (2012).
23. Seo, Y. *et al.* Ani9, A Novel Potent Small-Molecule ANO1 Inhibitor with Negligible Effect on ANO2. *PLoS one* 11, e0155771 (2016).
24. Hynds, R. E., Butler, C. R., Janes, S. M. & Giangreco, A. Expansion of Human Airway Basal Stem Cells and Their Differentiation as 3D Tracheospheres. *Methods in molecular biology (Clifton, N.J.)* 1576, 43–53 (2019).
25. Hild, M. & Jaffe, A. B. Production of 3-D airway organoids from primary human airway basal cells and their use in high-throughput screening. *Current Protocols in Stem Cell Biology* 37, IE.9.1-IE.9.15 (2016).
26. Duan, X. *et al.* An airway organoid-based screen identifies a role for the HIF1 α -glycolysis axis in SARS-CoV-2 infection. *Cell Reports* 37, 109920 (2021).
27. Spelier, S. *et al.* High-Throughput Functional Assay in Cystic Fibrosis Patient-Derived Organoids Allows Drug Repurposing. *bioRxiv* 2022.07.14.500147 (2022) doi:10.1101/2022.07.14.500147.
28. Hollenhorst, M. I., Richter, K. & Fronius, M. Ion Transport by Pulmonary Epithelia. *J Biomed Biotechnol* 2011, 174306 (2011).
29. Zajac, M., Dreano, E., Edwards, A., Planelles, G. & Sermet-gaudelus, I. Airway Surface Liquid pH Regulation in Airway Epithelium Current Understandings and Gaps in Knowledge. *International Journal of Molecular Sciences* 22, 3384 (2021).
30. Bayir, E., Sendemir, A. & Missirlis, Y. F. Mechanobiology of cells and cell systems, such as organoids. *Biophysical reviews* 11, 721–728 (2019).
31. Tarran, R. *et al.* Normal and cystic fibrosis airway surface liquid homeostasis. The effects of phasic shear stress and viral infections. *The Journal of biological chemistry* 280, 35751–35759 (2005).
32. Cheng, S. H. *et al.* Phosphorylation of the R domain by cAMP-dependent protein kinase regulates the CFTR chloride channel. *Cell* 66, 1027–1036 (1991).
33. Lérias, J. *et al.* Compartmentalized crosstalk of CFTR and TMEM16A (ANO1) through EPAC1 and ADCY1. *Cellular Signalling* 44, 10–19 (2018).
34. Oak, A. A. *et al.* Lubiprostone is non-selective activator of cAMP-gated ion channels and Clc-2 has a minor role in its prosecretory effect in intestinal epithelial cells. *Molecular pharmacology* 102, 106–115 (2022).
35. Salomon, J. J. *et al.* Generation and functional characterization of epithelial cells with stable expression of SLC26A9 Cl⁻ channels. *American journal of physiology. Lung cellular and molecular physiology* 310, L593–602 (2016).
36. Garnett, J. P. *et al.* Novel Role for Pendrin in Orchestrating Bicarbonate Secretion in Cystic Fibrosis Transmembrane Conductance Regulator (CFTR)-expressing Airway Serous Cells. *Journal of Biological Chemistry* 286, 41069–41082 (2011).
37. Devor, D. C. *et al.* Bicarbonate and Chloride Secretion in Calu-3 Human Airway Epithelial Cells. *Journal of General Physiology* 113, 743–760 (1999).
38. Laroche-Joubert, N., Marsy, S., Luriau, S., Imbert-Teboul, M. & Doucet, A. Mechanism of activation of ERK and H-K-ATPase by isoproterenol in rat cortical collecting duct. *American journal of physiology. Renal physiology* 284, F948–54 (2003).
39. Frizzell, R. A. & Hanrahan, J. W. Physiology of Epithelial Chloride and Fluid Secretion. *Cold Spring Harbor Perspectives in Medicine* 2, a009563 (2012).
40. Ibrahim, S. H. *et al.* CK2 is a key regulator of SLC4A2-mediated Cl⁻/HCO₃⁻ exchange in human airway epithelia. *Pflugers Archiv European Journal of Physiology* 469, 1073–1091 (2017).
41. Kunzelmann, K. *et al.* Cloning and function of the rat colonic epithelial K⁺ channel KVLQT1. *The Journal of membrane biology* 179, 155–164 (2001).
42. Smith, P. L. & Frizzell, R. A. Chloride secretion by canine tracheal epithelium: IV. Basolateral membrane K permeability parallels secretion rate. *The Journal of membrane biology* 77, 187–199 (1984).

43. Lee, R. J. & Kevin Foskett, J. cAMP-activated Ca²⁺ signaling is required for CFTR-mediated serous cell fluid secretion in porcine and human airways. *The Journal of clinical investigation* 120, 3137–3148 (2010).
44. Huang, F., Wong, X. & Jan, L. Y. International Union of Basic and Clinical Pharmacology. LXXXV: calcium-activated chloride channels. *Pharmacological reviews* 64, 1–15 (2012).
45. Yang, L. M., Rinke, R. & Korbmacher, C. Stimulation of the epithelial sodium channel (ENaC) by cAMP involves putative ERK phosphorylation sites in the C termini of the channel's beta- and gamma-subunit. *The Journal of biological chemistry* 281, 9859–9868 (2006).
46. Bargon, J., Viel, K., Daultbaev, N., Wiewrodt, R. & Buhl, R. Short-term effects of regular salmeterol treatment on adult cystic fibrosis patients. *The European respiratory journal* 10, 2307–2311 (1997).
47. Unwalla, H. J., Ivonnet, P., Dennis, J. S., Conner, G. E. & Salathe, M. Transforming growth factor- β 1 and cigarette smoke inhibit the ability of β 2-agonists to enhance epithelial permeability. *American journal of respiratory cell and molecular biology* 52, 65–74 (2015).
48. Vijftigschild, L. A. W. *et al.* β 2-Adrenergic receptor agonists activate CFTR in intestinal organoids and subjects with cystic fibrosis. *The European respiratory journal* 48, 768–779 (2016).
49. Wisler, J. W. *et al.* A unique mechanism of beta-blocker action: carvedilol stimulates beta-arrestin signaling. *Proceedings of the National Academy of Sciences of the United States of America* 104, 16657–16662 (2007).
50. Virtanen, P. *et al.* SciPy 1.0: fundamental algorithms for scientific computing in Python. *Nature Methods* 17, 261–272 (2020).
51. Fujii, M., Matano, M., Nanki, K. & Sato, T. Efficient genetic engineering of human intestinal organoids using electroporation. *Nature Protocols* 10, 1474–1485 (2015).
52. Saint-Criq, V. *et al.* Choice of Differentiation Media Significantly Impacts Cell Lineage and Response to CFTR Modulators in Fully Differentiated Primary Cultures of Cystic Fibrosis Human Airway Epithelial Cells. *Cells* 9, 2137 (2020).

SUPPLEMENTARY FIGURES

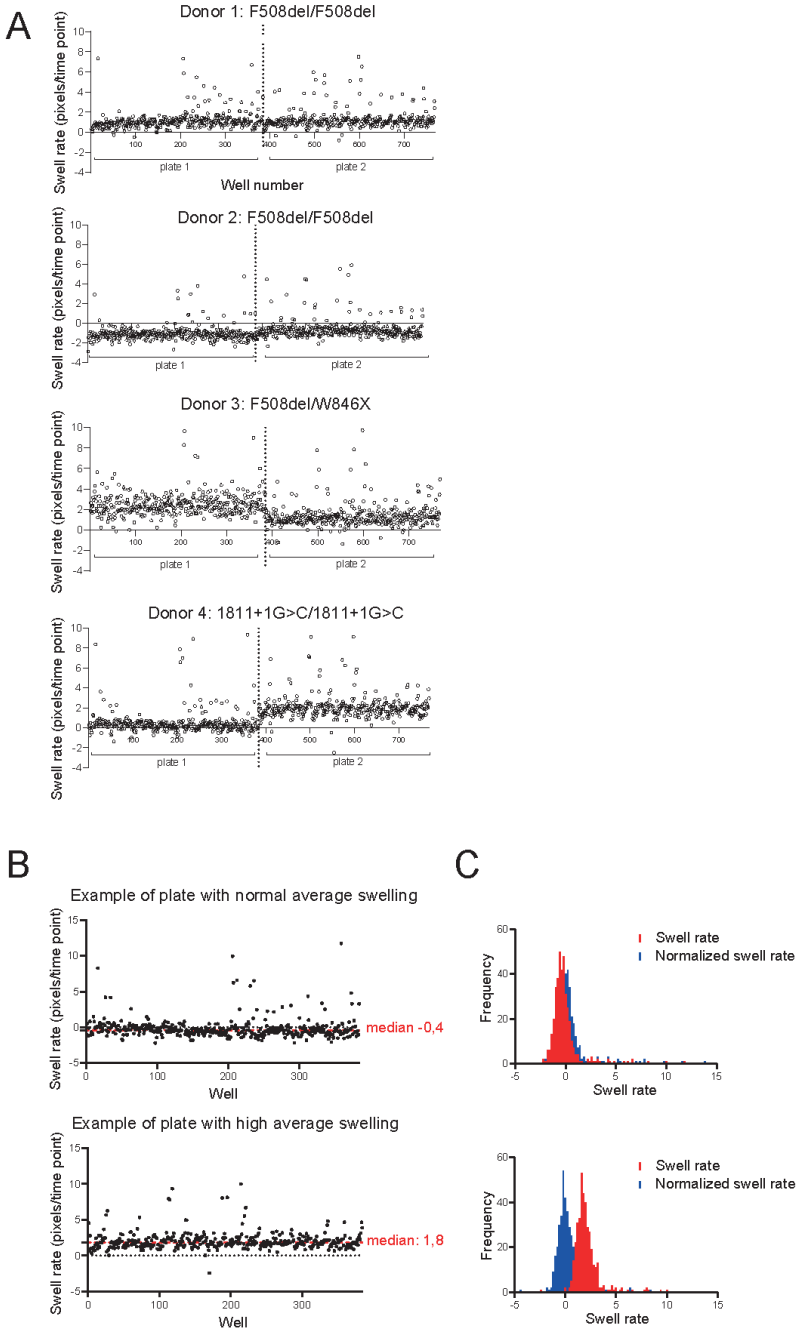
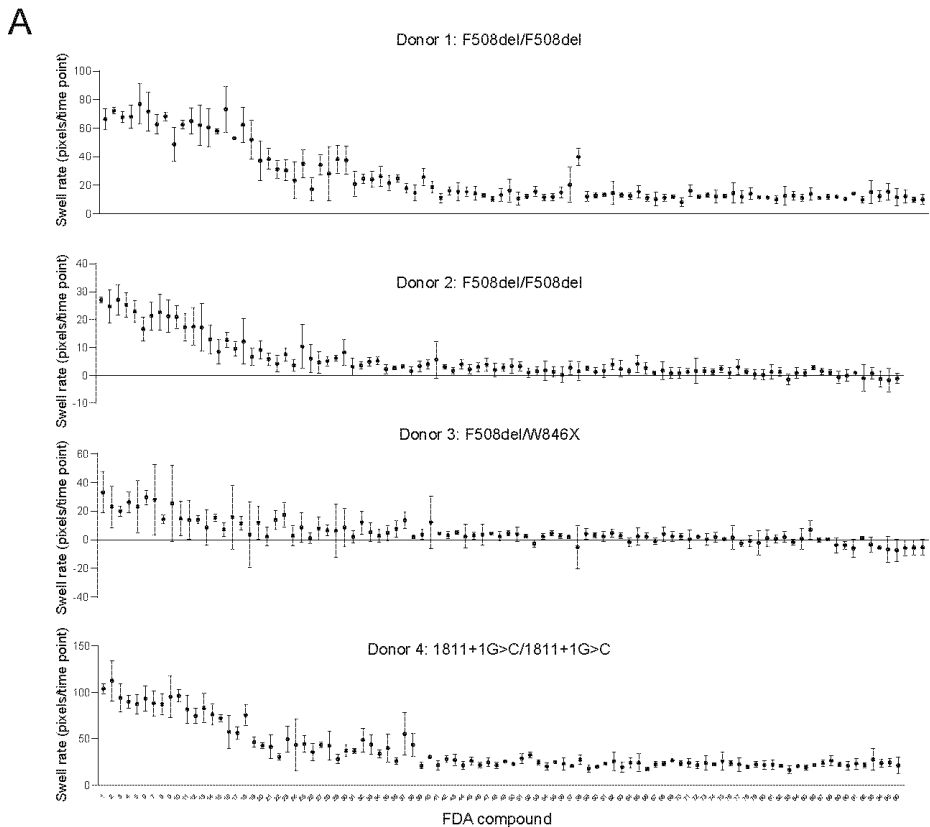


Figure S1. Primary screening assay in individual CF donors.

Figure S1. (continued)

(A) The primary screening assay was performed in four CF donors with different CFTR genotypes as indicated in the graphs (n=4 independent donors, 1-3 replicates per donor). Organoid swelling was determined in 384-wells plate format with 2 FDA compounds combined in a single well. Graphs depict the mean swell rate of all organoids in a well. Dotted lines represent different assay plates; (B) A plate normalization step was performed as median swell rates varied between assay plates and donors. Examples are shown from a plate with normal median swelling (upper panel) and from a plate with high median swelling (lower panel); (C) Histograms show the distribution of measurements before (red) and after (blue) plate normalization.

**Figure S2. Secondary screening assay in individual CF donors.**

(A) The secondary screening assay was performed in the more conventional 96-wells plate format in the same four CF donors as the primary screening assay, as indicated in the graphs. Organoid swelling is shown for individual donors.

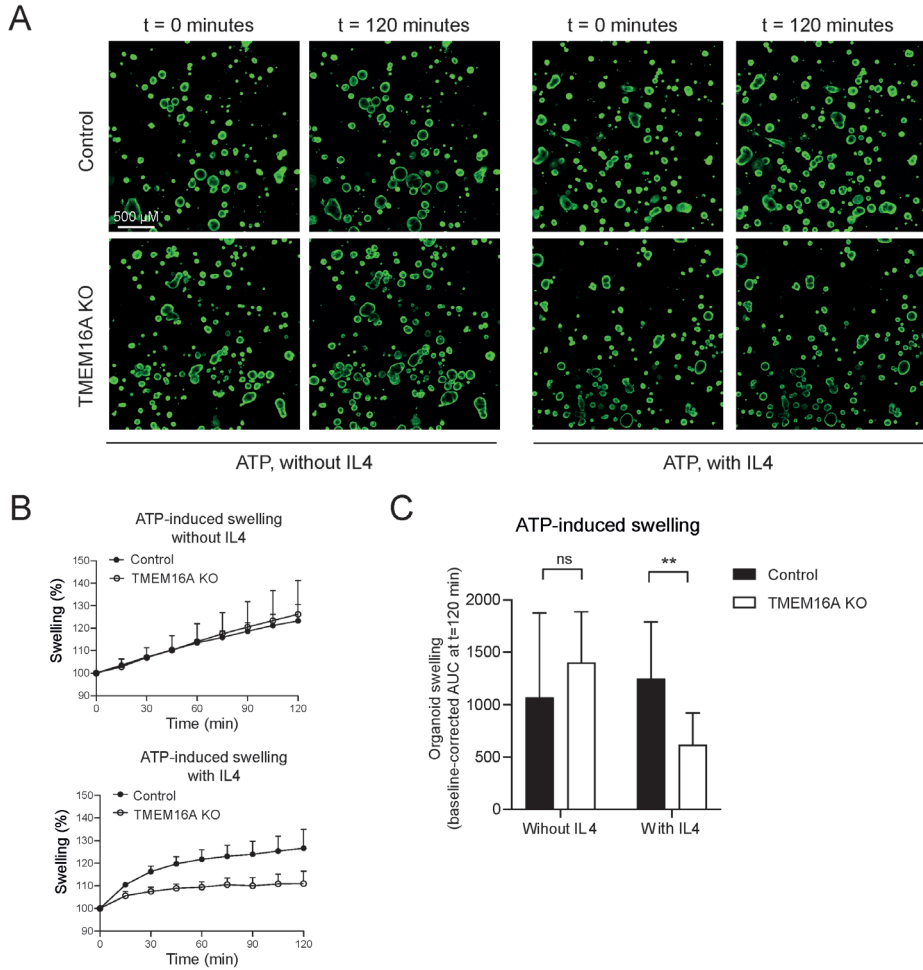


Figure S3. ATP-induced swelling in TMEM16A KO nasal organoids.

(A) Representative confocal images (G542X/CFTR Δ 2.3(21kb)) of TMEM16A KO and control nasal organoids after stimulation with ATP. Organoids were treated with or without IL-4 for 48h; (B,C) Quantification of ATP-induced swelling in TMEM16A KO and control nasal organoids, treated without (upper panel) or with (lower panel) IL-4 for 48h (n=3 independent CFTR-null donors, 1-7 measurements per donor). Analysis of difference was performed using unpaired t-tests. ** p < 0.01.

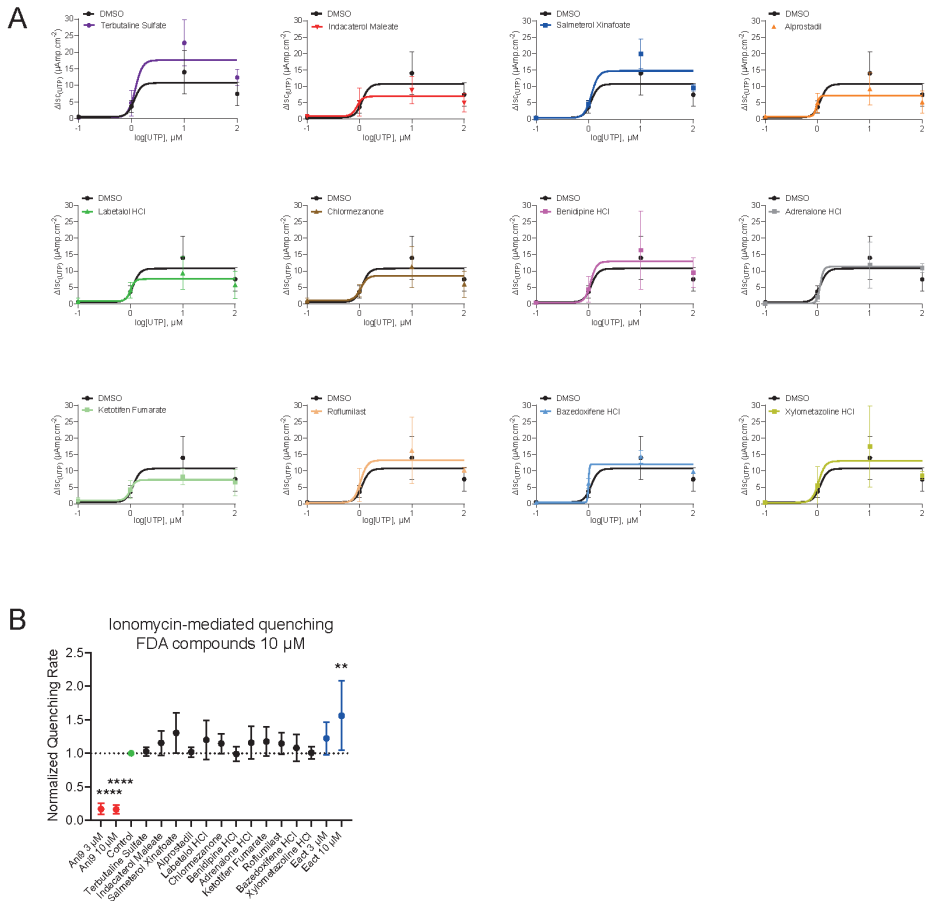


Figure S4. Effect of the hit compounds on TMEM16A in other *in vitro* model systems.

(A) The effect of hit compounds on UTP-dose response curves was analyzed in Ussing Chamber measurements with CFTR-null nasal cells. Data is shown for incubation with DMSO alone or with one of the 12 hit compounds. Nonlinear regression was used to fit a dose-response curve ($n=3$ independent donors, each compound was measured in at least 2 different donors; $n=2-3$ measurements per donor); (B) The Ionomycin-induced quenching assay in CFBE cells was also performed with a higher concentration of the FDA hit compounds (10 μ M instead of 3 μ M). TMEM16A-dependency was demonstrated with sensitivity for Ani9 (3 and 10 μ M, shown in red). DMSO was used as negative control (shown in green) and E_{act} (3 and 10 μ M) as positive control (shown in blue). For quantification, quenching rates were normalized to the control and a one-way ANOVA with Dunnett's post-hoc test was used to analyze differences with control. ** $p < 0.01$, **** $p < 0.0001$.

SUPPLEMENTARY TABLES

Table S1. Basal cell isolation and expansion medium

Reagents	Concentration	Company
Bronchial epithelial cell medium-basal (BEpiCM-b)	50 % (v/v)	ScienCell, Carlsbad, CA, USA
Advanced DMEM/F12	23.5 % (v/v)	Gibco, Waltham, MA, USA
B-27 Supplement, serum free	2 % (v/v)	Gibco, Waltham, MA, USA
GlutaMAX Supplement	1 % (v/v)	Gibco, Waltham, MA, USA
HEPES (1 M)	10 mM	Gibco, Waltham, MA, USA
(±)-Epinephrine hydrochloride	0.5 µg/mL	Sigma-Aldrich, St Louis, MO, USA
Hydrocortisone	0.5 µg/mL	Sigma-Aldrich, St Louis, MO, USA
3,3',5-Triiodo-L-thyronine sodium salt	100 nM	Sigma-Aldrich, St Louis, MO, USA
N-Acetyl-L-cysteine	1.25 mM	Sigma-Aldrich, St Louis, MO, USA
Nicotinamide	5 mM	Sigma-Aldrich, St Louis, MO, USA
SB 202190 (p38i)	500 nM	Sigma-Aldrich, St Louis, MO, USA
DMH-1 (BMPi)	1 µM	Selleck chemicals, Planegg, Germany
A83-01 (TGF-βi)	1 µM	Tocris, Bristol, UK
Y-27632 (ROCKi)	5 µM	Selleck chemicals, Planegg, Germany
DAPT (NOTCHI; only in expansion medium)	5 µg/mL	Fisher Scientific, Landsmeer, Netherlands
Recombinant human FGF-7	25 ng/mL	Peptotech, Rocky Hill, NJ, USA
Recombinant human FGF-10	100 ng/mL	Peptotech, Rocky Hill, NJ, USA
Recombinant human EGF	5 ng/mL	Peptotech, Rocky Hill, NJ, USA
Recombinant human HGF	25 ng/mL	Peptotech, Rocky Hill, NJ, USA
Rspondin 1 conditioned medium (from Rspo1 cells Cultrex®)	20 % (v/v)	Trevigen, Gaithersburg, MD, USA
Penicillin-Streptomycin	1 % (v/v)	Gibco, Waltham, MA, USA
Primocin	100 µg/mL	Invivogen, San Diego, CA, USA
Amphotericin B (only in isolation medium)	250 µg/mL	Gibco, Waltham, MA, USA
Gentamicin (only in isolation medium)	50 µg/mL	Sigma-Aldrich, St Louis, MO, USA
Vancomycin (only in isolation medium)	50 µg/mL	Sigma-Aldrich, St Louis, MO, USA

Table S2. ALI differentiation medium

Reagent	Concentration	Company
Advanced DMEM/F12	98.5% (v/v)	Gibco, Waltham, MA, USA
(±)-Epinephrine hydrochloride	0.5 µg/mL	Sigma-Aldrich, St Louis, MO, USA
Hydrocortisone	0.5 µg/mL	Sigma-Aldrich, St Louis, MO, USA
3,3',5-Triiodo-L-thyronine sodium salt	100 nM	Sigma-Aldrich, St Louis, MO, USA
Penicillin-Streptomycin	1 % (v/v)	Gibco, Waltham, MA, USA
A83-01 (TGF-β ₁)	50 nM	Tocris, Bristol, UK
TTNPB (Retinoic acid agonist)	100 nM	Cayman, Ann Arbor, MI
Recombinant human EGF	0.5 ng/mL	Peprotech, Rocky Hill, NJ, USA

Table S3. Airway organoid medium

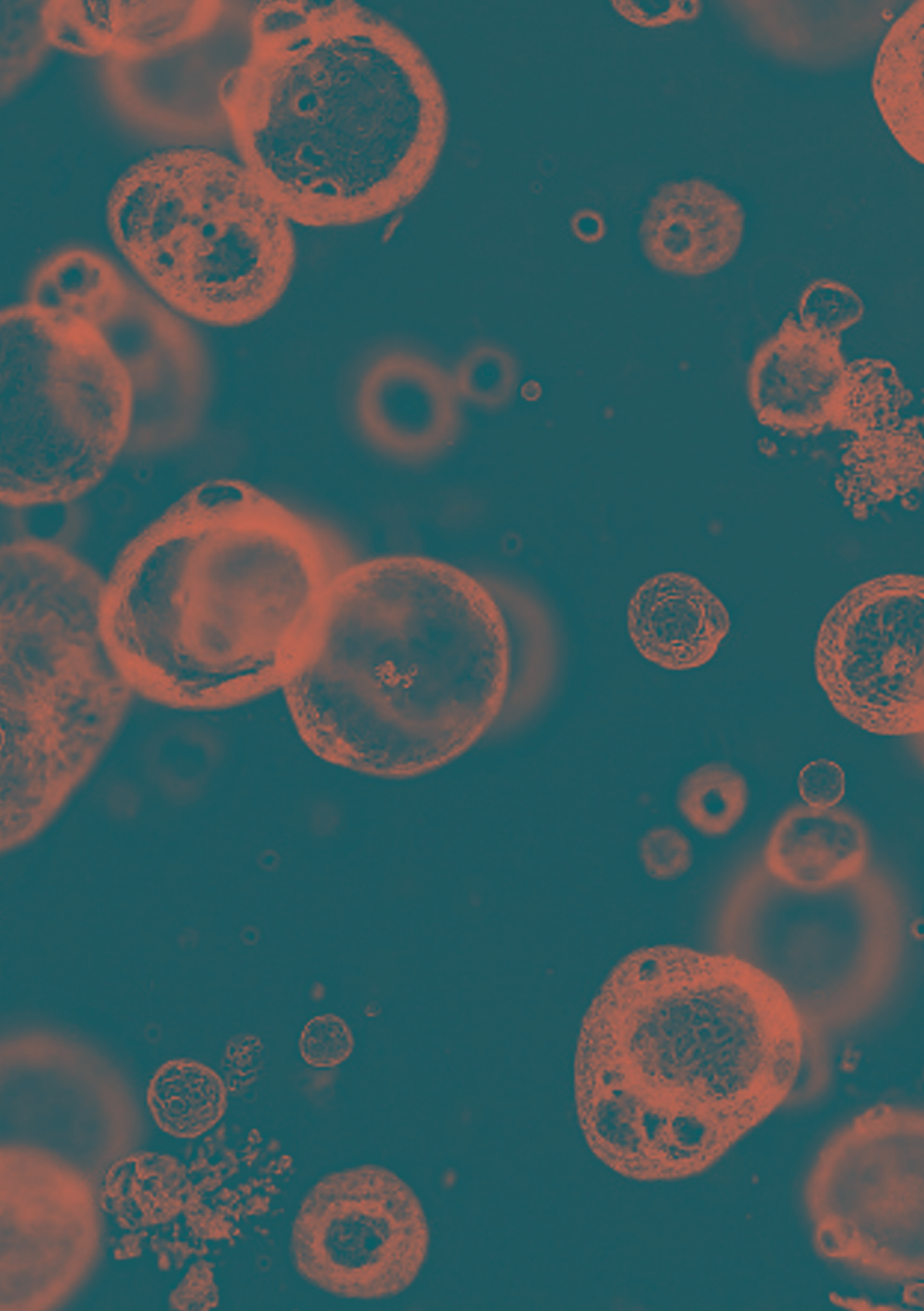
Reagent	Concentration	Company
Advanced DMEM/F12	95.5% (v/v)	Gibco, Waltham, MA, USA
B-27 Supplement, serum free	2 % (v/v)	Gibco, Waltham, MA, USA
GlutaMAX Supplement	1 % (v/v)	Gibco, Waltham, MA, USA
HEPES	10 mM	Gibco, Waltham, MA, USA
N-Acetyl-L-cysteine	1.25 mM	Sigma-Aldrich, St Louis, MO, USA
Nicotinamide	5 mM	Sigma-Aldrich, St Louis, MO, USA
SB 202190 (p38i)	500 nM	Sigma-Aldrich, St Louis, MO, USA
A83-01 (TGF-β ₁)	500 nM	Tocris, Bristol, UK
Y-27632 (ROCKi)	5 µM	Selleck chemicals, Planegg, Germany
Penicillin-Streptomycin	1 % (v/v)	Gibco, Waltham, MA, USA
Recombinant human FGF-7	5 ng/mL	Peprotech, Rocky Hill, NJ, USA
Recombinant human FGF-10	10 ng/mL	Peprotech, Rocky Hill, NJ, USA

Table S4. Antibodies

Antibody	Source	Identifier	Dilution
Mouse anti-MUC5AC	Thermo Fischer Scientific	#MA1-38223	1:500
Rabbit anti-β-tubulin IV	Abcam, Cambridge, UK	#ab179509	1:500
Rabbit anti-TMEM16A	Abcam, Cambridge, UK	AB64085	1:500
Rabbit anti-HSP90	Developed by laboratory of Prof. I. Braakman	NA	1:10.000
Goat anti-mouse IgG1, Alexa Fluor 647	Invitrogen, Waltham, MA, USA	A-21240	1:500
Goat anti-rabbit IgG, Alexa Fluor 488	Invitrogen, Waltham, MA, USA	A-11034	1:500
Goat anti-rabbit Immunoglobulins/HRP	Dako, Santa Clara, CA, USA	P0448;RRID:AB_2617138	1:2.000

Table S5. qPCR primers

Gene	Forward primer (5'- 3')	Reverse primer (5'- 3')
<i>ANO1</i>	AGGATTCTTTTTCGACAGCAA	CGTTTTCACCGTTGTAGTCTCC
<i>SLC26A9</i>	GACTACATCATTCTGACCTGC	AGGAGTAGAGGCCATTGACTG
<i>SLC26A4</i>	TGGTGGCTTGCAGATTGGAT	AGCTGTGAGACCAGCACTTG
<i>CLCN2</i>	TTGATCCTGCTCCCTCCAG	CATAAGCATGGTCCACTCCC
<i>SCNN1A</i>	TCTGCACCTTTGGCATGATGT	GAAGACGAGCTTGTCCGAG
<i>CFTR</i>	CAACATCTAGTGAGCAGTCAGG	CCCAGGTAAGGGATGTATTGTG
<i>ATP5B</i>	TCACCCAGGCTGGTTCAGA	AGTGGCCAGGGTAGGCTGAT
<i>RPL13A</i>	AAGGTGGTGGTCGTACGCTGTG	CGGGAAGGGTTGGTTCATCC



Chapter 4

Examining CRISPR knockouts of non-CFTR ion channels or transporters in cystic fibrosis nasal organoid fluid secretion

Lisa W. Rodenburg, Shannon M.A. Smits, Cornelis K. van der Ent, Jeffrey M. Beekman and Gimano D. Amatngalim

ABSTRACT

This study aimed to identify ion channels and transporters involved in CFTR-independent airway epithelial fluid secretion, with potential implications for reducing mucus obstruction in cystic fibrosis (CF). CRISPR gene editing was used to create knockouts of TMEM16A, SLC26A9, SLC26A4, CLCN2, and SCNN1A in CFTR null nasal airway organoids. This was followed by agonist-induced organoid swelling assays, studied under normal conditions and with interleukin-4 (IL-4) treatment. Gene knockout organoids did not show significant changes in agonist-induced swelling assays compared to control organoids. However, we observed involvement of the anion exchanger SLC26A4 (pendrin) in preventing intrinsic fluid secretion of organoids upon IL-4 treatment. This study provides proof-of-concept for utilizing CRISPR-gene editing and nasal organoid technology to investigate CFTR-independent fluid secretion. Moreover, our findings highlight the presence of unexplored CFTR-independent mechanisms, beyond the selected ion channels and transporters, which could be potential therapeutic targets for reducing airway mucus obstruction in CF.

INTRODUCTION

The airway epithelium plays a crucial role in defending the lungs against airborne pathogens through host defence mechanisms, such as mucociliary clearance¹. These host defence mechanisms involve the regulation of airway surface fluid balance through airway epithelial ion channels and transporters, including the cystic fibrosis transmembrane conductance regulator (CFTR) protein, which mediates chloride and bicarbonate conductance. Disturbances in airway epithelial ion conductance are considered significant contributors to the development of airway mucus obstruction and the subsequent decline in lung function seen in obstructive airway diseases². While CFTR function in airway epithelial cells has been well-studied, the precise functions of other ion channels and transporters remains largely unclear. Understanding the functions of these non-CFTR ion channels and transporters is critical for unraveling the pathogenesis of obstructive airway diseases.

The significance of restoring anion-dependent fluid transport is most well exemplified based on deficiencies in cystic fibrosis (CF). This genetic disorder is caused by mutations in the *CFTR* gene³, which attenuate CFTR-mediated anion transport in airway epithelial cells. This leads to reduced epithelial fluid secretion, accumulation of dehydrated mucus at the epithelial surface, and subsequent airway disease development². CFTR modulator drugs can restore CFTR protein function, with a new triple modulatory therapy, consisting of two correctors and a potentiator, showing highly effective therapeutic outcomes for the common F508del mutation⁴. However, 20% of people with CF are ineligible due to non-responding or uncharacterized rare mutations, and only 12% of people with CF have access due to high costs⁵. Therefore, alternative CF therapies are needed which are effective in all people with CF, independent of their mutation type.

Non-CFTR channels and transporters in the airway epithelium are potential drug targets to restore fluid balance, reduce airway mucus obstruction, and preserve lung function in individuals with CF⁶. Among these targets, TMEM16A is extensively studied as a calcium-activated chloride channel predominantly expressed in airway epithelial goblet cells⁷⁻¹¹. SLC26A9, another chloride channel expressed in airway epithelial cells, acts as a CF gene modifier, impacting CF disease severity and the efficacy of CFTR-directed therapies¹². CLCN2 (ClC-2) is a less studied chloride channel, but present in the airway epithelium and thus a potential alternative target^{13,14}. SLC26A4 (pendrin), belonging to the same SLC family as SLC26A9, serves as a chloride/bicarbonate anion exchanger and facilitates CFTR-dependent chloride transport and pH regulation, particularly during inflammatory conditions^{15,16}. The sodium transporter ENaC

becomes hyperactivated in CF airway epithelia, which subsequently drives the absorption of chloride and water via a paracellular shunt¹⁷.

In a previous study, we developed a nasal airway organoid-based swelling assay to investigate CFTR-independent fluid secretion in CF¹⁸. Building upon that work, the objective of our current study was to identify the specific involvement of TMEM16A, SLC26A9, SLC26A4, CLCN2 and SCNN1A (the α -subunit of ENaC) in CFTR-independent swelling of CF nasal organoids, using CRISPR-Cas9-based gene knockout techniques. Through organoid swelling assays, we examined the impact of individual ion transporters on epithelial fluid secretion under both normal and inflammatory conditions upon stimulation with IL-4. This approach allowed us to gain insights into the role of non-CFTR ion channels and transporters in CFTR-independent airway epithelial fluid secretion, thereby enhancing our understanding of alternative mechanisms to restore airway surface fluid balance in people with CF.

RESULTS

Generation of CRISPR-based gene knockouts in CF nasal epithelial cells

We first created gene knockouts of *TMEM16A*, *SLC26A9*, *CLCN2*, *SLC26A4*, and *SCNN1A* using highly efficient CRISPR-based genome editing with Cas9 ribonucleoprotein (RNP) as we previously described¹⁸. The gene knockouts were created in three independent CF donors without any CFTR protein function (G542X/CFTRdele2,3; W1282X/1717-1G>A; R553X/R553X) to exclude residual CFTR function in further analyses. Knockout cells exhibited large deletions compared to their controls, as demonstrated by DNA analysis (Figure 1A). Knockout efficiencies, estimated using the ICE analysis tool based on Sanger sequencing traces, ranged from 77 to 95% (Figure 1B). *TMEM16A* knockout cells were also validated on protein level by western blot, as published before¹⁸. Furthermore, these knockout cells were functionally validated in Ussing Chamber measurements where $\text{ani}9$ -dependent UTP-induced currents were absent in the *TMEM16A* knockout cells¹⁸.

Epithelial fluid secretion was not affected in gene-edited nasal organoids

To determine the impact of these gene knockouts on fluid secretion, we generated nasal organoids from the gene-edited and control cells (Figure 2A). The organoids were generated using a previously described method involving the differentiation of basal progenitor cells in air-liquid interface (ALI) cultures, fragmentation of the differentiated epithelial layer, and embedding of the fragments in Matrigel to promote self-organization into 3D organoids¹⁸. We then assessed the swelling response of the nasal organoids to various agonists, including ATP, E_{act} , forskolin, CPA, and ionomycin. These agonists are known to induce CFTR-independent chloride conductance in

primary airway epithelia. In our 2-hour measurements, all the agonists induced nasal organoid swelling. However, we did not observe significant differences in organoid swelling between the majority of the gene knockouts and the control organoids (Figure 2B). Notably, we did observe a non-significant trend of enhanced CPA- and ionomycin-induced organoid swelling in *CLCN2* knockout cells, although this observation was limited to two donors and did not reach statistical significance (Figure 2B). Furthermore, we examined the effect of a selection of FDA-approved drugs previously identified to induce CFTR-independent epithelial fluid secretion¹⁸. However, we did not observe significant differences in organoid swelling among any of the gene knockouts (Figure 2C). While the involvement of *CLCN2* in enhancing CPA- and ionomycin-induced organoid swelling warrants further investigation, our results indicate that the selected non-CFTR ion channels and transporters may not play major roles in CFTR-independent fluid secretion in CF nasal organoids under the examined experimental conditions.

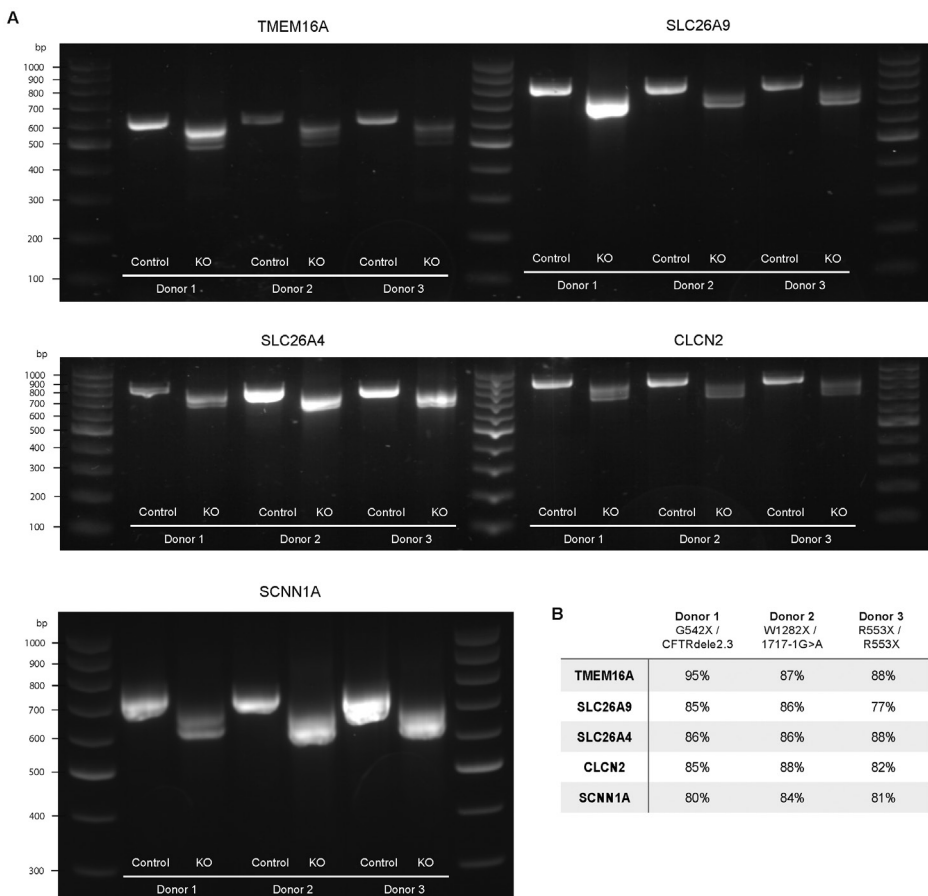
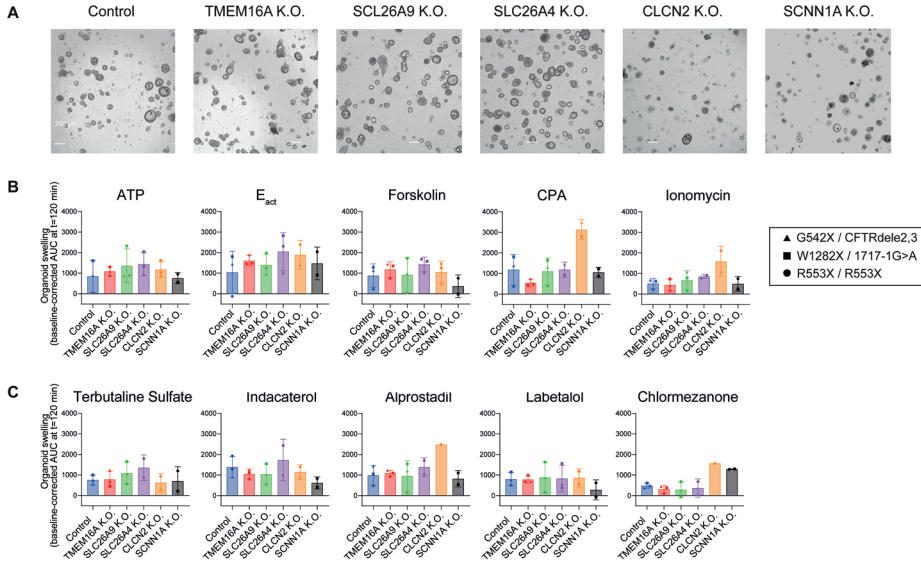


Figure 1. Generation of CRISPR-based gene knockouts in CF nasal epithelial cells.

Figure 1. (continued)

(A) DNA gel with PCR-amplified products from the gene knockouts of *TMEM16A*, *SLC26A9*, *SLC26A4*, *CLCN2* and *SCNN1A* in three CFTR null donors. (B) Knockout efficiencies of the gene knockouts estimated with the ICE analysis tool based on Sanger sequencing tracings.

**Figure 2. Epithelial fluid secretion was not affected in gene-edited nasal organoids.**

(A) Brightfield images showing the morphology of control and gene-edited nasal organoids two days after plating. Representative pictures are shown from one donor (G542X/CFTR Δ 2.3 and W1282X/1717-1G>A for the *SCNN1A* K.O.). (B) Organoid swelling induced by the agonists ATP, E_{act} , forskolin, CPA and ionomycin in control and gene-edited nasal organoids (n=2-3 independent donors, 1-8 replicates per donor). (C) Organoid swelling induced by a selection of FDA-approved drugs in control and gene-edited nasal organoids (n=1-3 independent donors, 1-6 replicates per donor). Organoid swelling is quantified as AUC values from two hour measurements, and depicted as mean per donor from several replicates. Analysis of difference between knockout and control organoids was performed with a two-way ANOVA with Dunnett post-hoc test (panel b-c). Only significant differences are shown.

Enhanced expression of alternative ion channels and transporters under inflammatory conditions

Previous studies have demonstrated an increased expression of *TMEM16A*, *SLC26A4*, and *SLC26A9* upon treatment with the Th2 cytokines IL-4 and IL-13^{11,15,19–21}. Based on this, we aimed to further investigate whether pro-inflammatory stimulation with IL-4 could enhance the sensitivity of the organoid swelling assay, specifically targeting these non-CFTR ion channels and transporters. First, we conducted a comprehensive analysis of the effects of IL-4 treatment on nasal organoids derived from three CFTR null donors using RNA-sequencing (RNA-seq). The principal component analysis (PCA) revealed a distinct gene expression pattern in IL-4-treated organoids compared to control cultures, indicating a significant impact of IL-4 stimulation (Figure 3A).

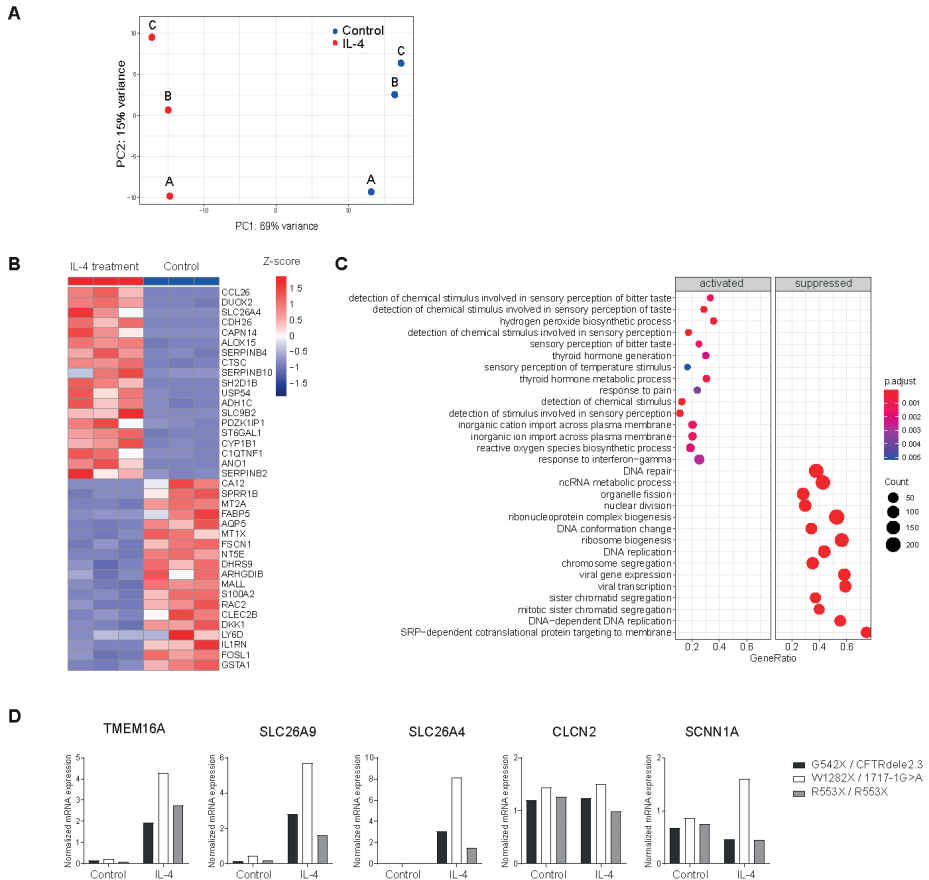


Figure 3. Enhanced expression of alternative ion channels and transporters under inflammatory conditions. (A) PCA to compare transcriptomic profiles from CFTR null nasal organoids treated with IL-4 or vehicle control (n=3 independent donors). A-C indicate individual donors. (B) Heatmap showing the 20 most enriched genes in donor-matched organoids treated with (red) or without (blue) IL-4 (n=3 independent donors). Data is shown as a Z score of the normalized expression. (C) Gene set enrichment analysis showing the top 15 enriched GO terms in IL4-treated and donor-matched non-IL4-treated nasal organoids (n=3 independent donors). Color indicates the degree of significance and dot size indicates gene count. (D) mRNA expression determined by qPCR of TMEM16A, SLC26A9, SLC26A4, CLCN2 and SCNN1A in nasal organoids from three CFTR null donors with IL-4 treatment or vehicle control (n=3 independent donors).

546 and 522 genes were significantly enriched in donor-matched organoids with or without IL-4 treatment, respectively (Table S1). The top 20 significantly enriched genes in IL-4 treated organoids included the chloride channel ANO1 (TMEM16A) and the chloride/bicarbonate exchanger SLC26A4 (Figure 3B). Pathway analysis showed enrichment of gene sets involved in sensory perception and ion transport in IL-4 treated organoids and an enrichment of pathways involved in DNA repair and replication in organoids without IL-4 treatment (Figure 3C). To validate our RNA-seq results,

we performed qPCR experiments, which confirmed the upregulation of *TMEM16A*, *SLC26A9*, and *SLC26A4* in IL-4-stimulated nasal organoids from the three CFTR null donors (Figure 3D). In contrast, mRNA expression of *CLCN2* and *SCNN1A* was unaltered under these conditions. In summary, our study demonstrates that pro-inflammatory stimulation with IL-4 enhances the expression of the non-CFTR channels *TMEM16A*, *SLC26A4*, and *SLC26A9*, and therefore likely also increase the sensitivity of the organoid swelling mediated by these ion channels and transporters.

FDA-approved β - and α -agonists induce CFTR-independent fluid secretion in IL-4-treated CF nasal organoids

We proceeded to characterize drugs that could potentially increase fluid secretion in IL-4-treated nasal organoids of individuals with CF. For this purpose, we performed a screening assay using an FDA-approved drug library consisting of 1400 compounds. The screening was conducted in nasal organoids from two CF donors with the F508del/F508del and G542X/CFTRdele2.3 mutations. The assay was carried out in a 384-well plate format, with each well containing a combination of two drugs. With the screening assay, we identified 21 drug combinations as hits based on their plate-normalized swell rates, which exceeded the threshold of 1 interquartile range (IQR) above the median (Figure 4A). To further analyze the hits, we compared them with FDA-approved compounds that were previously shown to increase CFTR-independent fluid secretion in organoids without IL-4 treatment¹⁸. We observed that 15 compound combinations were hits in both screening assays. Notably, the majority of these combinations included a β - or α -agonist, which are likely responsible for inducing organoid swelling (Figure 4B, box 1). Six compound combinations were exclusively identified in IL-4-treated organoids, although five of them were close to the threshold. One of the wells contained the compounds Bardoxolone Methyl and Vitamin E (Figure 4B, box 3). On the other hand, 32 hits were only found in nasal organoids without IL-4 treatment (Figure 4B, box 2). Three of these compound combinations contained a β -antagonist, specifically Carteolol, Labetalol, and Acebutolol. In conclusion, the FDA-approved drug screen conducted in IL-4-treated nasal organoids primarily identified β - or α -agonists as hits. No new compounds of interest were identified when compared to the screening assay performed in non-IL-4-treated nasal organoids. These findings suggest that the pro-inflammatory environment induced by IL-4 may not significantly alter the drug response in terms of CFTR-independent fluid secretion. In conclusion, the FDA-approved drug screen under inflammatory conditions mainly identified β - or α -agonists and no new compounds of interest were identified compared to the screening assay, previously conducted in non-IL-4-treated nasal organoids¹⁸.

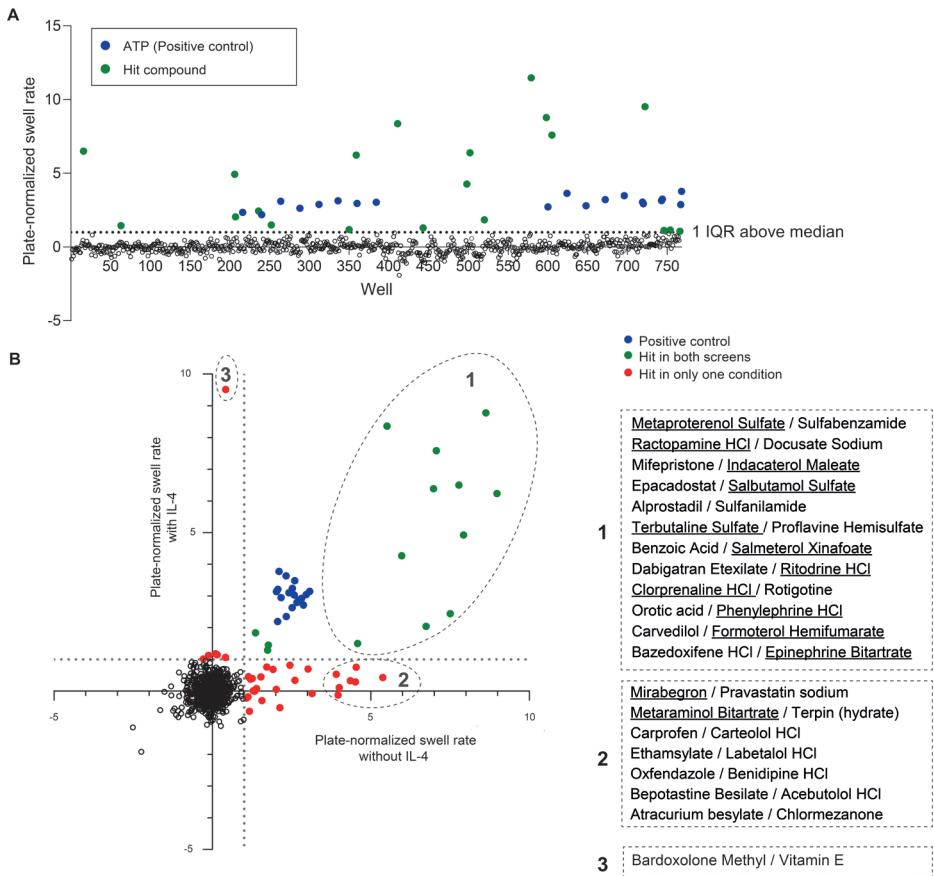


Figure 4. FDA-approved β - and α -agonists induce CFTR-independent fluid secretion in IL-4-treated CF nasal organoids.

(A) An FDA-approved drug screen was performed in nasal organoids treated with IL-4 for 48 hours. The screen was performed in 2 independent donors (F508del/F508del, G542X/CFTR Δ 2.3, n=2 replicates per donor) in 384-well plate format. 1400 compounds were screened with 2 compounds combined in a single well. ATP (100 μ M) was used as positive control. Data is shown as plate-normalized swell rate, averaged for all individual organoids in a well. A well containing hit compounds was defined by a threshold of a plate-normalized swell rate 1 IQR above the median plate-normalized swell rate. (B) Comparison between the FDA-approved drug screen performed in nasal organoids treated with and without IL-4. Organoid swelling is quantified as plate-normalized swell rate, averaged for all individual organoids in a well. ATP (100 μ M) or Eact (10 μ M) was used as positive control for the screen with or without IL-4 treatment respectively. A selection of wells containing hit compounds in both screens (box 1) or in one of both screens (box 2 and 3) are highlighted. Compounds with a function as β - or α -agonist are underlined.

SLC26A4 modifies fluid secretion in nasal organoids stimulated with IL-4

Subsequently, we conducted experiments using gene knockout cells in nasal organoids treated with IL-4. Initially, we observed a reduction in intrinsic fluid secretion in IL-4-treated control nasal organoids compared to untreated controls (Figure 5A). A similar

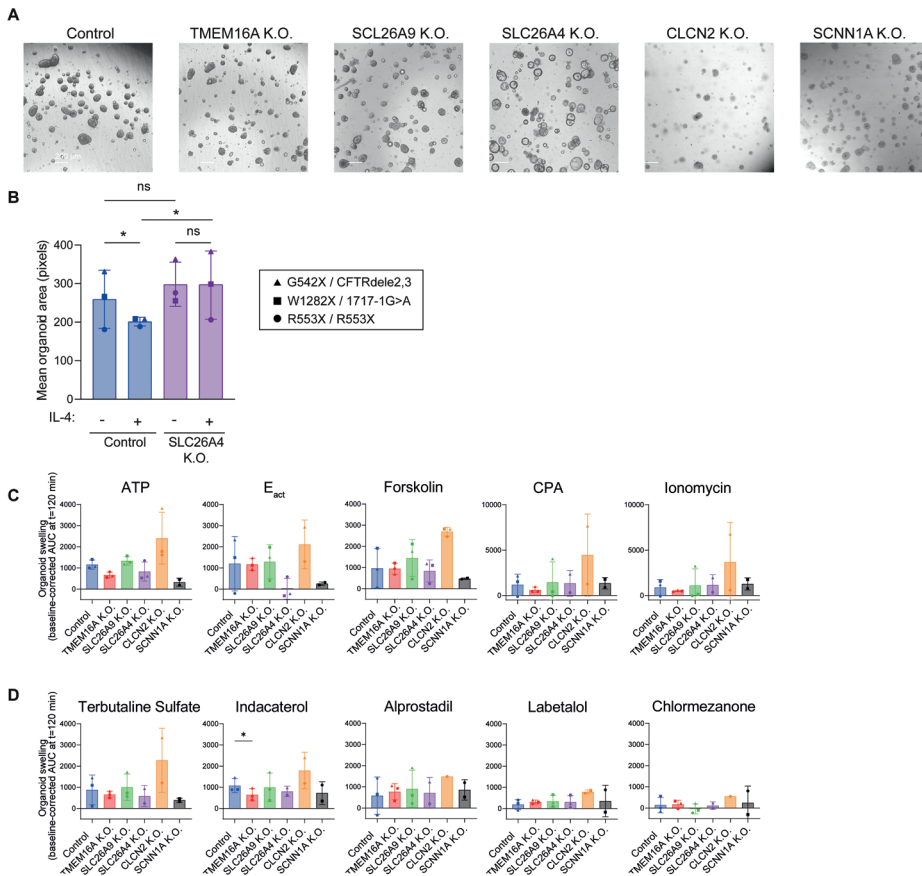


Figure 5. SLC26A4 modifies fluid secretion in nasal organoids stimulated with IL-4.

(A) Brightfield images showing the morphology of control and gene-edited nasal organoids two days after plating and with IL-4 treatment. Representative pictures are shown from one donor (G542X/CFTRdele2.3 and W1282X/1717-1G>A for the SCNN1A K.O.). (B) Individual organoid size compared between control and SLC26A4 K.O. organoids treated with or without IL-4 (n=3 independent donors). Data is shown as mean organoid size per well. (C) Organoid swelling induced by the agonists ATP, Eact, forskolin, CPA and ionomycin in control and gene-edited nasal organoids treated with IL-4 (n=2-3 independent donors, 1-7 replicates per donor). (D) Organoid swelling induced by a selection of FDA-approved drugs in control and gene-edited nasal organoids treated with IL-4 (n=1-3 independent donors, 1-7 replicates per donor). Organoid swelling is quantified as AUC values from two hour measurements, and depicted as mean per donor from several replicates. Analysis of difference was performed with a two-way ANOVA with Tukey (b) or Dunnett (c-d) post-hoc test. Only significant differences are shown. ns = non-significant, * p < 0.05.

reduction in intrinsic fluid secretion was also observed in *TMEM16A*, *SLC26A9*, *CLCN2*, and *SCNN1A* gene knockout organoids upon IL-4 treatment. However, interestingly, *SLC26A4* gene knockout organoids maintained their intrinsic fluid secretion even after IL-4 treatment (Figure 5A-B). To further investigate the effect of IL-4 on airway organoid fluid secretion, the swelling response to various agonists in IL-4-treated cultures was

examined, including a selection of FDA-approved drugs identified in the previous screening assays (Figure 5C-D). However, we did not observe significant differences in swelling between control organoids and gene-edited organoids under IL-4 treatment. It is noteworthy that E_{act} -induced organoid swelling was absent in *SLC26A4* knockout organoids, although the variation between the three donors limited the significance of this observation (Figure 5C). Overall, the results indicate that gene knockouts of *TMEM16A*, *SLC26A9*, *CLCN2*, and *SCNN1A* do not significantly alter agonist-induced organoid swelling in the presence of IL-4. The maintenance of intrinsic fluid secretion and attenuated E_{act} -induced swelling in IL-4 treated organoids suggest that upregulation of *SLC26A4* contributes to altered airway epithelial fluid secretion in CF.

DISCUSSION

The aim of this study was to identify specific ion channels and transporters involved in CFTR-independent nasal organoid swelling and evaluate their potential as therapeutic targets for restoring the epithelial fluid balance in people with CF. The lack of specific inhibitors for non-CFTR ion channels and transporters complicates mechanistic studies. Therefore, we utilized a highly efficient method to create gene knockouts in nasal brushing-derived epithelial cells, using CRISPR/Cas9 technology. Gene editing is a challenging procedure in primary nasal cells, as they have a limited expansion rate and do not survive as single cells²². A clonal selection step is therefore unfeasible. Other groups already reported gene editing in primary airway epithelial cells, but needed a fibroblast-feeder layer for cell expansion²³, used bronchial epithelial cells^{24,25} or cells derived from nasal biopsies during surgery²⁶ or lung explants²⁷. We developed a protocol to create gene knockouts in nasal epithelial cells derived from non-invasive nasal brushings and without the need for a clonal selection step because of high knockout efficiencies. After transfection, cells still could be expanded, cryostored and differentiated as ALI cultures.

In our experiments, we did not observe a significant reduction in agonist-induced swelling in any of the gene-edited organoids, including those treated with previously identified FDA-approved drugs¹⁸. Therefore, we proceeded with experiments using IL-4-treated nasal organoids. Consistent with previous studies, IL-4 treatment led to increased expression of *TMEM16A*, *SLC26A9*, and *SLC26A4* in CF nasal organoids^{11,15,19-21}. This finding suggests that IL-4 treatment enhances the sensitivity of the organoids to these specific ion channels and transporters. To explore if we could find FDA-approved drugs enhancing epithelial fluid secretion in IL-4-treated organoids, we repeated the FDA-approved drug screen under this inflammatory condition. However, only one new

compound combination was identified compared to the screen without IL-4, consisting of Bardoxolone Methyl and vitamin E. From previous experiments we know that Bardoxolone Methyl and not vitamin E induces the organoid swelling (unpublished). Bardoxolone Methyl is an activator of the Nrf2 pathway and inhibitor of the NF- κ B pathway. It was initially developed to treat chronic kidney disease, but appeared toxic as a phase 3 clinical trial was terminated due to a high rate of cardiovascular adverse events²⁸. In contrast to the screening assay conducted in non-IL-4-treated organoids, the screen performed in IL-4-treated organoids yielded fewer hits. This discrepancy could be attributed to several factors, such as the smaller number of donors used (two donors compared to four donors) or the possibility that some compounds may act via pathways that are not active under inflammatory conditions.

Consistent with our previous experiments conducted in non-inflammatory conditions, we did not observe a reduction in swelling in IL-4-stimulated gene knockout organoids in response to agonists, including FDA-approved drugs. This suggests that the gene knockouts of *TMEM16A*, *SLC26A9*, *SLC26A4*, *CLCN2*, and *SCNN1A*, under the influence of IL-4, do not significantly alter the responsiveness of the organoids to these drugs. However, we did observe a notable phenotypic difference in *SLC26A4* knockout organoids treated with IL-4. While IL-4 treatment led to a depletion of intrinsic fluid secretion, as indicated by a reduction in lumen formation, in control cultures and gene knockouts of *TMEM16A*, *SLC26A9*, *CLCN2*, and *SCNN1A*, the *SLC26A4* knockout organoids maintained lumen formation even in the presence of IL-4. The maintenance of lumen formation in *SLC26A4* knockout organoids even in the presence of IL-4 is an intriguing observation. It suggests that SLC26A4 may play a role in reducing fluid secretion in inflammatory airway conditions, as observed in CF. This finding aligns with previous studies that reported elevated airway surface liquid levels in SLC26A4-deficient ALI-cultured nasal epithelial cells, which was further increased upon stimulation with IL-13²⁹. SLC26A4, as an electroneutral anion exchanger, interacts with other ion channels and transporters to regulate fluid secretion in the airway epithelium. Previous studies have demonstrated an interaction between chloride conductance by CFTR and bicarbonate transport by SLC26A4, highlighting their cooperative roles in maintaining fluid balance^{16,30}. However, in the context of CFTR-null nasal organoids, as observed in our study, the specific ion channel or transporter responsible for lumen formation under resting conditions remains unknown. Additionally, SLC26A4 has been implicated in mucus secretion, and individuals with SLC26A4 mutations exhibit reduced mucus expression in the airway epithelium^{29,31}. In extent to these findings, our data support that inhibiting SLC26A4 could potentially increase airway epithelial fluid secretion in inflammatory conditions, independent of CFTR function. Consequently, targeting SLC26A4 inhibition may hold therapeutic potential for enhancing airway epithelial fluid secretion in

individuals with CF. Next to intrinsic fluid secretion, the observed reduction of E_{act} -induced swelling in *SLC26A4* knockout organoids treated with IL-4 suggests a potential interaction between *SLC26A4* and calcium-dependent organoid swelling mediated by TRPV4 activation³². E_{act} is known to increase intracellular calcium levels through its activation of TRPV4 channels. However, the exact mechanism by which *SLC26A4* influences calcium-dependent organoid swelling and its interaction with TRPV4 in this context is not yet fully understood and requires further investigation.

In summary, in our study we successfully generated gene knockouts targeting specific ion channels and transporters, revealing the involvement of *SLC26A4* in the regulation of airway epithelial fluid secretion during IL-4-mediated inflammation. However, the specific ion channels and transporters responsible for CFTR-independent nasal organoid swelling induced by FDA-approved drugs remain unidentified. The presence of swelling in CFTR null nasal organoids suggests the existence of alternative pathways in CF airway epithelia that can activate fluid secretion independently of the targeted ion channels and transporters investigated in this study. Therefore, to gain a deeper understanding of CFTR-independent fluid secretion and identify potential therapeutic targets, it is crucial to conduct further research using CRISPR-based gene knockout techniques. By characterizing unexplored mechanisms, we may uncover novel targets that hold promise for developing effective treatments aimed at restoring airway epithelial fluid balance and improving respiratory function in individuals with CF, but potentially also other airway diseases.

MATERIALS & METHODS

Cell culturing of nasal brushing-derived epithelial cells

Nasal brushings were collected from ten people with CF (F508del/F508del (2 female (F), 2 male (M)); W1282X/1717-1G>A (F); R553X/R553X (F); G542X/Dele2.3 (21kb) (M); F508del/W846X (F); 1811+1G>C/1811+1G>C (both F)). All subjects signed informed consent for the use and storage of their cells. The procedure was approved by a specific ethical board for the use of biobanked materials TcBIO (Toetsingscommissie Biobanks), an institutional Medical Research Ethics Committee of the University Medical Center Utrecht (protocol ID: 16/586). Basal progenitor cells were isolated from the nasal brushings and subsequently expanded and cryostored. Knockout epithelial cells were generated by electroporation of basal progenitor cells with RNP complexes, consisting of Cas9 protein and a mix of three sgRNA's. Knockout validation was performed by PCR amplification, gel electrophoresis and Sanger sequencing. Knockout efficiencies were estimated using the ICE analysis tool (<https://ice.synthego.com/>). Normal and

gene-edited basal progenitor cells were then differentiated at ALI conditions for 14-21 days towards a pseudostratified airway epithelium. The differentiated epithelial layer was then dissociated and disrupted into epithelial fragments. These were embedded in Matrigel and plated in 24-well plates to self-organize into organoids. When indicated, airway organoid medium was supplemented with IL-4 (10 ng/mL) instead of FGF7 and FGF10. The procedures were described in more detail previously¹⁸.

Organoid swelling assays

One day after plating in 24-well plates, organoids were passaged to 96-well plates. Swelling assays were performed one day later. At the day of the swelling assay, organoids were pre-treated with calcein green AM for 30 minutes. Organoids were then stimulated with an agonist (forskolin (5 μ M), ATP (100 μ M), E_{act} (10 μ M), CPA (100 μ M), ionomycin (1 μ M)), FDA compound (3 μ M) or vehicle control to analyze their effect on epithelial fluid secretion. Pictures were taken every 15 minutes for 2 hours in total. Swelling experiments were performed in quadruplets. Organoid swelling was quantified by assessing total organoid area in a well and calculating organoid surface area over time, normalized for $t = 0$ with 100% as baseline. Additionally, AUC values ($t = 120$ min) were calculated, corrected for the baseline by subtraction of the AUC values from DMSO-treated wells from the same experimental plate.

The FDA-approved drug screen was performed in 384-well plate format with two compounds combined in a single well, as previously described¹⁸. Organoid swelling was measured in 3 hour-measurements. ATP (100 μ M) was used as positive control. Organoid swelling was quantified by use of the neural network OrgaQuant, which automatically recognizes organoids in brightfield pictures³³. Linear regression was used to determine swell rates of individual organoids. The mean swell rate of all organoids in a well was used for further analysis. Plate-normalization was performed to compare swell rates across different plates and donors by the following formula: $(\text{swell rate}_{\text{well}} - \text{median swell rate}_{\text{plate}}) / \text{IQR swell rate}_{\text{plate}}$, where IQR is the inter quantile range.

The OrgaQuant neural network was also used to perform organoid size measurements without any stimulation³³. Organoid swelling experiments and the OrgaQuant analysis were described in more detail previously¹⁸.

mRNA expression analysis

To determine mRNA expression levels, RNA was isolated from organoids treated with IL-4 or vehicle control for 48-72 hours, using the RNeasy Mini Kit (Qiagen, Venlo, Netherlands) according to the manufacturer's protocol. For RNA-seq, RNA was sent to Single Cell Discoveries and an adapted version of the CEL-seq protocol was used

^{34,35}. Total RNA concentration was measured and normalized to 20 ng/μl using a Qubit fluorometer (Invitrogen, Waltham, MA, USA), and RNA quality was assessed via bioanalyzer and RNA Pico 6000 kit (Agilent, Santa Clara, CA, USA). Normalized total RNA (with RNA integrity number (RIN) scores >7) was used for library preparation and sequencing. Samples were barcoded with CEL-seq primers during a reverse transcription and pooled after second strand synthesis. The resulting cDNA was amplified with an overnight *in vitro* transcription reaction. From this amplified RNA, sequencing libraries were prepared with Illumina Truseq small RNA primers. The DNA library was paired-end sequenced on an Illumina Nextseq™ 500, high output, with a 1x75 bp Illumina kit (R1: 26 cycles, index read: 6 cycles, R2: 60 cycles). Read 1 was used to identify the Illumina library index and CEL-Seq sample barcode. Read 2 was aligned to the Human (hg38) reference transcriptome using BWA MEM³⁶. Reads that mapped equally well to multiple locations were discarded. Mapping and generation of count tables was done using the MapAndGo script³⁷. Differential gene expression analysis was performed using the R package DESeq2 (version 1.30.1)³⁸. Correction for donor and LFC shrinkage was performed using apeglm (version 1.12.0)³⁹. A gene was considered differentially expressed when the adjusted p value was <0.01 and fold change >1.5 or <-1.5. Gene set enrichment analysis for gene ontology of biological processes was performed using clusterProfiler (version 3.18.1)⁴⁰ and visualized using enrichplot (version 1.10.2)⁴¹.

For qPCR, cDNA was synthesized with the iScript cDNA synthesis kit (Bio-Rad, Hercules, CA, USA) according to the manufacturer's protocol. qPCR was performed with mixtures of specific primer pairs (Supplementary Table S2), with iQ SYBR Green Supermix (Bio-Rad) and a CFX96 real-time detection machine (Bio-Rad). CFX Manager 3.1 software (Bio-Rad) was used to calculate relative gene expression normalized to the housekeeping genes ATP5B and RPL13A according to the standard curve method. The housekeeping genes were selected based on their stable expression in airway epithelial cells using the "Genorm method"⁴². Experiments were performed with two technical replicates.

ACKNOWLEDGMENTS

We thank Single Cell Discoveries for their bulk RNA sequencing services and data analysis. This work was supported by grants of the Dutch Cystic Fibrosis Foundation (NCFS, HIT-CF grant) and SRC 013 from CF Trust-UK.

AUTHOR CONTRIBUTIONS

Conceptualization, J.M.B. and G.D.A.; Methodology, G.D.A.; Software, L.W.R.; Validation, Formal Analysis, Investigation and Data Curation, L.W.R., S.M.A.S. and G.D.A.; Resources, C.K.E. and J.M.B.; Writing – Original Draft, L.W.R. and G.D.A.; Writing – Review & Editing, S.M.A.S, C.K.E. and J.M.B.; Visualization, L.W.R.; Supervision, J.M.B. and G.D.A.; Funding Acquisition, C.K.E., J.M.B. and G.D.A.

DECLARATION OF INTERESTS

J.M.B. has a patent granted (10006904) related to CFTR function measurements in organoids and received personal fees from HUB/Royal Dutch academy of sciences, during the conduct of the study; nonfinancial support from Vertex Pharmaceuticals and personal fees and nonfinancial support from Proteostasis Therapeutics, outside the submitted work.

C.K.v.d.E. reports grants from GSK, Nutricia, TEVA, Gilead, Vertex, ProQR, Proteostasis, Galapagos NV, Eloxx pharmaceuticals, outside the submitted work; In addition, C.K.v.d.E. has a patent related to CFTR function measurements in organoids (10006904) with royalties paid.

The other authors declare no potential conflict of interest.

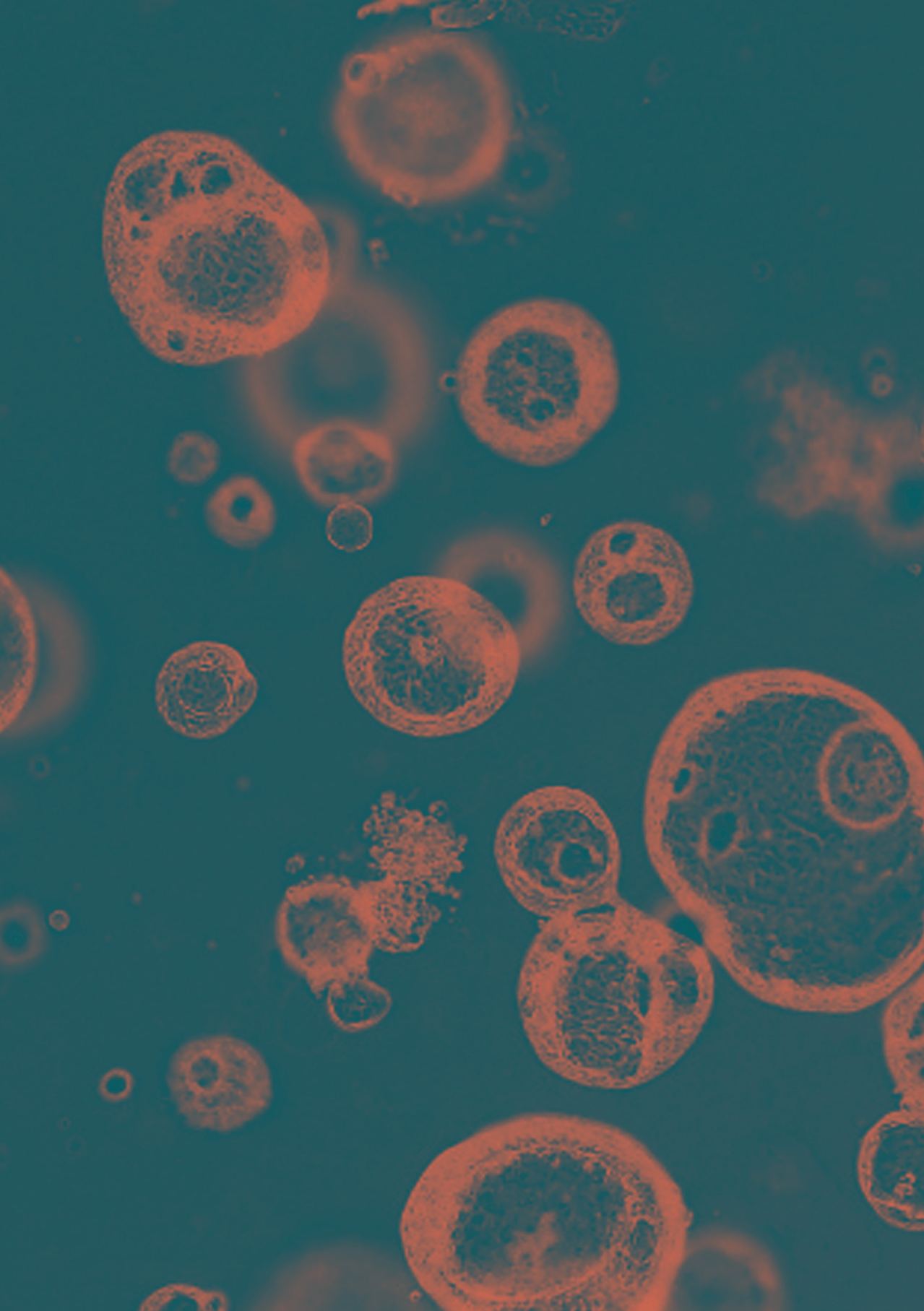
DATA AND CODE AVAILABILITY

Raw sequencing data cannot be provided with the manuscript due to privacy concerns of the human subjects.

REFERENCES

1. Amatngalim, G. D. & Hiemstra, P. S. Airway Epithelial Cell Function and Respiratory Host Defense in Chronic Obstructive Pulmonary Disease. *Chin Med J (Engl)* 131, 1099–1107 (2018).
2. Boucher, R. C. Muco-Obstructive Lung Diseases. *N Engl J Med* 380, 1941–1953 (2019).
3. Shteinberg, M., Haq, I. J., Polineni, D. & Davies, J. C. Cystic fibrosis. *Lancet* 397, 2195–2211 (2021).
4. McBennett, K. A., Davis, P. B. & Konstan, M. W. Increasing life expectancy in cystic fibrosis: Advances and challenges. *Pediatr Pulmonol* 57 Suppl 1, S5–S12 (2022).
5. Guo, J., Garratt, A. & Hill, A. Worldwide rates of diagnosis and effective treatment for cystic fibrosis. *Journal of Cystic Fibrosis* 21, 456–462 (2022).
6. Quesada, R. & Dutzler, R. Alternative chloride transport pathways as pharmacological targets for the treatment of cystic fibrosis. *Journal of Cystic Fibrosis* 19, S37–S41 (2019).
7. Danahay, H. & Gosling, M. TMEM16A: An Alternative Approach to Restoring Airway Anion Secretion in Cystic Fibrosis? *Int J Mol Sci* 21, 2386 (2020).
8. Sondo, E., Caci, E. & Galiotta, L. J. V. The TMEM16A chloride channel as an alternative therapeutic target in cystic fibrosis. *Int J Biochem Cell Biol* 52, 73–76 (2014).
9. Caputo, A. *et al.* TMEM16A, a membrane protein associated with calcium-dependent chloride channel activity. *Science* 322, 590–594 (2008).
10. Schroeder, B. C., Cheng, T., Jan, Y. N. & Jan, L. Y. Expression cloning of TMEM16A as a calcium-activated chloride channel subunit. *Cell* 134, 1019–1029 (2008).
11. Yang, Y. D. *et al.* TMEM16A confers receptor-activated calcium-dependent chloride conductance. *Nature* 455, 1210–1215 (2008).
12. Strug, L. J. *et al.* Cystic fibrosis gene modifier SLC26A9 modulates airway response to CFTR-directed therapeutics. *Hum Mol Genet* 25, 4590–4600 (2016).
13. Lipecka, J. *et al.* Distribution of ClC-2 chloride channel in rat and human epithelial tissues. *Am J Physiol Cell Physiol* 282, C805–16 (2002).
14. Thiemann, A., Gründer, S., Pusch, M. & Jentsch, T. J. A chloride channel widely expressed in epithelial and non-epithelial cells. *Nature* 356, 57–60 (1992).
15. Kim, D. *et al.* Pendrin Mediates Bicarbonate Secretion and Enhances Cystic Fibrosis Transmembrane Conductance Regulator Function in Airway Surface Epithelia. *Am J Respir Cell Mol Biol* 60, 705–716 (2019).
16. Tamma, G. & Dossena, S. Functional interplay between CFTR and pendrin: physiological and pathophysiological relevance. *Frontiers in Bioscience - Landmark* 27, 75 (2022).
17. Mall, M. A. ENaC inhibition in cystic fibrosis: potential role in the new era of CFTR modulator therapies. *European Respiratory Journal* 56, 2000946 (2020).
18. Rodenburg, L. W. *et al.* Drug Repurposing for Cystic Fibrosis: Identification of Drugs That Induce CFTR-Independent Fluid Secretion in Nasal Organoids. *Int J Mol Sci* 23, 12657 (2022).
19. Scudieri, P. *et al.* Association of TMEM16A chloride channel overexpression with airway goblet cell metaplasia. *J Physiol* 590, 6141–6155 (2012).
20. Anagnostopoulou, P. *et al.* SLC26A9-mediated chloride secretion prevents mucus obstruction in airway inflammation. *J Clin Invest* 122, 3629 (2012).
21. Simões, F. B., Kmit, A. & Amaral, M. D. Cross-talk of inflammatory mediators and airway epithelium reveals the cystic fibrosis transmembrane conductance regulator as a major target. *ERJ Open Res* 7, 247–2021 (2021).
22. Bukowy-Bieryłło, Z. Long-term differentiating primary human airway epithelial cell cultures: how far are we? *Cell Communication and Signaling* 19, 1–18 (2021).

23. Chu, H. W. *et al.* CRISPR-Cas9 mediated gene knockout in primary human airway epithelial cells reveals a pro-inflammatory role for MUC18. *Gene Ther* 22, 822 (2015).
24. Rapiteanu, R. *et al.* Highly efficient genome editing in primary human bronchial epithelial cells differentiated at air-liquid interface. *Eur Respir J* 55, 1900950 (2020).
25. Koh, K. D. *et al.* Efficient RNP-directed Human Gene Targeting Reveals SPDEF Is Required for IL-13-induced Mucostasis. *Am J Respir Cell Mol Biol* 62, 373–381 (2020).
26. Vaidyanathan, S. *et al.* High-Efficiency, Selection-free Gene Repair in Airway Stem Cells from Cystic Fibrosis Patients Rescues CFTR Function in Differentiated Epithelia. *Cell Stem Cell* 26, 161-171.e4 (2019).
27. Suzuki, S. *et al.* Highly Efficient Gene Editing of Cystic Fibrosis Patient-Derived Airway Basal Cells Results in Functional CFTR Correction. *Molecular Therapy* 28, 1–12 (2020).
28. de Zeeuw, D. *et al.* Bardoxolone Methyl in Type 2 Diabetes and Stage 4 Chronic Kidney Disease. *New England Journal of Medicine* 369, 2492–2503 (2013).
29. Lee, H. J. *et al.* Thick airway surface liquid volume and weak mucin expression in pendrin-deficient human airway epithelia. *Physiol Rep* 3, e12480 (2015).
30. Bajko, J., Duguid, M., Altmann, S., Hurlbut, G. D. & Kaczmarek, J. S. Pendrin stimulates a chloride absorption pathway to increase CFTR-mediated chloride secretion from Cystic Fibrosis airway epithelia. *FASEB Bioadv* 2, 526–537 (2020).
31. Gorrieri, G. *et al.* Goblet Cell Hyperplasia Requires High Bicarbonate Transport to Support Mucin Release. *Sci Rep* 6, 1–15 (2016).
32. Genovese, M. *et al.* TRPV4 and purinergic receptor signalling pathways are separately linked in airway epithelia to CFTR and TMEM16A chloride channels. *J Physiol* 597, 5859–5878 (2019).
33. Kassis, T., Hernandez-Gordillo, V., Langer, R. & Griffith, L. G. OrgaQuant: Human Intestinal Organoid Localization and Quantification Using Deep Convolutional Neural Networks. *Sci Rep* 9, 12479 (2019).
34. Hashimshony, T., Wagner, F., Sher, N. & Yanai, I. CEL-Seq: single-cell RNA-Seq by multiplexed linear amplification. *Cell Rep* 2, 666–673 (2012).
35. Simmini, S. *et al.* Transformation of intestinal stem cells into gastric stem cells on loss of transcription factor Cdx2. *Nat Commun* 5, 5728 (2014).
36. Li, H. & Durbin, R. Fast and accurate long-read alignment with Burrows-Wheeler transform. *Bioinformatics* 26, 589–595 (2010).
37. MapAndGo. <https://github.com/anna-alemany/transcriptomics/tree/master/mapandgo>.
38. Love, M. I., Huber, W. & Anders, S. Moderated estimation of fold change and dispersion for RNA-seq data with DESeq2. *Genome Biol* 15, 550 (2014).
39. Zhu, A., Ibrahim, J. G. & Love, M. I. Heavy-tailed prior distributions for sequence count data: removing the noise and preserving large differences. *Bioinformatics* 35, 2084–2092 (2019).
40. Yu, G., Wang, L.-G., Han, Y. & He, Q.-Y. clusterProfiler: an R package for comparing biological themes among gene clusters. *OMICS* 16, 284–7 (2012).
41. Yu G. enrichplot: Visualization of Functional Enrichment Result. <https://yulab-smu.top/biomedical-knowledge-mining-book/> (2022).
42. Vandesompele, J. *et al.* Accurate normalization of real-time quantitative RT-PCR data by geometric averaging of multiple internal control genes. *Genome Biol* 3, 1–12 (2002).



Chapter 5

Exploring intrinsic variability between cultured nasal and bronchial epithelia in cystic fibrosis

Lisa W. Rodenburg, Mieke Metzemaekers, Isabelle S. van der Windt, Shannon M.A. Smits, Loes A. den Hertog – Oosterhoff, Evelien Kruisselbrink, Jesse E. Brunsveld, Sabine Michel, Karin M. de Winter-de Groot, Cornelis K. van der Ent, Ralph Stadhouders, Jeffrey M. Beekman and Gimano D. Amatngalim

Based on: Scientific reports 2023, 13 (1); 18573

ABSTRACT

The nasal and bronchial epithelium are unified parts of the respiratory tract that are affected in the monogenic disorder cystic fibrosis (CF). Recent studies have uncovered that nasal and bronchial tissues exhibit intrinsic variability, including differences in mucociliary cell composition and expression of unique transcriptional regulatory proteins which relate to germ layer origin. In the present study, we explored whether intrinsic differences between nasal and bronchial epithelial cells persist in cell cultures and affect epithelial cell functioning in CF. Comparison of air-liquid interface-differentiated epithelial cells from subjects with CF revealed distinct mucociliary differentiation states of nasal and bronchial cultures. Moreover, using RNA sequencing we identified cell type-specific signature transcription factors in differentiated nasal and bronchial epithelial cells, some of which were already poised for expression in basal progenitor cells as evidenced by ATAC sequencing. Analysis of differentiated nasal and bronchial epithelial 3D organoids revealed distinct capacities for fluid secretion, which was linked to differences in ciliated cell differentiation. In conclusion, we show that unique phenotypical and functional features of nasal and bronchial epithelial cells persist in cell culture models, which can be further used to investigate the effects of tissue-specific features on upper and lower respiratory disease development in CF.

INTRODUCTION

The nasal and bronchial airway epithelium are unified parts of the human respiratory tract that originate from ecto- and endodermal germ layers, respectively^{1,2}. Despite differences in embryonic origin, both nasal and bronchial epithelial layers display a pseudostratified morphology and consist of ciliated, secretory and basal cells³. Moreover, nasal and bronchial epithelial cells employ common mechanisms to provide respiratory host defence⁴⁻⁶.

Nasal and bronchial epithelial cells are furthermore mutually affected in multiple respiratory diseases, including the monogenic disorder cystic fibrosis (CF)⁷. CF is caused by autosomal recessive inherited mutations in the *cystic fibrosis transmembrane conductance regulator (CFTR)* gene⁸. These genetic defects attenuate CFTR protein-dependent chloride conductance and fluid secretion at the surface of the airway epithelium⁹. This results in accumulation of dehydrated mucus at the epithelial surface, which cannot be removed via mucociliary clearance and consequently leads to the development of a muco-obstructive respiratory disease¹⁰.

In vitro models are widely used to study impaired airway epithelial cell functions in CF and the efficacy of novel CFTR-modulating therapies. These models use undifferentiated airway basal progenitor cells from nasal or bronchial tissues¹¹. Air-liquid interface (ALI) differentiated airway epithelial cell cultures are regarded as the golden standard¹¹, although airway organoids are emerging as a novel advanced 3D model system, uniquely suited for investigating fluid secretion^{12,13}.

Recent transcriptome studies with native airway tissue samples have uncovered intrinsic differences between the nasal and bronchial epithelium, including variations in ciliated and secretory cell composition and the expression of unique transcriptional regulatory proteins that relate to a difference in germ layer origin¹⁴⁻¹⁷. It remains unexplored whether these tissue-specific hallmarks affect nasal and bronchial epithelial cell functioning, and therefore have differential outcomes on upper and lower respiratory disease development in CF.

In the present study, we determined whether *in vitro* models can be used to explore the role of unique nasal and bronchial characteristics on airway epithelial cell functioning in CF. First, we compared paired nasal and bronchial epithelial cells from individuals with CF that were differentiated in ALI-cultures, and used RNA sequencing (RNA-seq) to determine persistent differences in epithelial differentiation and the expression of unique transcriptional regulatory proteins. Next, we performed an assay for

transposase-accessible chromatin using sequencing (ATAC-seq) to determine whether differences in transcriptional regulatory proteins are epigenetically imprinted already in basal progenitor cells. Moreover, we examined epithelial fluid secretion in nasal and bronchial organoids in a forskolin-induced swelling (FIS) assay, and investigated how CFTR-independent fluid secretion is affected by increased ciliated cell differentiation in CF nasal organoids.

RESULTS

Nasal and bronchial epithelial cell cultures exhibit a unique mucociliary differentiation state and transcriptome

Previous studies have revealed important variations in mucociliary differentiation states of freshly harvested nasal *versus* bronchial epithelial tissues¹⁵. These observations prompted us to uncover the phenotypes of cultured nasal and bronchial epithelial cells from paediatric individuals with CF. We isolated and expanded nasal and bronchial epithelial cells and confirmed their identity by immunofluorescence (IF) staining based on protein expression of basal progenitor cell markers (Fig. 1A). Paired nasal and bronchial cells were subsequently differentiated in an ALI model using similar culture conditions¹⁸. Differentiated nasal cell cultures contained a significantly higher percentage of MUC5AC⁺ secretory cells compared to differentiated bronchial cell cultures, which were enriched for β -tubulin IV⁺ ciliated cells (Fig. 1B). In line with IF staining, differentiated nasal and bronchial cells displayed higher mRNA expression of the transcription factors (TF) SPDEF and FOXJ1, respectively (Fig. 1C). In addition to a discrepancy in mucociliary cell composition, ALI-differentiated nasal cells displayed a significantly lower trans-electrical epithelial resistance (TEER) compared to cultured bronchial cells (Fig. 1D). Similar differences in mucociliary differentiation and TEER were observed in unpaired nasal and bronchial cultures from non-CF subjects (Supplementary Fig. S1A-C).

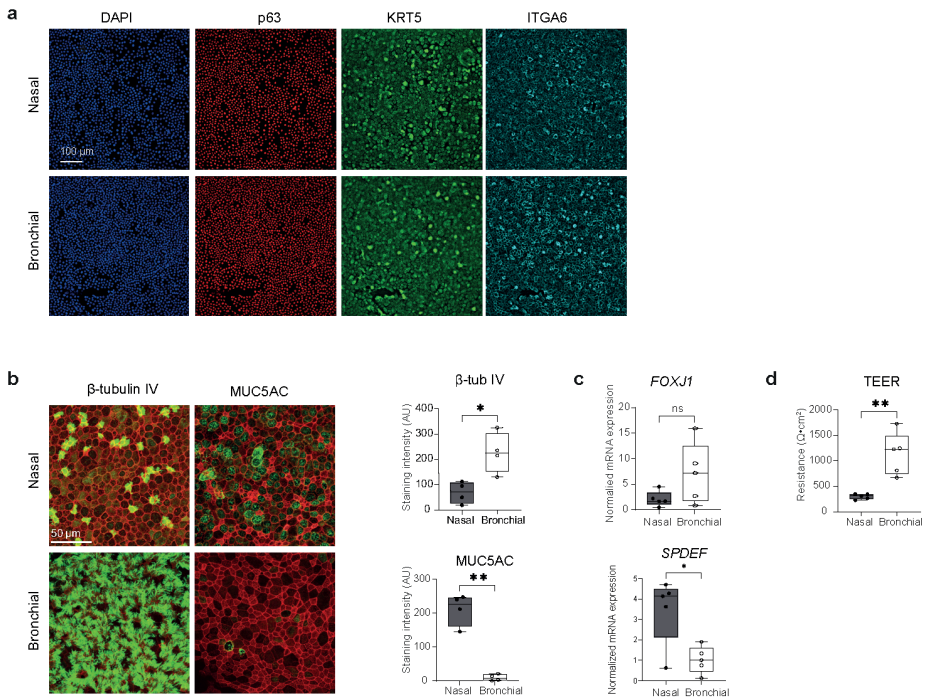


Figure 1. Nasal and bronchial epithelial cell cultures from individuals with CF exhibit unique mucociliary differentiation states.

(A) Representative IF staining of the basal cell markers p63 (red), KRT5 (green), and ITGA6 (cyan) in undifferentiated CF nasal and bronchial epithelial cells. DAPI (blue) was used to stain nuclei. Scale bar equals 100 μ m. (B) Representative IF staining (left panel) and quantification (right panel) of β -tubulin IV (ciliated cells) and MUC5AC (goblet cells) in paired ALI-differentiated nasal and bronchial cells of CF subjects (n=4 independent donors). Cultures were differentiated for 18 days. Epithelial markers are shown in green, phalloidin (red) was used as actin cytoskeleton staining. Scale bar equals 50 μ m. For quantification, 3 microscopic fields were analysed per well. (C) mRNA expression of the cell type-specific transcriptional factors *FOXJ1* (ciliated cells) and *SPDEF* (goblet cells) in paired ALI-differentiated nasal and bronchial epithelial cells of CF subjects (n=5 independent donors). (D) TEER measurements of paired ALI-differentiated nasal and bronchial epithelial cells of CF subjects (n=5 independent donors). Data is shown as mean \pm SD. Analysis of differences was conducted using paired t-tests (panel b, c, d). ns = non-significant, * p<0.05, ** p<0.01

Next, we profiled the transcriptomes of ALI-differentiated nasal and bronchial cultures from five individuals with CF by RNA-seq. Principal component analysis (PCA) showed clear clustering based on nasal or bronchial origin (Fig. 2A). We identified 919 and 735 differentially expressed genes (DEGs) that were higher expressed in differentiated bronchial and nasal cells, respectively (foldchange > 1.5 and adjusted p < 0.01) (Fig. 2B-C, Supplementary Table S1). Gene set enrichment analysis of these DEGs revealed higher expression of cilia-related gene sets in bronchial cells, while nasal cells showed enrichment of genes involved in neural development-related processes (Fig. 2D).

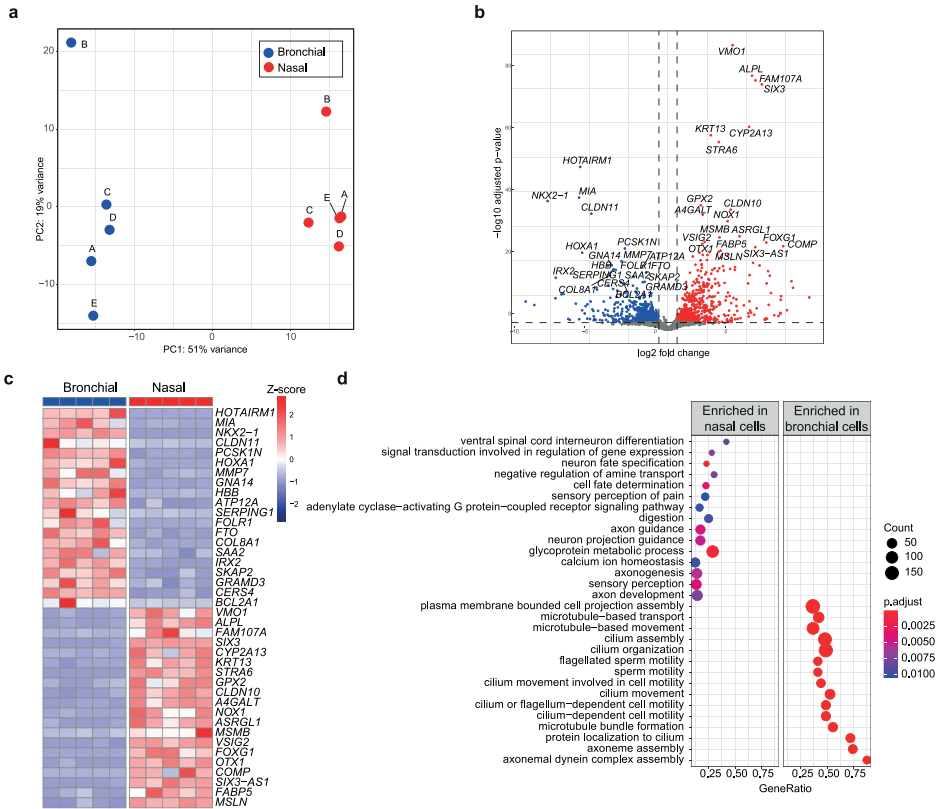


Figure 2. Transcriptome analysis of nasal and bronchial epithelial cells reveals unique core gene signatures. (A) PCA of transcriptomic analysis of paired ALI-differentiated nasal (red) and bronchial (blue) cells of CF subjects (n=5 independent donors). A-E indicate individual donors. (B) Volcano plot showing DEGs (defined as adjusted p value <0.01 and fold change > 1.5) between paired ALI-differentiated nasal and bronchial epithelial cells of CF subjects (n=5 independent donors). Red dots indicate enriched genes in nasal epithelial cells and blue dots indicate enriched genes in nasal epithelial cells. (C) Heatmap showing the 20 most significantly enriched genes in nasal (red) and bronchial (blue) epithelial cells. Z scores of normalized expression values are depicted. (D) Gene set enrichment analysis showing the top 15 of enriched GO terms in ALI-differentiated nasal and bronchial epithelial cells (n=5 independent donors). Color indicates the degree of significance and dot size indicates gene count. Gene ratio explains the fraction of DEG's in the specific GO term.

In addition to enhanced expression of genes associated with ciliated cells, bronchial cells displayed higher expression of distal airway club cell-related genes (Fig. 3A). In contrast, nasal cells more abundantly expressed goblet cell-related genes (Fig. 3A). We then determined expression of gene panels that were previously found to be specifically enriched in either nasal or tracheal/bronchial epithelial cells¹⁵. All of the known bronchial-enriched genes were indeed higher expressed in bronchial cell cultures compared to nasal cell cultures. Cultured nasal cells showed elevated expression of 8/14 of the reported nasal-specific genes (Fig. 3B)¹⁵. Overall, these results support the notion that nasal and bronchial epithelial cells exhibit unique cell type-specific differentiation characteristics that persists in cell culture.

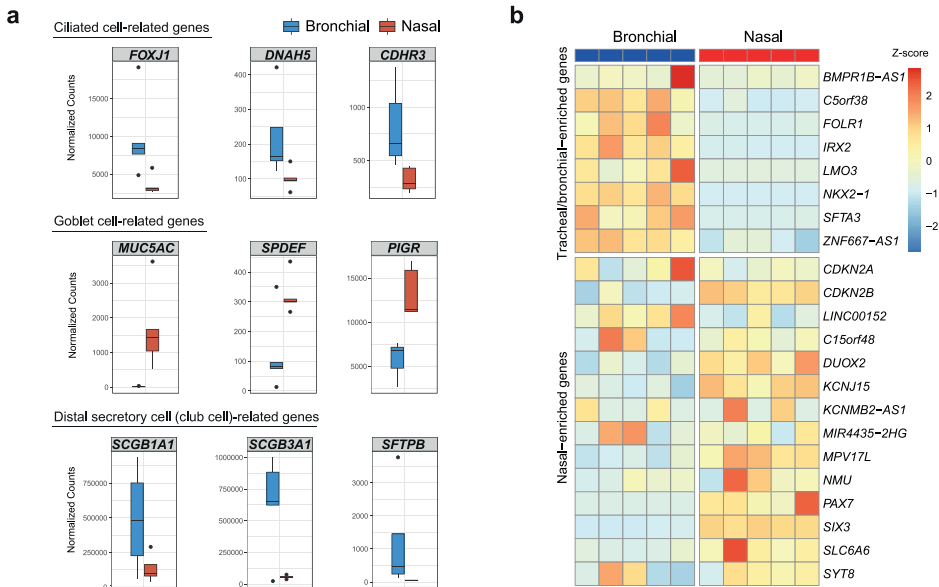
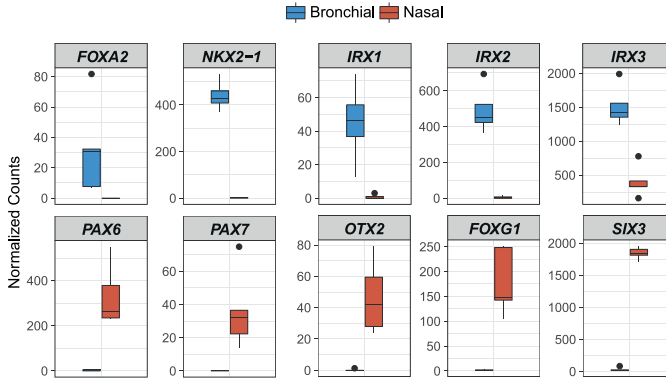


Figure 3. Transcriptome analysis of nasal and bronchial epithelial cells reveals differences in cell type-specific gene sets. (A) Normalized counts of ciliated cell-related genes (upper panel), goblet cell-related genes (middle panel) and distal airway secretory cell (club cell)-related genes (lower panel) in paired ALI-differentiated nasal (red) and bronchial (blue) cells of CF subjects (n=5 independent donors). (B) Heatmap showing gene expression in paired ALI-differentiated nasal (red) and bronchial (blue) cells of CF subjects (n=5 independent donors) of nasal- and trachea/bronchial-enriched genes based on scRNA-seq by Deprez et al.¹⁵

Identification of nasal and bronchial cell-specific signature TFs and epigenomic features

We employed our RNA-seq dataset to unravel whether specific TFs are putative regulators of differences in differentiation between nasal and bronchial epithelial cells. We searched for TFs among the top enriched DEGs in bronchial cells and identified the TFs *FOXA2*, *NKX2-1* and *IRX1-3*, which are all involved in lung endoderm morphogenesis (Fig. 4A, upper panel)^{19–23}. In contrast, top DEGs in nasal cells consisted of several unique TFs which are implicated in neural ectoderm development. These included *PAX6* and *PAX7*^{24–26}, *OTX2*^{27,28}, *FOXP2*²⁹ and *SIX3*³⁰ (Fig. 4A, lower panel). Differential expression of a subset of bronchial- and nasal-specific TFs was validated at the protein level in undifferentiated basal progenitor cells (Fig. 4B).

a



b

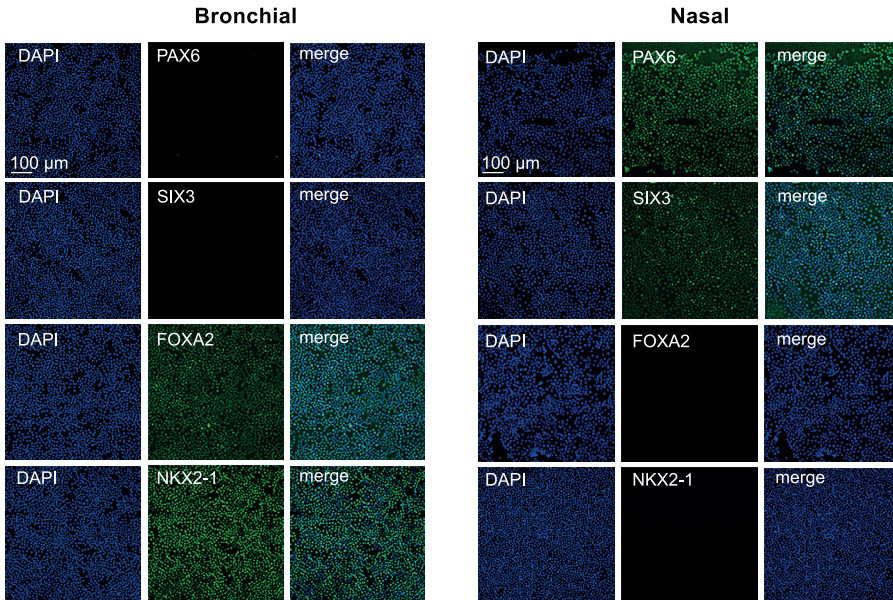


Figure 4. Identification of nasal and bronchial cell-specific signature TFs.

(A) Normalized counts of RNA-seq analysis from nasal- and bronchial-specific TFs in paired ALI-differentiated nasal (red) and bronchial (blue) cells of CF subjects (n=5 independent donors). (B) Representative IF staining of paired undifferentiated nasal and bronchial epithelial cells of an individual with CF. Cells were stained for the bronchial epithelial markers NKX2-1 and FOXA2 and the nasal epithelial markers PAX6 and SIX3. Scale bar equals 100 μm.

We next performed ATAC-seq to elucidate whether nasal and bronchial tissue-specific signature TFs and their cognate DNA binding sites were associated with accessible chromatin in basal progenitor cells. Of the five paired nasal and bronchial cell cultures, one bronchial sample was omitted for further analysis due to insufficient sample

quality. We reproducibly detected a total of 15,434 peaks of chromatin accessibility across samples, of which 147 regions were significantly more accessible and specific for nasal and 58 for bronchial cells (\log_2 fold change > 1 and adjusted $p < 0.1$) (Supplementary Fig. S2A-B, Supplementary Table S2). Pathway enrichment analysis of genes associated with nasal- or bronchial-specific accessible regions revealed distinct sets of biological processes (Supplementary Fig. S2C). Examples of individual genes near ATAC-seq peaks that were specifically enriched in bronchial cells include *IRX2* and *TBX3*, both involved in early lung development (Fig. 5A-B)^{31,32}. In accordance with mRNA expression in differentiated ALI-cultures, genes linked to nasal-specific regions of accessible chromatin included *PAX6* and *FOXP1* (Fig. 5A-B)^{24,29}. Integration of RNA-seq results from ALI-differentiated bronchial cells and ATAC-seq data from basal progenitor bronchial cells yielded twelve overlapping genes for bronchial cells, including *IRX1* and *IRX2* (Supplementary Fig. S2D, left panel). For nasal cells, 19 overlapping genes were found, including the signature TFs *PAX6* and *FOXP1* (Supplementary Fig. S2D, right panel). A TF motif enrichment analysis was conducted to search for known TF-binding motifs in accessible regions. Both bronchial- and nasal-specific regulatory regions were enriched for binding motifs of the stress-induced TF ATF-3³³ and AP-1, which regulates cellular functions including proliferation, differentiation and apoptosis³⁴ (Fig. 5C). Binding motifs for FOXM1, which has been implicated in several lung diseases³⁵ as well as those for FOXA1 and FOXA2, both involved in lung morphogenesis¹⁹, were significantly enriched in bronchial cells. Nasal-specific enriched binding motifs were found for *PAX6*, *SIX2* and *OTX2*. Altogether, we found unique nasal- and bronchial specific TF, which in part are imprinted epigenetically in airway basal progenitor cells.

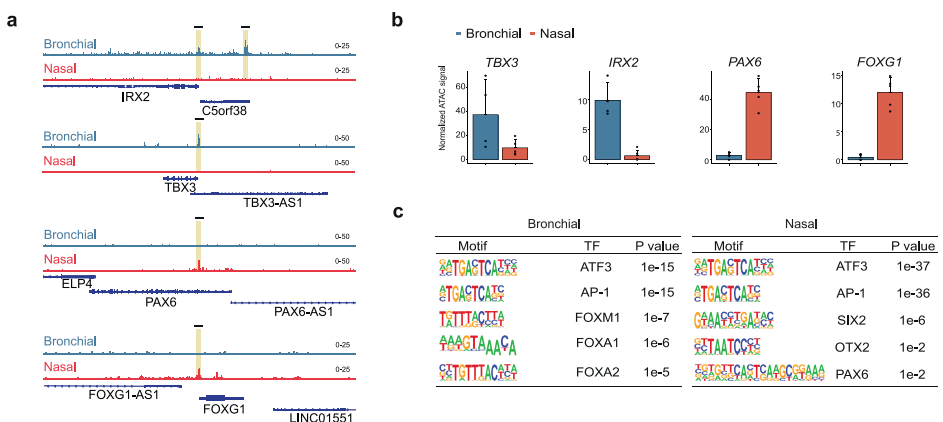


Figure 5. Unique epigenomic features of nasal and bronchial basal progenitor cells.

(A) Representative genome browser shots of ATAC-seq peaks across the genes *IRX2*, *TBX3*, *PAX6* and *FOXG1*. (B) Quantified ATAC-seq signals of selected genes in the different donors ($n=4-5$ independent donors). (C) Selection of enriched motif matrices and corresponding TF in nasal and bronchial epithelial cells, predicted by the HOMER motif analysis. Data is shown as mean \pm SD.

ALI culture-derived nasal and bronchial organoids display distinctive fluid secretion

Next, we determined whether differences in mucociliary differentiation between ALI-cultured nasal and bronchial epithelial cells affect fluid secretion. We employed 3D airway organoids generated from ALI-differentiated epithelial fragments (Fig. 6A)¹⁸. In line with our previous observations in ALI-cultures (Fig. 1), MUC5AC⁺ and β -tubulin IV⁺ cells were more abundant in CF nasal and bronchial organoids, respectively (Fig. 6B). Evaluation of organoid morphology revealed that nasal epithelial sheets formed into cystic organoids with clearly identifiable lumens, compared to CF donor-matched bronchial organoids that had no intrinsic lumen formation (Fig. 6C-D). Similar differences between nasal and bronchial organoid morphology were observed in cultures derived from healthy control (HC) subjects (Supplementary Fig. S3A). This suggests differences in intrinsic fluid secretion between nasal and bronchial organoids, presumably independent of CFTR under basal culture conditions.

To further investigate fluid secretion properties, we measured organoid swelling in response to the cAMP agonist forskolin, which we previously identified as an inducer of CFTR-independent fluid secretion in CF nasal organoids^{13,18}. Nasal and bronchial organoids from HC subjects (unpaired samples) were included in this FIS assay, to discriminate between CFTR-dependent and CFTR-independent swelling responses. We observed more prominent swelling responses in nasal and bronchial organoids from HC subjects compared to those from individuals with CF, which can be explained by a dysfunctional cAMP-dependent CFTR channel in CF organoids (Fig. 7A-C). Remarkably, nasal organoids from CF subjects displayed a significantly higher FIS when compared to paired bronchial organoids, which is likely CFTR-independent. Furthermore, bronchial organoids from subjects with CF with a F508del homozygous genotype displayed enhanced FIS in response to the CFTR-repairing drugs VX-809/VX-770 (Fig. 7D). Paired nasal organoids did not respond to these drugs, also probably due to abundant CFTR-independent organoid swelling.

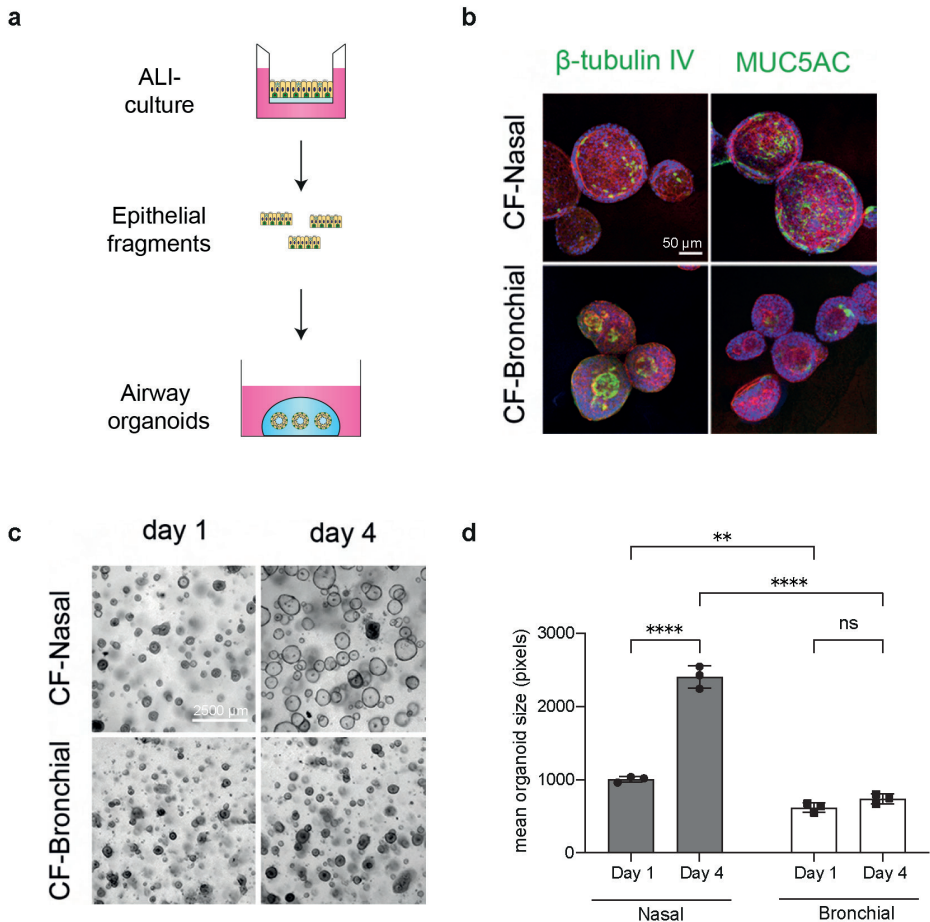


Figure 6. ALI culture-derived nasal and bronchial organoids display distinctive morphological features.

(A) Schematic representation showing how ALI-differentiated airway epithelia are converted into organoids to study organoid size and FIS. (B) Representative IF staining of paired nasal and bronchial airway organoids of a CF subject, showing β -tubulin IV (ciliated cells) and MUC5AC (goblet cells) staining (in green). Phalloidin (red) was used as actin cytoskeleton staining and DAPI (blue) to stain nuclei. Scale bar equals 50 μ m. (C) Representative brightfield images of paired CF nasal and bronchial airway organoids at day 1 and 4 after plating of epithelial fragments, showing lumen formation in nasal but not in bronchial organoids. Scale bar equals 2500 μ m. (D) Quantification of mean organoid size (pixels) of paired CF nasal and bronchial airway organoids at day 1 and 4 after plating of epithelial fragments ($n = 3$ wells of 1 donor). Data is shown as mean \pm SD. Analysis of differences was conducted with a two-way ANOVA with Tukey post-hoc test (panel d). ns = non-significant, ** $p < 0.01$, **** $p < 0.0001$.

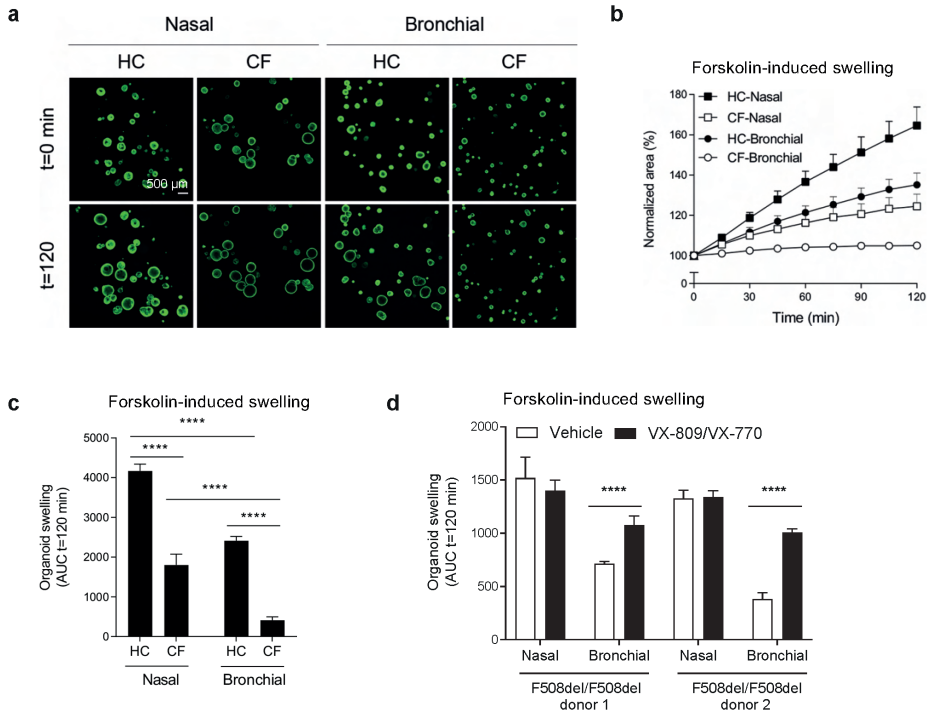


Figure 7. Differences in CFTR-independent forskolin-induced fluid secretion between nasal and bronchial organoids.

(A) Representative confocal images of calcein green-stained nasal and bronchial airway organoids from HC and CF at t=0 and t=120 min after stimulation with forskolin (5 μ M). Scale bar equals 500 μ m. (B) Nasal and bronchial airway organoids from HC (n=3 independent donors) and CF (n=3 independent donors) subjects were stimulated with forskolin (5 μ M) and organoid swelling was measured in time, demonstrating differences in fluid secretion. Results are depicted as percentage increase in normalized area in time. (C) Nasal and bronchial airway organoids from HC (n=3 independent donors) and CF (n=3 independent donors) subjects were stimulated with forskolin (5 μ M) and organoid swelling was measured in time, demonstrating differences in fluid secretion. Results are depicted as area under the curve (AUC) plots (t=120 min). (D) Paired nasal and bronchial airway organoids from CF subjects with a F508del/F508del genotype (n=2 independent donors) were pre-treated with VX-809 (10 μ M) for 48 h, and subsequently acute stimulated with forskolin (5 μ M) together with VX-770 (10 μ M) or vehicle. Airway organoid swelling is depicted as AUC plots (t=120 min). Data is shown as mean \pm SD. Swelling assays were conducted in quadruplicates for each condition. Analysis of differences was conducted with a two-way ANOVA with Bonferroni post-hoc test (panel c, d). **** p < 0.0001.

Next, we aimed to decipher whether the observed differences in differentiation state and capacity for fluid secretion between nasal and bronchial organoids had a causative relationship. To address this issue, we employed the γ -secretase inhibitor DAPT – an inhibitor of Notch signaling – to enrich for ciliated cells in nasal organoids^{36,37}. Microscopic evaluation showed the successful differentiation of DAPT-treated samples as evidence by an increased number of β -tubulin IV⁺ ciliated cells in ALI-differentiated nasal cell cultures of CF subjects (Fig. 8A). This was confirmed at the mRNA level, showing enhanced and reduced expression of *FOXJ1* (ciliated cells) and *MUC5AC* (goblet

cells), respectively (Supplementary Fig. S3B). After conversion of ALI cultures into organoids, we observed that differentiation with DAPT attenuated organoid lumen formation, suggesting reduced epithelial fluid secretion upon ciliated cell enrichment (Fig. 8B-C). However, FIS and responses to CFTR-repairing drugs were only minimally changed in CF nasal cultures differentiated with DAPT (Fig. 8D, Supplementary Fig. S3C). Altogether, the distinct swelling responses of nasal and bronchial organoids suggest that their unique differentiation states and morphological characteristics coincide with intrinsic differences in their potency to secrete fluid in a CFTR-independent manner.

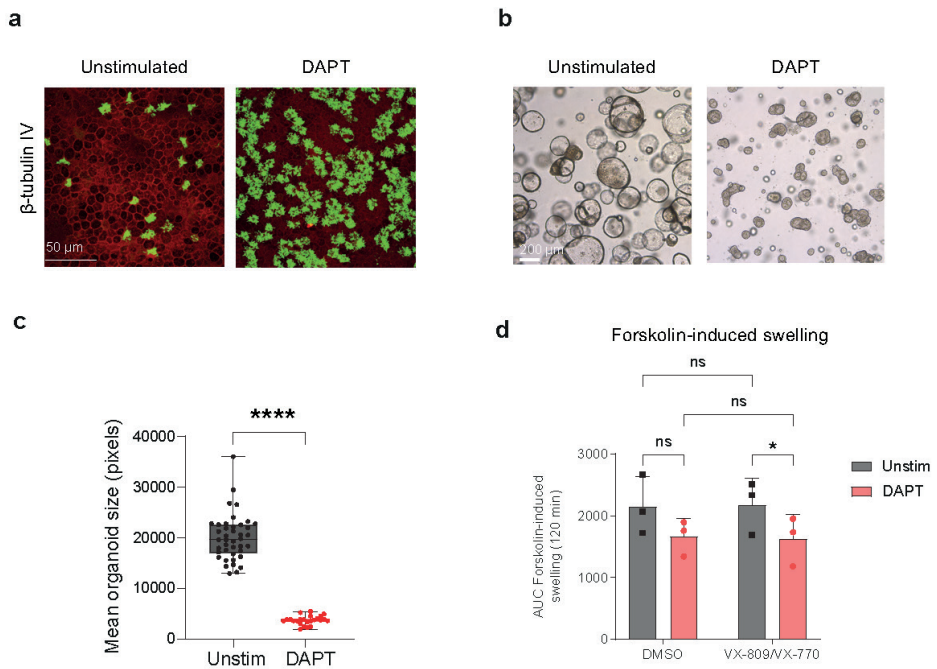


Figure 8. Intrinsic fluid secretion in nasal organoids is reduced by ciliated cell enrichment.

(A) Representative IF staining of β -tubulin IV (ciliated cells) in nasal cells cultured with or without the γ -secretase inhibitor DAPT (20 μ M) from an individual with CF (F508del/F508del). Cultures were differentiated for 18 days. Epithelial markers are shown in green, phalloidin (red) was used as actin cytoskeleton staining. Scale bar equals 50 μ m. (B) Representative brightfield images of nasal organoids treated with or without the γ -secretase inhibitor DAPT (20 μ M), from an individual with CF (F508del/F508del), 6 days after plating. Scale bar equals 200 μ m. (C) Quantification of mean organoid size of nasal organoids treated with or without the γ -secretase inhibitor DAPT (20 μ M) from an individual with CF (F508del/F508del) ($n = 24/41$ wells). (D) Nasal organoid swelling assay with organoids from individuals with CF ($n=3$ independent donors), treated with or without the γ -secretase inhibitor DAPT (20 μ M). Organoids were stimulated with forskolin (5 μ M) alone, or with forskolin (5 μ M) together with VX-770 (10 μ M) and pre-treatment with VX-809 (10 μ M) for 48 h. Results are depicted as AUC plots ($t=120$ min). Data is shown as mean \pm SD. Swelling assays were conducted in quadruplicates for each condition. Analysis of differences was conducted with an unpaired t-test (panel c) or two-way ANOVA with Tukey post-hoc test (panel d). ns = non-significant, * $p < 0.05$, **** $p < 0.0001$.

DISCUSSION

This study aimed to explore whether cultured nasal and bronchial epithelia can be used to investigate imprinted tissue-specific characteristics in CF. Upon cultivation under similar culturing conditions, ALI-differentiated nasal and bronchial cell cultures displayed significant enrichment for goblet and ciliated cells respectively. These observations are in line with previously published single cell and bulk RNA-seq studies on freshly isolated nasal and tracheal or lower airway cells¹⁴⁻¹⁷. Therefore, we demonstrate that tissue-specific differences are preserved in cell cultures with our culture media after multiple weeks of culturing. The unique differentiation characteristics of nasal and bronchial cells appear to be independent of CF disease since similar observations were made for cells from healthy donors.

IF analysis revealed the presence of key TF proteins related to nasal (PAX6 and SIX3) and bronchial (NKX2-1 and FOXA2) epithelial cells already in basal progenitor cells. Moreover, using ATAC-seq we have demonstrated that multiple key TF genes and their putative binding sites are associated with accessible chromatin specifically in nasal or bronchial progenitor cells. These findings support the hypothesis that the high abundance of goblet cells in nasal cell cultures is due to the absence of certain transcriptional regulatory proteins that are expressed in bronchial epithelial cells. For instance, the TFs FOXA1/2 and NKX2-1, which are not expressed in nasal cells, are known for their inhibitory effect on goblet cell metaplasia in bronchial epithelial cells^{20,38,39}.

Besides FOXA1/2, nasal cells lacked both mRNA expression in ALI-cultures and accessible TF DNA binding motifs in basal cell cultures of other regulatory proteins that have been previously reported to regulate endoderm-derived lung development, such as IRX1-3^{22,23}. In contrast, nasal cell-enriched TFs included PAX6, FOXG1, OTX2, and SIX3, which have been reported to regulate the development of ectoderm-derived tissues^{24,29,30}. This suggests that unique nasal- and bronchial-specific TFs are likely related to differences in their germ layer origin. Further research is required to demonstrate the role of nasal cell-specific TFs in both nasal epithelial development and the regulation of mucociliary differentiation. For instance, as shown in ectoderm-derived epithelial tissues^{40,41}, PAX6 may act as key regulator of nasal epithelial cell differentiation. It will be interesting for subsequent studies to characterize the role of these nasal cell-specific TFs, as they likely drive tissue-specific differences in upper and lower respiratory disease development - both in CF and other respiratory diseases.

Our results further revealed clear differences in nasal and bronchial organoid fluid secretion. In earlier studies we showed that nasal organoids from subjects with CF

displayed high intrinsic and cAMP-induced CFTR-independent fluid secretion^{13,18}. In the current study we observed that bronchial organoids of subjects with CF lacked CFTR-independent fluid secretion. In contrast to CF nasal organoids, bronchial organoids responded to CFTR-modulating drugs, further suggesting differences in CFTR-dependent fluid secretion. In an attempt to link these differences in fluid secretion to altered cell differentiation, we used the Notch inhibitor DAPT to enrich for ciliated cells in nasal organoids. While this indeed reduced intrinsic fluid secretion, we did not observe changes in FIS, suggesting different mechanisms underlying the intrinsic and cAMP-induced CFTR-independent fluid secretion. Moreover, differentiation with DAPT did not improve CFTR modulator responses, which is likely due to a depletion of CFTR-expressing secretory cells^{42,43}. Overall, our data suggest that epithelial cell differentiation is an important determinant of CFTR-independent epithelial fluid secretion. Additionally, it provides a proof-of-concept that differentiation studies in ALI-cultures can be combined with the assessment of fluid secretion in ALI-culture derived organoids.

It should be mentioned that the effect of CFTR modulator responses was measured in a limited number of available donors. Furthermore, we showed previously that adaption of the culturing conditions of CF nasal organoids is needed to boost CFTR expression and make them suitable for CFTR-dependent FIS-assays¹⁸. Therefore, the effects of CFTR modulators between nasal and bronchial organoids should be validated in future efforts using a larger cohort and optimized organoid culture conditions. Of note, in contrast to our observation made in nasal and bronchial organoids, others did not observe differences in CFTR-dependent chloride conductance between ALI-differentiated nasal and bronchial epithelial cells^{44,45}. More research is needed to gain insight into the mechanisms underlying the differential CFTR-independent fluid secretion between nasal and bronchial organoids, which may relate to differences in cell type-dependent activity of ion channels or transporters such as cAMP-mediated chloride-, calcium-, bicarbonate-, sodium- or potassium transporters¹³.

Together, our data show that nasal and bronchial epithelia have unique phenotypic and functional characteristics that persist in cell culture, including intrinsic differences in germ layer-specific gene regulatory networks and cellular differentiation, which may affect epithelial fluid secretion in CF. Cultured nasal and bronchial epithelial cells may therefore serve as excellent models to further explore the contribution of tissue-specific characteristics on upper and lower respiratory disease development in CF.

MATERIALS & METHODS

Patient materials and sample collection

Paired nasal and bronchial samples were collected as part of the Precision study (protocol ID: NL54885.041.16), which was approved by the Medical Research Ethics Committee of the University Medical Center Utrecht (Utrecht, The Netherlands). Paired samples were collected from 1 child without CF (Female (F)) and 8 children with CF with the following *CFTR* mutations: F508del/F508del (F), F508del/F508del (F), F508del/F508del (F), F508del/F508del (F), F508del/A455E (Male (M)), F508del/A455E (F), F508del/1717-1G>A (M), F508del/2183AA>G (F). Additionally, nasal brushings were obtained from subjects that gave signed informed consent for use and storage of their cells, which was approved by a specific ethical board for the use of biobanked materials TcBIO (Toetsingscommissie Biobanks), an institutional Medical Research Ethics Committee of the University Medical Center Utrecht (protocol ID: 16/586). These non-paired nasal brushings were obtained from 1 child with CF (F508del/F508del (F)), 3 adults with CF (all F508del/F508del (M)) and 7 adult healthy controls. Furthermore, residual bronchial tissues from lung transplantation donors at the University Medical Center Utrecht, the Netherlands, were accessible for research within the framework of patient care, in accordance with the “Human Tissue and Medical Research: Code of conduct for responsible use” (2011) (www.federa.org), describing the no-objection system for coded anonymous further use of such tissue without necessary written or verbal consent. These bronchial tissues were obtained from 3 subjects without CF. All nasal samples were obtained as brushings from both inferior turbinates by use of a cytological brush. Bronchial samples from the CF subjects were obtained as brushings during a bronchoscopy and from the healthy controls as explant material. All samples were collected in advanced DMEM/F12 containing glutaMAX (1% v/v), HEPES (10 mM), penicillin-streptomycin (1% v/v) and primocin (50 mg/mL).

Isolation and expansion of airway epithelial cells

Nasal and bronchial airway epithelial cells were isolated from nasal and bronchial brushings as previously described¹⁸. In brief, cells were scraped off the brush, incubated with TrypLE express enzyme (Fisher Scientific, Landsmeer, The Netherlands) supplemented with sputolysin for 10 min at 37 °C, strained with a 100 µM strainer and plated in a collagen IV-precoated (50 µg/mL) 6-well culturing plate. Cells were refreshed three times a week with basal cell (BC) isolation medium (Supplementary Table S3). After one week, antibiotics were withdrawn from the medium and DAPT was added to the medium, which was called BC expansion medium (Supplementary Table S3) from now on. These basal progenitor cells were cultured until 80-90% confluence. Confluent cell layers were frozen in CryoStor CS10 freezer medium (STEMCELL technologies,

Vancouver, Canada) supplemented with Y-27632 (5 μM ; Selleck chemicals, Planegg, Germany), or passaged using TrypLE express enzyme. Bronchial airway epithelia were isolated from explant tissue by first incubating resected bronchial tissues in Protease type XIV (Sigma-Aldrich, St Louis, MO, USA) at 4 °C overnight. The next day, dissociated epithelial cells were treated with TrypLE express enzyme (Thermo Fischer Scientific, Waltham, MA, USA) to obtain single cells, which were isolated and expanded in 2D cell cultures, using similar culture conditions as the nasal epithelial cells.

ALI differentiation of airway epithelial cells

Mucociliary differentiation of nasal and bronchial airway epithelial cells (passage = 4) was conducted in ALI-Transwell cultures as previously described¹⁸. In brief, 0.2×10^6 or 0.5×10^6 basal progenitor cells (24 or 12 well-inserts respectively) were seeded on PureCol-coated (30 $\mu\text{g}/\text{mL}$, Advanced BioMatrix, Carlsbad, CA, USA) Transwell inserts (0.4 μm pore size polyester membrane, Corning, Corning, NY, USA). Cells were first cultured in submerged conditions with BC expansion medium (Supplementary Table S3) until 100% confluence. Medium was then changed to ALI differentiation medium (Supplementary Table S4) supplemented with A83-01 (500 nM). After 2 days, apical medium was removed to culture the cells under air-exposed conditions. A83-01 was withdrawn from the medium after 3-4 days at air-exposed conditions. Medium was refreshed twice a week, and the apical side of the cells was washed with PBS once a week. Cells were differentiated for 18 days at air-exposed conditions. In indicated experiments, DAPT (20 μM) was added to ALI-differentiation medium from the 4th day of air-exposure.

Conversion of ALI-differentiated airway epithelia into 3D organoids

Differentiated ALI-cultures were converted into 3D airway organoids, as previously described¹⁸. In brief, ALI-cultures were treated with collagenase type II (1 mg/mL, Thermo Fisher Scientific) for 45-60 min at 37 °C to detach the epithelial layer from the Transwell membrane. After detachment, the epithelial layer was mechanically disrupted into fragments by pipetting and subsequently strained with a 100 μm strainer. After centrifugation, epithelial fragments were resuspended in ice-cold 75% Matrigel (Corning, v/v in airway organoid medium) and plated as 30 μl droplets on pre-warmed 24-well suspension plates. These plated were then placed upside down in a tissue incubator for 20-30 min to solidify the Matrigel droplets. Airway organoid medium was added and refreshed twice a week to stimulate airway organoid formation (Supplementary Table S5). It takes 1-3 days for organoid formation and the development of intrinsic lumen. In indicated experiments, DAPT (20 μM) was added to the airway organoid medium.

Forskolin-induced swelling (FIS) measurements in airway organoids

One or two days before fluid secretion measurements, airway organoids were transferred to 96-well plates in 4 μl droplets of 75% Matrigel (v/v in airway organoid medium). Organoids were cultured with 100 μl airway organoid medium. For a FIS assay, airway organoids were stained with calcein green AM (3 μM , Invitrogen, Waltham, MA, USA) 30 min before the experiment. Airway organoids were then stimulated with forskolin (5 μM) and organoid swelling was visualized by imaging at 15-min time intervals for a period of 2 h. Images were made with a Zeiss LSM800 confocal microscope (Zeiss, Breda, Netherlands) at 37°C and 95% O₂/5% CO₂, using a 5x objective. To determine CFTR modulator responses, CF airway organoids were pre-incubated with the CFTR corrector VX-809 (10 μM , Selleck chemicals, Planegg, Germany) for 48 h, followed by stimulation with the CFTR potentiator VX-770 (10 μM , Selleck Chemicals, Planegg, Germany) together with forskolin (5 μM , Sigma-Aldrich, St Louis, MO, USA). Total organoid area per image was quantified using Zen Blue Software (Zeiss). Organoid swelling was then calculated over time, normalized for t=0 and the baseline was set at 100%. Organoid swelling was also expressed as area under the curve (AUC) values to better compare different conditions. Organoid swelling experiments were performed in quadruplicates.

Organoid size measurements

Organoid size was quantified by use of the OrgaQuant convolutional neural network which automatically recognizes organoids in brightfield images^{13,46}. The organoid surface area was estimated using OrgaQuant bounding boxes, assuming organoids had a disk shape. The mean surface area of all individual organoids within a culture well was used for further analyses.

Immunocytochemistry

Undifferentiated airway epithelial cells cultured at collagen IV-coated ibidi 18-well slides, ALI-differentiated airway epithelia, and organoids plated in a 96-well plate, were stained as previously described^{12,18,47}, using indicated antibodies (Supplementary Table S6), with or without phalloidin and DAPI. Images were acquired with a Leica SP8X confocal microscope or Leica THUNDER imager and processed with LAS X software and ImageJ/FIJI. For quantification, MUC5AC⁺ and β -tubulin IV⁺ cells were counted in three microscopic fields per well.

Quantitative real time PCR

Total RNA was extracted from ALI-differentiated nasal and bronchial airway epithelial cells using the RNeasy Mini Kit (Qiagen, Venlo, Netherlands) according to the manufacturer's protocol. For quantitative real-time PCR (qPCR), cDNA was first

synthesized with the iScript cDNA synthesis kit (Bio-Rad, Hercules, CA, USA) according to the manufacturer's protocol. qPCR was conducted using mixtures of specific primer pairs (Supplementary Table S7) and iQ SYBR Green Supermix (Bio-Rad), using a CFX96 real-time detection machine (Bio-Rad). CFX Manager 3.1 software (Bio-Rad) was used to calculate relative gene expression normalized to the housekeeping genes *ATP5B* and *RPL13A* according to the standard curve method. The housekeeping genes were selected based on stable expression in airway epithelial cells using the "Genorm method"⁷⁴⁸. Experiments were performed with two technical replicates.

RNA-seq

RNA-seq was performed at Single Cell Discoveries, using an adapted version of the CEL-seq protocol^{49,50}. Total RNA concentration was measured and normalized to 20 ng/μl using a Qubit fluorometer (Invitrogen, Waltham, MA, USA), and RNA quality was assessed via bioanalyzer and RNA Pico 6000 kit (Agilent, Santa Clara, CA, USA). Normalized total RNA (with RNA integrity number (RIN) scores >7) was used for library preparation and sequencing. Samples were barcoded with CEL-seq primers during a reverse transcription and pooled after second strand synthesis. The resulting cDNA was amplified with an overnight *in vitro* transcription reaction. From this amplified RNA, sequencing libraries were prepared with Illumina Truseq small RNA primers. The DNA library was paired-end sequenced on an Illumina Nextseq™ 500, high output, with a 1x75 bp Illumina kit (R1: 26 cycles, index read: 6 cycles, R2: 60 cycles). Read 1 was used to identify the Illumina library index and CEL-Seq sample barcode. Read 2 was aligned to the Human (hg38) reference transcriptome using BWA MEM⁵¹. Reads that mapped equally well to multiple locations were discarded. Mapping and generation of count tables was done using the MapAndGo script⁵². Differential gene expression analysis was performed using the R package DEseq2 (version 1.30.1)⁵³. Correction for donor and LFC shrinkage was performed using apeglm (version 1.12.0)⁵⁴. A gene was considered differentially expressed when the adjusted p value was <0.01 and fold change >1.5 or <-1.5. Gene set enrichment analysis for gene ontology of biological processes was performed using clusterProfiler (version 3.18.1)⁵⁵ and visualized using enrichplot (version 1.10.2)⁵⁶.

Initial processing of ATAC-seq data, peak calling and peak-gene assignment

ATAC-seq reads were aligned to the human genome (hg38) with HISAT2 using the Octopus Toolkit⁵⁷. HOMER's⁵⁸ makeTagDirectory command was used to make Tag Directories, which were manually filtered to remove reads mapping to the Y chromosome or mitochondrial genome. The fragment length estimate was set to 64 as a representative estimate for all samples. The average signal at all transcription start sites (TSS) in the genome, and the local background signal surrounding these

TSS, were calculated using HOMER's `annotatePeaks` command (options `tss hg38 -size 10000 -hist 40`). The relative quality of each individual sample was determined based on its specific TSS enrichment ratio, which was defined as the average TSS signal (-80 to +80 bp from TSS) divided by the average local background signal (-5kb to -4.96kb and +4.96kb to +5kb away from TSS). Peak calling was performed using HOMER's `findPeaks` command (options `-region -size 100 -minDist 75 -localSize 50000`). HOMER's `mergePeaks` command was used to identify peaks that were present in at least 3/4 (for bronchial samples) or 3/5 (for nasal samples) biological replicates. Only these 'reproducible peaks' were kept for downstream analysis. Peaks that were present in all samples ('universal peaks') were identified as overlapping reproducible peaks found in both experimental groups. HOMER's `makeUCSCfile` command was used to create `bedGraph` files for data visualization of in the IGV genome browser. Peaks were assigned to putative target genes using GREAT with default settings (*i.e.* Basal plus extension; proximal: 5kb upstream, 1kb downstream, distal: up to 1000kb)⁵⁹.

Downstream analysis of ATAC-seq data

Raw counts were determined at all reproducible peaks using HOMER's `annotatePeaks` command (options `hg38 -size given -raw`)⁵⁸. Counts were normalized using the R package `DESeq2`⁵³. To accommodate for the relative lack of zero's in ATAC-seq data at regions without true signal, we slightly modified `DESeq2`'s standard normalization method. Briefly, scaling factors were determined for each sample based on the set of universal peaks (*i.e.* peaks that were present in all samples) and were used to normalize counts at all peaks. PCA of all reproducible peaks ($n=15,434$) was performed with `FactoMineR`⁶⁰. Differentially enriched ATAC-Seq peaks were identified using `DESeq2` (\log_2 fold change > 1 , adjusted p value < 0.1), with scaling factors based on the universal peak set. Pathway enrichment analysis of genes near bronchial-specific and nasal-specific ATAC-seq peaks was performed using `Metascape`⁶¹. Bronchial-specific and nasal-specific ATAC-seq peaks were used as input for HOMER's `findMotifsGenome` script (options `-size 200 -mask -len 6,8,10,12 -S 20`) to search for known transcription factor binding motifs.

Statistical analysis

Statistical analyses were performed using Graphpad version 9.3.0 or R version 4.0.3. Data is presented as mean \pm SD, unless otherwise indicated. Statistical tests used for analysis of differences are indicated in corresponding figure legends. Differences were considered significant at $p < 0.05$.

ACKNOWLEDGEMENTS

We thank Single Cell Discoveries for their bulk RNA sequencing services and data analysis. We thank Michal Mokry and Noortje van den Dungen for conducting ATAC sequencing.

This work was supported by grants of the Dutch Cystic Fibrosis Foundation (NCFS, HIT-CF grant) and SRC 013 from CF Trust-UK. MM is supported by a postdoctoral fellowship from the European Molecular Biology Organization (EMBO ALTF 992-2021).

DATA AVAILABILITY

Normalized counts of sequencing can be found in the supplementary tables. Raw sequencing data cannot be provided with the manuscript due to privacy concerns of the human subjects.

ETHICS DECLARATIONS

The study was conducted according to the guidelines of the Declaration of Helsinki, and approved by the Medical Research Ethics Committee of the University Medical Center Utrecht (Utrecht, The Netherlands) (protocol ID: NL54885.041.16, approved on 16 November 2016 and protocol ID: 16/586, approved on 25 January 2017). Informed consent was obtained from all subjects involved in the study.

COMPETING INTERESTS

J.M.B. has a patent granted (10006904) related to CFTR function measurements in organoids and received personal fees from HUB/Royal Dutch academy of sciences, during the conduct of the study; nonfinancial support from Vertex Pharmaceuticals and personal fees and nonfinancial support from Proteostasis Therapeutics, outside the submitted work.

C.K.v.d.E. reports grants from GSK, Nutricia, TEVA, Gilead, Vertex, ProQR, Proteostasis, Galapagos NV, Eloxx pharmaceuticals, outside the submitted work; In addition, C.K.v.d.E. has a patent related to CFTR function measurements in organoids (10006904) with royalties paid.

The other authors declare no potential conflict of interest.

AUTHOR CONTRIBUTIONS

Conceptualization, J.M.B. and G.D.A.; Methodology, G.D.A., R.S.; Software, L.W.R., M.M. and R.S.; Validation, Formal Analysis, Investigation and Data Curation, L.W.R., M.M., I.S.W., S.M.A.S., L.A.H.O., E.K., J.E.B., R.S. and G.D.A.; Resources, S.M., K.M.W.G., C.K.E. and J.M.B.; Writing – Original Draft, L.W.R. and G.D.A.; Writing – Review & Editing, M.M., I.S.W, S.M.A.S., L.A.H.O, E.K., J.E.B., S.M., K.M.W.G., C.K.E., R.S. and J.M.B.; Visualization, L.W.R., M.M. and G.D.A.; Supervision, R.S, J.M.B. and G.D.A.; Funding Acquisition, M.M., C.K.E., R.S., J.M.B. and G.D.A.

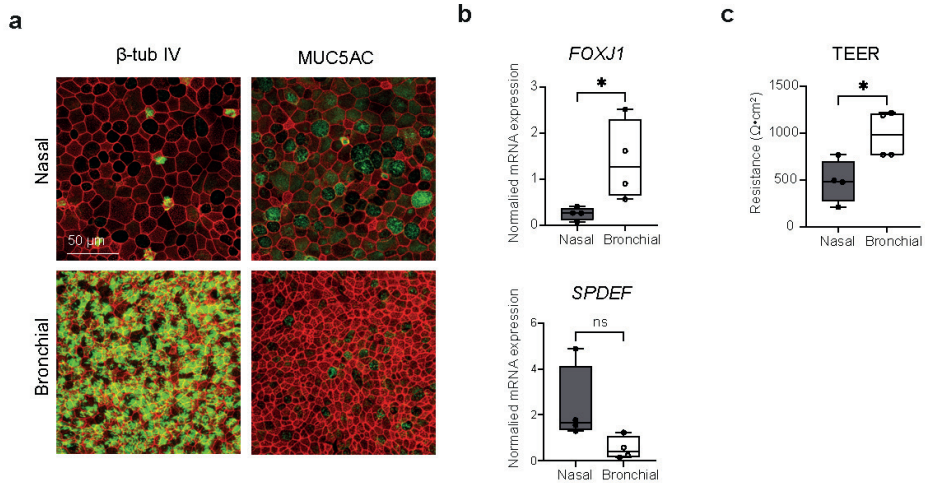
REFERENCES

1. Som, P. M. & Naidich, T. P. Illustrated review of the embryology and development of the facial region, part 1: Early face and lateral nasal cavities. *AJNR Am J Neuroradiol* 34, 2233–2240 (2013).
2. Herriges, M. & Morrisey, E. E. Lung development: orchestrating the generation and regeneration of a complex organ. *Development* 141, 502–513 (2014).
3. Widdicombe, J. H. Early studies on the surface epithelium of mammalian airways. *Am J Physiol Lung Cell Mol Physiol* 317, L486–L495 (2019).
4. Kojima, T. *et al.* Regulation of tight junctions in upper airway epithelium. *Biomed Res Int* 2013, 947072 (2013).
5. Knowles, M. R. & Boucher, R. C. Mucus clearance as a primary innate defense mechanism for mammalian airways. *J Clin Invest* 109, 571–577 (2002).
6. Ganz, T. Antimicrobial polypeptides in host defense of the respiratory tract. *J Clin Invest* 109, 693–697 (2002).
7. Loebinger, M. R., Bilton, D. & Wilson, R. Upper airway 2: Bronchiectasis, cystic fibrosis and sinusitis. *Thorax* 64, 1096–1101 (2009).
8. Riordan, J. R. *et al.* Identification of the cystic fibrosis gene: cloning and characterization of complementary DNA. *Science* 245, 1066–1073 (1989).
9. Knowles, M. R. *et al.* Abnormal ion permeation through cystic fibrosis respiratory epithelium. *Science* 221, 1067–1070 (1983).
10. Boucher, R. C. Muco-Obstructive Lung Diseases. *N Engl J Med* 380, 1941–1953 (2019).
11. Cholon, D. M. & Gentsch, M. Recent progress in translational cystic fibrosis research using precision medicine strategies. *J Cyst Fibros* 17, S52–S60 (2018).
12. Sachs, N. *et al.* Long-term expanding human airway organoids for disease modeling. *EMBO J* 38, e100300 (2019).
13. Rodenburg, L. W. *et al.* Drug Repurposing for Cystic Fibrosis: Identification of Drugs That Induce CFTR-Independent Fluid Secretion in Nasal Organoids. *Int J Mol Sci* 23, 12657 (2022).
14. Vieira Braga, F. A. *et al.* A cellular census of human lungs identifies novel cell states in health and in asthma. *Nat Med* 25, 1153–1163 (2019).
15. Deprez, M. *et al.* A Single-Cell Atlas of the Human Healthy Airways. *Am J Respir Crit Care Med* 202, 1636–1645 (2020).
16. Kicic, A. *et al.* Assessing the unified airway hypothesis in children via transcriptional profiling of the airway epithelium. *J Allergy Clin Immunol* 145, 1562–1573 (2020).
17. Imkamp, K. *et al.* Gene network approach reveals co-expression patterns in nasal and bronchial epithelium. *Sci Rep* 9, 15835 (2019).
18. Amatngalim, G. D. *et al.* Measuring cystic fibrosis drug responses in organoids derived from 2D differentiated nasal epithelia. *Life Sci Alliance* 5, e202101320 (2022).
19. Wan, H. *et al.* Compensatory roles of Foxa1 and Foxa2 during lung morphogenesis. *J Biol Chem* 280, 13809–13816 (2005).
20. Wan, H. *et al.* Foxa2 regulates alveolarization and goblet cell hyperplasia. *Development* 131, 953–964 (2004).
21. Lazzaro, D., Price, M., de Felice, M. & di Lauro, R. The transcription factor TTF-1 is expressed at the onset of thyroid and lung morphogenesis and in restricted regions of the foetal brain. *Development* 113, 1093–1104 (1991).
22. Gómez-Skarmeta, J. L. & Modolell, J. Iroquois genes: Genomic organization and function in vertebrate neural development. *Curr Opin Genet Dev* 12, 403–408 (2002).
23. van Tuyl, M. *et al.* Iroquois genes influence proximo-distal morphogenesis during rat lung development. *Am J Physiol Lung Cell Mol Physiol* 290, L777–L789 (2006).
24. Zhang, X. *et al.* Pax6 is a human neuroectoderm cell fate determinant. *Cell Stem Cell* 7, 90–100 (2010).

25. Basch, M. L., Bronner-Fraser, M. & García-Castro, M. I. Specification of the neural crest occurs during gastrulation and requires Pax7. *Nature* 441, 218–222 (2006).
26. Kawakami, A., Kimura-Kawakami, M., Nomura, T. & Fujisawa, H. Distributions of PAX6 and PAX7 proteins suggest their involvement in both early and late phases of chick brain development. *Mech Dev* 66, 119–130 (1997).
27. Beby, F. & Lamonerie, T. The homeobox gene Otx2 in development and disease. *Exp Eye Res* 111, 9–16 (2013).
28. Simeone, A. Otx1 and Otx2 in the development and evolution of the mammalian brain. *EMBO J* 17, 6790–6798 (1998).
29. Kumamoto, T. & Hanashima, C. Evolutionary conservation and conversion of Foxg1 function in brain development. *Dev Growth Differ* 59, 258–269 (2017).
30. Kobayashi, M., Nishikawa, K., Suzuki, T. & Yamamoto, M. The homeobox protein Six3 interacts with the Groucho corepressor and acts as a transcriptional repressor in eye and forebrain formation. *Dev Biol* 232, 315–326 (2001).
31. Lütke, T. H. *et al.* Tbx2 and Tbx3 Act Downstream of Shh to Maintain Canonical Wnt Signaling during Branching Morphogenesis of the Murine Lung. *Dev Cell* 39, 239–253 (2016).
32. Becker, M. B., Zülch, A., Bosse, A. & Gruss, P. Irx1 and Irx2 expression in early lung development. *Mech Dev* 106, 155–158 (2001).
33. Ku, H. C. & Cheng, C. F. Master Regulator Activating Transcription Factor 3 (ATF3) in Metabolic Homeostasis and Cancer. *Front Endocrinol (Lausanne)* 11, 556 (2020).
34. Hess, J., Angel, P. & Schorpp-Kistner, M. AP-1 subunits: quarrel and harmony among siblings. *J Cell Sci* 117, 5965–5973 (2004).
35. Li, Y. *et al.* The multifaceted roles of FOXM1 in pulmonary disease. *Cell Commun Signal* 17, 35 (2019).
36. Rock, J. R. *et al.* Notch-dependent differentiation of adult airway basal stem cells. *Cell Stem Cell* 8, 639–648 (2011).
37. Amatngalim, G. D. *et al.* Aberrant epithelial differentiation by cigarette smoke dysregulates respiratory host defence. *Eur Respir J* 51, 1701009 (2018).
38. Paranjpye, A., Mutolo, M. J., Ebron, J. S., Leir, S. H. & Harris, A. The FOXA1 transcriptional network coordinates key functions of primary human airway epithelial cells. *Am J Physiol Lung Cell Mol Physiol* 319, L126–L136 (2020).
39. Maeda, Y. *et al.* Airway epithelial transcription factor NK2 homeobox 1 inhibits mucous cell metaplasia and Th2 inflammation. *Am J Respir Crit Care Med* 184, 421–429 (2011).
40. Nomi, K. *et al.* Generation of functional conjunctival epithelium, including goblet cells, from human iPSCs. *Cell Rep* 34, 108715 (2021).
41. Bannier-Hélaouët, M. *et al.* Exploring the human lacrimal gland using organoids and single-cell sequencing. *Cell Stem Cell* 28, 1221–1232.e7 (2021).
42. Plasschaert, L. W. *et al.* A single-cell atlas of the airway epithelium reveals the CFTR-rich pulmonary ionocyte. *Nature* 560, 377–381 (2018).
43. Okuda, K. *et al.* Secretory cells dominate airway CFTR expression and function in human airway superficial epithelia. *Am J Respir Crit Care Med* 203, 1275–1289 (2021).
44. Brewington, J. J. *et al.* Brushed nasal epithelial cells are a surrogate for bronchial epithelial CFTR studies. *JCI Insight* 3, e99385 (2018).
45. Pranke, I. M. *et al.* Correction of CFTR function in nasal epithelial cells from cystic fibrosis patients predicts improvement of respiratory function by CFTR modulators. *Scientific Reports* 2017 7:1 7, 1–11 (2017).
46. Kassis, T., Hernandez-Gordillo, V., Langer, R. & Griffith, L. G. OrgaQuant: Human Intestinal Organoid Localization and Quantification Using Deep Convolutional Neural Networks. *Sci Rep* 9, 12479 (2019).
47. Dekkers, J. F. *et al.* High-resolution 3D imaging of fixed and cleared organoids. *Nat Protoc* 14, 1756–1771 (2019).

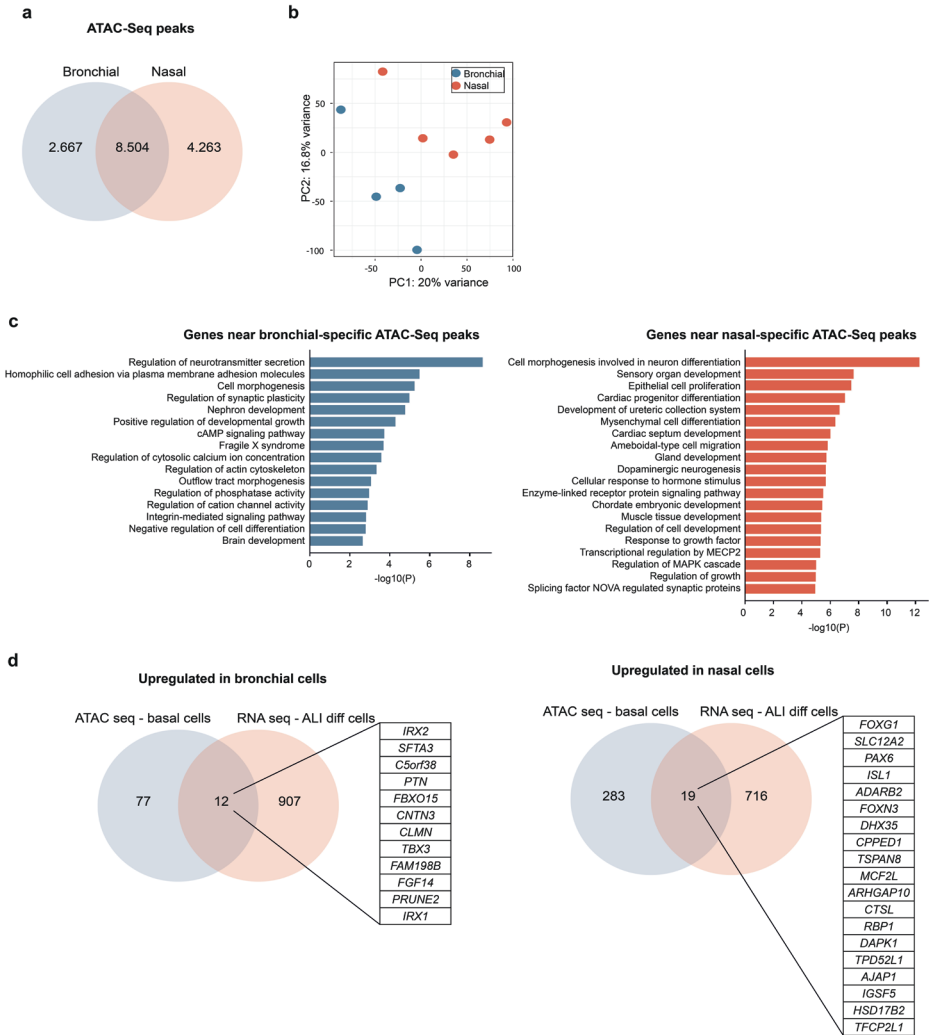
48. Vandesompele, J. *et al.* Accurate normalization of real-time quantitative RT-PCR data by geometric averaging of multiple internal control genes. *Genome Biol* 3, 1–12 (2002).
49. Hashimshony, T., Wagner, F., Sher, N. & Yanai, I. CEL-Seq: single-cell RNA-Seq by multiplexed linear amplification. *Cell Rep* 2, 666–673 (2012).
50. Simmini, S. *et al.* Transformation of intestinal stem cells into gastric stem cells on loss of transcription factor Cdx2. *Nat Commun* 5, 5728 (2014).
51. Li, H. & Durbin, R. Fast and accurate long-read alignment with Burrows-Wheeler transform. *Bioinformatics* 26, 589–595 (2010).
52. MapAndGo. <https://github.com/anna-alemany/transcriptomics/tree/master/mapandgo>.
53. Love, M. I., Huber, W. & Anders, S. Moderated estimation of fold change and dispersion for RNA-seq data with DESeq2. *Genome Biol* 15, 550 (2014).
54. Zhu, A., Ibrahim, J. G. & Love, M. I. Heavy-tailed prior distributions for sequence count data: removing the noise and preserving large differences. *Bioinformatics* 35, 2084–2092 (2019).
55. Yu, G., Wang, L.-G., Han, Y. & He, Q.-Y. clusterProfiler: an R package for comparing biological themes among gene clusters. *OMICS* 16, 284–7 (2012).
56. Yu G. enrichplot: Visualization of Functional Enrichment Result. <https://yulab-smu.top/biomedical-knowledge-mining-book/> (2022).
57. Kim, T., Seo, H. D., Hennighausen, L., Lee, D. & Kang, K. Octopus-toolkit: a workflow to automate mining of public epigenomic and transcriptomic next-generation sequencing data. *Nucleic Acids Res* 46, e53 (2018).
58. Heinz, S. *et al.* Simple combinations of lineage-determining transcription factors prime cis-regulatory elements required for macrophage and B cell identities. *Mol Cell* 38, 576–589 (2010).
59. McLean, C. Y. *et al.* GREAT improves functional interpretation of cis-regulatory regions. *Nat Biotechnol* 28, 495–501 (2010).
60. Lê, S., Josse, J. & Husson, F. FactoMineR: An R Package for Multivariate Analysis. *J Stat Softw* 25, 1–18 (2008).
61. Zhou, Y. *et al.* Metascape provides a biologist-oriented resource for the analysis of systems-level datasets. *Nat Commun* 10, 1523 (2019).

SUPPLEMENTARY FIGURES



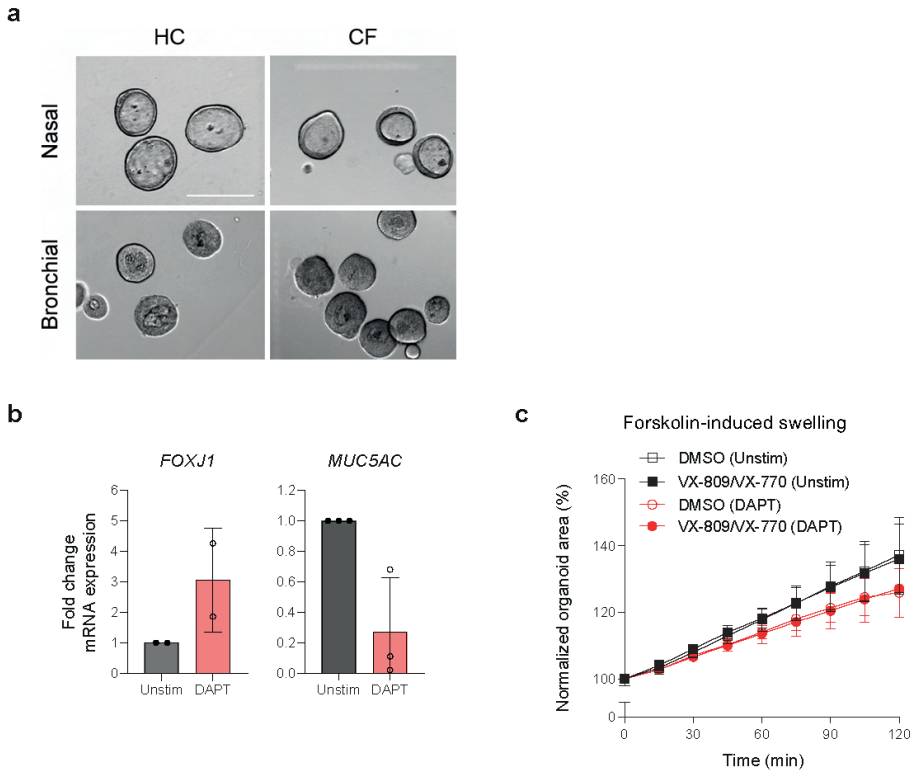
Supplementary Figure S1. Nasal and bronchial epithelial cell cultures from HC subjects exhibit unique mucociliary differentiation states.

(A) Representative IF staining of β -tubulin IV (ciliated cells) and MUC5AC (goblet cells) in paired ALI-differentiated nasal and bronchial cells of a HC subject. Cultures were differentiated for 18 days. Epithelial markers are shown in green, phalloidin (red) was used as actin cytoskeleton staining. Scale bar equals 50 μ m. (B) mRNA expression of the cell type-specific transcriptional factors *FOXJ1* (ciliated cells) and *SPDEF* (goblet cells) in ALI-differentiated nasal (grey bars) and bronchial (open bars) epithelial cells of HC subjects (n=4 independent donors). (C) TEER measurements of ALI-differentiated nasal (grey bars) and bronchial (open bars) epithelial cells of HC subjects (n=4 independent donors). Data is shown as mean \pm SD. Analysis of differences was conducted using unpaired t-tests (panel b, c). ns = non-significant, * $p < 0.05$.



Supplementary Figure S2. Unique epigenomic features of nasal and bronchial basal progenitor cells.

(A) Venn diagram showing the identified ATAC-seq peaks, indicating chromatin accessible regions, and discriminates nasal- and bronchial-specific ATAC-seq peaks. (B) PCA of differentially enriched ATAC-seq peaks in undifferentiated nasal (n=5 donors, of which 4 paired donors) and bronchial epithelial cells (n = 4 paired donors) (log₂ fold change >1, adjusted p < 0.1). (C) Pathway enrichment analysis with genes assigned to the bronchial- (left panel) and nasal- (right panel) specific differentially expressed ATAC-seq peaks. (D) Venn diagram showing overlap between genes corresponding to differentially expressed ATAC-seq peaks in undifferentiated bronchial (left panel) and nasal (right panel) epithelial cells and DEGs from RNA-seq, enriched in ALI-differentiated bronchial epithelial cells.



Supplementary Figure S3. ALI culture-derived nasal and bronchial organoids display distinctive fluid secretion, which is dependent on the number of ciliated cells.

(A) Representative brightfield images of nasal and bronchial airway organoids from HC and CF subjects, demonstrating pre-swollen lumens in HC and CF nasal organoids, and a lack of lumen formation in bronchial organoids. Scale bar equals 500 μm . (B) mRNA expression of the cell type-specific transcription factors *FOXJ1* (ciliated cells) and *MUC5AC* (goblet cells) in nasal cells from individuals with CF (n=2-3 independent donors), treated with (red) or without (grey) the γ -secretase inhibitor DAPT (20 μM). mRNA expression is calculated using the ddCt method and shown as a fold change compared to unstimulated cells. (C) Nasal organoid swelling assay with organoids from individuals with CF (n=3 independent donors), treated with or without the γ -secretase inhibitor DAPT (20 μM). Organoids were stimulated with forskolin (5 μM) alone, or with forskolin (5 μM) together with VX-770 (10 μM) and pre-treatment with VX-809 (10 μM) for 48 h. Results are depicted as percentage increase in normalized area in time. Data is shown as mean \pm SD. Analysis of differences was conducted with a one-sample t-test (panel b).

ONLINE SUPPLEMENTARY TABLES

Available online at <https://doi.org/10.1038/s41598-023-45201-4>

Supplementary Table S1: Differentially expressed genes between ALI-differentiated nasal and bronchial epithelial cells

Supplementary Table S2: Differentially enriched ATAC-seq peaks between nasal and bronchial basal progenitor cells

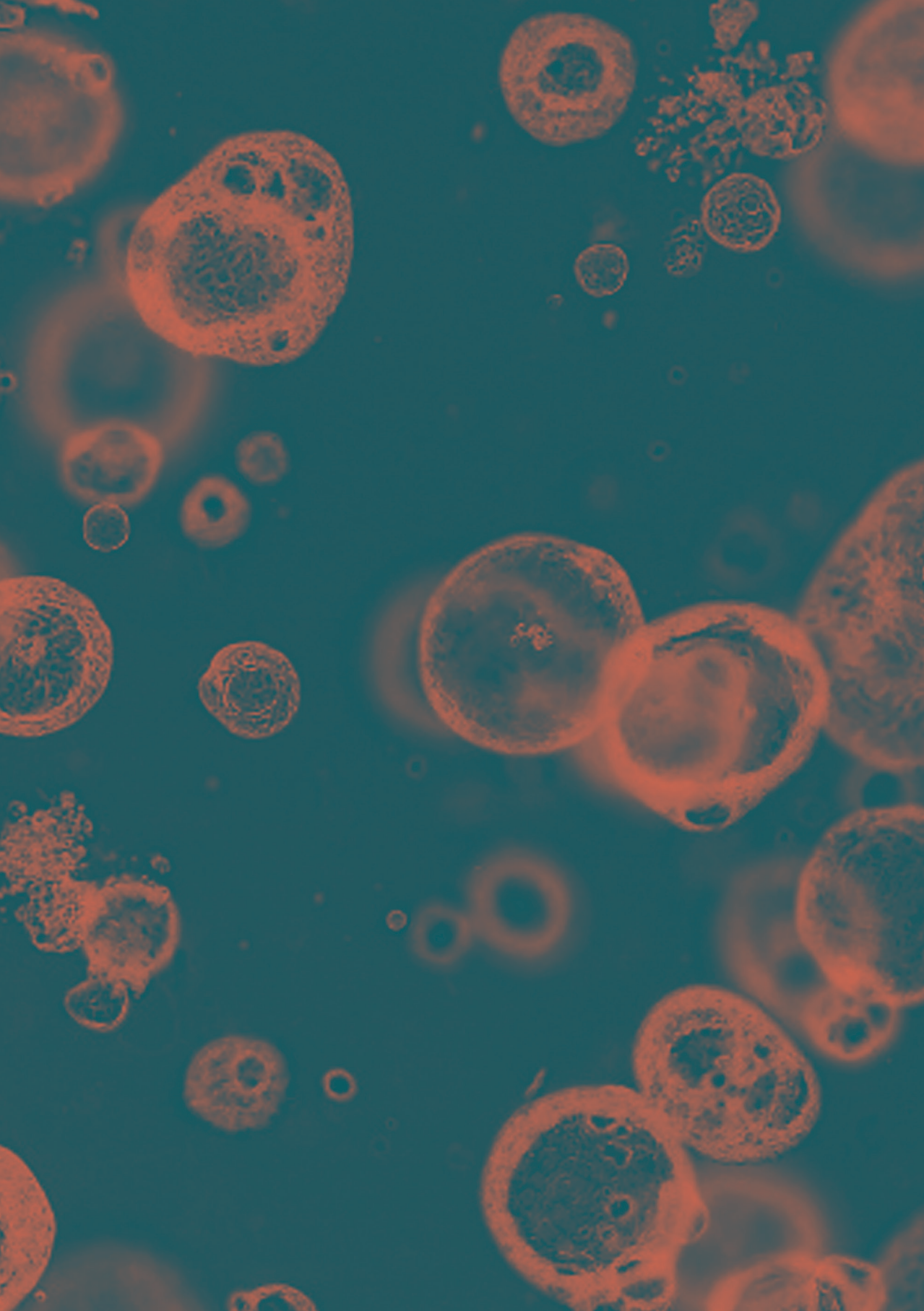
Supplementary Table S3: BC isolation and BC expansion medium

Supplementary Table S4: ALI-differentiation medium

Supplementary Table S5: Airway organoid medium

Supplementary Table S6: Antibodies for immunofluorescence

Supplementary Table S7: Primers for qPCR



General discussion

GENERAL DISCUSSION

The aim of this thesis was to investigate the use of cultured nasal brushing-derived airway epithelial cells as preclinical model for cystic fibrosis (CF). In this general discussion, I will first focus on strengths and limitations of the newly developed culturing protocols for human nasal epithelial cells (HNEC). Next, I will discuss the use of cultured HNEC as personalized disease model for CF and other airway diseases.

PROS AND CONS OF WORKING WITH NASAL BRUSHING-DERIVED EPITHELIAL CELLS

In **chapter 1**, we describe protocols to culture nasal brushing-derived airway epithelial cells and to generate organoids from these cells to apply in a functional CFTR assay. Nasal brushing-derived airway epithelial cells have already been widely used in airway epithelial culture models ^{1,2}, but the application was impeded by a low yield of cells harvested during nasal brushings, a limited proliferative capacity of isolated cells and limited scalability of functional CFTR assays. Therefore, we developed new protocols for the collection of HNEC by nasal brushing and the subsequent isolation, expansion and cryopreservation of basal progenitor cells. Novel culture media recipes were developed for the expansion of basal progenitor cells without the need of feeder cells. Feeder cells are growth-arrested animal-derived cells that produce growth factors to stimulate the proliferation of difficult growing primary cell cultures, such as airway epithelial cells. However, drawbacks are the risk for contamination of patient-derived cells with animal-derived components and the extra workload of using an extra cell line ¹. Our culturing method does not need feeder cells and is based on small molecules which inhibit the ROCK, NOTCH and MAPK signaling pathways and induce dual SMAD inhibition ^{1,3,4}. The culture medium further contains growth factors and WNT activators. However, the requirement of WNT activators is arguable as others cultured airway organoids without their need ⁵. The small molecules increase the proliferative lifespan of basal progenitor cells by preventing differentiation and postponing senescence. This enabled us to isolate appropriate numbers of basal progenitor cells for expansion up to passage 13 and cryopreservation. As the culture media only stimulates expansion of basal progenitor cells, and not of differentiated epithelial cells, immune cells or fibroblasts, we did not need a selection step by flow cytometry.

An advantage of our culturing protocols is the availability of culturing media recipes with fully defined ingredients. Many of the widely used culturing media are from commercial agencies with undefined ingredients. Different culturing media were shown to induce different cellular morphologies and experimental outcomes in ALI-

differentiated cell cultures, thus impeding experimental reproducibility^{6,7}. With a defined ingredient list, users can understand differences between different media. Therefore, targeted improvements can be applied when needed for specific assays, e.g. by withholding specific ingredients or adding components. Furthermore, the culture media has an animal-free composition. Noteworthy, we did not directly compare our culturing media with other available culturing media, which might be useful in future to better understand the effect of culture medium on experimental outcomes.

Using our culturing protocols, we established a biobank with cryopreserved nasal brushing-derived basal progenitor cells (Table 1). All donors signed a broad informed consent for the storage and future use of their cells. The biobank currently consists of nasal brushing-derived basal progenitor cells of approximately 320 donors, including 145 people with CF with varying *CFTR* mutations and 54 controls without CF. Further, our nasal brushing-derived cell culturing protocols are used to study other genetic respiratory disorders, e.g. primary ciliary dyskinesia (PCD), respiratory infections, e.g. covid-19, and the role of the airway epithelium in congenital disorders, e.g. oesophagus atresia. The biobank enables the use for personalized disease modeling, such as understanding disease pathology, disease stratification, or predicting therapeutic responses on individual basis. In **chapter 1 and 2**, we show the implementation of *CFTR* function measurements in nasal organoids, derived from air-liquid interface (ALI)-differentiated basal progenitor cells. Furthermore, biobanked HNEC can be shipped abroad to collaborating research groups. As example, we shared HNEC with an international collaborating group to perform Ussing Chamber measurements in similar HNEC as used for nasal organoid swelling assays, as shown in **chapter 2 and 3**.

Table 1. Overview of the nasal epithelial cell cultures included in our biobank.

Disease	Number of biobank inclusions
CF	145
<i>F508del/F508del</i>	55
<i>Class I genotype</i>	9
<i>Class II genotype (other than F508del/F508del)</i>	34
<i>Class III genotype</i>	10
<i>Class IV genotype</i>	4
<i>Class V genotype</i>	7
<i>Unclassified genotype</i>	15
COVID-19	81
Primary ciliary dyskinesia (PCD)	15
Oesophagus atresia	13
Children with recurrent respiratory infections	12
Healthy control	54
Total	320

Besides biobanking, the new culturing protocol facilitates bulky expansion of basal progenitor cells for multiple passages. This provided us with a high yield of HNEC at high passages to implement in screening assays or gene-editing approaches. In **chapter 4**, we screened 1400 FDA-approved drugs in 384-well plate format to investigate their effect on epithelial fluid secretion in nasal organoids. In **chapter 5**, we created multiple gene knockouts using CRISPR/Cas9 technology in basal progenitor cells which still could be expanded and cryostored after the electroporation procedure. Based on a published protocol for human bronchial epithelial cells (HBEC) from explanted lung tissue⁸, we developed a gene editing protocol for nasal-brushing derived epithelial cells by the direct delivery of ribonucleoprotein (RNP) complexes, consisting of sgRNA and Cas9, into the cells by electroporation. A selection step was not needed, because of high knockout efficiencies. Gene-editing was performed earlier in biopsy-derived HNEC⁹ and in nasal brushing-derived epithelial cells, but without further expansion of the gene-edited cells^{10,11}. To my knowledge, we are the first who reported gene-editing and subsequent expansion and cryostorage in nasal brushing-derived epithelial cells¹². In total, we created 46 gene-edited cell cultures from biobanked HNEC.

Despite the huge progress in the culturing of nasal brushing-derived airway epithelial cells, challenges remain. First, the expansion capacity of basal progenitor cells is still limited because of cellular senescence at higher passages. This is related to the confined regenerative capacity of the airway epithelium *in vivo*, which is only activated upon injury. This is in contrast to the unlimited expansion of intestinal epithelial stem cells in organoid cultures, which reflects the continuous high cellular turnover observed in intestinal tissue¹³. Because of its characteristics *in vivo*, it is uncertain if the *in vitro* proliferative capacity of basal progenitor cells can be improved further. This would not raise issues for personalized disease modeling, as only a low number of cells is needed. However, when a high number of cells is needed, e.g. for large drug screenings, cells can be further expanded at multiple passages, or it might be needed to re-brush a patient. Future research should establish how passage number affects fluid secretion in nasal organoids, as other studies showed a gradual decrease of CFTR- and ENaC-dependent currents in HNEC at higher passages¹⁴. Alternatively, the lifespan of basal progenitor cells might be expanded by the introduction of human telomerase reverse transcriptase (hTERT) to generate an immortalized cell culture¹⁵. However, it has to be investigated if these immortalized cultures still represent the native genetic and epigenetic profile of individual patients.

Another challenge of the use of patient-derived airway epithelial cells is the substantial donor-to-donor variation, when aiming to draw conclusions on group level. Many experiments in this thesis were performed with a limited number of donors (n = 3 - 5),

which often was not enough to reach statistical significance between experimental groups. However, for personalized medicine applications this donor-to-donor variation is not a limitation as the cultures represent the individual. The variation within one donor is limited, but seems to increase when using cells from different passages or from different vials. The variation between donors occurred in cell culturing properties, such as the expansion rate of basal progenitor cells, the time needed to obtain well-differentiated cultures and the number of organoids formed from a fixed number of cells. These variations require thorough planning and may lead to the spread of experimental steps from different donors across different days. We also observed variation in the cellular composition after ALI-differentiation and in fluid secretion properties of nasal organoids. The variation between donors might be caused by technical variation, e.g. during the collection procedure (e.g. yield of cells, type of cells), the media batch and correct freeze/thawing procedures. The variation might also relate to biological variation between the cell cultures, such as genetic and epigenetic differences. Factors which might cause biological variation are chronic inflammation, acute infection at the moment of brushing, sinonasal problems, medication, age, sex, smoking and severity of disease. Other studies already showed that age affects mucociliary differentiation and TMEM16A-dependent chloride transport, but not ENaC- and CFTR-dependent transport ¹⁶. In contrast, another study looked into predictive factors for the success of generating a fully differentiated ALI culture in more than 400 bronchial cell cultures and only found the presence of ciliated beating cells in the brush as predictive factor, and not age, lung function or having asthma or COPD ¹⁷. All these aspects require the need for many donors to observe differences and reach statistical significance between experimental groups. Other improvements which might help to decrease variation between donors are establishing similar experimental conditions, e.g. by planning experimental assays at the same time, on similar culturing plates, using similar media batches, increasing the number of technical replicates or by automatizing experimental steps. However, it will always be a difficult balance between the labour-intensive experimental work with patient-derived cells and having enough replicates and donors to draw strong conclusions.

NASAL ORGANOIDS COMPARED TO OTHER PERSONALIZED *IN VITRO* MODELS FOR CF

Besides the introduction of improved culturing protocols, we described how nasal organoids, derived from ALI-differentiated HNEC, can be used as model for CF. **Chapter 1 and 2** describe their application in the CFTR-dependent FIS assay to predict CFTR modulator efficacy on individual basis. This might facilitate access to therapy

for people with rare *CFTR* mutations. Moreover, **chapter 3** describes the application of nasal organoids in *CFTR*-independent fluid secretion assays. It aimed to find drugs which restore epithelial fluid secretion by alternative ion channels or transporters, thus bypassing *CFTR*. This approach might be applicable for all people with CF, independent of their mutation type. But how do fluid secretion assays in nasal organoids compare to other personalized *in vitro* models for CF?

Ussing chamber measurements in ALI-differentiated HBEC are considered as the golden standard for *in vitro* *CFTR* function measurements¹⁸. As the collection of HBEC requires an invasive bronchoscopy, *CFTR* function measurements with the Ussing chamber were also successfully performed in HNEC^{19,20}. However, the Ussing chamber limits scalability as only 4 – 8 samples can be measured simultaneously in this system. The number of samples can be increased by using the Multi Transepithelial Current Clamp (MTECC) 24-well system²¹, but still not enable the use of 96- or 384-well plates, which we did for organoid assays. Therefore, the main advantage of nasal organoids over Ussing chamber measurements are its scalability and potential for high-throughput settings to screen drug libraries or large patient cohorts.

The other widely used personalized model for CF is the FIS assay in intestinal organoids^{22,23}. The advantage of intestinal above nasal organoids is their inexhaustible supply and fast growth. HNEC stop growing at a certain passage, and the effect of passage number is still unknown. Furthermore, the FIS assay in intestinal organoids is performed in organoids derived from expansion culture conditions, while nasal organoids first have to be differentiated before they express *CFTR*²¹. Therefore, nasal organoids take more time to be applied in FIS assays after their collection. However, a rectal biopsy is more invasive compared to a nasal brushing and intestinal organoids are not airway-derived, which is the most affected epithelial tissue in people with CF. Comparison studies between donor-matched nasal and intestinal organoids showed a similar FIS response in **chapter 2**, but has to be repeated in a larger subject-matched cohort.

HNEC distinguish themselves from intestinal organoids by the expression of alternative ion channels and transporters. This makes them suitable for epithelial fluid secretion studies focusing on alternative chloride channels, which we did in **chapter 3 and 4**. In **chapter 5**, we did not observe this *CFTR*-independent fluid secretion in organoids derived from ALI-differentiated HBEC. However, as people with CF mostly suffer from problems in the lower airways, it can be argued how relevant this cAMP-mediated *CFTR*-independent organoid swelling in HNEC is, when not observed in our 2-hour experiments in HBEC. On the other hand, only a little improvement in fluid secretion might already relieve symptoms and might not be picked up in HBEC

in vitro. Therefore, clinical translation of compounds stimulating CFTR-independent fluid secretion should answer this question. One example is the TMEM16A potentiator ETD002. It increased anion secretion in cultured HBEC from subjects with CF, without affecting calcium signaling or increasing mucus production^{24,25}. In animal studies, it accelerated mucociliary clearance in an ovine model after blocking CFTR function²⁴. Furthermore, it did not induce bronchoconstriction in rats, which could have been an unwanted consequence of TMEM16A activation²⁵. The first-in-human trial with ETD002 is now ongoing^{24–26}. Besides potentiating TMEM16A, multiple pharmaceutical companies developed compounds inhibiting ENaC as strategy to rehydrate the CF airway epithelium. So far, none of the compounds showed therapeutic benefit in clinical trials because of modest, short-term or toxic effects, but other trials are ongoing^{27,28}.

Another source of patient-derived cells to perform CFTR function measurements are induced pluripotent stem cells (iPSCs). These are patient-derived somatic cells, usually fibroblasts or peripheral blood mononuclear cell (PBMCs), reprogrammed *in vitro* towards pluripotent stem cells. These stem cells are subsequently differentiated towards airway basal progenitor cells by mimicking key embryological events. The airway basal progenitor cells can be ALI-differentiated towards a mucociliary epithelium or transformed into airway organoids. These differentiated iPSCs represent the unique genetic code of an individual patient and thus can be applied for assessing baseline CFTR function and potential rescue by CFTR modulators in Ussing Chamber measurements or by FIS assays in airway organoids²⁹. Advantages of iPSCs in comparison to the other discussed models are the limitless supply of patient-derived cells, the non-invasive collection and the availability of established gene-editing protocols. Downsides are the long and labour-intensive protocols for reprogramming and differentiation, including many quality control checks. Therefore, the use of iPSCs for CFTR function measurements is not suited for a widely use around different labs or to screen large patient cohorts.

Despite the advantages of nasal organoids as personalized model of CF, good validation studies of the FIS assay in nasal organoids with clinical data are still needed. One retrospective validation study by another group showed a correlation between baseline FIS in nasal organoids and baseline sweat chloride *in vivo*. Furthermore, they found a significant correlation between the effect of CFTR modulator treatment on the *in vitro* organoid response and the *in vivo* lung function. Sweat chloride values post modulator treatment were not included as these were not routinely measured. Noteworthy, the sample size was very small (n=8) and included people with CF with a large variety in CFTR function and drug responsiveness³⁰. For the other personalized *in vitro* models for CF, more validation studies have been reported. For example, it has been shown

that CFTR modulator responses in ALI-differentiated HNEC measured in the Ussing chamber correlated with *in vivo* clinical drug responses^{31,32}. Furthermore, The FIS assay in intestinal organoids was shown to correlate with long-term disease progression³³ and the effect of CFTR modulators correlated with donor-matched *in vivo* drug responses²³. Future research should therefore focus on clinical validation of the FIS assay in nasal organoids, especially with our own culturing protocols. They should include enough donors, equally divided over different mutation groups and preferably include both lung function and sweat chloride measurements pre- and post-treatment.

DO NASAL EPITHELIAL CELLS REPRESENT THE LOWER AIRWAYS?

In **chapter 5**, we focused on the research question to what extent cultured HNEC may act as surrogate model of the diseased lower airway epithelium. To investigate this, we compared CF donor-matched HNEC and HBEC using several molecular and functional analysis methods, including transcriptomics, epigenetics and studies focused on characterizing mucociliary differentiation and fluid secretion. Through these analyses, we found a predominant secretory phenotype in ALI-differentiated HNEC and a ciliated phenotype in ALI-differentiated HBEC. This corresponds with studies conducted by others, although they did not quantify the expression. Images seem to show higher expression of the secretory cell marker MUC5AC in HNEC and more expression of the ciliated cell marker acetylated α -tubulin in HBEC²⁰. In contrast, others showed ciliated cells as the predominant cell type in HNEC, but did not make a comparison with HBEC¹⁹. Furthermore, we observed major differences in the epithelial barrier integrity between nasal and bronchial cell cultures, as reflected by a lower transepithelial electrical resistance (TEER) in ALI-differentiated HNEC compared to ALI-differentiated HBEC. This difference was observed in cultures of donors with CF and in cultures of non-CF controls. Differences in barrier integrity also corresponded with observations made in other studies which observed a non-significant trend in higher baseline barrier integrity in ALI-differentiated HBEC from people with CF compared to HNEC, measured by the Ussing Chamber. However, this trend was seen only in a minority of the donors²⁰. Another study only found a lower baseline resistance in ALI-differentiated HBEC from healthy controls, and not in CF cultures¹⁹. A potential explanation for the differences seen in mucociliary differentiation are epigenetic differences, imprinted in the basal progenitor cells. This might relate to their different embryonic origin, as we showed in **chapter 5** that ectoderm-related transcription factors are higher expressed in HNEC and endoderm-related transcription factors more in HBEC. The differences in barrier integrity might be caused by lower expression of adherent proteins in HNEC, maybe

related to the different cellular phenotype. However, as others observed many donor variation, it might also be related to inflammation status during the collection, or due to technical issues, e.g. sampling yield or monolayer differentiation.

Despite differences in the mucociliary epithelial composition, the question is whether cultured HNEC can be applied in a similar manner as HBEC in organoid swelling assays. In previous studies, others have shown a good correlation between paired ALI-differentiated HNEC and HBEC for CFTR-dependent currents and CFTR modulator responses, determined in Ussing chamber measurements²⁰. In contrast, we observed CFTR-dependent swelling and CFTR rescue by CFTR modulators in FIS assays in bronchial organoids, but not in subject-matched nasal organoids, cultured in similar conditions. Similar to earlier observations made in **chapter 2**, nasal organoids demonstrated CFTR-independent swelling, which affected the detection of CFTR modulator responses. Thus, previous studies examining forskolin-induced chloride currents in Ussing chamber measurements in HNEC, did not correspond with our observation in FIS assays with nasal organoids. Indeed, in **chapter 2**, we furthermore demonstrated that CFTR specificity in nasal organoids can be enhanced by modifying the culture conditions. Further studies are required to explore how CFTR modulator responses in FIS assays are affected in nasal and bronchial organoids using this optimized culture condition. Moreover, it should be investigated how FIS assays in nasal organoids correspond to forskolin-induced chloride currents in donor-matched HNEC measured by the Ussing chamber.

Altogether, we and others showed clear differences between cultured nasal and bronchial epithelial cells. This is actually not surprising as both epithelia have different cellular compositions and functions *in vivo*. The nasal cultures therefore might recapitulate the *in vivo* situation, but HNEC should display similar characteristics as HBEC when used as surrogate model. We showed that culturing conditions of HNEC can be adapted to skew cellular differentiation to a lower airway phenotype or to increase CFTR expression. Therefore, HNEC should not necessarily mimic all characteristics of HBEC, but they should provide similar outcomes as HBEC in the experimental assays of interest. To assess if HNEC are appropriate as surrogate model, outcomes should be validated with HBEC or with clinical data for each specific assay.

NASAL EPITHELIAL CELLS AS MODEL FOR OTHER AIRWAY DISEASES

This thesis focuses on the application of HNEC as personalized model for CF. However, the culturing methods described in **chapter 1** have the potential for broader application as *in vitro* model in various other airway diseases. First, these methods can be employed for other genetic airway diseases, characterized by airway epithelial cell dysfunction. Most notably is the monogenic disorder PCD, characterized by genetic defects in motile cilia assembly or functional proteins, resulting in impaired ciliary function. ALI-differentiated HNEC and nasal spheroids have already been used for diagnostic purposes^{34,35}. In extent to this, there is a promising potential for using HNEC of subjects with PCD for personalized medicine.

In addition to monogenic disorders, cultured HNEC may also serve as proxy model for chronic inflammatory airway diseases, such as asthma and COPD. In the field of asthma research, the united airway disease hypothesis proposes that the upper and lower airways exhibit a similar disease manifestation because a single inflammatory process affects both regions^{36,37}. This hypothesis may explain why many people with asthma also suffer from allergic rhinitis³⁷. Indeed, transcriptomic profiles of fresh upper and lower airway brushings from children with asthma, wheeze and/or atopy showed large homology and could be used to identify different sub phenotypes of asthma^{38,39}. *In vitro* cell cultures from asthmatics have been used to study inflammation at resting conditions or in response to inflammatory stimuli. Comparisons between ALI-differentiated HNEC and HBEC from children with asthma showed morphological differences, with a higher number of both ciliated and goblet cells in HBEC⁴⁰. Upon stimulation with the cytokine IL-13, which is used to mimic Th2 inflammation observed in allergic asthma, both HBEC and HBEC show an increased number of goblet cells, but only HBEC show a decrease in ciliated cells. In contrast to these morphological differences, the physiological response upon IL-13 stimulation was comparable between ALI-differentiated HNEC and HBEC, as measured by the apical and basolateral secretion of cytokines⁴⁰. Other studies demonstrated a constitutively higher release of IL-6 and IL-8 in cultured HNEC compared to HBEC from asthmatics.^{41,42} The same studies examined respiratory viral infections and demonstrated similarities in host responses. However, it should be noted that most of the studies were performed in submerged non-differentiated cell cultures^{41,42}. One study compared ALI-differentiated cells from asthmatic patients on their response to human rhinovirus (HRV) infection and found a higher susceptibility for infection in HBEC compared to HNEC⁴³.

In COPD research, it is hypothesized that lower airway epithelial remodelling follows a distal-to-proximal repatterning ⁴⁴. This remodelling process in COPD resembles the genetic and phenotypic characteristics of the non-diseased upper airways, leading to an increase in goblet cells and a decrease in ciliated and club cells ⁴⁴⁻⁴⁶. Furthermore, studies have shown that gene expression changes induced by cigarette smoke exposure in the bronchial airway epithelium are also reflected in the nasal epithelium ⁴⁷⁻⁴⁹. Nasal epithelial cell cultures from people with COPD have further been used to study epithelial host defence responses to inflammatory stimuli. In one study, a correlation was found in Toll-like receptor 4 (TLR-4) expression, a key player in epithelial host defence, between paired nasal and tracheal undifferentiated cell cultures of COPD patients ⁵⁰. In contrast, others observed a more pronounced downregulation of TLR-4 in ALI-differentiated HBEC upon cigarette smoke exposure, compared to HNEC ⁵¹. TLR-4 activation with lipopolysaccharide (LPS) induced a comparable IL-8 response ALI-differentiated HNEC and HBEC from COPD subjects. However, induction of IL-6 response was lower in HBEC ⁵¹. Altogether, these findings suggest structural differences between cultured HNEC and HBEC, which highly depend on culturing conditions and different experimental setups. However, it is also shown that these differences not necessarily lead to differences in functional assays focusing on the intended outcome measure.

Cultured HNEC may also serve as viable model to study respiratory viral infections, as the nasal epithelium serves as the main tissue that is initially infected by airborne viral particles. ALI-differentiated HNEC have been applied to study a broad range of respiratory viruses, including respiratory syncytial virus (RSV) ⁵², severe acute respiratory syndrome coronavirus 2 (SARS-CoV-2) ^{53,54} and influenza ^{55,56}. These studies have utilized HNEC to study viral entry and the efficacy of antiviral drugs, such as vaccines and monoclonal antibodies.

In addition to viral infection research, HNEC can be utilized in toxicology studies to evaluate the effects of pollutant-induced hazard ^{57,58}. For instance, the molecular alterations induced by diesel engine exhaust were assessed in HNEC from diesel engine factory workers and were shown to overlap with smoking-induced signatures ⁵⁸.

To summarize, the culturing protocols developed for HNEC in this thesis have a broad applicability beyond CF. By optimizing and validating the culturing protocols for specific assays, the potential of HNEC in various research fields can be fully realized.

CONCLUDING REMARKS AND FUTURE PERSPECTIVE

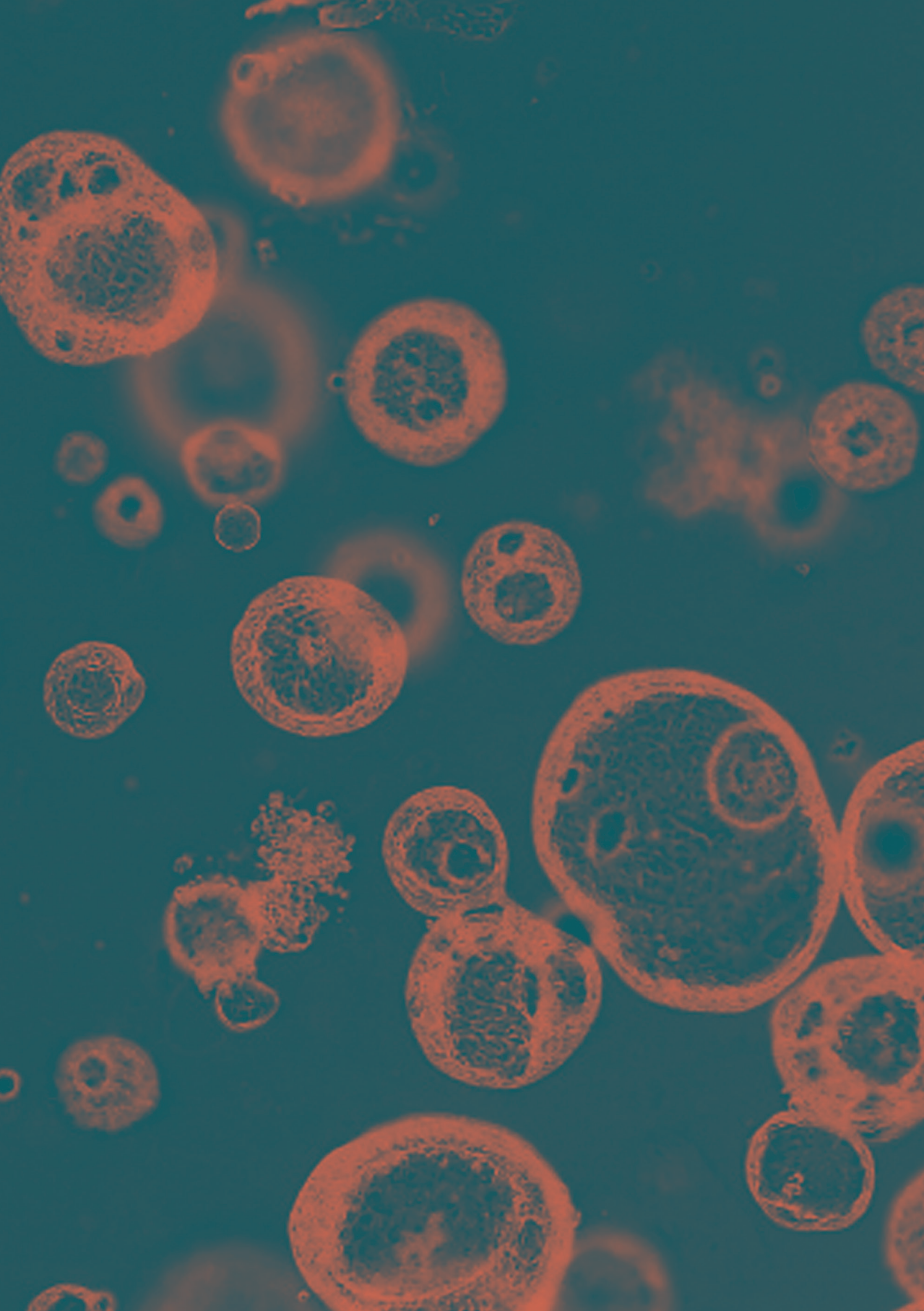
We developed culturing protocols for nasal-brushing derived cells and utilized them for biobanking, disease modeling, drug screenings and CRISPR/Cas9-gene editing. The easy and minimally invasive collection method make HNEC particularly attractive for personalized disease modeling. When considering whether nasal epithelial cells are the ideal model system for CF research, it is worth examining the criteria proposed by Mou et al. for an ideal CF model system⁵⁹. According to these criteria, an ideal model system should be patient-specific, provide an unlimited supply of cells, be clean, easily screenable, shareable, shippable, universally applicable, and have a fully defined and efficient protocol. In my opinion, an ideal model system should also involve minimally invasive collection, reproducibility, a high success rate in the isolation procedure, validated with clinical data and approved by regulatory and ethical instances. Nasal organoids comply with many of these criteria, as they are patient-specific, screenable, shareable, shippable, have a fully defined protocol, acquired via minimally invasive procedures and have regulatory approval. Therefore, HNEC are a very promising preclinical disease model, but future research should draw attention to the success rate of isolation, the reproducibility and validation with clinical responses. Moreover, by optimizing the culturing conditions for specific assays and research objectives, HNEC have the potential to be utilized in a much broader range of preclinical models for airway epithelial diseases than what has been described in this thesis. This further highlights the versatility and potential of nasal epithelial cells as a valuable tool in biomedical research.

REFERENCES

1. Bukowy-Bieryłło, Z. Long-term differentiating primary human airway epithelial cell cultures: how far are we? *Cell Communication and Signaling* 19, 1–18 (2021).
2. Keegan, D. E. & Brewington, J. J. Nasal Epithelial Cell-Based Models for Individualized Study in Cystic Fibrosis. *Int J Mol Sci* 22, 4448 (2021).
3. Mou, H. *et al.* Dual SMAD Signaling Inhibition Enables Long-Term Expansion of Diverse Epithelial Basal Cells. *Cell Stem Cell* 19, 217–231 (2016).
4. Horani, A., Nath, A., Wasserman, M. G., Huang, T. & Brody, S. L. Rho-associated protein kinase inhibition enhances airway epithelial Basal-cell proliferation and lentivirus transduction. *Am J Respir Cell Mol Biol* 49, 341–347 (2013).
5. Salahudeen, A. A. *et al.* Progenitor identification and SARS-CoV-2 infection in human distal lung organoids. *Nature* 588, 670–675 (2020).
6. Saint-Criq, V. *et al.* Choice of Differentiation Media Significantly Impacts Cell Lineage and Response to CFTR Modulators in Fully Differentiated Primary Cultures of Cystic Fibrosis Human Airway Epithelial Cells. *Cells* 9, 2137 (2020).
7. Luengen, A. E. *et al.* Choosing the Right Differentiation Medium to Develop Mucociliary Phenotype of Primary Nasal Epithelial Cells In Vitro. *Scientific Reports* 2020 10:1 10, 1–11 (2020).
8. Koh, K. D. *et al.* Efficient RNP-directed Human Gene Targeting Reveals SPDEF Is Required for IL-13-induced Mucostasis. *Am J Respir Cell Mol Biol* 62, 373–381 (2020).
9. Vaidyanathan, S. *et al.* High-Efficiency, Selection-free Gene Repair in Airway Stem Cells from Cystic Fibrosis Patients Rescues CFTR Function in Differentiated Epithelia. *Cell Stem Cell* 26, 161-171.e4 (2019).
10. Cao, H. *et al.* Testing gene therapy vectors in human primary nasal epithelial cultures. *Mol Ther Methods Clin Dev* 2, 15034 (2015).
11. Geurts, M. H. *et al.* CRISPR-Based Adenine Editors Correct Nonsense Mutations in a Cystic Fibrosis Organoid Biobank. *Cell Stem Cell* 26, 503-510.e7 (2020).
12. King, N. E. *et al.* Correction of Airway Stem Cells: Genome Editing Approaches for the Treatment of Cystic Fibrosis. *Hum Gene Ther* 31, 956 (2020).
13. Kotton, D. N. & Morrissey, E. E. Lung regeneration: mechanisms, applications and emerging stem cell populations. *Nature Medicine* 2014 20:8 20, 822–832 (2014).
14. Schmidt, H. *et al.* Serially passaged, conditionally reprogrammed nasal epithelial cells as a model to study epithelial functions and SARS-CoV-2 infection. *Am J Physiol Cell Physiol* 322, C591–C604 (2022).
15. Bodnar, A. G. *et al.* Extension of life-span by introduction of telomerase into normal human cells. *Science* 279, 349–352 (1998).
16. Balázs, A. *et al.* Age-Related Differences in Structure and Function of Nasal Epithelial Cultures From Healthy Children and Elderly People. *Front Immunol* 13, 822437 (2022).
17. Gras, D. *et al.* Epithelial ciliated beating cells essential for ex vivo ALI culture growth. *BMC Pulm Med* 17, 80 (2017).
18. Ramalho, A. S. *et al.* Assays of CFTR Function In Vitro, Ex Vivo and In Vivo. *Int J Mol Sci* 23, (2022).
19. Pranke, I. M. *et al.* Correction of CFTR function in nasal epithelial cells from cystic fibrosis patients predicts improvement of respiratory function by CFTR modulators. *Sci Rep* 7, 7375 (2017).
20. Brewington, J. J. *et al.* Brushed nasal epithelial cells are a surrogate for bronchial epithelial CFTR studies. *JCI Insight* 3, e99385 (2018).
21. Zomer-van Ommen, D. D. *et al.* Comparison of ex vivo and in vitro intestinal cystic fibrosis models to measure CFTR-dependent ion channel activity. *J Cyst Fibros* 17, 316–324 (2018).

22. Dekkers, J. F. *et al.* A functional CFTR assay using primary cystic fibrosis intestinal organoids. *Nat Med* 19, 939–945 (2013).
23. Berkers, G. *et al.* Rectal Organoids Enable Personalized Treatment of Cystic Fibrosis. *Cell Rep* 26, 1701–1708.e3 (2019).
24. Danahay, H. L. *et al.* TMEM16A Potentiation: A Novel Therapeutic Approach for the Treatment of Cystic Fibrosis. *Am J Respir Crit Care Med* 201, 946–954 (2020).
25. Danahay, H. *et al.* Potentiating TMEM16A does not stimulate airway mucus secretion or bronchial and pulmonary arterial smooth muscle contraction. *FASEB Bioadv* 2, 464 (2020).
26. A First in Human Study to Evaluate the Safety, Tolerability and Pharmacokinetics of Single and Multiple Ascending Doses of Inhaled ETD002 in Healthy Subjects - Full Text View - ClinicalTrials.gov. <https://clinicaltrials.gov/ct2/show/NCT04488705?term=etd002&draw=2&rank=1>.
27. Mall, M. A. ENaC inhibition in cystic fibrosis: potential role in the new era of CFTR modulator therapies. *European Respiratory Journal* 56, 2000946 (2020).
28. Pinto, M. C., Silva, I. A. L., Figueira, M. F., Amaral, M. D. & Lopes-Pacheco, M. Pharmacological Modulation of Ion Channels for the Treatment of Cystic Fibrosis. *J Exp Pharmacol* 13, 693–723 (2021).
29. Berical, A. *et al.* A multimodal iPSC platform for cystic fibrosis drug testing. *Nat Commun* 13, 4270 (2022).
30. Anderson, J. D., Liu, Z., Odom, L. V., Kersh, L. & Guimbellot, J. S. CFTR function and clinical response to modulators parallel nasal epithelial organoid swelling. *Am J Physiol Lung Cell Mol Physiol* 321, L119–L129 (2021).
31. Pranke, I. *et al.* Might Brushed Nasal Cells Be a Surrogate for CFTR Modulator Clinical Response? *Am J Respir Crit Care Med* 199, 123–126 (2019).
32. Debley, J. S. *et al.* Correlation between ivacaftor-induced CFTR activation in airway epithelial cells and improved lung function: A proof-of-concept study. *Ann Am Thorac Soc* 17, 1024–1027 (2020).
33. Muilwijk, D. *et al.* Forskolin-induced organoid swelling is associated with long-term cystic fibrosis disease progression. *Eur Respir J* 60, 2100508 (2022).
34. Hirst, R. A., Rutman, A., Williams, G. & O'Callaghan, C. Ciliated air-liquid cultures as an aid to diagnostic testing of primary ciliary dyskinesia. *Chest* 138, 1441–1447 (2010).
35. Marthin, J. K., Stevens, E. M., Larsen, L. A., Christensen, S. T. & Nielsen, K. G. Patient-specific three-dimensional explant spheroids derived from human nasal airway epithelium: a simple methodological approach for ex vivo studies of primary ciliary dyskinesia. *Cilia* 6, 3 (2017).
36. Khan, D. A. Allergic rhinitis and asthma: Epidemiology and common pathophysiology. *Allergy Asthma Proc* 35, 357–361 (2014).
37. Compalati, E. *et al.* The link between allergic rhinitis and asthma: the united airways disease. *Expert Rev Clin Immunol* 6, 413–423 (2010).
38. Poole, A. *et al.* Dissecting childhood asthma with nasal transcriptomics distinguishes subphenotypes of disease. *J Allergy Clin Immunol* 133, 670–8.e12 (2014).
39. Kicic, A. *et al.* Assessing the unified airway hypothesis in children via transcriptional profiling of the airway epithelium. *J Allergy Clin Immunol* 145, 1562–1573 (2020).
40. Thavagnanam, S. *et al.* Nasal epithelial cells can act as a physiological surrogate for paediatric asthma studies. *PLoS One* 9, e85802 (2014).
41. McDougall, C. M. *et al.* Nasal epithelial cells as surrogates for bronchial epithelial cells in airway inflammation studies. *Am J Respir Cell Mol Biol* 39, 560–568 (2008).
42. Pringle, E. J. *et al.* Nasal and bronchial airway epithelial cell mediator release in children. *Pediatr Pulmonol* 47, 1215–1225 (2012).
43. Lopez-Souza, N. *et al.* In vitro susceptibility to rhinovirus infection is greater for bronchial than for nasal airway epithelial cells in human subjects. *J Allergy Clin Immunol* 123, 1384–90.e2 (2009).

44. Yang, J. *et al.* Smoking-Dependent Distal-to-Proximal Repatterning of the Adult Human Small Airway Epithelium. *Am J Respir Crit Care Med* 196, 340–352 (2017).
45. Puchelle, E., Zahm, J.-M., Tournier, J.-M. & Coraux, C. Airway epithelial repair, regeneration, and remodeling after injury in chronic obstructive pulmonary disease. *Proc Am Thorac Soc* 3, 726–733 (2006).
46. Shaykhiev, R. & Crystal, R. G. Early events in the pathogenesis of chronic obstructive pulmonary disease. Smoking-induced reprogramming of airway epithelial basal progenitor cells. *Ann Am Thorac Soc* 11 Suppl 5, S252–8 (2014).
47. Sridhar, S. *et al.* Smoking-induced gene expression changes in the bronchial airway are reflected in nasal and buccal epithelium. *BMC Genomics* 9, 259 (2008).
48. Zhang, X. *et al.* Similarities and differences between smoking-related gene expression in nasal and bronchial epithelium. *Physiol Genomics* 41, 1–8 (2010).
49. Boudewijn, I. M. *et al.* Nasal gene expression differentiates COPD from controls and overlaps bronchial gene expression. *Respir Res* 18, 213 (2017).
50. MacRedmond, R. E., Greene, C. M., Dorscheid, D. R., McElvaney, N. G. & O'Neill, S. J. Epithelial expression of TLR4 is modulated in COPD and by steroids, salmeterol and cigarette smoke. *Respir Res* 8, 84 (2007).
51. Comer, D. M., Elborn, J. S. & Ennis, M. Comparison of nasal and bronchial epithelial cells obtained from patients with COPD. *PLoS One* 7, e32924 (2012).
52. Besteman, S. B. *et al.* Recurrent Respiratory Syncytial Virus Infection in a CD14-Deficient Patient. *J Infect Dis* 226, 258–269 (2022).
53. Hou, Y. J. *et al.* SARS-CoV-2 Reverse Genetics Reveals a Variable Infection Gradient in the Respiratory Tract. *Cell* 182, 429–446.e14 (2020).
54. Pizzorno, A. *et al.* Characterization and Treatment of SARS-CoV-2 in Nasal and Bronchial Human Airway Epithelia. *Cell Rep Med* 1, 100059 (2020).
55. Forero, A. *et al.* Evaluation of the innate immune responses to influenza and live-attenuated influenza vaccine infection in primary differentiated human nasal epithelial cells. *Vaccine* 35, 6112–6121 (2017).
56. Tan, K. Sen *et al.* Comparative Transcriptomic and Metagenomic Analyses of Influenza Virus-Infected Nasal Epithelial Cells From Multiple Individuals Reveal Specific Nasal-Initiated Signatures. *Front Microbiol* 9, 2685 (2018).
57. Bardet, G. *et al.* A model of human nasal epithelial cells adapted for direct and repeated exposure to airborne pollutants. *Toxicol Lett* 229, 144–149 (2014).
58. Drizik, E. *et al.* Transcriptomic changes in the nasal epithelium associated with diesel engine exhaust exposure. *Environ Int* 137, 105506 (2020).
59. Mou, H., Brazauskas, K. & Rajagopal, J. Personalized medicine for cystic fibrosis: Establishing human model systems. *Pediatr Pulmonol* 50, S14–S23 (2015).



Nederlandse samenvatting

INTRODUCTIE

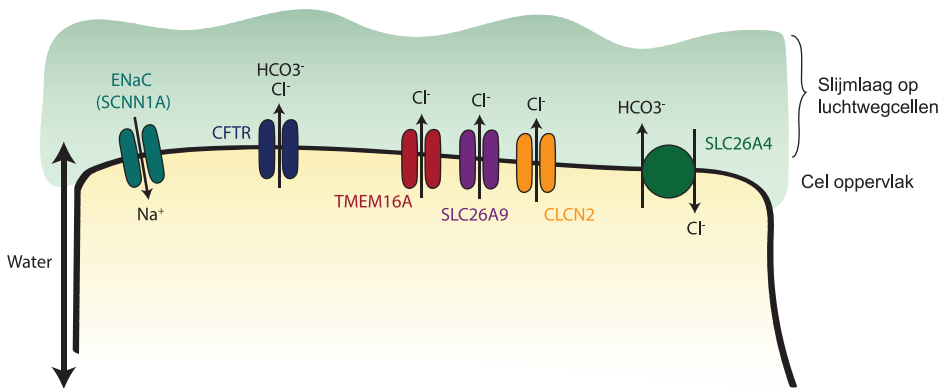
Taaismijziekte of cystic fibrosis (CF) is een aangeboren aandoening waarbij het eiwit cystic fibrosis transmembrane conductance regulator (CFTR) niet goed werkt. CFTR is een zoutkanaal dat chloor de cellen uit transporteert. Vanwege osmose wordt dit zouttransport gevolgd door water en ontstaat er een dunne soepele slijmlaag op de cellen. Bij taaismijziekte werkt het zoutkanaal CFTR niet goed. Hierdoor is er geen zout- en watertransport de cellen uit, waardoor er dik en taai slijm ontstaat. Dit geeft met name problemen in de longen. Vastzittend dik slijm kan hier zorgen voor benauwdheid en hoestbuien. Daarnaast kunnen bacteriën vast gaan zitten in dit dikke slijm en zo infecties veroorzaken. Deze kunnen zo ernstig verlopen dat patiënten moeten worden opgenomen in het ziekenhuis of hier zelfs vroegtijdig aan overlijden. CFTR heeft niet alleen een belangrijke rol in de longen, maar ook in andere organen zoals de darmen, alvleesklier, lever en geslachtsorganen. Symptomen waar mensen met CF daarom ook last van kunnen hebben zijn darmproblemen, slechte voedselvertering, vermoeidheid, groeiachterstand, diabetes, leverziekte en verminderde vruchtbaarheid. De gemiddelde levensverwachting van mensen met CF in Nederland is momenteel 50 jaar.

In Nederland worden per jaar 25-30 kinderen geboren met CF en in totaal leven er in Nederland ongeveer 1650 mensen met CF. De diagnose wordt meestal vlak na de geboorte gesteld via de hielprik screening. CF wordt veroorzaakt door een foutje in een specifiek stukje van het DNA, dat codeert voor het CFTR-eiwit. Deze foutjes in het DNA worden mutaties genoemd. Alleen als van beide ouders deze mutatie is geërfd, krijgt een kind CF. Er bestaan meer dan 2000 verschillende soorten mutaties in het DNA die CF kunnen veroorzaken. Het type mutatie bepaalt de ernst van de ziekte. Dit kan variëren van een CFTR eiwit dat minder zout doorlaat, tot helemaal geen aanmaak van het CFTR eiwit.

De levensverwachting voor mensen met CF is de laatste jaren enorm toegenomen. Dit komt door de ontwikkeling van medicijnen die specifiek het CFTR eiwit repareren. Dit worden CFTR-modulatoren genoemd. Voor 2012 was er alleen maar symptoombestrijding mogelijk. Ongeveer 80% van de mensen met CF komt in aanmerking voor deze CFTR-modulatoren. Dit is afhankelijk van het type mutatie in het DNA. De 20% die niet in aanmerking komen voor de CFTR-modulatoren hebben een mutatie die niet reageert op de medicijnen, of ze hebben een zeldzame mutatie waarvan onbekend is hoe die zal reageren op de medicijnen. Uit schattingen blijkt echter dat wereldwijd maar 12% van de mensen met CF CFTR-modulatoren krijgt. Dit heeft te maken met de zeer hoge prijs waardoor de CFTR-modulatoren in veel landen

niet worden vergoed. Er is dus een grote groep van mensen met CF voor wie momenteel geen goede therapie beschikbaar is.

Een alternatieve therapie voor deze groep kan zijn om andere zoutkanaaltjes in de cellen extra te stimuleren ter compensatie voor het mindere zouttransport via CFTR. Andere chloor kanaaltjes zijn bijvoorbeeld TMEM16A, SLC26A9, SLC26A4 en CLCN2 (figuur 1). Deze methode zou kunnen werken voor alle mensen met CF, ongeacht het type mutatie.



Figuur 1. De verschillende zoutkanalen in luchtwegcellen die in dit proefschrift besproken worden.

Cl⁻: chloride, HCO₃⁻: bicarbonaat, Na⁺: natrium.

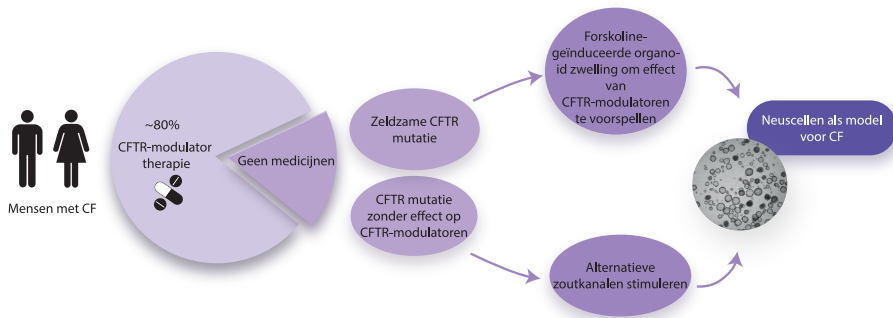
De effectiviteit van (nieuwe) medicijnen voor CF kan worden getest in het lab door water- en zouttransport na te bootsen in gekweekte cellen. Bij voorkeur zijn dit cellen afkomstig van mensen met CF. Dit wordt al gedaan op gekweekte mini-darmpjes van mensen met CF, een methode die in ons lab is ontwikkeld. Hierbij worden stamcellen uit een darmbiopt gekweekt als 3D bolletjes, ook wel organoïden of mini-darmpjes genoemd. Bij stimulatie van het CFTR eiwit stromen zout en water de organoïden in, wat zorgt voor zwelling. Stimulatie van CFTR gebeurt met de stof forskoline en daarom wordt deze methode forskoline-geïnduceerde zwelling (FIS) genoemd. Bij organoïden van mensen met CF is geen of minder zwelling te zien. Deze organoïden kunnen worden behandeld met CFTR-modulatoren om te kijken of deze de CFTR functie verbeteren en dus wel zwelling geven. De mate van organoïd zwelling wordt dus gebruikt als maat voor CFTR functie en voor het voorspellen van effectiviteit van CFTR-modulatoren. Dit kan toegepast worden om patiënt-specifiek te voorspellen of medicijnen werken, maar ook om op grote schaal nieuwe medicijnen te testen. Deze methode is gevalideerd met klinische data en wordt wereldwijd al toegepast. Echter, mensen met CF hebben de grootste problemen in de luchtwegen, en daarom zou een model met luchtwegcellen

beter geschikt kunnen zijn. Daarnaast komen de andere zoutkanalen weinig voor in darm organoïden, waardoor de alternatieve therapie om andere zoutkanalen te simuleren niet in darm organoïden bestudeerd kan worden.

Luchtwegcellen kunnen verkregen worden door een bronchiale brush of biopsie tijdens een bronchoscopie. Na het opkweken van de stamcellen moeten de cellen gedifferentieerd worden naar luchtweg-specifieke cellen. CFTR functie kan in deze cellen worden gemeten via elektrofysiologische metingen met de Ussing kamer. Hierbij wordt stroomverschil gemeten als maat voor zouttransport. Dit is wereldwijd de meest geaccepteerde methode voor CFTR functie metingen in gekweekte luchtwegcellen van mensen met CF. Nadelen van deze methode zijn de invasieve bronchoscopie om de cellen te verkrijgen, en de kleine schaal waarop de elektrofysiologische metingen worden uitgevoerd. De schaalbaarheid kan worden vergroot door de luchtwegcellen te kweken als organoïden, mini-longetjes. De protocollen voor luchtweg organoïden zijn echter nog niet zo goed en gevalideerd als voor de darm organoïden.

Als alternatief voor de invasieve methode om luchtwegcellen te verkrijgen, kunnen neuscellen worden gebruikt als model voor de luchtwegen. Neuscellen worden verkregen met een simpele neusbrush. Het is echter nog niet duidelijk of gekweekte neuscellen een goed model zijn voor de luchtwegen. De neus is onderdeel van de luchtwegen, en bezit in het DNA dus ook eventuele CFTR mutaties. Echter, tijdens de embryonale ontwikkeling stammen de neuscellen van een andere kiemlaag dan de rest van de luchtwegen. Daarnaast hebben de cellen in de bovenste luchtwegen een andere functie en samenstelling dan de cellen in de onderste luchtwegen.

Het doel van dit proefschrift is om de toepasbaarheid van neuscellen, specifiek neus organoïden, te onderzoeken als model voor CF (figuur 2). Enerzijds zullen ze gebruikt worden voor forskoline-geïnduceerde zwellings metingen in neus organoïden om patiënt-specifiek te voorspellen of CFTR-modulatoren effectief zullen zijn. Dit is nuttig voor patiënten met zeldzame CFTR mutaties waarvan niet bekend is hoe ze op medicijnen zullen reageren. Anderzijds zullen neus organoïden gebruikt worden om medicijnen te vinden die andere zoutkanaaltjes dan CFTR activeren. Op deze manier hopen we medicijnen te vinden voor alle mensen met CF, ongeacht het type mutatie.

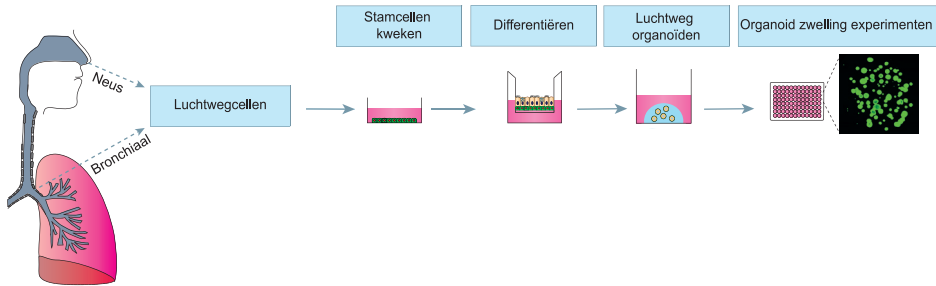


Figuur 2. Het nut van neuscellen als model voor CF.

Enerzijds kunnen neuscellen gebruikt worden om te voorspellen of CFTR-modulatoren effectief zullen zijn bij mensen met een zeldzame CFTR mutatie. Anderzijds kunnen neuscellen gebruikt worden om medicijnen te vinden die alternatieve zoutkanalen stimuleren voor mensen die geen baat hebben bij CFTR-modulatoren.

HOOFDSTUK 1: NIEUWE PROTOCOLLEN VOOR HET KWEKEN VAN NEUSCELLEN

Hoofdstuk 1 beschrijft nieuwe protocollen om neuscellen te verzamelen, te kweken, organoïden van te maken en CFTR functie metingen mee uit te voeren (figuur 3). We hebben nieuwe methodes ontwikkeld waardoor de luchtweg stamcellen beter en sneller groeien. Hierdoor kunnen we neuscellen invriezen in een biobank om bij toekomstig onderzoek te gebruiken. Na het opkweken van de stamcellen, worden deze aan de bovenkant aan lucht blootgesteld zodat ze zich differentiëren naar luchtweg-specifieke celtypes. Deze cellaag wordt vervolgens in stukjes in een 3D matrix geplaatst zodat ze zich vormen tot 3D organoïden. Deze neus organoïden kunnen worden gebruikt voor CFTR functie metingen. Hierbij wordt het CFTR kanaal gestimuleerd met de stof forskoline waardoor zout en vervolgens water de organoïden in stroomt. Dit zorgt voor zwelling van de organoïden. Organoïden van mensen met CF kunnen worden behandeld met CFTR-modulatoren om de effectiviteit van deze medicijnen patient-specifiek te voorspellen.



Figuur 3. Het kweekproces van luchtwegcellen.

Luchtwegcellen worden verkregen met een neusbrush of bronchoscopie. Vervolgens worden de stamcellen gekweekt en gedifferentieerd tot verschillende celtypes. Deze cellen worden gebruikt om organoïden van te maken en organoid zwellings experimenten mee uit te voeren.

HOOFDSTUK 2: CFTR FUNCTIE METINGEN IN NEUS ORGANOÏDEN

In hoofdstuk 2 beschrijven we de optimalisatie van het protocol om CFTR functie metingen in neus organoïden uit te voeren. We zagen namelijk dat de forskoline-geïnduceerde zwelling van neus organoïden niet volledig afhankelijk was van CFTR, maar ook van andere zoutkanalen. Hierdoor was het nog niet mogelijk om het effect van CFTR-modulatoren nauwkeurig te bepalen. We hebben het kweekmedium verbeterd om de expressie van CFTR te verhogen, en de zwelling grotendeels afhankelijk van CFTR te maken. Om dit te bewijzen maakten we organoïden van gezonde controles zonder werkend CFTR (een CFTR knockout). In deze CFTR knockouts was geen forskoline-geïnduceerde zwelling meer aanwezig, wat dus bewijst dat deze zwelling CFTR-afhankelijk was. Ook testten we de effectiviteit van CFTR-modulatoren op CF organoïden van personen met verschillende mutaties. Afhankelijk van de mutatie zagen we al dan niet een toename in organoïd zwelling, wat betekent dat personen met verschillende mutaties anders reageren op de CFTR modulatoren.

HOOFDSTUK 3: ALTERNATIEVE ZOUTKANALEN ACTIVEREN IN NEUS ORGANOÏDEN

Hoofdstuk 3 focust op een alternatieve aanpak voor herstel van de water- en zoutbalans bij mensen met CF, door activatie van andere zoutkanalen dan CFTR. Neus organoïden zijn een goed model om deze alternatieve zoutkanalen te onderzoeken, aangezien we zwelling zagen in organoïden van mensen met een ernstige vorm van CF, zonder

enige CFTR functie. Deze zwelling moet dus veroorzaakt zijn door andere zoutkanalen dan CFTR. Het doel in dit hoofdstuk was om een medicijn te vinden dat één van deze alternatieve zoutkanalen stimuleert. De focus was op medicijnen die al op de markt zijn (FDA-approved) voor andere ziektebeelden, aangezien deze snel en veilig naar de patiënt gebracht zouden kunnen worden. Er werden 1400 medicijnen op grote schaal getest, in 384-well platen. Van deze screen werden 12 medicijnen geselecteerd die zwelling in de neus organoïden veroorzaakten, onafhankelijk van CFTR. De selectie medicijnen bevatte voornamelijk α - en β -agonisten. β -agonisten, zoals salbutamol, zijn met name bekend als luchtwegverwijder voor astma of COPD therapie. Eerder onderzoek onderzocht al deze middelen bij mensen met CF, maar hierbij ontstonden helaas bijwerkingen voordat een effectieve dosering was bereikt.

Om te onderzoeken via welk zoutkanaal de geselecteerde medicijnen werken, knipten we in het DNA van CF organoïden zodat het zoutkanaal TMEM16A niet meer werkzaam was (TMEM16A knockout). TMEM16A is namelijk het meest onderzochte alternatieve chloor kanaal in de luchtwegen. In deze organoïden zonder TMEM16A werd de selectie medicijnen opnieuw getest, maar we zagen nog steeds organoïd zwelling. Zo concludeerden we dat TMEM16A dus niet betrokken was bij de CFTR-onafhankelijke organoïd zwelling. Samenvattend, in dit hoofdstuk ontdekten we medicijnen die CFTR-onafhankelijk vloeistof transport stimuleren in neus organoïden van mensen met CF, maar het blijft onbekend via welk zoutkanaal.

HOOFDSTUK 4: WELK ZOUTKANAAL ZORGT VOOR ZWELLING IN NEUS ORGANOÏDEN?

Het doel van hoofdstuk 4 was om uit te vinden welk zoutkanaal verantwoordelijk is voor het vloeistof transport in neus organoïden. De focus was zowel op voorzwelling van de organoïden, als na stimulatie met de medicijnen die in het vorige hoofdstuk zijn ontdekt. We knipten in het DNA van CF organoïden met CRISPR/Cas9 zodat een specifiek zoutkanaal niet meer werkzaam zou zijn, dit heet een knockout. We deden dit voor de zoutkanalen TMEM16A, SLC26A9, SLC26A4, CLCN2 en SCNN1A (figuur 1) en onderzochten of de medicijnen nog steeds organoïd zwelling gaven in deze knockouts. Bij alle varianten was dit het geval. We zagen nog steeds voorzwelling van de organoïden, en zwelling na stimulatie met de medicijnen.

Omdat we geen verschillen zagen in de knockouts, herhaalden we de experimenten in een situatie die ontsteking nabootst. Uit literatuur is het namelijk bekend dat behandeling van de celkweken met het ontstekingsiwit IL-4 de expressie van een aantal

zoutkanalen verhoogt. We zagen inderdaad dat behandeling met IL-4 de expressie van de zoutkanalen TMEM16A, SLC26A9 en SLC26A4 verhoogde. In deze omstandigheden met ontsteking herhaalden we de screen met 1400 bestaande medicijnen om medicijnen te ontdekken die zwelling geven van neus organoïden. We vonden deels dezelfde α - en β -agonisten als in de screen zonder IL-4 behandeling uit het vorige hoofdstuk. Helaas ontdekten we geen nieuwe medicijnen. Vervolgens onderzochten we de zwelling in de verschillende knockouts behandeld met IL-4. We zagen dat de voorzwelling die we normaal in neus organoïden zien, we noemen dit het basale vloeistof transport, verdwijnt met IL-4 behandeling. Opmerkelijk genoeg zagen we dit niet in de SLC26A4 knockout organoïden. Dit suggereert dat het zoutkanaal SLC26A4 betrokken is bij het basale vloeistof transport in neus organoïden in omstandigheden met ontsteking. Na stimulatie met de medicijnen uit het vorige hoofdstuk zagen we in alle knockout organoïden nog steeds zwelling. Samenvattend, we ontdekten dat het zoutkanaal SLC26A4 betrokken is bij de basale vloeistofsecretie in neus organoïden behandeld met IL-4, maar weten nog steeds niet via welk zoutkanaal de gevonden medicijnen vloeistoftransport stimuleren in de neus organoïden van mensen met CF.

HOOFDSTUK 5: HOE VERSCHILLEN NEUS EN BRONCHIALE CELLEN VAN ELKAAR?

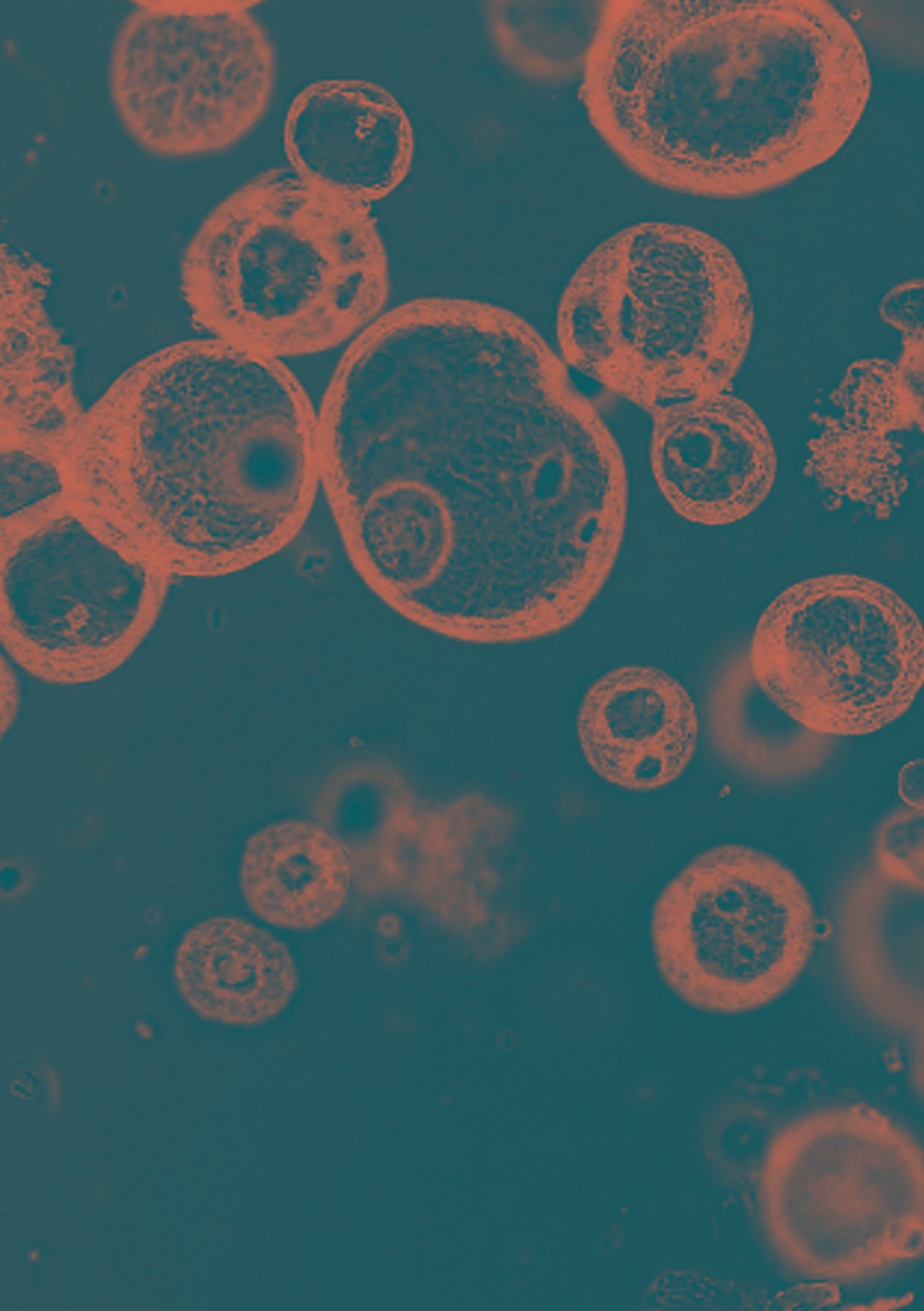
Na de verschillende toepassingen van neus organoïden bestudeerd te hebben, wilden we weten hoe representatief de neuscellen eigenlijk zijn voor de onderste luchtwegen (de bronchiën), waar de meeste symptomen bij mensen met CF voorkomen. We weten dat tijdens de embryonale ontwikkeling neuscellen van een andere kiemlaag ontstaan (ectoderm) dan de bronchiale cellen (endoderm). Daarnaast zijn neuscellen gespecialiseerd in het afweren van bacteriën, terwijl bronchiale cellen gespecialiseerd zijn in het geleiden van lucht. In hoofdstuk 5 vergeleken we daarom gekweekte neus en bronchiale cellen met elkaar, afkomstig van dezelfde CF donoren (figuur 3). Na het opkweken van stamcellen uit neus- en bronchiale brushes, zagen we dat de stamcellen differentieerden naar verschillende celtypes. De neuskweken bevatten meer mucusproducerende cellen en de bronchiale kweken meer gecilieerde cellen. Deze kweken werden vervolgens gebruikt om organoïden van te maken. Zoals gezien in de vorige hoofdstukken waren de neus organoïden voorgezwollen door CFTR-onafhankelijk basaal vloeistoftransport. De bronchiale organoïden hadden deze voorzwelling niet. Naast de voorzwelling, zwelden de CF neus organoïden verder na stimulatie met forskoline, iets wat we niet zagen in de bronchiale CF organoïden. Voorbehandeling met CFTR-modulatoren gaf wel forskoline-geïnduceerde zwelling in de bronchiale organoïden, terwijl neus organoïden niet reageerden op deze medicijnen. Deze

verschillen in vloeistof transport tussen neus en bronchiale CF organoïden tonen dus aan dat in de neus organoïden meer alternatieve zoutkanalen actief zijn die CFTR-onafhankelijk vloeistof transport stimuleren.

Vervolgens onderzochten we of het verschil in vloeistoftransport veroorzaakt werd door de verschillende samenstelling van celtypes tussen neus en bronchiale cellen. We behandelden de neuscellen zodanig dat er meer gecilieerde cellen ontstonden, net als in de bronchiale cellen. We zagen dat hierdoor de voorzwelling in neus organoïden verdween, en dat het basale vloeistof transport dus afhankelijk is van de aanwezige celtypes. Echter, na stimulatie met forskoline zagen we dat er nog steeds CFTR-onafhankelijke organoid zwelling aanwezig was in de neus organoïden. Dit suggereert dus dat basale vloeistofsecretie afhankelijk is van de aanwezig celtypes, terwijl de forskoline-geïnduceerde zwelling via een ander mechanisme werkt. Samenvattend, in dit hoofdstuk zagen we verschillen tussen neus en bronchiale cellen in het soort celtypes, en in basaal en forskoline-geïnduceerd vloeistof transport. CFTR-onafhankelijk vloeistoftransport is meer aanwezig in neus organoïden, in vergelijking met bronchiale organoïden.

CONCLUSIE

In dit proefschrift verbeterden we de kweekprotocollen om neuscellen en neus organoïden, afkomstig van een simpele neusbrush, te gebruiken als model voor CF. We optimaliseerden de protocollen voor forskoline-geïnduceerde zwellings metingen om patiënt-specifiek te voorspellen of CFTR-modulators effectief zullen zijn. Daarnaast gebruikten we de neus organoïden om medicijnen te vinden die andere zoutkanalen dan CFTR activeren. Dit zou als alternatieve therapie kunnen werken om het zout- en watertransport te herstellen, onafhankelijk van het type mutatie. We selecteerden medicijnen die organoid zwelling gaven, maar het is nog onduidelijk via welke zoutkanalen deze medicijnen werken. Toekomstig onderzoek moet zich vooral richten op het verder ontwikkelen van kweekprotocollen van neuscellen en de klinische validatie van de beschreven toepassingen. Naast CF kunnen de protocollen voor het kweken van neuscellen ook gebruikt worden voor het bestuderen van andere luchtwegaandoeningen.



Acknowledgements – Dankwoord

ACKNOWLEDGEMENTS – DANKWOORD

Jeffrey (Jeff), het begon met dat ik heel graag stage wilde lopen in jouw labgroep. Na 2 onbeantwoorde e-mails wist ik via Myriam een kennismaking met jou te regelen. Hoe lastig het was om contact te krijgen, zo makkelijk was het om daarna te blijven gezien jouw enthousiasme tijdens ons kennismakingsgesprek. Na wetenschapsstage volgde een PhD-traject, want je enthousiasme werkt aanstekelijk. Tijdens mijn PhD was je was een heel relaxte begeleider, die me voornamelijk bijstond tijdens de UK Trust meetings. Als ik ergens mee zat, dan was je er echt voor me. Dank voor alle kansen die je me geboden hebt. Ik bewonder hoe jij op jonge leeftijd professor bent geworden, grote beurzen binnensleept, en zo'n uitgebreid netwerk hebt. Ook naast werk hebben we mooie herinneringen: het hand-in-hand synchroon schaatsen tijdens de schaatstraining voor de Weissensee en de eindeloze hoeveelheid rondjes op de ijsbaan in de weekenden. Daarnaast ook de villa met privé zwembad tijdens congres in Barcelona, en natuurlijk de bbq in je tuin in Maarn.

Kors, van de achtergrond heb je mijn promotietraject begeleid en mogelijk gemaakt. Ik bewonder de infrastructuur die jullie hebben opgezet waar het lab en de kliniek samenwerken om patiënten te helpen. Jouw terugkerende vraag bij lab-praatjes 'hoe kunnen we de patiënt hiermee helpen' heeft mij geïnspireerd om translationeel te blijven denken. De mogelijkheden die jij zoekt en creëert om patiënten te helpen via onderzoeksbevindingen inspireert mij om later dokter en onderzoek te kunnen combineren.

Gimano, jij staat aan de basis van dit proefschrift. Het begon tijdens mijn wetenschapsstage waar je me leerde hoe een pipet werkt en hoe ik steriel moest werken. Ik heb de nieuwsgierigheid van je overgenomen om op maandag ochtend als eerste, nog voor een kop koffie, onder de microscoop te kijken hoe het met de cellen gaat. Na mijn stage mocht ik blijven als jouw eerste PhD-student en werd ik onderdeel van het luchtweg team. Inmiddels heb je een heel luchtweg model opgezet wat ingezet wordt voor verschillende ziektebeelden en zelfs de basis is voor een eigen bedrijf. Ik bewonder je eindeloze stroom aan nieuwe ideeën en experimenten. Je baalde niet van een mislukt experiment of negatief resultaat, maar wist dit om te zetten in nieuwe inzichten of experimenten. Ooit hoop ik ook zoveel inspiratie te hebben. Heel veel dank voor je begeleiding, alles wat je me geleerd hebt en de kansen die je me geboden hebt.

Myriam en Wilma, niet alleen hielpen jullie me uit de brand met het inplannen van afspraken in de drukke agenda's van mijn begeleiders, ook was het altijd gezellig om even bij te kletsen. Ook dank voor de organisatie van de altijd geslaagde kerstontbijten en familiedagen.

Beekman lab team, wat waren jullie leuke collega's en wat mis ik de gezelligheid in Beekman-office (aka "flexwerkplek"). Mooie herinneringen aan de congressen, zoals de yoga ochtend sessie op het strand in Albufeira, en mijn referentie wat betreft hotels is verpest sinds we in het luxe resort in Dubrovnik hebben geslapen. **Juliet**, sportieve buddy vanaf het begin, en mijn vaste ideale kamergenoot op congressen (als de airco het maar doet) en de Weissensee. **Hetty**, samen gestart in het airway team, met de WKZ auto toeren om PCD-neusbrushes te verzamelen (van Scheveningen tot Den Helder) en op avontuur naar Toronto waar jij heel stoer kampeerde met 0 graden. **Sacha**, ik waardeer jouw positiviteit en initiatiefrijkheid. Dank voor alle blauwe plekken en blaren die ik overhield aan de survivalrun en de clinics 😊. **Suzanne**, ik bewonder hoe jij je PhD startte rondom de geboorte van Owen. **Nefeli**, super cool you are a PhD student yourself now. When will we eat APPLE pie together? **Bente**, mooi om te zien hoe jij de brug vormde tussen het lab en de volwassenen CF zorg. En respect voor het geduld dat jij met de Ussing kamer hebt. **Lieve PhD-maatjes**, succes met de afronding van jullie PhD's en ik ben heel benieuwd waar jullie carrière naar toe gaat!

Het sterke **lab tech team Isabelle, Shannon, Loes, Heleen, Natascha, Roos-Anne**: zonder jullie geen medium, geen stockjes, chaos in de stikstof, en geen gezelligheid. Tijdens het schrijven miste ik het lekker kletsen in de celkweek. Bedankt dat ik op mijn laatste dag nog mocht helpen met het uitvullen van stockjes, een waardig afscheid 😊. **Shannon**, dank voor je hulp bij alle zwellings experimenten met oneindig veel verschillende compounds. Ook al hadden de organoids er niet altijd zin in, we hebben het project weten af te ronden! En dank voor de pottery avonden waar ik heb ontdekt dat creativiteit best leuk is. **Isabelle**, dank voor je hulp bij het STAR protocols paper, ik vond het heel motiverend om dit samen aan te pakken. **Loes**, je was een heel fijne en gezellig collega die altijd klaar stond om te helpen en je hebt onwijs veel voor ons geregeld: dank! **Heleen**, super werk heb jij verricht met het opzetten van de mooie Castor database en ik ben onder de indruk hoe snel jij je weg en netwerk hebt gevonden als biobank manager. **Natascha**, ik bewonder hoe jij je analisten baan combineert met je passie en talent voor taarten bakken via je eigen bedrijf.

Sam, heel fijn om met jou te kunnen sparren over R, programmeren en data-management. Ik heb veel van je geleerd en ben onder de indruk van 'jouw' robolab. **Bahar**, ik waardeer onze gesprekken in de celkweek die binnen no time gingen over toekomstplanning en carrière keuzes. Je hebt me van wat waardige adviezen voorzien. **Martijn**, de verbinder tussen 2 groepen en die opvallend vaak heerlijke zelfgemaakte taarten trakteerde. En stiekem ben ik jaloers op je dieren en moestuin thuis.

Dear **SRC members from Newcastle, Lisbon and Regensburg**, thank you for the fruitful collaboration. I learned a lot from our monthly discussions and working with different techniques on the same research topic. I thank CF Trust, UK for creating this opportunity.

Studenten **Casper, Dounia en Elyse**, dank voor jullie hulp en enthousiasme met mijn experimenten in het lab. Ik vond het erg leuk om met jullie samen te werken en ben benieuwd hoe jullie carrières gaan lopen.

Oud-collega's **Eyleen (makreel 😊), Evelien, Sylvia, Jesse, Annelotte**, jullie hebben me wegwijs gemaakt in de Beekman groep en het lableven, dank hiervoor!

Maaïke, iets om naar uit te kijken waren onze koffiedates bij GenMab om lekker bij te kletsen. Fijn dat jij elke barista kende en wist wie de lekkerste koffie zet. Laten we vooral koffie blijven drinken!

Marlou, Danya, Sabine vd L, Gizem met jullie heb ik vooral samengewerkt voor het Kafrio-cohort. Voor mij een kans om weer patiënten contact te hebben naast alle uren in de celkweek en waardoor ik nu weer in de kliniek ben gaan werken. Credits voor Marlou en Danya voor al het logistieke regelwerk. Ook waardeerde ik de schrijfdagen (schrijfclubje) op de flexwerk plekken met heerlijke koffie pauzes en het uitwisselen van allerlei PhD zaken.

Afdeling KLZ, mooi en uniek hoe de samenwerking tussen lab en kliniek hier staat als een huis. Ieder jaar een heerlijk kerstontbijt en team uitje, wat een fijne afdeling. Dank voor al jullie hulp en gezelligheid.

Mariska, beiden gingen we heel jong op kamers in Utrecht om in de hordengroep van Henk te trainen. Op ons 16^e al mee op trainingskamp naar Monte Gordo en later Mallorca waar we vele mooie herinneringen hebben gemaakt. Super leuk om nog steeds samen te trainen en weer op <10 min fietsafstand te wonen. Heel leuk dat je als paranimf mijn sportieve hobby wilt representeren 😊

Jill, ik ben blij dat ik iemand ken die net zo enthousiast wordt van geocaching als ik. Nog zoveel avonturen om samen aan te gaan: Lunetten hebben we al uitgespeeld, nu nog alle gemeentes van NL (na ons pensioen..?) en oriëntatielopen.

SUMMA-vriendinnetjes Emma, Iris en Ilja, het contact begon op de eerste dag van SUMMA tijdens het etentje in Humphreys en resulteerde in samenwonen in Appie

de gekste, weekendjes weg in Leersum, Middelburg en Leuven en onze traditionele kerstdiners. Ook al zijn jullie meer van de chirurgische kant en komen er af en toe vieze operatie verhalen voorbij, fijn om met jullie te kunnen sparren over mijn artsen carrière. Ik bewonder jullie passie als dokter en hoop dat er nog vele bourgondische etentjes zullen volgen tussen de diensten door.

Lotte, trouwe vriendin sinds de bachelor, van koffietjes in het Hubrecht naar etentjes bij elkaar thuis. Wie weet komen we elkaar in de toekomst wel weer tegen op de werkvloer...

Loes, waar ik dacht dat CRISPR/Cas best een ingewikkelde techniek is, blijkt dat jij dit gewoon in de biologie les al leert aan middelbare scholieren. Super leuk dat we zo regelmatig bij kletsen.

Phoenix-atletiek maatjes bij de sprint- en krachtttrainings groep, jullie zorgden voor de ontspanning en afleiding na dagen in het lab of het schrijven van dit proefschrift. Zo fijn om 's avonds in zo'n vertrouwde omgeving te komen, of het weekend te starten met de bostraining. Ik waardeerde jullie medeleven tijdens mijn Weissensee-trainingen, en ook fijn dat ik nu nog welkom ben als mila-sprinter. Ik heb mooie herinneringen aan alle wedstrijden, vooral de competitiedagen met het hele team. Met name dank voor de trainers **Bas, Egbert en Mariska** dat jullie al jarenlang vrijwillig klaar staan om de trainingen te verzorgen. De volgende klassiekers zal ik niet snel vergeten: de '6-minuten buik', 'alles halen uit je contributie', en uiteindelijk zelfs een naar mij vernoemde oefening: 'de Lisa'.

Surfboyz&girlz: James, Mirte, Ivo, Iris, Léon, Anish, Isabel. Ik begon als aanhang van een surfboy, maar ben inmiddels een surfgirl. Veel leuke herinneringen al gemaakt: op de camping in Limburg, de blokhut in Soest (gourmetten), elkaar helpen verhuizen, en mooie schilderijen als aandenken, nog steeds wachtend om opgehangen te worden. Op naar het maken van meer mooie herinneringen. Wanneer gaan we eigenlijk een keer surfen?

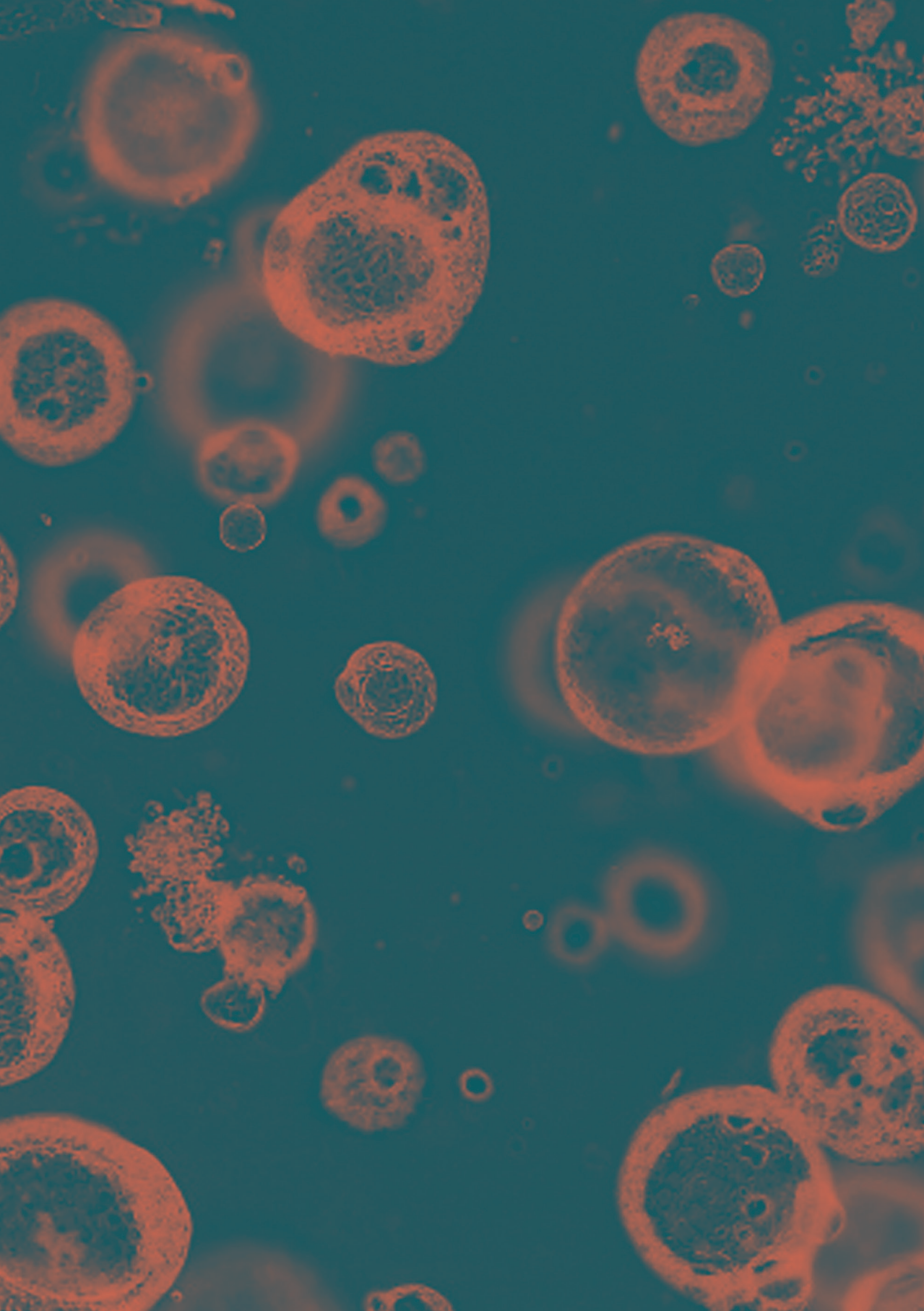
Lieve Gerard, Gentia, Niels en Anne Fleur. Fijn hoe jullie ons steunen en altijd voor ons klaar staan. Leuk dat jullie nieuwsgierig zijn naar de wondere wereld van DNA, en ook kritisch zijn op de grenzen van alle medische innovaties. Geniet van jullie pensioen met mooie caravan-vakanties en ritjes met de MG. Bedankt voor al jullie steun in het najagen van onze dromen. **Anne Fleur**, ik ben onder de indruk van je doorzettingsvermogen om fysiotherapeut te worden, naast de vele uren die je steekt in je bijbaantjes. **Niels**, ik bewonder je creatieve talent wat je gebruikt op je werk en in hobby-projecten, zoals onze afstudeer-cadeaus.

Lieve papa en mama, Wim en Trudy, bedankt voor het altijd er voor mij zijn. Bedankt voor alle kansen die jullie me geboden hebben, zoals de combinatie van school, sport en een muziekinstrument leren spelen. Dankzij jullie vind ik een gezonde leefstijl normaal. Ik kom nog altijd heel graag ‘thuis’ in huize Amersfoort. Fijn dat ik jullie altijd mag bellen als ik ergens mee zit, maar ook om successen mee te delen. Ik hoop dat jullie lekker samen van het pensioen genieten, een mooie moestuin opbouwen en nog vele mooie ritjes op de tandem zullen maken.

Lieve Jeroen, soms wist jij zulke lastige vragen over mijn PhD onderzoek te stellen dat ik zelf vastliep. Stiekem vind ik jouw huidige baan ook reuze interessant. Ik bewonder je nieuwsgierigheid, doorzettingsvermogen en ondernemendheid, onder andere met avontuurlijke reizen. Daarnaast leuk om samen spelletjes te doen en fijn dat je af en toe wilt helpen met het oplossen van een lastige geocache puzzel 😊.

Lieve Remco, Rutchanna, Liam en Elena. Altijd fijn om bij jullie op bezoek te gaan. Bij jullie heb ik koffie leren drinken, krijg ik altijd heerlijk eten, en heb ik geleerd dat kwaliteit best wat mag kosten. Leuk om jullie als gezin te zien ontwikkelen en af en toe lekker blokkentorens te kunnen bouwen of boekjes te lezen.

Lieve Jasper, mijn maatje waar ik zo trots op ben. Af en toe was je ook gewoon mijn PhD-collega, als we op werk even met elkaar belden via Teams om elkaar te helpen in R. Ik ben trots hoe we naast werk en het vele sporten quality time houden met de inmiddels beroemde datenight op woensdagavond. Ik ben onder de indruk hoe jij momenteel onderzoek combineert met het doktersleven. Bedankt dat je er altijd voor me bent en je onvoorwaardelijke steun. Ik kijk er naar uit om nog heel veel mooie herinneringen samen te maken. Lieve schat, ik ben heel erg gek op jou.



List of publications

LIST OF PUBLICATIONS

THIS THESIS

Rodenburg LW, van der Windt IS, Dreyer HHM, Smits SMA, den Hertog – Oosterhoff LA, Aarts EM, Beekman JM and Amatngalim GD. Protocol for generating airway organoids from 2D air-liquid interface differentiated nasal epithelia for use in a functional CFTR assay. *STAR protocols* **4**, 102337 (2023).

Amatngalim GD, **Rodenburg LW**, Aalbers BL, Raeven HH, Aarts EM, Sarhane D, Spelier S, Lefferts JW, Silva IA, Nijenhuis W, Vrendenburg S, Kruisselbrink E, Brunsveld JE, van Drunen CM, Michel S, de Winter-de Groot KM, Heijerman HG, Kapitein LC, Amaral MD, van der Ent CK, Beekman JM. Measuring cystic fibrosis drug responses in organoids derived from 2D differentiated nasal epithelia. *Life science alliance* **5**, e202101320 (2022).

Rodenburg LW, Delpiano L, Railean V, Centeio R, Pinto MC, Smits SMA, van der Windt IS, van Hugten CFJ, van Beuningen SFB, Rodenburg RNP, van der Ent CK, Amaral MD, Kunzelmann K, Gray MA, Beekman JM, Amatngalim GD. Drug Repurposing for Cystic Fibrosis: Identification of Drugs That Induce CFTR-Independent Fluid Secretion in Nasal Organoids. *Int J Mol Sci* **23**, 12657 (2022).

Rodenburg LW, Metzemaekers M, van der Windt IS, Smits SMA, den Hertog – Oosterhoff LA, Kruisselbrink E, Brunsveld JE, Michel S, Winter-de Groot KM, van der Ent CK, Stadhouders R, Beekman JM, Amatngalim GD. Exploring intrinsic variability between cultured nasal and bronchial epithelia in cystic fibrosis. *Sci Rep* **13**, 18573 (2023).

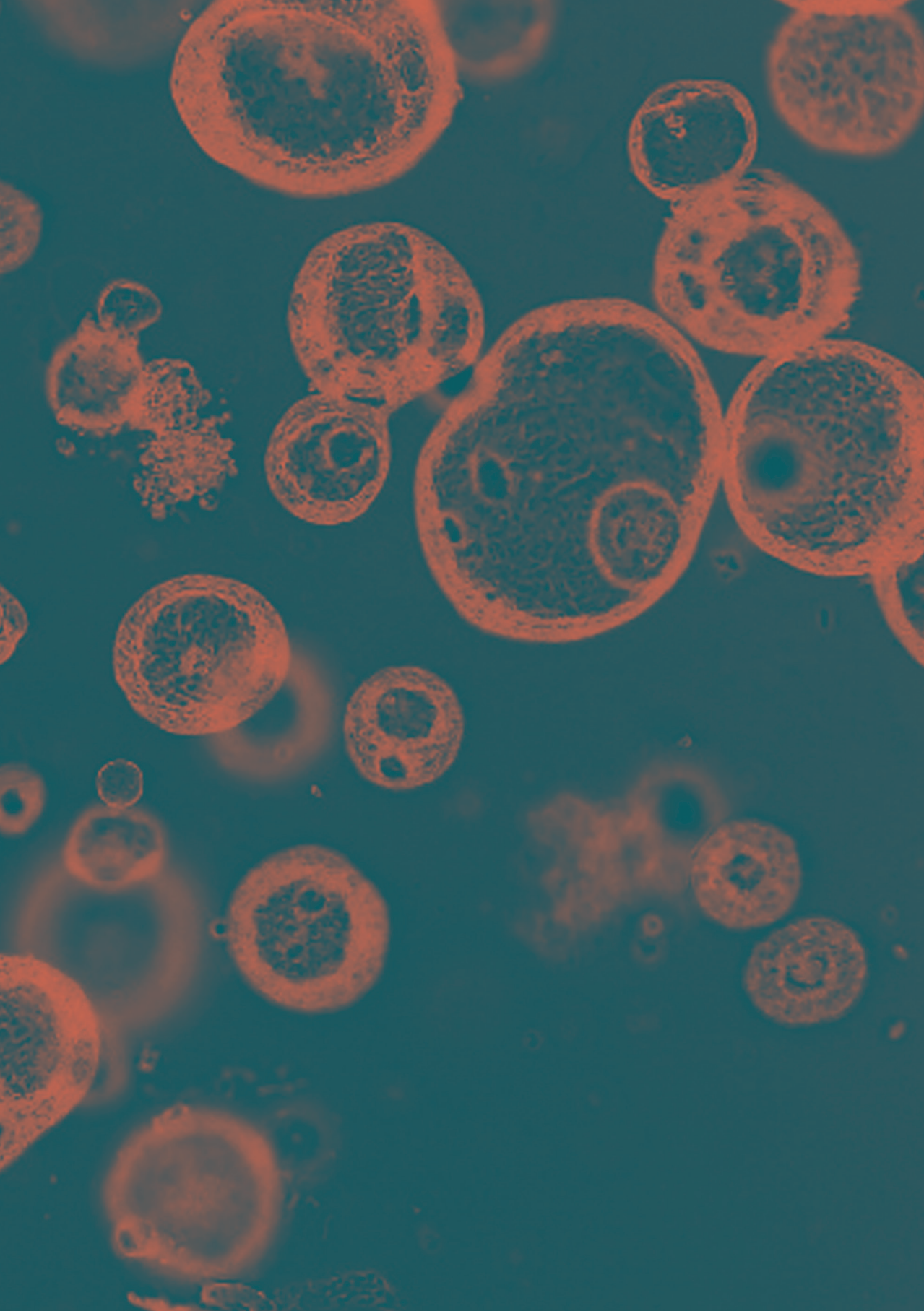
OTHER PUBLICATIONS

Delpiano L, **Rodenburg LW**, Burke M, Amatngalim GD, Beekman JM, Gray MA. Dynamic regulation of airway surface liquid pH by TMEM16A and SLC26A4 in cystic fibrosis nasal epithelia with rare mutations. *Proc Natl Acad Sci U S A* **120**, e2307551120 (2023).

Dreyer HHM, van Tuyll van Serooskerken ES, **Rodenburg LW**, Bittermann AJN, Arets HGM, Reuling EMBP, Verweij JW, Haarman EG, van der Zee DC, Tytgat SHAJ, van der Ent CK, Beekman JM, Amatngalim GD, Lindeboom MYA. Airway Epithelial Cultures of Children with Esophageal Atresia as a Model to Study Respiratory Tract Disorders. *Children* **10**, 1020 (2023).

Jo S, Centeio R, Park J, Ousingsawat J, Jeon DK, Talbi K, Schreiber R, Ryu K, Kahlenberg K, Somoza V, Delpiano L, Gray MA, Amaral MD, Railean V, Beekman JM, **Rodenburg LW**, Namkung W, Kunzelmann K. The SLC26A9 inhibitor S9-A13 provides no evidence for a role of SLC26A9 in airway chloride secretion but suggests a contribution to regulation of ASL pH and gastric proton secretion. *FASEB J* **36**, e22534 (2022).

Besteman SB, Phung E, Raeven HHM, Amatngalim GD, Rumpret M, Crabtree J, Schepp RM, **Rodenburg LW**, Siemonsma SG, Verleur N, van Slooten R, Duran K, van Haaften GW, Beekman JM, Chang LA, Meyaard L, van der Bruggen T, Berbers GAM, Derksen N, Nierkens S, Morabito KM, Ruckwardt TJ, Kurt-Jones EA, Golenbock D, Graham BS, Bont LJ. Recurrent Respiratory Syncytial Virus Infection in a CD14-Deficient Patient. *J Infect Dis* **226**, 258-269 (2022).



About the author

ABOUT THE AUTHOR



Lisa Rodenburg was born on 7 April 1994 in Amersfoort. She attended high school at the Johan van Oldenbarnevelt gymnasium in Amersfoort. She obtained a bachelor's degree in Biomedical Sciences and continued with the selected Utrecht medical master (SUMMA) to obtain her medical degree, both at Utrecht University.

During her studies she developed a great interest for translational medicine. Therefore, she did her scientific master internship in the research group of Prof. Dr. Jeffrey Beekman and Prof. Dr. C.K. van der Ent, under daily supervision of Dr. Gimano Amatngalim, affiliated with the department of paediatric pulmonology in the Wilhelmina Children's hospital (WKZ) and with the Regenerative Medicine Center Utrecht (RMCU). The research project was focused on the application of nasal brushing-derived airway epithelial cells as preclinical model for cystic fibrosis. After obtaining her master's degree, she continued this research project as PhD student in 2019.

After finishing her PhD in 2023, she started working as a resident (ANIOS) in internal medicine at the St. Antonius hospital in Nieuwegein to acquire working experience as a clinical doctor. In October 2023, she continued as a resident (ANIOS) in clinical genetics at the University Medical Center Utrecht (UMCU).

In her spare time she loves doing sports. After many years of performing sprint and hurdles at competitive level for Altis (Amersfoort) and av Phoenix (Utrecht), she is now focusing more on endurance sports like running, cycling, mountain biking and ice skating.

